Aston University

If you have discovered material in AURA which is unlawful e.g. breaches copyright, (either yours or that of a third party) or any other law, including but not limited to those relating to patent, trademark, confidentiality, data protection, obscenity, defamation, libel, then please read our Takedown Policy and contact the service immediately.

APPLICATION OF THERMAL NEUTRON RADIOGRAPHY FOR THE MASS TRANSPORT OF MOISTURE THROUGH FREEZING SOIL

MICHAEL ANTHONY CLARK
Doctor of Philosophy

ASTON UNIVERSITY
APRIL 1989

This copy of the thesis has been supplied on condition that anyone who consults it is understood to recognise that its copyright rests with its author and that no quotation from the thesis and no information derived from it may be published without the author's prior, written consent.

THESIS SUMMARY

Aston University
Application of Thermal Neutron Radiography for the Mass Transport of Moisture Through Freezing Soil
Michael Anthony Clark
Ph.D
1989.

This thesis reports on the development of a technique to evaluate hydraulic conductivities in a soil (Snowcal) subject to freezing conditions. The technique draws on three distinctly different disciplines, Nuclear Physics, Soil Physics and Remote Sensing to provide a non–destructive and reliable evaluation of hydraulic conductivity throughout a freezing test. Thermal neutron radiography is used to provide information on local water / ice contents at anytime throughout the test. The experimental test rig is designed so that the soil matrix can be radiated by a neutron beam, from a nuclear reactor, to obtain radiographs. The radiographs can then be interpreted, following a process of remote sensing image enhancement, to yield information on relative water / ice contents. Interpretation of the radiographs is accommodated using image analysis equipment capable of distinguishing between 256 shades of grey. Remote sensing image enhancing techniques are then employed to develop false colour images which show the movement of water and development of ice lenses in the soil . Instrumentation is incorporated in the soil in the form of psychrometer / thermocouples, to record water potential, electrical resistance probes to enable ice and water to be differentiated on the radiographs and thermocouples to record the temperature gradient. Water content determinations are made from the enhanced images and plotted against potential measurements to provide the moisture characteristic for the soil. With relevant mathematical theory pore water distributions are obtained and combined with water content data to give hydraulic conductivities. The values for hydraulic conductivity in the saturated soil and at the frozen fringe are compared with established values for silts and silty–sands. The values are in general agreement and, with refinement, this non–destructive technique could afford useful information on a whole range of soils. The technique is of value over other methods because ice lenses are actually seen forming in the soil, supporting the accepted theories of frost action. There are economic and experimental restraints to the work which are associated with the use of a nuclear facility, however, the technique is versatile and has been applied to the study of moisture transfer in porous building materials and could be further developed into other research areas.

Key Words: Partially frozen soil, Hydraulic conductivity, Neutron radiography, Remote sensing.

ACKNOWLEDGEMENTS

I thank my supervisor Dr Roger Kettle who has been a constant source of technical advice and has been both a friend and a colleague to me in my days as an undergraduate and postgraduate student.

I wish to thank the staff of The Universities of Manchester and Liverpool Research Reactor, particularly Dr Chris Bates, and the staff of Harwell Research Laboratories, particularly Rusty Harris and Jack Seymour. My thanks go also to the technical support staff of Aston University, whose skill in constructing the test apparatus was considerable.

The help and advice of Dr Hawkesworth, Dr Giles D'Souza and Dr Andrew Binley, which was given freely and with enthusiasm, is gratefully acknowledged and special thanks is reserved for Dr David Barnes, whose constant support and advice throughout the years of this study has been invaluable.

Finally I thank my wife, Ashley, who has tolerated everything to support this work, and my Mum and Dad for their help.

To Ash, Ben, Joe and Laura.

CONTENTS

LIST OF FIGURES

LIST OF TABLES

LIST OF PLATES

CHAPTER 1 INTRODUCTION

Large areas of the Earths land surface are subject to climatic freezing. In the temperate regions much of the land is subject to seasonal freezing while, in the high latitudes, permafrost is the predominant feature of the environment.

In such regions problems associated with frost action are of great importance. In Canada, Alaska and the U.S.S.R, where permafrost covers a total area of approximately 22 million square kilometres, the problems of differential frost heave and thaw weakening cause damage to buildings, roads and pipelines.

The first detailed work on frost heave was carried out by Taber (1) some 60 years ago. Freezing experiments, under controlled conditions, were conducted with the specimen frozen from the top and the upward movement of pore water permitted from an artificial water table. As the zero isotherm penetrated deeper into the soil it was noted that the surface displaced vertically as segregated ice lenses were formed. As one lens ceased to enlarge and another formed below it no change was noted in the rate of vertical displacement. Such testing demonstrated, in a controlled laboratory environment, many of the features that had been observed in field exposures.

Initially freezing air temperatures set up thermal gradients that induce upward heat flow through the soil. As heat is extracted, moisture in the frost susceptible soil nucleates at the freezing front leading to the formation of ice crystals. The growth of these ice crystals produces planar ice lenses. The upward migration of soil water feeds these ice lenses and so enables them to enlarge. Thus the development of ice lenses produces an upward displacement of the ground surface, termed "Frost Heave". Frost heave can range from 20 to 50cm over a winter season and, if restrained, can produce measurable heaving pressures (2).

In order to develop frost heave in a soil three conditions must be satisfied. There must be a subzero temperature at the soil surface, water must be available to sustain the freezing process and the soil must be frost susceptible. As particle size decreases freezing induced effects increase and hence, in general, silts are more frost susceptible than sands and gravels. This trend does not however, apply to soil particles in the colloidal range, freezing (wet) silts develop larger frost heaves, than clay soils but the heave pressures induced in such clays are capable, of lifting great loads (2).

The rate of heat removal and the upward movement of soil water are critical factors in frost heave development. The flow lines for heat conduction and water movement are in general parallel to one another and perpendicular to the soil surface which results in ice forming in lenses parallel to the soil surface. The 9% expansion of water on phase change from liquid to solid is not the cause of frost heave. This has been proven (1) in experiments where Benzene and Nitrobenzene, which contract when frozen, have been used to wet the soil. The subsequent exposure to nucleation temperatures gave rise to the formation of solid lenses with the soil exhibiting expansion. The heave has consequently been attributed (1) to the movement of additional water into the zone of freezing and so study of the moisture flow and the factors influencing such flow are of paramount importance to understanding soil freezing on both the macroscale and microscale.

The second damaging factor associated with frost action in soils arises from the changes that accompany thawing. During thawing previously frozen soil becomes drenched in melt water which may result in complete loss of strength, this is referred to as Thaw Weakening. The problem is enhanced if heaving has occurred. When the frozen zone thaws excess melt water from the segregated ice lenses can permeate upward to the soil surface, if the downward migration is prevented by the presence of frozen soil lower in the ground. When heave takes place beneath a road surface, thawing leaves the pavement supported by wet soil and water which can lead to wheel load damage in the road pavement.

In addition to Frost Heave and Thaw Weakening, the repeated freezing and thawing of the soil can produce other problems which may be of relevance to both the geotechnical engineer and the (soil) agronomist. Cyclic freezing and thawing can lead to migration of coarse particles and alterations in the texture of fine grained soils. The moisture fluxes associated with freezing and thawing can produce changes in the concentrations of nutrients in the soil water which may influence the growth of plants. In addition during freezing, the frozen zone is filled with ice which seals the infiltration pathway of the hydrological cycle.

This thesis details the development of a multi discipline experimental technique to study the mass transport of moisture through a freezing soil. The technique involves nuclear physics, a neutron beam from a nuclear reactor is used to obtain neutron radiographs of ice lensing in a highly frost susceptible matrix. The images obtained depict water in the matrix and enhancement of the images, using remote sensing image enhancing techniques, actually shows the development of ice lensing in the soil.

The images are digitised so that values for water contents can be obtained and these are combined with data from suction probes, installed in the freezing sample, so that hydraulic conductivities can be determined. Knowledge of the hydraulic conductivity, the ease with which moisture moves through the soil, is essential for the successful modelling of frost action in soils and consequently measurement of the parameter has been attempted by renowned researchers with varying degrees of success. Values for hydraulic conductivities obtained in the experimental work reported in this thesis are compared with values obtained by other researchers to validate the technique.

The technique has certain advantages over other methods, notably the soil remains undisturbed throughout the test and the external parameters, temperature, water flow to the soil etc., can be varied without affecting measurements. There are also limitations to the technique when applied to the study of freezing soils. The technique, however, can also be applied to other research areas outside soil freezing and some of these applications are discussed later in the thesis.

CHAPTER 2. FROST HEAVE: LITERATURE REVIEW

2.1 Theories

There are three main theories of frost heave:

1. Capillary Theory.
2. Secondary Heaving Theory.
3. Adsorption Force Theory.

An additional theory developed in 1979 by Konrad and Morgenstern, has gained some support and limited success. The theory is known as the Segregation Potential or Mechanistic Theory of Frost Heave, and will be included for discussion.

All the theories are in agreement that the film water separating the ice lenses from the soil grains is responsible for the phenomenon of frost heave.

2.1.1 Capillary Theory.

The Capillary Theory states that the capillary suction present at a curved ice/water interface causes water to move to a growing ice lens, (3).

The condition for ice lens growth at the freezing front is given by equation 1, (4):

$$P_i - P_w = 2.\ \sigma_{iw} / r_p \quad \text{.......}(1)$$

where:

P_i = Ice pressure
P_w = Pore water pressure
σ_{iw} = Surface tension of the ice/water interface
r_p = Radius of ice pores containing ice/water interface

The equation shows the pressure difference required for ice to penetrate the neck between soil grains and the situation is represented diagramatically in figure 1.

The changes in pressure influence the freezing point. Ice lens temperature can be determined from the Clausius – Clapeyron equation :

$$LdT = -(\ V_i\, dP_i - V_w\, dP_w\ ) / T_0 \quad \text{.......}(2)$$

where:

T_0 = Equilibrium temperature of bulk ice and water (°K)
dT = Drop in temperature below To (°K)

dP = Change in pressure
V = Specific volume
L = Latent heat
subscripts i and w refer to ice and water

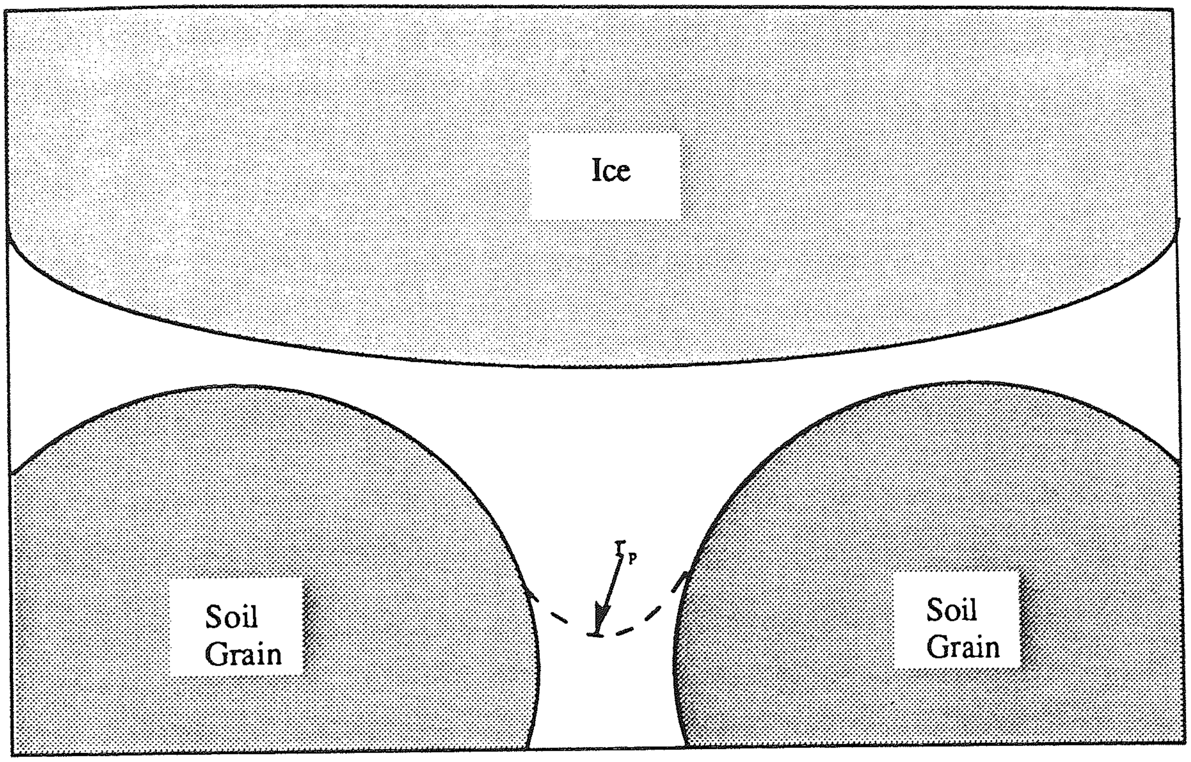

Figure 1 – Ice Penetrating Neck Between Soil Grains.

The rate of heave is dependent on mass transfer of water to the freezing front. The mass transfer of water is dependent on the suction induced at the freezing front, the availability of water in the unfrozen soil and the hydraulic conductivity of the frozen soil.

For growth of ice lenses to continue at the stationary freezing front the rate of heat removal from the supply of water and phase change transformation must equal the rate of heat removal from the freezing plane.

Above the ice front the heat flow is non steady which gives rise to a strong tendency for lowering the temperature at the freezing front. Changes in local temperature thus alter the radius of the ice/water surface enabling the ice to penetrate the neck between soil grains and forming a new lens at a lower elevation.

In this way a series of ice lenses are formed by the penetrating freezing front and consequently the rate of heave is influenced by the rate of heat extraction. Application of overburden pressure increases P_i modifies the suction and limits flow to the freezing front which causes the rate of heave to be lowered. As the ice lenses accumulate the stress beneath ice lenses increases which may decrease the pore size in the unfrozen soil. As hydraulic conductivity is affected by changes in pore size this limits the movement of water to the growing ice lenses.

There are five basic assumptions in the Capillary Theory :

1. The angle of contact between ice and water is zero.
2. The pores are of circular cross–section.
3. Osmotic and adsorption effects can be neglected.
4. The pores are air free.
5. Ice pressure remains constant during freezing.

These assumptions are best satisfied by granular soils and hence the Capillary model is not suited to the study of long term freezing involving secondary heaving.

2.1.2 Secondary Heaving Theory.

The Secondary Heaving Theory, developed by Miller (2), can be used to predict both primary and secondary heave.

In the primary heave stage ice lenses grow at the freezing front where development is sustained by the inability of the ice / water interface to pass through the pores. Secondary heave concerns the development of the frozen fringe, the growth of the ice phase into some of the pores formed by stationary particles below the ice lens.

The stages in the development of ice in a soil are given in figure 2. (2)

The theory divides a sample of soil, subject to freezing into three distinct regions :

1. A solid frozen region of soil which may contain ice lenses.
2. A partially frozen region of soil, the frozen fringe, which contains soil, ice and unfrozen water.
3. An unfrozen region of wet soil.

Secondary heaving involves the mass movement of water through the frozen fringe via the liquid films (200 Å thick) between the pore ice and pore walls.

This mass movement is dominated by the movement of solid ice in the direction of decreasing temperature and together with water transport, is termed "Series Parallel Transport".

Millers model is termed a rigid–ice model because the ice present in the frozen fringe is considered rigidly connected to the ice of the growing lens (5). The movement of pore ice through the pores is by a microscopic regelation process where fusion is achieved by a temporary thawing into the frozen mass. The ice phase appears to move as a contiuous rigid body, however, with a uniform linear velocity equal to the observed rate of heave.

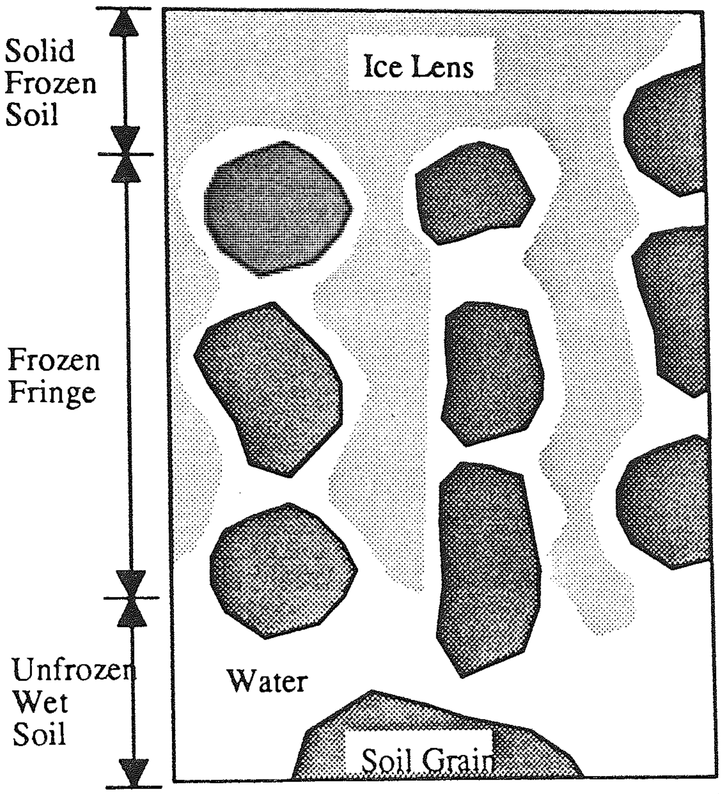

Figure 2 – Secondary Heaving Model.

The overburden, P, is partially supported in two ways. By the reaction of the mineral framework, effective stress σ_e and by the reaction of the pore content, effective stress σ_n.

$$P = \sigma_e + \sigma_n \quad (3)$$

Which can be expressed as :

$$P = \sigma_e + (X P_w + (1 - X) P_i) \quad (4)$$

Where.

X = Stress partition factor.
P_w= Water pressure.
P_i= Ice pressure.

The maximum heaving pressure that can be developed during secondary heaving depends on the temperature, dTo, at the base of the nominal ice lens (the upper limit of the continious films) and pore water pressure, P_w.

$$P_i \max = \rho_i ((P_w)o / \rho_w + L\, dT_0 / T) \quad (5)$$

Where:

ρ_i = Density of ice.
ρ_w = Density of water.

L = Latent heat of phase transition.
T = Absolute temperature (K).
$(P_w)_o$ = Pore water pressure at elevation of nominal ice lens

The rate of secondary heaving is largely controlled by the rate of water flow through the frozen fringe. An increase in temperature gradient reduces the width of this fringe and its impedance to moisture flow. Hence the rate of secondary heaving is inversely proportional to the thickness of the fringe and proportional to the temperature gradient in the fringe.

The rate of primary heaving is proportional to net rate of heat extraction at the frost line.

The secondary heaving theory is most often applied to fine grained soils or soils with a substantial fines content.

2.1.3 Adsorption Force Theory

It has been observed that mineral particles may be carried by growing ice. The particles being transported by floating on the surface of the ice on the thin layer of unfrozen water between the ice lens and the adjacent soil particles. The water molecules in this film water are constantly replenished by the influx of water from an adjacent reservoir. This happens because the freezing film water generates suction that draws water from the surrounding reservoir,the phenomenon being known as segregation freezing.

In the Adsorption Force Theory, (6) the soil particles are assumed to be non–deformable spheres of equal size and the film water is assumed to remain a constant thickness. Relating this to figure 3, providing the soil particles remain in the same positions during freezing the surface AA will rise by the thickness of the frozen portion.

The theory treats the film water as a solid attributing the primary cause of heaving to the stress generated within the film. The stress in the film water is highest where there is closest contact with overlying particles and is negligible in the region near the free pore space.

The depressed freezing point of the film water, due to this stress, is known as the Segregation Freezing Temperature (T_s). It is lower than the in–situ freezing temperature by an amount proportional to the frost heaving pressure.

$$T_s = T_i\,(1 - (W + \rho_i g x)/(\rho_i L)) \qquad \text{.......(6)}$$

T_i = temperature of in–situ freezing.
W = surcharge overlying the ice lens.
ρ_i = density of ice.

g = acceleration due to gravity.

x = thickness.

L = latent heat.

$W + \rho_i g x$ = ice pressure increment.

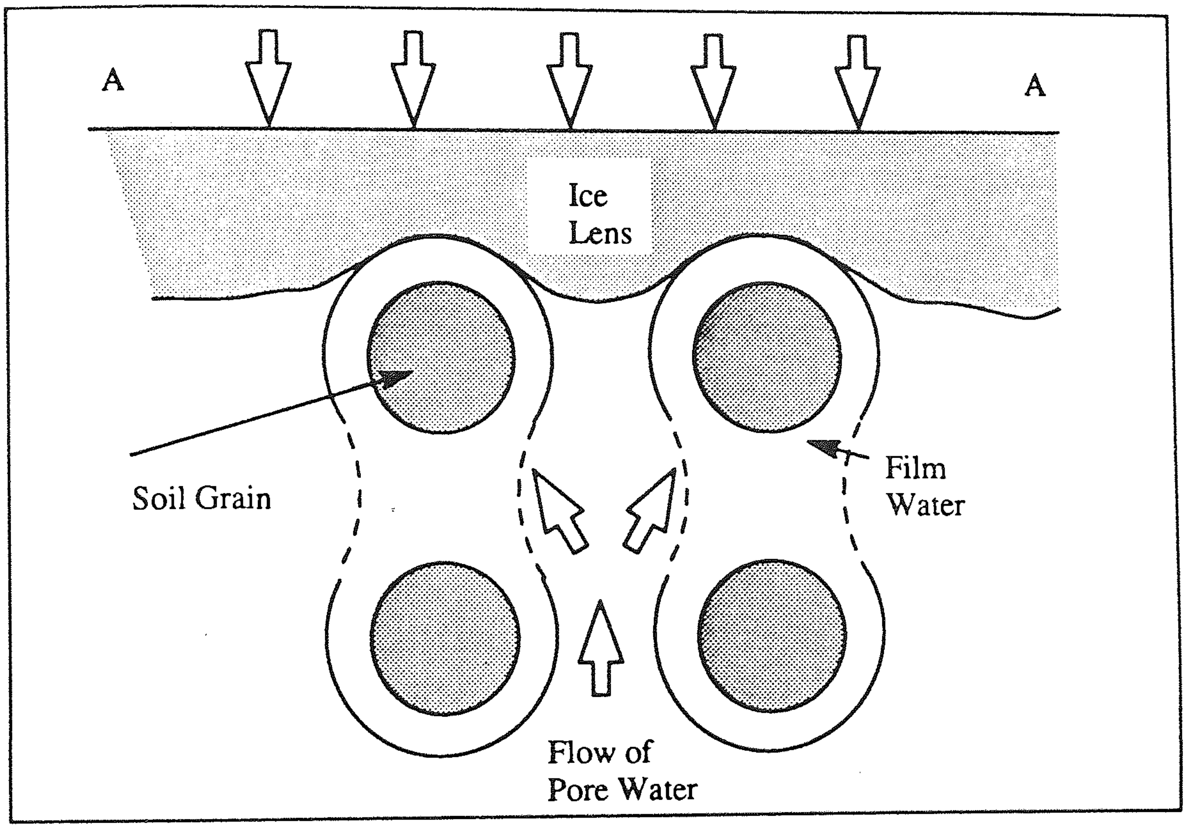

Figure 3 – Pore Water Flow During Freezing.

The ice pressure increment is the overall average of the excess ice stress at the freezing front caused by the surcharge and may be interpreted to be the frost heaving pressure.

The distribution of the segregation freezing temperature in the film water layer is determined by the distribution of the stress. The interaction of the segregation freezing temperature and the actual temperature distribution is complicated and creates a partially frozen zone (zone of diffused freezing). At the boundary of the zone in–situ freezing occurs which governs the supply of water to the freezing zone but does not contribute to frost heave. At the upper boundary of the zone there is segregation freezing and ice lenses grow.

The Capillary Theory considers the adsorption force in the intergranular space to be in equilibrium with the capillary force in the pore and hence neglects it. The Adsorption Force Theory disputes this and states that the adsorption force is the agent causing frost heave.

As with the other theories rate of heave depends on rate of heat extraction, rate of water flow towards the zone of diffused freezing and the composition of the soil.

2.1.4 Segregation Potential

The Segregation Potential Theory, developed by Konrad and Morgenstern (7–13), attempts to characterise a freezing soil by two parameters, the segregation–freezing temperature (T_s) and the overall permeability of the frozen fringe (K_f).

The theory is based upon continuous frost penetration during unsteady heat flow and concentrates on the properties within the frozen fringe that vary in response to temperature changes.

At the start of freezing the rate of frost penetration is high. The water drawn into the sample flows to the accumulation zone which thickens as the thin unfrozen water layers surround the soil particles, the location of the zone being controlled by local permeability. At this stage the thermodynamic equilibrium is altered, the free energy of the water is higher than that of adjacent ice. The equilibrium is re–established by freezing incoming water so that the thickness of the unfrozen water films is maintained.

The advancing frost front delays the accumulation of water allowing the development of a continuous ice lens and hence segregation freezing occurs preferentially along the top of the soil particles.

As the soil temperature decreases the suction in the frozen fringe develops a non–linear profile as a result of the decreasing permeability of the frozen soil. As the rate of frost penetration decreases the rate of temperature change across the sample is reduced. This results in accumulation of water at a given level for longer periods and gives rise to the formation of a discreet ice lens. The ice lens is unstressed and at the base thermodynamic equilibrium is described by the Clausius–Clapeyron equation. This is not the situation with ice between soil grains which is highly stressed and unsuited to application of the Clausius–Clapeyron equation.

Initially ice lenses are very thin but as the freezing front advances and the temperature gradient decreases the thickness and spacing of the lenses increases. At steady state conditions the frozen fringe attains a maximum thickness.

Konrad and Morgenstern suggest that under zero external load, various cold side temperatures and a constant warm side temperature the segregation freezing temperature of the final ice lens formation and the permeability of the frozen fringe will be unique for a given soil.

Applying the theory, frost heave is controlled by the temperature gradient within the frozen fringe.

$dh / dt = 1.09\ v$ ....(7)

$dh / dt = SP(Pe)\ \text{grad}\ T$ ....(8)

Where :

dh / dt = Rate of segregation heave.
v = Velocity of water intake (mm/s).
Pe = Overburden pressure (N/mm^2).
$SP(Pe)$ = Segregation potential as a function of overburden pressure.
grad T = Temperature gradient across frozen fringe (°C/mm).

Hence segregation heave is directly related to segregation potential.

Segregation potential is related to several variables, cold side temperature, warm side temperature and overburden pressure. In tests Konrad and Morgenstern (8) suggest the highest segregation potential for a soil, which occurs when the suction at the frozen–unfrozen interface is zero, should be determined. The suction decreases as the warm side temperature decreases, hence by conducting tests at warm side temperatures approaching 0 °C the segregation potential value can be maximised.

Konrad and Morgenstern (9) have found that maximum segregation potential occurs with the formation of the final ice lens, when the rate of cooling is near zero. It is therefore suggested that v and gradT be determined when the final ice lens begins to develop.

2.2. Frost Susceptibility Tests

In the majority of cases soils are classified for frost susceptibility through measurements of frost heave. Other tests have been used involving empirical assessment of soil–physical characteristics, heaving pressure in restrained tests or thaw weakening (14).

Two direct simulation tests for measuring frost heave, based on the work of Taber (15,16), are in common use. The tests have been developed in Britain by The Transport and Road Research Laboratory (TRRL)(17) and in America by The Cold Regions Research and Engineering Laboratory (CRREL)(18).

2.2.1 TRRL and CRREL Frost Heave Tests

The TRRL test, originally designed to be carried out in a cold room, is now performed in a Self Refrigerated Unit (SRU), shown in figure 4 which is produced commercially by P.S.Snow and Co. Ltd. and based on a prototype developed at Nottingham University (14).

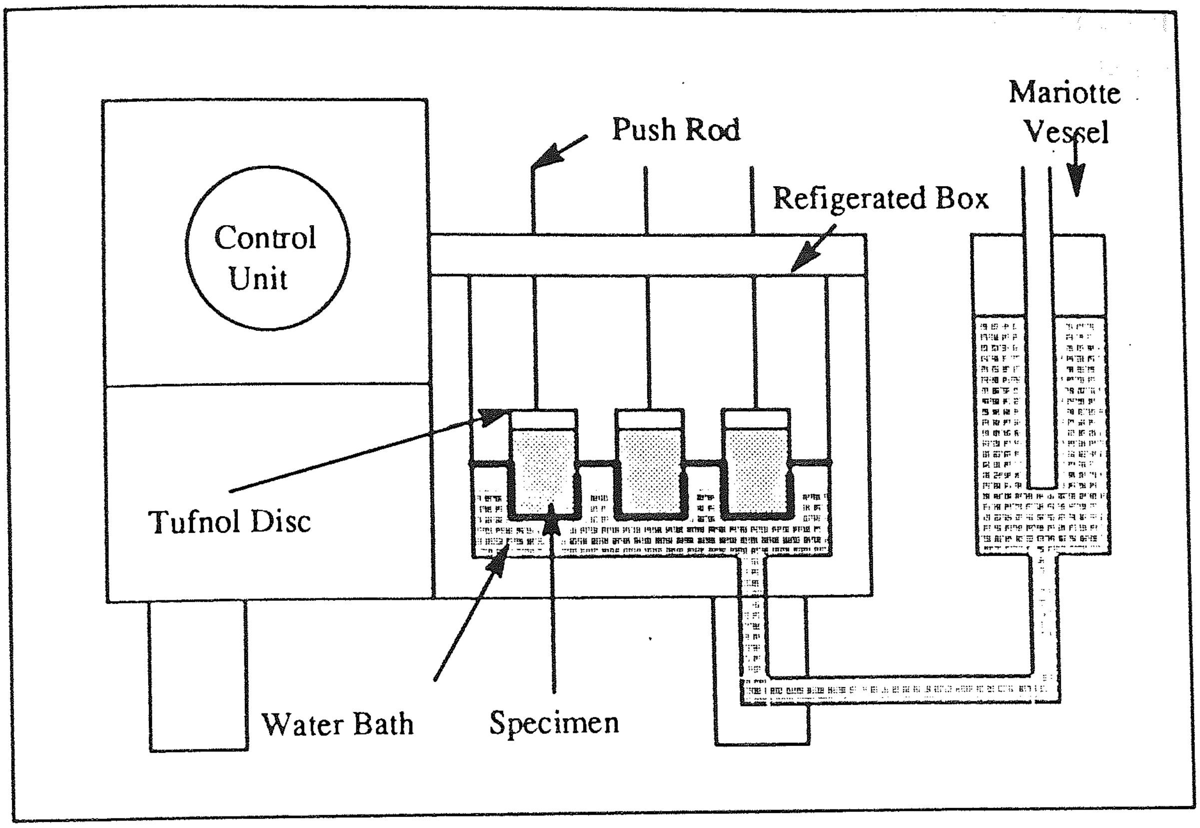

Figure 4 – Self Refrigerated Unit (SRU)

The unit is equipped with an insulated box containing a water bath. The temperature of the water is maintained at 4 °C +/– 0.5 °C (modified to 4 °C +/– 0.1 °C by the use of mercury thermometers) by a heater and the water level is kept constant by means of a Mariotte vessel. A wooden removable box with holes for nine specimen holders sits on the water bath.

The soil specimens are prepared (17) to give 101mm diameter x 152.6mm final dimensions and are wrapped in waxed paper. The specimens rest on porous discs which, on location in brass specimen holders fitted into the wooden box, become saturated with water. Cardboard discs 98.4mm diameter (modified to Tufnol discs 101.6mm diameter) rest on top of the specimens to locate push rods which extend through holes in the top of the cabinet and enable the heave developed in the specimens to be measured.

The specimens are insulated along their length with coarse sand (modified to Vermiculite) and the insulated box is maintained at –17 °C to give a temperature at the top of the specimens of –10 °C.

Results (19) indicate that the test has large systematic errors. Moderation of the water bath temperature, a major source of error, has been improved by using a water bath stirrer (20,21).The method of compaction is questioned in memorandum MM64 (22) and a recommendation made that vibration techniques would be an improvement over the current static compaction. The length of the test (250 hours) is considered too long and it is suggested that the duration be reduced to 100 hours as a correlation between heave established at 250 and 100 hours has been demonstrated.

In the CRREL test the temperature at the top of the specimen is adjusted to give a specified rate of frost penetration (6.7mm/day). The test is broadly similar to the TRRL test in all other respects. A detailed comparison of the two tests is given by Sutherland and Gaskin (23).

2.2.2 Other Frost Susceptibility Tests

This thesis does not attempt to examine in any great detail the numerous tests available for determining frost susceptability of soils. Chamberlain (24) has made a comprehensive review of frost susceptibility tests.

2.2.2.1 Empirical Assessment

Most of the empirical assessment methods are based on particle size characteristics and a few study the effects of minerology, moisture, density, structure, boundary conditions, overburden etc. (3).

Taking a particle size characteristic assessment Casagrande (25) states:

"One should expect considerable ice segregation in non–uniform soil containing more than 3% of grains smaller than 0.02mm and in very uniform soils containing more than 10% smaller than 0.02mm. No ice segregation was observed in soils containing less than 1% smaller than 0.02mm."

2.2.2.2 Simulation Assessment

With simulation assessment frost susceptibility is assessed in terms of total heave or rate of heave.

A comparison of open system methods of simulation assessment of frost susceptibility is made by Jones (14) and illustrated in table 1. The TRRL and CRREL tests have previously been covered, the Precise Freezing Cell (PFC) (16) will now be discussed in some detail.

A cut away view of the PFC is shown in figure 5 (16).The specimens used in the PFC are compacted by a combination of vibrating hammer and static compaction and when

wrapped in waxed paper (as in the TRRL test) rest on a porous disc in a copper holder located in a wooden ring. An insulated container, of PVC filled with vermiculite, surrounds the ring forming a cavity along the length of the specimen. The lower end of the cavity forms a water bath which feeds the specimen, the water level being maintained by a constant head device (as in the TRRL test). From the wooden ring to the top of the specimen the cavity is filled with loose sand. A guard ring, supplied with a coolant (methyl alcohol) rests on the sand and surrounds a peltier cell, which rests on a copper plate located on the specimen, and is supplied with cooling water. Temperature regulation of this freezing head, to +/- 0.1 °C, is achieved by a thermistor embedded in the lower face of the copper plate and coupled to a feedback control on the external cooler. A dial gauge is positioned on the peltier cell for recording heave during freezing.

Table 1 – Comparison of Frost Heaving Tests.

EXPERIMENTAL CHARACTERISTICS	TRRL	CRREL	PFC
Freezing regulated by:			
Air temp. – constant	x		
Air temp. – varying		x	
Surface temp – constant			x
Other details:			
Surcharge (KPa)	0	35	0
Specimen – height (mm)	152	152	152
Specimen – diameter (mm)	102	109	102
No. of specimens per test	3x3	4	1
Test duration (days)	10	10–14	< 10
Characteristics measured:			
Total heave	x		x
Heaving rate		x	

The system is operated at constant temperature by housing the cell in a commercial refrigerator with control and monitoring equipment in a constant temperature enclosure maintained at 21 °C +/- 1 °C.

In tests using the PFC it was found that all heave ceased before 250 hours of freezing had elapsed, consequently future tests were terminated when the rate of heave became negligible (<0.1mm/day).

In the PFC radial heat flow is very small, particularly in the frozen zone, giving a better approximation to unidirectional flow than can be achieved in the TRRL test. The rate of penetration of the zero isotherm is also much faster and together with constant boundary temperatures leads to smaller heaves and more repeatable results.

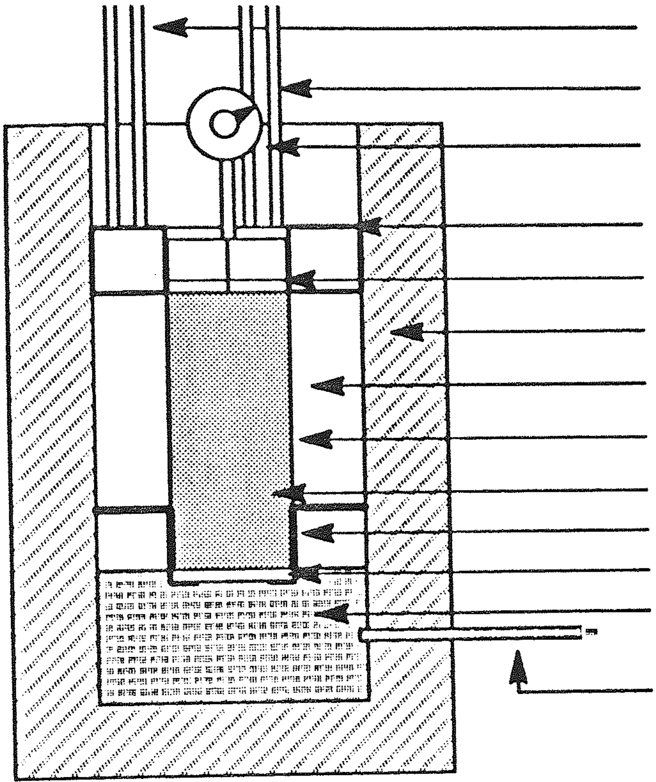

Figure 5 – Precise Freezing Cell (PFC).

A closed system method of simulation assessment of frost action has been developed by Kettle and McCabe (26). Initial work on the system looked at ways of reducing side wall resistance, which has been shown (26,3) to have a marked effect on heaving pressure.

Initial designs were based on an original system used at CRREL. The specimen was housed in a steel mould, coated with Polytetrafluoroethylene (PTFE) dry lubricant and tapered to reduce side wall resistance. At the lower end of the mould a recessed steel plate was incorporated to locate a porous stone.

Freezing was by means of a thermoelectric device (TED) which rested on an aluminium cold plate at the top of the mould and maintained the top temperature at –4.2 °C. The bottom temperature was held constant at +4 °C by the cabinet containing the specimen. Tests continued until maximum pressure was reached, defined as the pressure at which the rate of increase is less than 0.001 MN/m/hr.

Results from these initial tests indicated that side wall resistance had not been sufficiently reduced by the use of PTFE dry lubricant and a tapered mould. To rectify the problem a multi–ring system for specimen support was developed.

Perspex rings located inside a modified steel mould, giving 1mm clearance between rings and mould, were used both during compaction and freezing. It was found however that moisture exuded between the rings during compaction producing adfreeze on testing. To eliminate this, following compaction, the steel mould was lifted from the ring system, the rings are coated with grease, a rubber membrane slid over them and then a further coating of grease applied to the outer face of the membrane before the steel mould was replaced.

A comparison of heaving pressures against time for the three methods of reducing side wall resistance is given in figure 6.

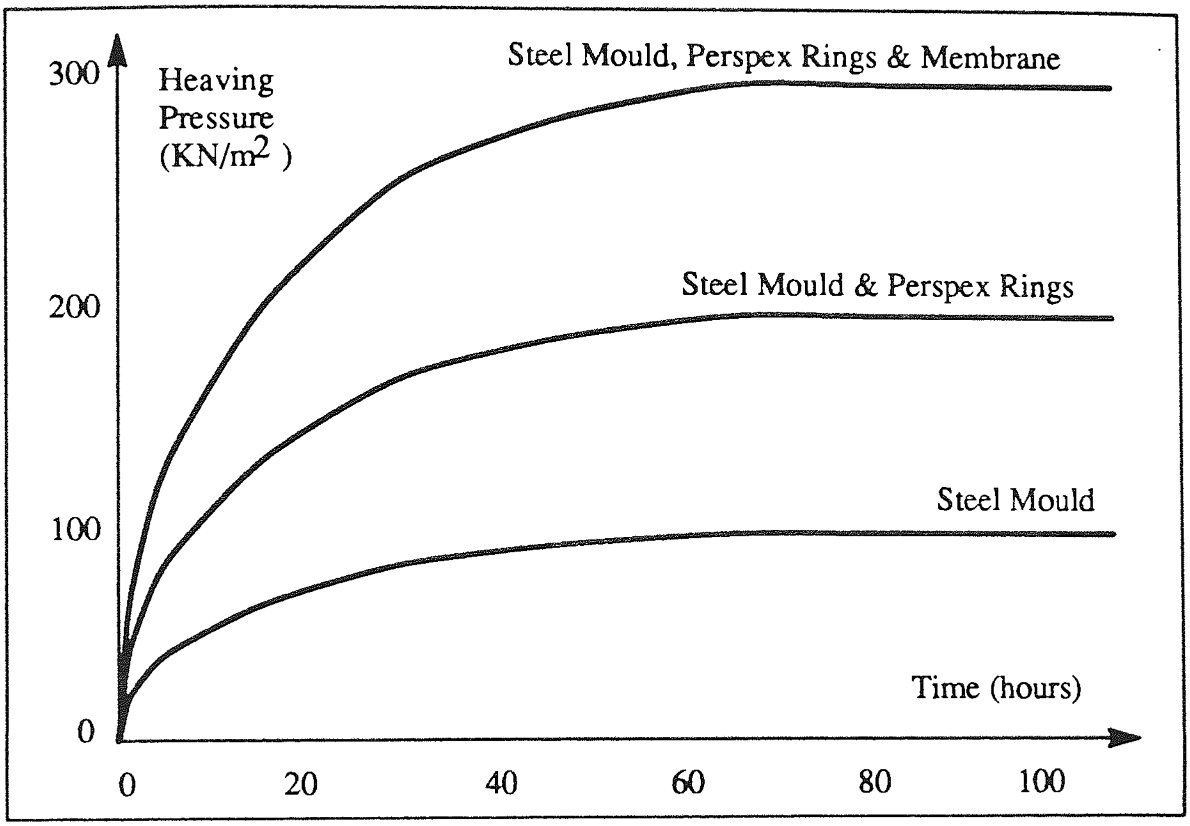

Figure 6 – Relative Effects of Modifications to Measured Heaving Pressures.

The system was further improved by changing the TED for a cold plate containing refrigerant from a central cryostat which enabled several tests to be run from one cryostat at the same time.

Work by Kettle and McCabe (26) and McCabe (3) has shown that heaving pressure and frost heave are not uniquely related, other influences such as particle type and grading are important.

2.3 Heaving Pressure and Surcharge

Restriction of frost heave leads to the development of heaving pressures. The pressure is associated with the accumulation of water, as ice, and occurs in the ice phase (27), its magnitude being influenced by many factors (3).

1. Pore size (particle size).
2. Rate of heat removal
3. Tension in the ice/water interface.

4. Hydraulic conductivity of the frozen soil.
5. Hydraulic conductivity of the unfrozen soil.
6. Hydraulic conductivity of the frozen fringe.
7. Availability of water.
8. Temperature gradient in the frozen fringe.
9. Compressibility of the unfrozen soil.
10. External pressure on the soil.
11. Rigidity of structures adjacent to the freezing soil.

The energy released when ice lenses are formed encourages water migration to the freezing front and aids in lifting overlying soil overburden. A consequence of this is that as overburden pressure increases less energy is available for transporting water and hence ice lens development is restricted.The pressure (shut off pressure) at which no further ice lensing occurs, in reality, does not exist.

There is a tailing off of ice lens development with increased overburden pressure but the key factor determining heaving pressure is thought to be cold side temperature.

The Clausius–Clapeyron equation can be used to determine heaving pressure from ice lens temperature:–

$$LdT = -(V_i\,dP_i - V_w\,dP_w)/T_0 \qquad \text{.....(2)}$$

Assuming the heaving pressure during the freezing process does not change, this gives:–

$$dP = (T_0\,LdT)/(V_i - V_w) \qquad \text{.....(9)}$$

Hence the heaving pressure is related to the freezing point depression which is related to the soil texture (pore size).

Considering heaving pressures in freezing soils, in addition to Millers theory of Secondary Heave (2) , The Adsorption Force Theory has merit and the heaving pressure expression derived by Takagi(6) can be used.

The effect of overburden is twofold. The suction potential, established beneath the warmest ice lens, is reduced by an amount equal to (V_i/V_w)Pe which influences the rate of water migration and rate of heave. Changes in pressure effect the unfrozen water content in frozen soil. Raising the overburden pressure increases the amount of unfrozen water, resulting in changes in local permeability and changes in the frozen fringe characteristics (segregation freezing temperature Ts and overall permeability Kf (28). It also results in the freezing point moving further into the soil, lengthening the frozen fringe and so reducing the hydraulic gradient across the fringe. Interest in heaving pressure is concentrated in two main areas. Evaluation of the effects of heaving pressures on structural facilities involving low temperatures (ice rinks etc.) and developing the use of heaving pressures to replace heave as a test for frost susceptibility in soils.

Work directed towards the second of these areas has been carried out by McCabe (3) and Kettle and McCabe (26,29). The work involves the use of a controlled heave unit (CHU), described in section 2.2.2.2 of this thesis and illustrated in figure 7 (29).

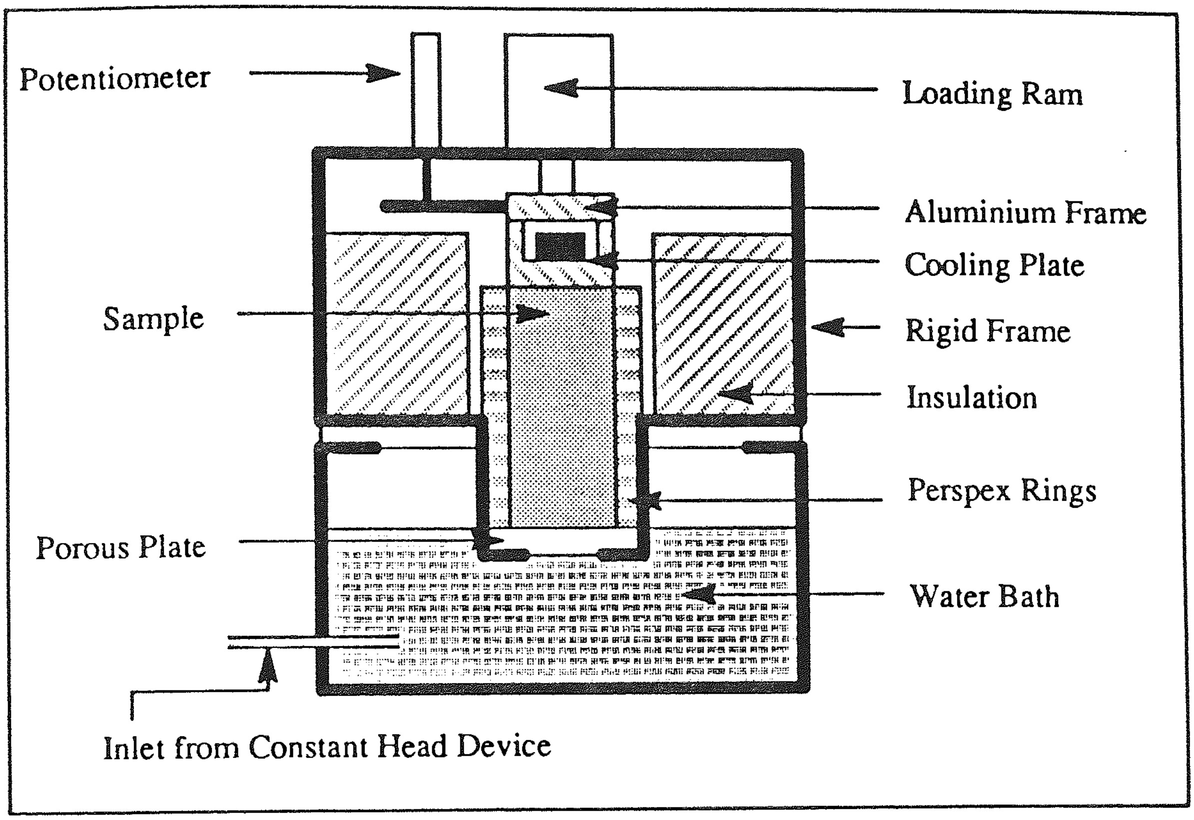

Figure 7 – Controlled Heave Unit (CHU).

The work has encompassed heaving pressure measurement for coarse granular, clay and mixed materials with particular interest paid to thermal parameters, side wall resistance, temperature of the cooling plate and the influence of the specimen size and material properties. A full appraisal of the tests is given by McCabe (3). Information gained indicates that relatively low surcharges can produce reductions in frost heave and that frost heave is related to surcharge by a hyperbolic curve that is dependent on material (27), figure 8. It is also suggested that the ratio of surcharge pressure to heaving pressure can be used to predict the reduction in heave.

Using heaving pressures, rather than frost heave, to determine frost susceptibility is desirable as testing time can be greatly reduced.

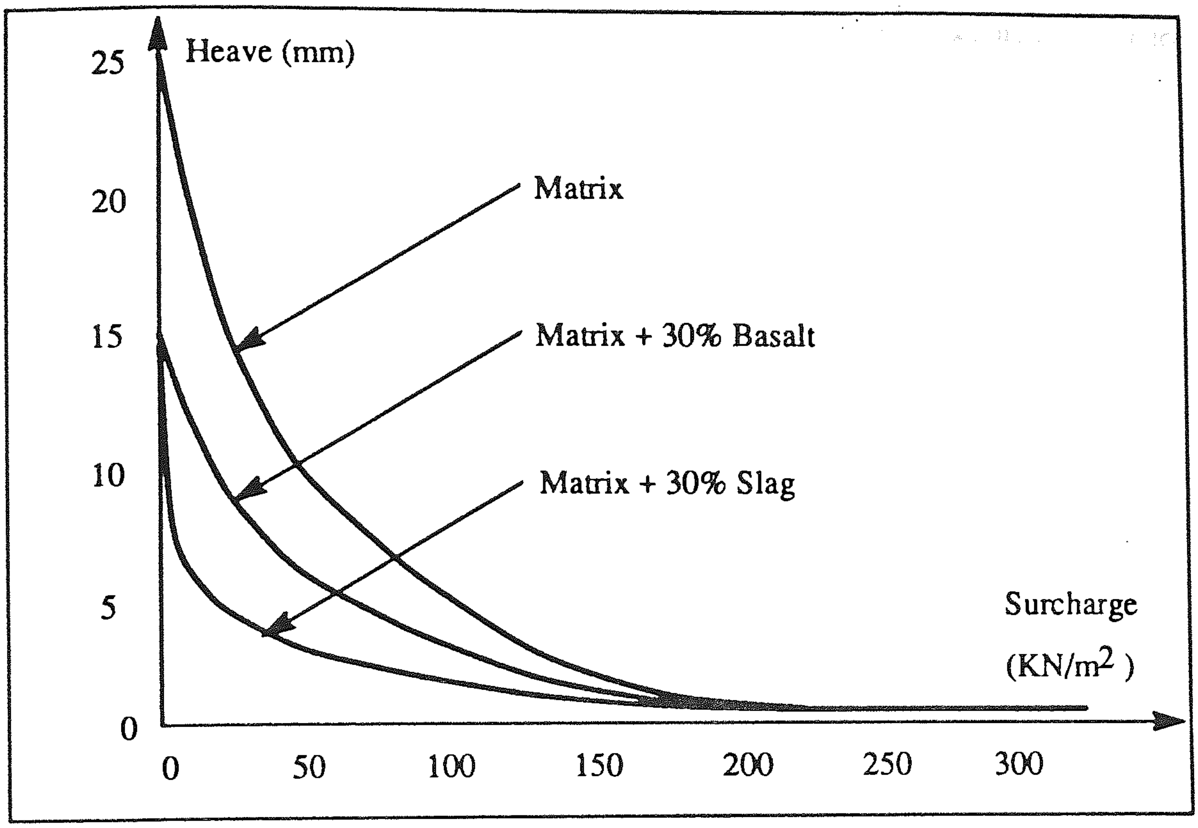

Figure 8 – Frost Heave Against Surcharge.

2.4 Models

Pure modelling, employing the laws of physics, is difficult due to the complexity of frost heave. Most frost heave models view the soil as a continuum looking at the process on a macroscopic level, though Takagi (6) has examined the microscopic interactions in the film water surrounding particles in the freezing soil.

Involved in most models is a set of coupled partial differential equations of heat and mass flow. Both are typically parabolic with second and first derivatives in space and first derivatives in time. The system is non–linear with a complexity which results in numerical solution with finite differences applied in time and either finite differences or finite elements applied in space (30).

Hysteresis, an inherent feature of the freezing process, is not covered by any model although latent heat affects from phase change must be included if the model is to succeed.

A model, Guymon et al (31,32), developed from the work of Berg assumes the liquid content and hydraulic conductivity in the frozen zone to be independent of the temperature, being taken as functions of liquid pressure head. The model, developed for uni–directional freezing, is macro thermodynamic and one–dimensional and is representative of the type which monitor ice accumulation, with heave occurring when ice accumulation is 85 or 90% of the porosity. The model however continues to treat the frozen soil as if it were continious, a false situation when ice lensing has occurred.

A more physically elaborated mathematical model for coupled mass and energy transfer in freezing soils has been developed by Hopke (33). The Clapeyron equation is used to calculate ice pressure from temperature and water pressure, and Galerkin's finite element scheme is used to solve for one dimensional energy and mass balances. The model takes into account the effects of overburden with heaving allowed to occur whenever the ice pressure is at least as large as the overburden. This works as increased overburden reduces heave, but too much heave is predicted for low overburdens or high temperature gradients (conditions which relate to a thin frozen fringe).

In addition to models concerned with heave prediction, a theoretical model for predicting thermal conductivity in frozen soils has been developed by Gori (34). The model assumes parallel isotherms and heat flux lines for the determination of effective thermal conductivity and gives a fair approximation to experimental data. An indepth review of modelling techniques and specific models is given by O'Neill (30).

CHAPTER 3. FREEZING INDUCED EFFECTS: LITERATURE REVIEW

3.1 Introduction

This chapter looks at the mode of ice lens formation in soils and the importance of unfrozen water in frozen soils. Important freezing induced effects, suction and hydraulic conductivity, are then discussed and experimental techniques for determining these parameters covered in detail. Following on from Chapter 2, which looked at the mechanism of frost action, the formation of ice lenses in soils and the subsequent effects are now described.

3.2 Ice Lensing

The formation of ice lenses in (incompressible, non–cohesive) soils results in heave in the ground surface equivalent to the total thickness of the lenses, (35). The negative pore pressures which are generated in compressible soils, at the freezing front as the ice lenses develop, can, however, produce positive effective stresses in the unfrozen soil leading to consolidation. Williams (36) has carried out work on compressible soils to calculate the degree of consolidation. He was able to demonstrate the existence of negative pore pressures the magnitude of which were dependent on the freezing temperature.

Ice lenses are generally formed discretely in large numbers separated by layers of soil. This rhythmic ice banding is a result of periods of inbalance between the heat and moisture flows, (35). The formation of an ice lens is accompanied by the liberation of the latent heat of fusion which augments the heat flow through the frozen layer, (37). This has been recently demonstrated experimently by McCabe (38). A specimen of artificial soil was tested under uniaxial freezing conditions and subjected to several different overburden loads. With no surcharge and the correspondingly increased ice lensing, higher heat flows were recorded in the frozen soil.

Techniques to examine the structure of ice lenses normally involve the slicing of frozen soils into thin sections. A fairly successful attempt at this approach has been made by Osterkamp (39). Frozen soils were cut into thin sections using a diamond wire saw, the sections then being photographed to obtain information on ice lenses at or near melting point. It was suggested (39) that water flow through ice lenses near the freezing front is facilitated by a three dimensional network of veins lying in three–grain intersections which can result in a water flux of 1cm/day. However even at temperatures well below 0 °C, where ice lenses are well developed, water can be present and water flows through these frozen zones have been recorded.

Variations in soil type lead to variations in the shape of ice lenses. In granular soils the direction of the major axis of the lens is normal to the heat flow and the shape is dual convex. In clay soils drying and shrinkage along the ice/water interface results in shell shaped ice lenses, (35). Arvidson et al (40) report on several incidences with fine grained soils when the movement of pore water away from the freezing front has prevented the formation of ice lenses. Any resulting heave has then been due to insitu freezing of the remaining pore water.

3.3 Unfrozen Water in Frozen Soils

The unfrozen water content of frozen soils is dependent on (41):

i) Temperature and overburden pressure (external forces)
ii) Specific surface area of the solid phases within the soil system.
iii) Chemical and minerological composition of the soil.
iv) Physicochemical characteristics of the soil, particularly the nature of exchangeable cations.

In a given soil the unfrozen water content is primarily dependent on temperature and is also influenced by capillarity and osmotic effects, which serve to suppress the freezing point, and by adsorption with soil particles, (42).The effect of externally applied forces is to increase the unfrozen water content particularly in fine grained soils.

It is now generally considered that the unfrozen water is present as a thin layer adsorbed between soil particles and the ice (43). This layer is replenished during heaving by the influx of water from adjacent reservoirs (open system) or from the unfrozen soil (closed system). As the zero isotherm penetrates, a portion of the boundary layer supporting the ice lens solidifies which thickens the lens and locally reduces the thickness at the boundary layer. This film is replenished by imbibing water from the moist unsaturated soil below, thus the temperature gradient has induced a hydraulic gradient which facilitates the continual upward flow of water, thereby allowing the lens(es) to continue to grow.

The existence of this water film was experimentally shown by Corte (44) when he demonstrated that particles can be carried upward in a soil by floating on ice. Water and ions are conducted via this unfrozen film under the influence of temperature, electrical, and external pressure gradients. The rate of water migration is dependent on the surface area and thickness of the film. As the temperature in the soil is lowered the thickness of the film is reduced and water flow through the frozen soil decreases, (45). The coexistence of unfrozen water with ice in capillaries or as an absorbed layer at temperatures below 0 °C can be accounted for by considering the thermodynamics of the soil water system.

As water is drawn from the unfrozen soil during freezing, it produces a fall in the pore water pressure resulting in the development of a suction in the remaining unfrozen soil water, Williams (36) and Burt (46). The term 'suction' implies a pressure state, however at low water contents osmotic forces due to disolved salts and surface adsorption effects are more important, and so it is more appropriate to refer to soil water in terms of 'Free Energy'. The free energy of the soil water (dG) is defined as the difference in the absolute Gibbs free energy of the soil water and that of pure bulk water at atmospheric pressure.

The Clausius–Clapeyron equation states:

$LdT = -(Vi\ dPi - Vw\ dPw) / T_0$ ......(2)

Equation 10 is derived from equation 2 and shows the relationship between Gibbs free energy (dG) and freezing point depression.

$dG = (T_0 - T) L / T$ ......(10)

Where:

$T_0 - T$= Freezing point depression relative to the free energy of pure bulk water.

Equation 10 however only applies to the situation where the ice phase is pure and under atmospheric pressure. With soil water, dG may be divided into various components:

$dG = dG1 + dG2 + dG3$ ......(11)

Where 1, 2 and 3 represent capillarity, surface absorption and osmotic effects. The relative importance of components 1, 2 and 3 is dependent on water content which in frozen soils is dependent on freezing point depression.

At temperatures around 0 °C capillarity is the dominant effect and the capillary equation, Taylor (47)

$H = (2 \sigma_{aw}) / (r \rho_w g)$ ......(12)

Where:

H = Height of a column of water supported by a meniscus of radius r.
ρ_w = Density of water.
g = Acceleration due to gravity.
σ_{aw}= Surface tension of air–water interface.

can be written as, (4):

$P_i - P_w = 2 \sigma_{iw} / r$ ......(1)

dG can then be related to P_i–P_w using the fundamental equation:

$$dG = V\,(P_i - P_w) \qquad (13)$$

It is these potentials which are dominant in primary heaving with water movement through the unfrozen zone to the frost line.

Within the colder frozen layer the relative Gibbs free energy of the unfrozen soil water varies in accordance with equation 11.

The change in free energy which accompanies the reduction in unfrozen water content is thus the cause of the coexistence of ice and water in soils below 0 °C. There is no tendency for the water to freeze because it possesses the same relative free energy as the ice and hence water moves through the frozen zone via the continuous liquid films facilitating secondary heaving.

3.4 Suction

This section is concerned with the methods of measurement that have been used to determine suction in the unfrozen and frozen soils.

The decrease in pressure on the free unabsorbed water is termed the soil suction. At low suctions the surface tension of water and the curvature of the air–water interface can be used in the capillary model to calculate suction using equation 1:

$$P_i - P_w = 2\,\sigma_{iw} / rp \qquad (1)$$

As soil water suction increases, the capillary model can not be used on its own, interactions between water molecules and the surfaces of soil particles must also be taken into account. If there are differences in potential in a system, matter is transferred until equilibrium is achieved. The rate of movement of the water is assumed proportional to the potential gradient. For one dimensional water movement this can be expressed as (48):

$$Vf = -k\,d\phi/dx \qquad (14)$$

where:

Vf = Volume flux of water.
k = Constant of proportionality.
ϕ = Potential.
x = Distance.

In this equation, unlike Darcy's flow equation, the constant of proportionality is a function of water movement or suction.

The flow equation for one dimension is obtained by combining equation 14 with the principle of conservation of matter:

$d\phi/dt = -d/dx(k\ d\phi/dx)$ ....(15)

where:

t = Time.

For one dimensional flow, in the vertical direction, equation 15 becomes:

$d\phi/dt = d/dz(D\ d\phi/dz) + dk/dz$ ....(16)

where:

D = k dh/dϕ = Diffusivity.
T = Suction.

In a heterogeneous matrix D and k will vary with position.

These equations, however, only apply to isothermal systems where liquid and vapour movement may be treated together. When temperature gradients are present this may not be the case, liquid and vapour movement may be in opposite directions and both vapour pressure and soil suction are temperature dependent.

In swelling clays the capillary model probably fails at suctions above 1 bar (49) and therefore it can be concluded that the suction of water in a swollen clay should be thought of as the difference of Gibbs potential rather than a difference of hydrostatic pressure.

3.4.1 Suction in Unfrozen Soils

Water movement in soils is largely governed by soil suction gradients (49). If the soil pores are filled with water, the gravitational field is responsible for water movement. In partially filled pores the interaction between the water and the surfaces of the soil particles provides the forces for water movement. The total potential can again be expressed as the sum of three components, gravitational potential, osmotic potential and capillary potential. The capillary potential is of major importance in the context of this thesis and the various methods available for measuring it are discussed.

3.4.1.1 The Pressure Membrane Apparatus

With the pressure membrane apparatus the potential energy of the soil water is raised to that of the free water by applying an appropriate pressure. The results obtained are expressed as a series of moisture content versus suction curves (50).

The pressure membrane apparatus can operate to high suctions with air pressures of up to 14 bars. A pressure membrane apparatus has been developed (50) to measure pressures up to 1382 bars. The design is based on an apparatus constructed at the Road Research Station in the UK, a full description of which is given by Williams (50).

3.4.1.2 Mercury Manometer Tensiometer

These are the most commonly used instruments for the measurement of the moisture potential in the field (51). The tensiometer functions by reducing the potential of the free water to that of the soil water by reducing the pressure acting on it. The potential is then calculated from the product of the pressure difference and the specific volume of water. Reliable readings can be achieved with mercury manometer tensiometers over the range 0–0.7 bars or 0–0.85 bars if tensiometers are equipped with pressure transducers. Although the potentials of the soil moisture can be far below the measuring range of tensiometers, water movements associated with these low potentials are of little consequence in hydrological determinations where tensiometers have their main application.

3.4.1.3 Psychrometers

Soil hygrometer/psychrometers are an alternative method of measuring water potentials from less than 1 bar to greater than 30 bars, in–situ and in the laboratory. In the psychrometric (wet bulb method) a thermocouple is cooled below the dew point by means of the Peltier effect. This results in a film of condensed water forming on the junction surface. The condensed water evaporates which results in the temperature of the junction being depressed below ambient temperature. The cooling is a function of the rate of evaporation, this is a function of the vapour pressure of the atmosphere which is a function of the water potential of the soil (52).

Psychrometer probes require careful calibration in the laboratory prior to use and hence errors in the field are possible if sufficient care is not taken. Temperature gradients in field situations can cause serious problems as laboratory calibrations are made under isothermal conditions.

3.4.1.4 Osmotic Method

A method of applying suction to soil water by osmosis has been devised (53). The osmotic pressure of an aqueous solution of polyethylene glycol applies a suction to specimens through a semi–permeable membrane. The osmotic method has a similar pressure range to the pressure membrane apparatus, the applied suction being varied by concentration of solution.

3.4.1.5 The pF Scale

The pF scale of measuring suction has been developed to enable low suctions (10cm water) and high suctions (1000cm water) to be represented by more manageable units. The pF value is equivalent to the logarithum to base ten of the suction expressed in cm water, so that a suction of 10cm water has a pF value of 1 and a suction of 1000 cm water has a pF value of 3.

3.4.2 Suction in Frozen Soils

When a frost susceptible soil is frozen with frost heave in an advanced stage, ice lenses will be present in the soil fabric. This lensing occurs as as result of potentials being generated in the freezing zone which cause water to migrate from regions of greater potential, to the developing ice lens(es).

It is suggested (54) that the potentials developed by freezing may be regarded as hydraulic and, by balancing against a water column, may be measured as hydrostatic pressures. An experiment along these lines, has been undertaken by Williams (54). A soil sample is frozen from the top down with a column of water feeding the bottom of the sample. If the column is closed, as shown in figure 9, water is prevented from entering the specimen and the potential developed at the frost line is represented by the hydrostatic pressure (suction) at the point of measurement.

Aston University

Illustration removed for copyright restrictions

Figure 9 – Schematic Representation of Williams's Apparatus (54)

Using this type of apparatus it has been suggested (54) that the magnitude of the potential developed is dependent on soil type. Developing this work an apparatus has been devised (54) to produce the temperature gradients likely to occur in nature, with the aim of assessing potentials which are likely to be developed. This was achieved by the use of a pressure transducer, instead of a manometer, for measuring the pressures in the water with controlled cooling achieved by a thermoelectric device. A detailed account of the operating characteristics of the pressure transducer arrangement and thermoelectric cooling system is given by Williams (54). Results obtained using this apparatus indicate that the fall in the water pressure at the frost line is a function of the temperature gradients within the frozen layer and, to a lesser extent, of the hydraulic conductivity of the frozen soil.

An alternative method for assessing suction in freezing soils has also been developed by Williams (36). The negative pore pressures accompanying ice lens growth, result in an equal positive effective stress (stress acting across grain to grain contacts). In compressible soils the increase in effective stress causes consolidation, Williams considered a method of relating the consolidation in the unfrozen soil, resulting from effective stress increases, to the negative pore pressures developed in the soil. The experimental apparatus used by Williams in this work is depicted in figure 10 and has been described in detail elsewhere (36). It is designed so that ice lenses form at atmospheric pressure, separated from the unfrozen soil by rubber membranes. In this way consolidation in the unfrozen soil can be measured.

Aston University

Illustration removed for copyright restrictions

Figure 10 – Section Through Freezing Apparatus (Williams) (36).

The negative pore pressure (suction), in unconfined samples can be related to temperature by the following equation (48):

$$H = L/Tg \ dT \qquad (17)$$

where:

H = Suction (height of a column of water in cm).
L = Latent heat of freezing of water (3.336×10^9 erg/g).
T = Temperature (°K).
dT = Negative temperature (°C).
g = Acceleration due to gravity (m/s^2).

This equation is compatible with the results obtained by Williams (36) down to the level at which shrinkage is reached. By separating the ice phase from the unfrozen phase the uncertainties with boundary conditions in using this equation are greatly reduced.

An indirect method of determining frost susceptibility in limestones, by evaluating suction characteristics, has been described by Jones and Hurt (55). The suction characteristics (soil moisture content relationships) are determined by an osmotic method. The method works by predicting the frost susceptibility of a soil from critical pore size. Simplifying assumptions in translating effective size to equivalent suction, are avoided by direct use of suction characteristics.

A method using a tensiometer containing ethylene glycol–water solution has been developed (56) which is reported to function at sub–zero temperatures. There may, however, be problems if the tensiometer membrane is not perfectly semi–permeable. The ethylene glycol–water solution may diffuse into the frozen soil, so increasing the osmotic pressure associated with leachable solutes in the unfrozen water adjacent to the tensiometer. Other research (57), however, indicates that ethylene glycol does not diffuse into the soil water of the sandy silts under test.

3.5 Hydraulic Conductivity

In this section, methods of measuring the hydraulic conductivity in unfrozen and frozen soils are reported.

3.5.1 Hydraulic Conductivity in Unfrozen Soils

Saturated flow through a soil is assumed to obey Darcy's law. In figure 11 water is introduced into the cylinder and allowed to flow through it until the soil pores are filled with water and inflow and outflow rates are equal. The velocity of flow is then given by the following equation:

$v = Q/A$ ....(18)

where:

v = Velocity of flow.
Q = Inflow and outflow rates.
A = Cross sectional area of cylinder.

Darcy's experiments showed that:

$v \propto H1-H2$ with L constant and
$v \propto 1/dL$ with H1–H2 constant.

If H1–H2 is then defined as dH:

$v \propto -dH$ and Darcy's law can be stated as:

$v = -k\ dH/dL$ ....(19)

Where k is the constant of proportionality (hydraulic conductivity) and has dimensions of velocity and is a function of the media and the permeating fluid.,

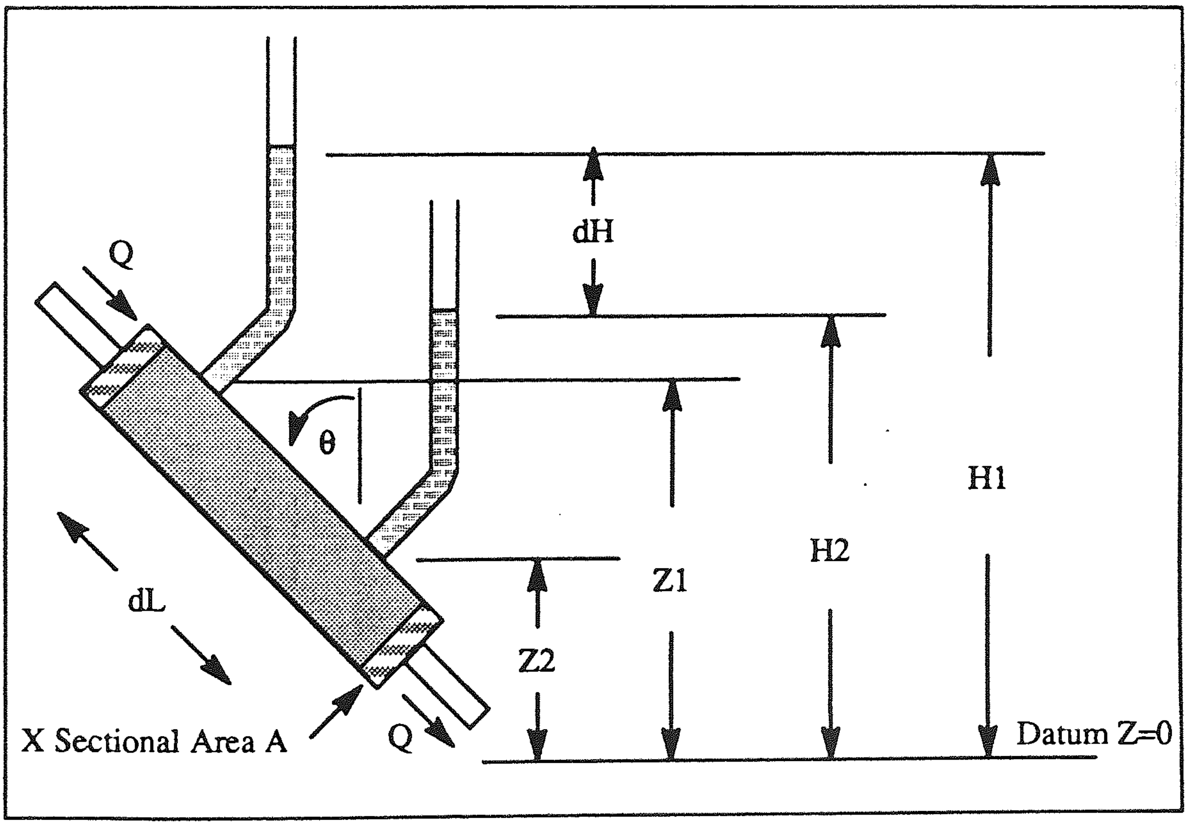

Figure 11 – Constant Head Apparatus for Permeability Determination.

For measurements of the hydraulic conductivity in unsaturated soils, in addition to water flow rates, the water potentials and the potential gradient must be determined. A complete account of the methods of measuring hydraulic conductivities in unsaturated, unfrozen soils is given by Thompson (58) and so only those methods of greatest interest in the context of this investigation will be considered.

The first direct measurement of hydraulic conductivity in unsaturated soil was made by Richards (59) in 1931. The experimental set up is shown in figure 12 and involves a soil column at reduced potential. Suction is applied to water held in porous plates, which controls the potential of the water in the soil. When equal inflow and outflow rates are achieved the potential gradient due to gravity is measured by two tensiometers a known distance apart. Knowing flow rate, cross sectional area and potential gradient, Darcy's equation can be used to solve for the average potential between two measured points. An improvement to this method was made by Richards and Moore (60) in 1952 through the use of a pressurised soil column to increase the potential at which the conductivity could be measured.

Aston University

Illustration removed for copyright restrictions

Figure 12 – Permeability Apparatus (Richards) (59)

Moore (61) was the first to use steady state evaporation from a soil column for hydraulic conductivity measurement. In this technique, water in a reservoir is allowed to evaporate upward through an enclosed soil column under isothermal conditions. Tensiometers are inserted in the column to measure potential at various positions. When a constant evaporation rate is achieved the soil is sectioned at each tensiometer location to obtain the moisture content. Knowing rate of flow (from rate of evaporation) and potential gradient through the soil column, hydraulic conductivity can be determined for a range of tensiometer readings.

This method has been subsequently adapted by Childs and Collis–George (62) 1950 and Nielsen et al (63) 1960. Childs and Collis–George used a 3m long tilting tube, potential gradients were controlled by the inclination of the tube and the length of the tube ensured that zones of uniform water content and suction were set up. Evaporation rates were increased (63) by circulating air over the specimens and by applying a reduced potential to the water reservoir, drier equilibrium conditions were achieved. To accelerate data collection a non–steady state evaporating column is used (64). Soil moisture content/ potential relationships are determined for the wetting or drying cycle to supply input for equation 20.

$$dQ = A \, . \, \phi \, . \, dz/z \ldots\ldots (20)$$

where

dQ = Volume of water.
A = Soil sample cross–sectional area.
z = Height.
ϕ = Volume of water / unit volume of dry soil.

The potential of the soil water determines the value of ϕ which can be used, in equation 20, to give the volume of water in the soil at that potential. By plotting the values for volume of water against time, the rate of accumulation or depletion of water from that point is given by the slope of the graph and, knowing the inflow and outflow from the tube of soil, the flow rates at the tensiometer locations can be found. Having obtained flow rates Darcy's equation can be solved for a range of soil suctions.

Techniques involving nuclear radiation have been available since 1961 for evaluating water contents in unsaturated soils and this data can be employed for hydraulic conductivity determinations. The gamma–ray adsorption technique (65) uses a gamma–ray emitting radioactive source to scan the soil sample, the rate of absoption being dependant on matrix material and water content, the proportion of gamma–rays passing through the soil is detected and the results analysed to determine water contents. The method is sensitive to soil density and to small errors in the gamma–ray trajectory distances between the emitter and detector. The accuracy is improved by collimating the radiation, through shielding, to a narrow beam to give good resolution at the scanning position. A further more detailed description of gamma–ray adsorption techniques is given later in the chapter. The neutron scattering method (66) estimates the moisture content of the soil by measurement of the hydrogen content, the water being the major source of hydrogen in soil. This technique which, unlike that of the gamma–ray, is specific to water is discussed in some detail later in this chapter.

Measurements of hydraulic conductivity have also been made using pressure plate outflow data, with the system initially being designed in 1956 (67), and successive modifications being made between 1958 and 1965 (68–70). A pressurised chamber is used to house a soil specimen of known dimensions. One surface is held in contact with water , at atmospheric pressure, via a porous stone. Equilibrium between the soil water potential and the surrounding air pressure is established before a small increment of pressure is applied causing water to flow from the soil through the porous disc to the water at atmospheric pressure. Flow continues until the new soil water potential is restored to an equilibrium condition with the air pressure. The soil matrix and the impedance to flow of the porous stone determine the rates and total amounts of outflow.

Indirect estimates of hydraulic conductivity in unsaturated soil fall into two main groups, those involving the probability of pore to pore contact and based on statistical theory and those involving the use of power functions. A full account of these methods, which are quick, reproducible but of dubious accuracy, is given by Thompson (58).

3.5.2 Hydraulic Conductivity in Frozen Soils

The water within the frozen fringe, the zone between the 0 °C isotherm and the ice lens, exits at reduced potentials thus creating potential differences between points within the frozen fringe. These potential differences cause water to flow towards the freezing front, the rate of water flow being determined by the magnitude of the potential gradient and the hydraulic conductivity of the soil in the frozen fringe. A knowledge of the hydraulic conductivity, together with the potentials and temperatures, is therefore essential for the successful modelling of the behaviour of soils under freezing conditions.

For hydraulic conductivity determinations within frozen soils there are problems which, under normal conditions, prevent direct measurement. In a standard permeameter, used for unfrozen soils, water enters and leaves the specimen via inlet and outlet reservoirs. If such a permeameter were to be used with frozen soils it would need to be maintained below 0 °C. This would result in the inlet and outlet reservoirs freezing and, despite capillary and adsorbed water around the soil particles, this ice would block the flow. With such difficulties it is clear that specific equipment must be developed to determine the hydraulic conductivity of frozen soils, and this section describes the various direct and indirect methods that have been employed, under both laboratory and field conditions.

The permeameter cells developed independently by both Miller (71) and Burt (46) are the most commonly cited direct methods for determining the hydraulic conductivity of frozen soils. The other techniques fall broadly into the category of indirect methods but can be subdivided into:

a) Methods involving determinations on frozen soils and
b) Methods involving determinations on unfrozen unsaturated soils for comparison with frozen soils.

3.5.2.1 "Ice Sandwich" Permeameter

Miller (71) developed a constant volume permeameter to determine the apparent hydraulic conductivity of ice in a central chamber, sandwiched between end chambers, containing pure supercooled water. Using this permeameter Miller proved that flow is possible through a frozen porous medium even when ice lenses exist. The explanation for the mechanism of flow is that water moves through the porous medium to the ice lens where it freezes, the heat liberated causes a thawing on the other side of the lens and the resultant effect is of transport of water across the lens. This process of fusion, achieved by temporary thawing into the frozen mass, is termed regelation.

Alternative explanations have been suggested (71) such as, flow along grain boundaries in polycrystalline ice or leakage between the ice and the side wall of the chamber. By inserting a thin, impermeable foil barrier into the ice, Miller demonstrated (71) that the flow rate was virtually independent of the area of the foil, so disproving that flow through the ice was via the grain boundaries. In order to determine the effect of peripheral leakage on the overall flow determinations the rig was operated with two alternative central chambers, one having a diameter of 16mm and the other having a diameter of 32mm. Doubling the diameter should have doubled the flow if peripheral leakage was the cause and quadrupled the flow if the transport had involved regelation or grain boundary flow. Experiments carried out using this rig demonstrated that flow in the 32mm diameter chamber was exactly four times that for the 16mm diameter chamber, proving conclusively that flow through the ice must be attributed to regelation.

Sahin (72) modified the experiment by replacing the ice with frozen soil. The frozen soil being separated from the end chambers, containing supercooled water, by porous phase barriers that mechanically exclude ice but transmit liquid water. The permeameter (73) is shown in figure 13. De–aired, de–ionised water is delivered to one side of the permeameter and outflow from the other side is directed into a capillary, the hydraulic gradient being imposed by a temperature gradient across the sample. The capillary is finely divided and read with a travelling telescope. Millipore GSWP (0.1μm) filters are used as phase barriers to exclude ice from the supercooled water as dialysis membranes have too high an impedance for use in the ice free range. Experiments using the permeameter (73) have centred on one material (4–8μm silt fraction) and have demonstrated that, with precise and stable control of temperature and long equilibriation times, the permeameter was effective in the limited temperature range 0 to –0.35 °C. Within this range water fluxes increased in direct proportion to the temperature imposed hydraulic gradient according to Darcy's Law (73).

Later work with the permeameter (74) examined the hydraulic conductivity of eight frozen soils in the temperature range 0 °C to –0.35 °C. The eight soils were made up of four natural silts (Chena, NWA, Manchester and Calgary) a 4–8 μm silt fraction separated from the Manchester silt and samples of Illite, Kaolinite and Zeolite. During setting up, the apparatus was held in the dilatometer mode for each freezing increment and equilibriation period, subsequently being switched to permeameter mode to allow measurements of the hydraulic conductivity. With the sample at slightly below 0 °C, freezing was initiated by the introduction of a frozen tube of water through a port in the side of the sample chamber. For measurements of the volume of water emerging from unit area of sample per unit of time estimates were made of the hydraulic conductivity.

Aston University

Illustration removed for copyright restrictions

Figure 13 – Ice Sandwich Permeameter (Miller) (71)

Generally the eight specimens gave the expected results. However, important discrepancies were observed in the hydraulic conductivity values at the time of ice intrusion into the pore system which casts serious doubts over the reliability of the ice seeding technique. Successive measurements of hydraulic conductivity following freeze thaw cycling showed increased hydraulic conductivity for all eight specimens. This would appear logical, since pores penetrated by ice would be expected to enlarge so that upon thawing and re–freezing, the hydraulic conductivity would increase.

3.5.2.2 Osmotic Permeameter

In the Osmotic Permeameter developed by Burt (46) a sample of frozen, de–aired soil is placed between two reservoirs of lactose and water solution. The sample and reservoirs are maintained at sub–zero temperatures by immersion in a bath of ice and lactose solution. There is no temperature gradient across the sample and an hydraulic gradient is established by applying pressure to one reservoir to induce flow. The discharge from the sample is then recorded by the meniscus movement of water in a capillary attached to the outlet reservoir. The experimental scheme is shown in figure 14.

Aston University

Illustration removed for copyright restrictions

Figure 14 – Osmotic Apparatus (Burt) (46)

The unfrozen water in the frozen soil possesses a negative pore water pressure and consequently if pure water were to be used in the reservoirs, even without freezing, water would tend to be drawn into the soil. Using lactose overcomes this problem by equalising the potentials in the reservoirs and soil. To limit the movement of lactose molecules into the sample, by diffusion or transport in the flowing water, a dialysis membrane is fitted to each end of the sample. Lactose molecules which pass through the membrane effect the equilibrium between the soil water potential and that of the lactose solution. However the effect of this on the overall hydraulic conductivity of the sample has been shown (75) to be minimal. This was demonstrated in parallel experiments where the lactose was replaced with polyethylene glycol which has a greater molecular weight, and so was unable to pass through the dialysis membrane. Burt and Williams (76) continued to use lactose over polyethylene glycol as lactose has low viscosity and its use enables the freezing point to be depressed to –1 °C. For experiments requiring lower temperatures more soluble chemicals, such as sodium chloride, have to be used. The disadvantage of using sodium chloride was that molecules rapidly passed through the membrane and soil which resulted in total thawing of the sample after only 36hours (76).

To comply with Darcy's Law, a constant head should produce a constant flow velocity over time. However with some clays it was found (76) that when a constant head was maintained for several hours a substantial fall in flow velocity occurred. Another problem was encountered when large heads were applied to produce measurable flow in the clay soils. As the water was effectively being forced into the frozen soil, by the applied hydraulic gradient, some thawing was experienced at the inflow end of the sample. This thawing developed slowly and only became noticable after about two days of testing. Burt and Williams (76) reported, however, that after four days of testing the thawing effected up to a third of the sample. Despite these problems by applying the technique to a variety of soils Burt and Williams (76) were able to make some useful conclusions. Notably that hydraulic conductivity in frozen soils decreases with decreasing temperature and that the most frost susceptible soils, the silts and clays, still achieve relatively high conductivities well below 0 °C. They also noted, as did Miller, that the presence of ice lenses did not prevent water flow in the soils.

3.5.2.3 Other Permeameter Cells

Following from the formative work of Burt, the method was further developed by Perfect and Williams (77). Instead of applying an air pressure, a temperature gradient was used to induce flow through the sample, the flow being in the direction of decreasing temperature. Before a temperature gradient could be established the Gibbs free energies of the water in the reservoirs and in the soil sample were equalised and, as in Burt's experiments, this was achieved by the use of lactose. Uni–axial heat flow was achieved by heavily insulating the system, since radial heat flow would result in non–uniform temperature and moisture distributions accross the sample.

The reservoir temperatures, which determined the temperature gradient across the sample, were set using Peltier modules, controlled by a thermoelectric cooling control system, which were able to maintain the required sub–zero temperatures to within + or – 0.02 °C. Concentrations of lactose in the reservoirs were dependent on the relative temperatures but in the recorded tests (77) a concentration giving a freezing point depression corresponding to the cold end temperature was used in both reservoirs. The inflow and outflow for the reservoirs was measured by timing the movement of the meniscii in the attached capillary tubes. The apparatus is shown in figure 15.

Results from the recorded experiments have demonstrated that the movement of unfrozen water within soils, at sub–zero temperatures with applied temperature gradients, can be described by application of Darcy's Law. Perfect and Williams (77) performed some experiments using supercooled water in the reservoirs and obtained results which indicated a flow from the cold reservoir through the sample to the warm reservoir. They attributed this apparent reversal of flow by suggesting that the supercooled water was not in thermodynamic equilibrium with the unfrozen soil water. The largest thermal imbalance was at the cold end of the sample so causing water to move from the cold reservoir into the sample with flow into the warm reservoir occurring as a direct result of the increase in pore water pressure.

Aston University

Illustration removed for copyright restrictions

Figure 15 – Permeameter Apparatus (Perfect & Williams) (77)

Through the design of a new permeameter cell, Aguirre–Puente et al (78) avoided the need for lactose or other freezing point depressant. The apparatus is shown in figure 16. The central portion of the test sample was kept at the required sub–zero temperature and the end portions maintained at the required positive temperature by the use of circulating temperature regulating fluid. Water inflow and outflow for the specimen was via pistons, with porous plates, fitted at the extremities of the specimen tube.

The matrix was compacted in layers into the cell with the moisture content closely controlled. The effective length of the test specimen (the frozen portion) was not pre-determined, but was defined by the two freezing fronts (zero isotherms) formed in the specimen. In experiments using the permeameter, temperature variations have given rise to variations in the quantity of unfrozen water resulting in additional flow. Furthermore, the water inlet/outlet pistons may have developed leakage problems, as water was being forced through the frozen soil via the pistons. This may be of particular importance for the case of low flow rate.

Aston University

Illustration removed for copyright restrictions

Figure 16 – Permeameter Apparatus (Aguirre–Puente) (78)

3.5.2.4 X–Ray Technique

Although some of the indirect techniques have applicability both in the laboratory and in situ, the X–ray technique is only suited to laboratory testing. The X–ray technique has been reported (79) as a method for determining the water flow in the unfrozen and frozen parts of a freezing saturated soil, subject to an overburden pressure. The test specimen is saturated with pure water. To determine the temperature profile, copper–constanton thermocouples are located along the specimen at 10mm intervals and small lead shots (2mm diameter) are imbedded in the sample at intervals of 5mm in two vertical rows, on a single plane. For positional reference, additional lead shots are located on the outside of the specimen. The sample is then consolidated under the desired applied load and the end plates held at constant temperatures, cooling the specimen from the bottom upward. A drainage tube from the upper end plate is connected to a volume change indicator to measure water inflow and outflow from the soil sample. Data from the thermocouples, volume change indicator and a dial gauge, located at the top of the sample, are collected periodically by a digital data aquisition system.

The specimen and associated rig were located between the X–ray source and an X–ray film recorder. In this way the positions of the lead shot in the specimen were monitored, throughout the test, and were shown by small circular images on the film. The recorded images were analysed to accurately determine the relative positions of the embedded lead shot throughout a 502 hour freezing test. This information was combined with the other data to determine the water flow rates in the frozen and unfrozen sections of the specimen. Of particular interest to this work was the appearance , on the X–ray films, of the main large ice lens and subsequent smaller ice lenses. The quality of the images was suprisingly good indicating a coincidental contrast in X–ray diffraction between the water, as ice, and the soil matrix.

3.5.2.5 The Neutron Probe

The neutron probe (80) is a portable device for the determination of water content, in any physical state, insitu. The probe incorporates a high energy neutron emitting isotope, most commonly Amercium Beryllium (Am–Be), and a neutron detector. High energy neutrons (energy of a million electron volts (eV) or more) are slowed by elastic collision with the nuclei of atoms, the energy lost per collision being greatest with atoms of low atomic weight.

In soils the only element of low atomic weight, present in large quantities, is the hydrogen in water. Consequently when the probe is activated at the required depth in the soil, the size of the cloud of slow neutrons (energy of 100 eV) remaining after collisions within the soil is directly related to the water content of the soil at that depth. Within the neutron probe the number of slow neutrons reaching the detector, per unit time over a known soil volume, is recorded and the soil moisture contents are determined by comparison with a calibration curve.

For insitu measurements of water content, the probe is located within an access tube, tamped into a previously drilled and slightly undersized hole to ensure a tight fit. The neutron probe is a useful tool for determining water contents in the field, the readings being taken automatically so enabling rapidly changing water contents to be recorded. There are, however, precautions to be taken for accurate determinations. The sphere of influence of the probe is critical and can result in errors at low penetration depths, if not accurately set. Account has also to be taken of the physical and chemical properties of the soil as these will affect the water content reading as different elements attenuate neutrons to different extents, and so individual calibration curves will be needed for different soils.

Neutrons are not readily collimated and as the counting technique determines the scattered rather than unscattered neutrons, the probe should be used with a large bulk of soil (resolution over 400 mm), to minimise errors.

3.5.2.6 Gamma–ray Attenuation

Gurr (65) put forward a method for measuring water contents in unsaturated columns of soil using gamma–rays. The soil sample was scanned with gamma–rays from a 25mc Cesium (Cs) source, and the proportion of radiation reaching a scintillation counter detector was recorded. As the method is sensitive to small errors in the gamma–ray trajectory distances, between emitter and detector, a lead collimator with a 4.8mm diameter hole was used to give a narrow beam. The degree of scattering and adsorption of gamma–rays was dependent on the density of matter in the path. Changes in the wet density of the matrix could therefore be recorded and moisture contents determined from the changes.

Hoekska (81) used a single gamma–ray technique to evaluate moisture transport in a partially frozen soil under a temperature gradient. Samples of Fairbanks silt were compacted into 152.4mm long by 112mm diameter perspex cylinders, at various initial water contents. Thermistors, located along the length of the cylinders, recorded temperature throughout the tests. The samples were sealed at one end with a perspex lid and cooled from the other end by a brass cooling plate, which was fed with circulating glycol coolant from a constant temperature bath. The density, porosity and water content of the soil were recorded throughout the test.

In this study (81) it was assumed that density remained unchanged, which was acceptable if no ice lensing occurred. During the test the cylinder was supported in a horizontal position, located between the gamma radiation source and the detector. In this way the sample could be mechanically moved along the supporting carriage which enabled the attenuation of gamma radiation to be determined along the sample, throughout the test. The source was 20mc Cs^{137} and the beam was collimated by a 2mm x 20mm slit in the lead shielding. The gamma rays passing through the sample were detected, 300mm from the source, by a scintillation counter connected to a pulse height analyser which could be linked to an automatic scaler and printer.

The attenuation of gamma rays by a moist soil column was determined (81) using:

$$I = Io \exp -(u_s \rho_s d + u_w \rho_w d) \qquad (21)$$

where:

I = Intensity of beam after passage through the soil.
Io = Intensity of beam without passage through the soil.
u_s = Mass adsorption coefficient of the soil (cm^2/g).
ρ_s = Density of the soil (g/cm^3).
u_w = Mass adsorption coefficient of water (cm^2/g).
ρ_w = Volumetric water content (g/cm^3).
d = Path length of gamma rays through the soil (cm).

The pulse height analyser enabled the mono–energetic gamma–rays of Cs^{137} to be rejected, a requirement for the above relationship to be valid. It was assumed that us, ρs and d were unaltered throughout the test, the volumetric water content can then be determined (79) from:

$$\ln Io - \ln It = u_w (\rho_w o - \rho_w t) \ldots\ldots\ldots\ldots (22)$$

where:

$\rho_w o$ = Water content at time 0 (g/cm^3).
$\rho_w t$ = Water content at time t (g/cm^3).

Counting times of ten minutes were selected for each measurement of gamma ray attenuation to give a large count and so reduce errors. It was found (81) that the technique failed at high water contents which correspond to the formation of ice lenses with the subsequent disruption of the soil matrix. The technique was limited to non ice lensed soils where moisture flow could be determined from the local change in water content at various times throughout the test.

A dual energy gamma scanning system has been used (82) to measure the location of the growing ice lens relative to the freezing front, in columns of New Hampshire Silt under various overburden pressures and temperature gradients. The information gained was used to evaluate modes of water redistribution in freezing soils.

The sample chamber was a perspex cylinder of 37.3mm internal diameter. Thermoelectric temperature control plates, at either end of the chamber, controlled the temperature gradient across the sample. Porous stainless steel plates made the thermal contact between the control plates and the sample. The expansion of the soil, due to frost heave, was monitored by the use of a copper piston which contained the upper cooling unit. Connected to the porous plates were water access tubes, the top tube feeding the sample with free water whilst freezing was initiated in the base. Thermocouples were installed at 10mm intervals to record the temperature gradient in the soil. Two gamma–ray sources were used, 300mc Am^{241} (Amercium) and 200mc Cs^{137}, each being aligned and collimated to give a single beam of 25mm x 3mm. The intensity of radiation was measured with a single scintillation counter and photomultiplier, the signal was then split into two and each half was viewed with the aid of pulse height analysis, to determine bulk density and moisture content for each scan location.

To create unidirectional heat flow conditions, the sample was encased in 25mm thick polystyrene and installed in a perspex air bath maintained between 0 °C and 1 °C. The reported values for the temperature profiles (82) indicated that the approach had been successful with radial heat flow reduced to a negligible amount. The results of the tests were as expected, showing that rates of water intake and heave increase with increasing temperature gradient and decreasing overburden.

The dual gamma–ray scanning technique gave the position of the ice lens and the location behind the 0 °C isotherm was determined from temperature profiles. The results indicated that the ice lens forms some 2–4mm behind the freezing front, in accordance with the mechanism of secondary frost heave. The particular water and heat flow condition assumed steady state behaviour and therefore it was considered acceptable, after 10 to 12 hours, to apply Darcy's Law to describe the water flow in the unfrozen soil and the frozen soil, up to the ice lens. An equation involving Darcy's Law and the Clapeyron equation was subsequently used to calculate the hydraulic conductivities of the frozen fringe.

Similar dual energy gamma-ray techniques have been developed (83–84) to accurately determine soil moisture movements and bulk densities simultaneously in soils during freezing. It has been reported (83–84) that the accuracy of the dual gamma–ray system depends mainly on the attenuation coefficients of the matter through which the beams pass. In order therefore, to minimise errors, considerable effort must be put into accurate determinations of the attenuation coefficients for the soil, water and perspex container.

Initial experiments on unfrozen soils, carried out to check the system, gave good agreement between the results obtained with gamma ray attenuation and gravimetric methods for bulk density and water content. In subsequent freezing tests, as expected, density increases were coupled with reductions in moisture content indicating consolidation in the unfrozen layer. The results showed that the frozen and unfrozen regions of the soil matrix were marked by an abrupt change in moisture content profile. Various experiments were conducted (83–84) to produce results for different rates of freezing front advance. It was shown that the slower the advance of the freezing front the greater was the increase in water content in the freezing soil.

The gamma–ray attenuation technique can be applied in the field (80), to obtain moisture content values in local soil thicknesses of up to 20mm, by determining changes in wet density. The technique is comparable to the neutron probe but with the added advantage of allowing determinations to be made over small distances. The technique however requires that the soil be of relatively constant specific gravity,which is seldom the case in field situations.

3.5.2.7 Pulsed Nuclear Magnetic Resonance

This technique, although little used for field measurements, has been used since 1962 (85) as a laboratory based technique for determining the phase composition of soils. With the soil matrix located in two magnetic fields, one fixed and one variable, an increased absorption of energy is noticed at a specific frequency of the varying field. This frequency is referred to as the nuclear magnetic resonance (NMR) and can be directly related to water content in the soil (80).

In a preliminary study (86) pulsed NMR has been used to determine unfrozen water contents in frozen soils. In the reported experiments sixteen frozen samples of each of three representative soil types were analysed. All the experiments took place in an environmental chamber where temperatures were accurately controlled down to –30 °C, this being necessary as the NMR probe is sensitive to temperature changes. It is assumed that the first pulse amplitude is directly proportional to the amount of unfrozen water in the matrix, however there is a signal reduction associated with decreasing temperature. This was accounted for (86) by multiplying the raw signal at each temperature by a normalising factor to obtain a reading which could be compared with one taken at room temperature.

The results obtained (86) showed that the ice content had an effect on the unfrozen water contents. From this it was concluded (86) that the unfrozen water content can be separated into water associated with the soil minerals and water associated with the ice. One problem with the experimental work was that the first pulse amplitude signal for the soil ice was infact made up from unfrozen water at the ice / water interface and protons within the ice crystals, in uncertain proportions.

Researchers report good correlation between unfrozen water contents across a range of sub–zero temperatures (87) but the presence of ferromagnetic minerals in soils can cause difficulties in the measurement of the unfrozen water content with NMR (88). A demagnetising procedure has been introduced to counter the problem (89) and further recent advances (90) in the field have increased the speed of measurement of unfrozen water content as a function of temperature in unconfined samples.

3.5.2.8 Time Domain Reflectometry

This is an electromagnetic technique which is reported as being rapid and reliable (91). Time–domain reflectometery is used to measure the dialectric constant of a soil, the dialectric constant being a measure of the ability of the soil to store electrical potential energy under the influence of an electrical field, relative to that of air. In the frequency range 1 MHz to 1 GHz the real part of the complex dialectric constant is not strongly frequency dependent but is highly sensitive to volumetric water content and weakly sensitive to soil type and density (92). Through tests (92) on varying soils an empirical curve which relates the apparent dialectric constant to water content has been produced and which accurately represents the findings from all tests.

A TDR source generates a pulse which is transmitted along transmission lines of known length. The travel time (t) of the pulse through the soil is then a function of the apparent dialectric constant (Ka) and the line length (l) and the relationship can be expressed in the form :

$$Ka = (ct / l) \ldots\ldots\ldots\ldots (23)$$

where c is the velocity of an electromagnetic wave in free space (3×10^8 m/s).

The technique has been applied (91–93) to the determination of unfrozen water contents in frozen soils, and invokes the use of an empirical formula (92) to convert dialectric values to values for unfrozen water contents. The dialectric constant for ice is 3.2 and for dry soils varies between 2.5 and 3.5, for water the value is approximately 80 which is markedly different to soil or ice. TDR has been used to determine the unfrozen water contents in frozen soils and for estimating the hydraulic conductivity of frozen ground (91,93). It shows great promise for both laboratory and field applications (94) which is a flexibility afforded by few other methods. The main design considerations for laboratory or field application concern the cross–sectional geometry and line length of the transmission lines. There are upper and lower limits to the spacing between transmission lines to ensure that a representative volume of soil is sampled and line length must be carefully determined to give an easily measurable trace.

Both coaxial and parallel transmission lines have been used (91,93) to test saturated soil samples and results achieved have been in general agreement with previous determinations on freezing soils. To calibrate the TDR technique for the measurement of unfrozen water content the relationship between the dielectric constant (Ka) and the unfrozen water content must be established. Measurements of Ka are made for ice / water mixtures in coaxial tubes and a modified dialatometer is used to evaluate the volume expansion of the soil due to freezing to determine the unfrozen water content.

The results were in close agreement with the previously referenced empirical curve for frozen soils (92) and demonstrate the lack of variation of Ka with varying ice content. Subsequent tests have been performed to develop the freezing characteristic curves which relate the unfrozen water content to temperature.

TDR has been used in the field (95) to monitor unfrozen water content continuously and to determine the snowmelt infiltration into seasonally frozen soils. Although the results compared favourably with those from dual gamma ray attenuation studies, problems were encountered with the TDR probes. When installed vertically to obtain a water profile with depth, water flowing along the probes influenced the wetting and drying cycles of the soil and the high thermal conductivity of the probes affected the freezing and thawing cycles. It has been concluded (95) that for the technique to be used for continuous measurement of unfrozen water content in the field the probes must be installed horizontally.

In comparisons between TDR and NMR methods it has been found (96) that best data correlations are obtained with an average dialectric constant for water somewhat less than that for bulk water.

3.5.2.9 Dilatometer Method

An early attempt to determine the water content of a freezing soil involved the use of a Dilatometer (97). Underlying this approach was the conception that: "If the amount of expansion, upon freezing, of a known quantity of water is known then the water content of a freezing soil can be determined by the magnitude of the expansion."

This relies on the misconception that the expansion of soil under freezing conditions is due to the 9% volume expansion of water upon freezing. It is now agreed that the expansion of the soil is due to a complex freezing process involving the development of ice lenses.

3.5.2.10 Gravimetric Determinations

Information on water migration in frozen soil samples has been obtained (87,98) by slicing the matrix and performing a gravimetric determination of water content on each section.

In one such investigation (98) a sample was immersed in liquid Nitrogen in an attempt to obtain a uniform homogeneous frozen sample. The sample was then trimmed, encased in a rubber membrane and inserted in a frost cell where a constant temperature gradient was applied. At the completion of each closed test the frozen sample was cut into slices and water content determinations performed. The technique has also been applied to an open system (98) in which a pre–made ice lens was inserted into the soil matrix. The experiments demonstrated the occurrence of moisture migration due to temperature gradients in frozen soil and indicated that the rate of migration was dependent on the apparent permeability of the frozen soil.

As an alternative approach (87) closed soil columns, initially at uniform total water content, were subjected to a nearly linear temperature gradient and at various times throughout the test these columns were sectioned to gravimetrically determine water contents, as a function of position. Temperature, water and pressure gradients were carefully controlled and separated so that only one type of gradient acted on the free water in a given experiment.

Subsequent analyses can lead to the determination of the hydraulic conductivities. For the case where temperature gradient acts on the free water, this involves calculating the water fluxes across the boundaries of adjacent sections, with fluxes towards the cold end being considered positive. Individual mass balances are calculated for each section together with the average water content for all the sections.

The flux from one section to another is then given by:

$f_i = f_{i-1} + (w_i - w_{ave})$..........(24)

where:

f_i = Flux in section i
f_{i-1} = Flux in section i–1
w_i = Water content of section i
w_{ave} = Average water content

The form of the Clausius–Clapeyron equation used is:

$H = L / Tg \; dT$..........(17)

Hence, the effective pressure gradient can be calculated from the temperature gradient. Hydraulic conductivities are then determined by employing a form of Darcy's Law:

$Q = -k \; A \; dH/dL$..........(25)

where:

Q = Flux of water (cm^3/day)
A = Cross sectional area available for flow (cm^2)
dH/dL = Pressure head per unit length of the sample (see figure 12)
k = Hydraulic conductivity (cm/day)

3.5.2.11 Isothermal Calorimetery

Isothermal calorimetery is used to calculate the proportion of ice and unfrozen water in a soil in order that phase composition curves (unfrozen water content versus temperature) can be obtained. A calorimeter permits the measurement of the amount of heat added to or removed from a soil sample when the temperature is changed by a given amount.

The technique has been used (99) to establish an equation for predicting the apparent specific heat capacity and the cumulative heat adsorption versus temperature curves for frozen soils from the water–ice phase composition. The data obtained has been represented by a simple power equation:

$$w_u = \alpha\ T\beta \qquad (26)$$

where:

w_u = Unfrozen water content
T = Freezing point depression (°C)
α & β = Parameters characteristic of the soil.

The values for α and β are obtained by a least squares regression of experimentally measured values of T and Wu and regression against specific surface area (S) to give:

$$\ln w_u = a + b \ln S + cS^d \ln T \qquad (27)$$

where a,b,c and d are constants.

In frozen soils phase change is usually a gradual occurrence and so the term apparent specific heat capacity has been used instead of specific heat capacity, the specific heat capacity being the quantity of heat required to raise the temperature of a substance 1 °C, expressed per unit weight. The apparent specific heat capacity is calculated (99) as the sum of the heat capacities corresponding to the soil matrix, unfrozen water and ice phase plus a term which accounts for the latent heat involved in changing the proportion of unfrozen water to ice:

$$C_a = C_s + C_i(w_w - w_u) + C_u w_u + 1/dT \int_{T1}^{T2} L\ (dw_u/dT)\ dT \qquad (28)$$

where:

C_a = Apparent specific heat capacity (cal/°C/weight of soil).
C_s = Specific heat capacity of soil matrix.
C_i = Specific heat capacity of ice.
C_u = Specific heat capacity of unfrozen water.
w_w = Total water content.
w_u = Unfrozen water content.
T = Temperature (°C).
L = Latent heat of fusion of ice.

The term $\int_{T1}^{T2} L(dw_u/dT)\,dT$ is evaluated using equation (27).

Work using this technique (100) for determining specific heats and unfrozen water contents in frozen soils has facilitated various observations.

The calorific observations differ slightly from the thermal properties of the soil under natural conditions, particularly where overburden is thick. The specific heats during freezing are often increased, apparently by the migration of water and the associated ice lens growth. Consequently the method is best suited to near surface conditions with consideration made to overburden pressures and moisture supply.

Another application of the technique (86) has been to establish the unfrozen water contents which can then be linked with liquid limit determinations. The aim of this work was to correlate unfrozen water contents of frozen soils with simpler more widely used soil indices, in an effort to make water–ice phase composition information more widely available.

The accuracy of the results is effected by soil composition. For example, soluble salts effect the amount of unfrozen water without appreciably effecting the the liquid limit determinations.

3.5.2.12 Comparison of Properties of Unfrozen, Unsaturated Soils and Frozen Soils.

An analogy between the mechanisms of water transport in partially frozen soils and those in unsaturated soils has been presented (101). The storage and transmission properties of frozen and partially frozen soils were assumed to be directly analogous to those of unfrozen soil at a similar energy state, represented by the soil water pressure head. From a phenomenological point of view a numerical model, incorporating a Darcian approach, was used to examine freezing affected soil water redistribution and infiltration to the frozen soil. Unfortunately a qualitative comparison between simulated and observed responses has not been given, due to the unavailability of reliable data on physical, thermal and hydraulic transmission properties of partially frozen soils.

A similar analogy (102) between water transport in a frozen porous medium, under isothermal conditions, and water transport in unfrozen soil, is claimed to be accurate for volumetric water contents of 10% or less. The experimental procedure involved the use of two plastic pipettes, one containing a uniformly dry sample and one containing a uniformly wet sample. The tubes were held at −1 °C and connected. After a specified time the connected pipette was removed, sectioned into 64 equal segments and the dry density and water content of each section determined gravimetrically.

CHAPTER 4 NUCLEAR TECHNIQUES

4.1 Radioisotopes

Radioisotopes were considered for use in determining mass transport of water in freezing soils. It was intended that they should be used to label water in a sample during the freezing process and by detecting the emitted radiation, the water movements could be monitored. This method is used frequently and to great effect in the medical profession. After an extensive literature search one isotope, tritium (H), was considered suitable for the work. The reasons for this are many, but in essence a labelling compound for use in frost heave experiments has to:

(a) be unreactive with the soil matrix or water,
(b) emit radiation of a measurable quantity,
(c) have a realistic half life (the time taken for half the atoms in radioactive matter to decay), i.e. not too long so that disposal of waste material is a problem and not too short so that measurement of radiation is a problem,
(d) not be adsorbed into the soil matrix,
(e) be cheap and readily available.

Tritium is an isotope of hydrogen which occurs naturally in rain water and, in a more concentrated form, is available from radiochemical firms as tritiated water ($H^1H^3O^{16}$) produced as a by–product in nuclear reactors. Tritium has a half life of 12.36 years and is a Beta particle emitter. Concentrations of tritium are measured in tritium units (TU) (1 TU is a concentration of one atom of tritium per 10^{18} atoms of Protium). As tritium is an isotope of hydrogen it does not react with the soil matrix or water. The other element in water, oxygen, would be unusable in its radioactive form as it has a half life of 5.5 seconds. Tritium was first discovered in atmospheric hydrogen in 1950 (103) and in surface water in 1951 (104).

Approximately 97% of the tritium deposited on the land surface occurred during the years 1961 to 1965 (105) due to nuclear weapon testing. The detonation of hydrogen bombs introduced tritium into the atmosphere, as a result tritium content in precipitation in South Africa increased from 20 TU in 1958 to 50 TU in 1963 (106).

As concentrations of tritium increased, in the late fifties and early sixties, its use as a natural tracer in ground water studies became apparent. The presence of tritium in rainfall was used to develop an approximation of the amount retained in the soil and its distribution under insitu conditions (106). The water extracted from the soil was then assayed for tritium using electrolyte concentration and gas counting techniques.

Tritium has also been used to estimate the amount of water moving laterally into an aquifer (107) and to establish the existence of considerable amounts of water in permafrost rocks and in ground ice in zones of annual temperature fluctuations (108). High tritium concentrations were found in wedge ice and golets ice (under 30 years old) but none was found in buried wedge ice and primary ice lenses. Evaluation of tritium concentrations has hence been used to gain information on water transportation in the permafrost ground system.

The usual practice is to detect the emissions with a liquid scintillation counter which entails analysing the specimens after freezing to determine water content distribution. This technique is of little use in this study as the same or better could be achieved by a simple gravimetric water content determination. It was intended, therefore, that emissions be detected during the freezing process using a solid scintillation counter, a photomultiplier and the relevant electronics. The scintillation counter would detect emissions from water at the extremities by travelling up the side of the specimen. Using an initial specified concentration of tritiated water of given volume, readings of Beta emissions at a point in the sample would give information on the water/ice content at that point. Extending this could lead to information on the flows of water and, in particular, to the flows across the frozen fringe and through the film water.

A thorough experimental investigation was not carried out as problems were encountered in detecting the Beta particles. For a reasonable reading (10 counts/second from a 100 mL sample) 1 mc of tritiated water would be required. Such a high concentration would present some problems with disposal of waste. However, the problem, is that the detected Beta particles are emitted from a layer of water 1×10^{-3} mm thick and, if the method of detection previously described was used, the readings, would be of film water wetting the sides of the container.

A possible solution to the problem of detection might be to use a scintillation counter attached to a fibreoptic probe, since this could allow information on detected particles to be transmitted to a photomultiplier. This idea is fairly new and research work on scintillation counters with fibre optic probes is in its infancy, and so it was decided that accurate experimentation with radioisotopes would not be suitable for this particular investigation.

4.2 Thermal Neutron Radiography

Through the consideration of radioisotopes as possible aids to measuring moisture fluxes, it became clear that a variety of applications of nuclear radiation could be considered for such work. Indeed the literature studies indicated several radiographic methods which might be suitable for differentiating water from matric materials.

Some success with radiographs, produced using X–rays, has been achieved (79). The work is reported in Section 3.5.2.4 but, in essence, these investigations (79) demonstrated that the water and ice were clearly discernable from the soil matrix on a series of X–radiographs produced during a freezing experiment.

X–rays are electromagnetic waves of short wavelength (0.01–10nm) which readily penetrate materials containing light elements but are attenuated by heavy elements. Thermal neutrons (neutrons of energy 0.01–0.3eV in thermal equilibrium with their environment) are uncharged, with small magnetic moments, and hence, do not interact with atomic elements in their path, but react only with nuclei. A neutron loses most energy in a head–on, rather than glancing, collision with a nucleus of an atom.

Looking at the kinetic energy of an elastic head on collision:

$$1/2\, m_1 v_1^2 = 1/2\, m_1 v_1'^2 + 1/2\, m_2 v_2'^2 \quad \text{.......(29)}$$

where:

m_1 = mass of neutron
v_1 = initial velocity of neutron
v_1' = velocity of neutron after collision
m_2 = mass of nucleus
v_2' = velocity of nucleus after collision

and from conservation of linear momentum:

$$m_1 v_1 = m_2 v_2' - m_1 v_1' \quad \text{.......(30)}$$

Dividing equation 30 by equation 31 gives:

$$v_1' = v_1 - v_2' \quad \text{.......(31)}$$

and substituting equation 32 into equation 31 gives:

$$v_n' = 2 m_1 v_1 / (m_1 + m_2) \quad \text{.......(32)}$$

Hence, the kinetic energy transfer is given by:

$$K_2'/K_1 = m_2 v_2'^2 / m_1 v_1^2 = 4\, m_1 m_2 / (m_1 + m_2)^2 \quad \text{.......(33)}$$

Hence, when a neutron is in a head–on collision with a proton (hydrogen aton) almost all the energy is lost. This strong dependence of absorption of neutrons on the particular element is contrasted with the smooth variation founded in X–rays, as shown in figure 17.

The soil matrix used in the experiments is calcium–carbonate ($CaCO_3$), the constituent elements of which contrast dramatically in mass absorbtion coefficients for neutrons, with hydrogen in water. The variation in mass absorption coefficients for X–rays, however is slight. Neutron radiography techniques were therefore employed as a method of distinguishing water/ice from the soil.

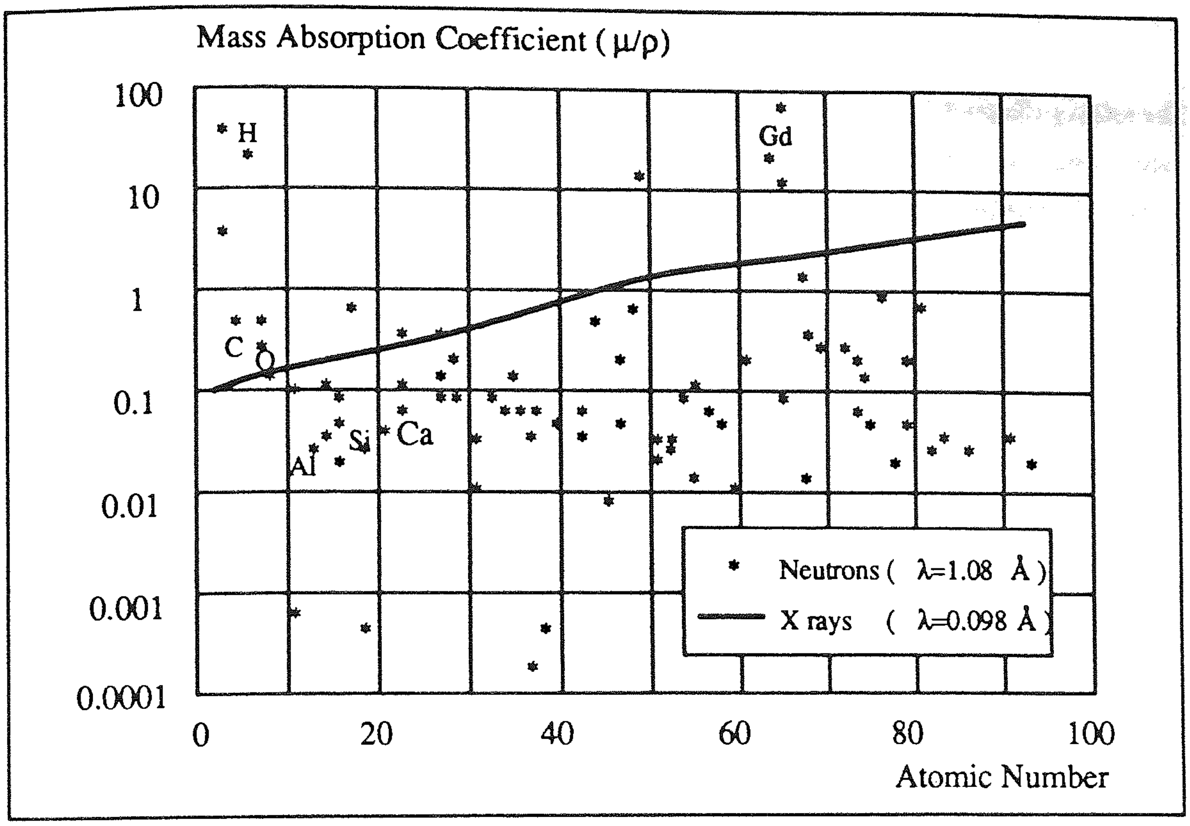

Figure 17 – Mass Absorption Coefficient against Atomic Number.

4.2.1 The Technique

The nucleus of an atom is made up of protons and neutrons, protons are positively charged and of approximately equal mass to neutrons which have no charge (109). High energy neutrons (energy of a million electron volts (eV) or more) are slowed by elastic collisions with the nuclei of atoms. The energy lost per collision is greatest with atoms of low atomic weight (66) and consequently hydrogen, having the lowest atomic weight of the elements, is most effective at slowing neutrons. A widely used practical application of this is the Neutron Probe which employs a neutron scattering and detection technique. The probe is discussed in some detail in Section 3.5.2.5 of Chapter 3.

The neutron radiography technique reported here is a different application of the effect of neutron slowing by collision with hydrogen atoms. A soil matrix which is subject to freezing conditions is irradiated with neutrons. The neutrons which pass through the matrix are detected in order to establish the quantity and location of water in the matrix. The object of the experiment is to obtain a series of radiographs throughout a test which can be subsequently assayed to determine water movements in the matrix. The inclusion of additional instrumentation to record suctions and temperatures would facilitate determinations of the hydraulic conductivity in both the unfrozen and frozen regions of the soil.

4.2.2 Neutron Production

For neutron radiography neutrons are available from three sources, in descending order of source intensity they are Nuclear Reactors, Particle Accelerators and Radioisotopes. This work was carried out at The Universities of Manchester and Liverpool Research Reactor, the basic layout of which is given in figures 18a and 18b, and so this discussion is limited to the radiographic techniques which are relevant to beam production at a nuclear reactor.

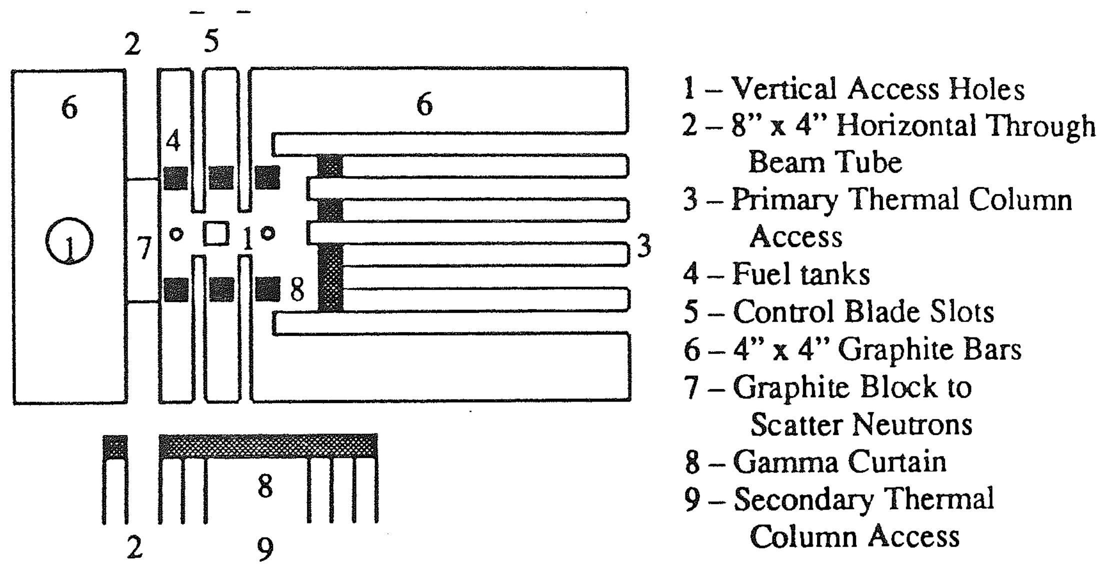

Figure 18a – Plan View of Universities Research Reactor Core.

Neutrons which originate from the primary source of the reactor, the reactor core, are too energetic for radiographic purposes. It is, therefore, necessary to reduce the average energy, using a moderator, to give greater differences between the neutron attenuation coefficients of materials to give a well moderated or thermal neutron flux (110). Neutron flux is measured in neutrons per square centimetre per second ($n\ cm^{-2}\ s^{-1}$) and base flux can range from $10^7\ n\ cm^{-2}\ s^{-1}$ to $5x10^{14}\ n\ cm^{-2}\ s^{-1}$ (110).

To extract a usable beam of neutrons from a reactor, a collimator has to be introduced into the moderator. The collimator is in the form of a long steel tube formed in the concrete shielding and normally of rectangular or circular cross–section. In this way only neutrons with a direction close to the collimator axis reach the radiographic position where the beam intensity can vary between $10\ n\ cm^{-2}\ s^{-1}$ and $10^8\ n\ cm^{-2}\ s^{-1}$. The reduction in intensity follows an inverse square law and can be calculated using the following equation (110):

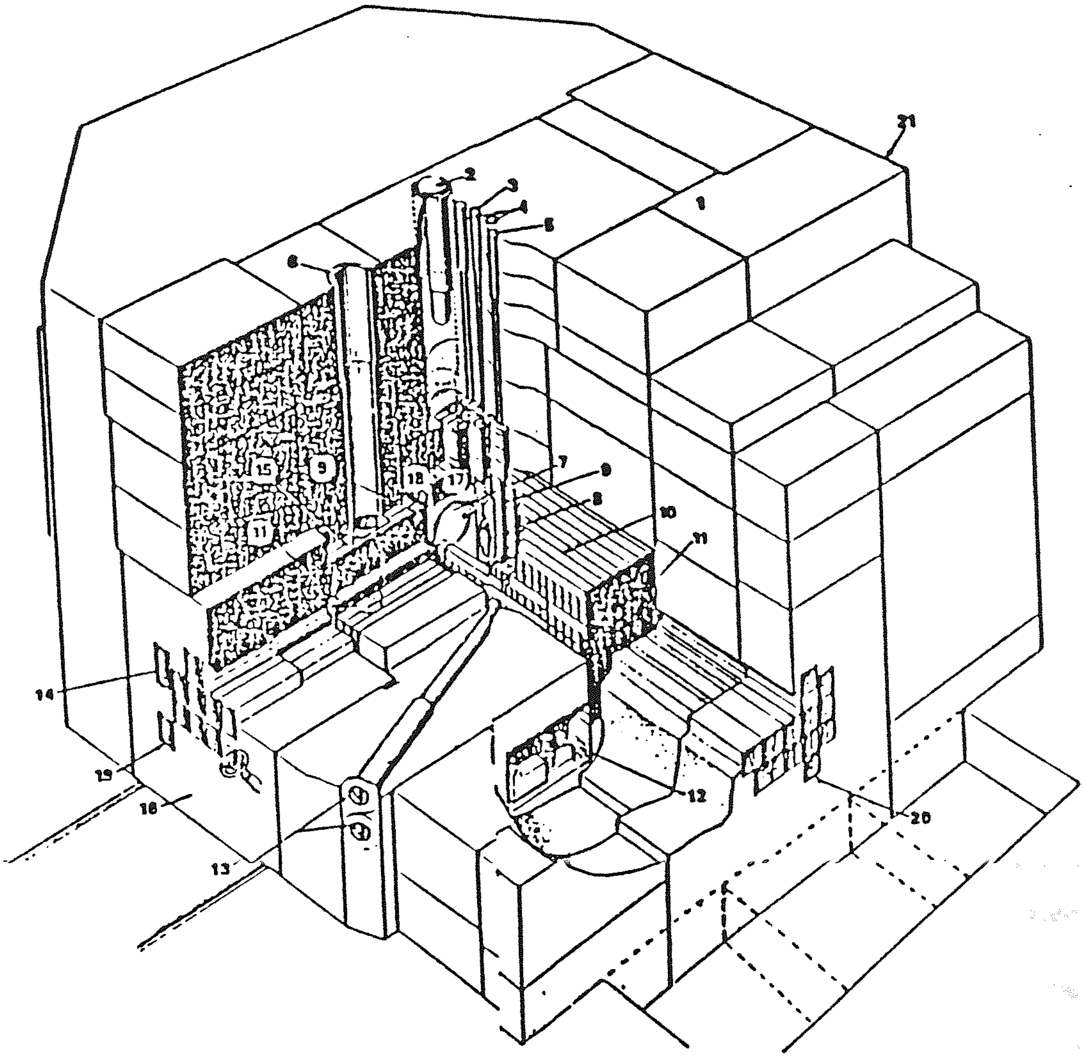

Figure 18b – View of Universities Research Reactor Core.

Key

1. Removable concrete shielding
2. 6" verticle access hole
3. 4" x 4" verticle access hole
4. 1.5" verticle access holes
5. Neutron source
6. 6" verticle access hole
7. Control blade
8. Fuel elements in fuel tank
9. Lead gamma shields
10. Primary thermal column
11. Removable graphite stringers
12. Control blade drive
13. Diagonal beam tubes
14. **8" x 4" horizontal through beam tube**
15. Secondary thermal column access
16. Rolling shield
17. Main thermal column
18. Rabbit tubes
19 Secondary thermal column access
20. Primary thermal column access
21. **4" x 4" horizontal access hole**

$I(E) = Z\ O(E) / LD^2$ ....(34)

where:

$I(E)$ = Neutron beam intensity at the object.
$O(E)$ = Neutron flux at the collimator base (assumed isotropic).
LD = Distance from beam tube base to object (source / object separation).

and Z is a constant given by:

$Z = A / 4\pi$ ....(35)

where:

A = Effective area of the beam tube base.

The neutron beam can be improved in a number of ways to provide more discernable radiographs. Variations in beam intensity across the object plane, geometric unsharpness of the beam, unwanted gamma radiation and neutron scattering in the air and from the walls of the of the collimator can all be countered to improve the quality of the beam.

A non–uniform base flux may cause variations in flux across the object plane. This can be corrected by inserting a graphite moderator, of calculated thickness, at the filter position. It is desirable to place the filters as far away from the image as possible but not less than three neutron diffusion lengths from the base to prevent the source flux being reduced.

The geometric unsharpness (UG) of the beam is dependent on the separation between the object detail and the image recorder. A simple equation can be used to express the relationship:

$UG \approx S\ X/LD$ and $S\ Y/LD$ ....(36)

where:

S = Separation between object detail and image recorder.
X & Y = Dimensions of a rectangular cross–section beam.

It is suggested (110) that approximately 5% per m of beam intensity is lost through scattering in the air. By using evacuated or helium filled flight tubes the problem can be overcome. In addition, by coating the walls of the collimator with a neutron absorbing material, neutrons from the walls are prevented from reaching the image recorder and so reducing the quality of the radiograph.

An overall improvement in the technique would be to use a cold neutron beam instead of a thermal neutron beam. In a study of hydrogen in palladium (111) using a cold neutron beam a visual hydrogen detection sensitivity of better than 2 μgmm^{-2} is recorded.

4.2.3 Other Applications of Neutron Radiography

Thermal neutron radiography has been used in many fields, to provide extensive non–destructive assessments of test samples. In neutron radiography tests carried out at a low flux reactor in The Netherlands (112) successful results have been obtained for non–destructive testing on :

i. Metal bonded specimens.
ii. Reinforced plastics.
iii. Electric and hydraulic components.
iv. Distribution of borium in stainless steel.
v. Liquid sodium detection in irradiated capsules.
vi. Non–irradiated fuel pins.
vii. Geologic specimens.
viii. Electrical heaters.
ix. Bio–mechanical connections, prothesis.
x. High tension isolation materials.

It is interesting to note that in i and ii the use of neutron radiography has been notably more successful in detecting air voids and determining porosities than similar work with X–rays.

Other applications include the use of neutron beams to test 'hot' irradiated fuel elements (113). Of particular interest is work using neutron radiography to study the growth of young roots in soil (114). Excellent results have been obtained with a beam of 10^7 n cm^{-2} s^{-1} and irradiation times of 8 to 10 minutes to give a total exposure of $5x10^9$ ncm^{-2}. Roots of 0.3mm diameter growing in low soil moisture conditions were clearly visible on the radiographs (114).

A thermal neutron beam from a TRIGA Mark 11 reactor has been used (115) to observe microcracks in concrete which are optically invisible at 40x magnification. Neutron radiographs obtained with a neutron flux of $5.6x10^5$ n cm^{-2} s^{-1} at the radiographic position have been compared with X–radiographs. By impregnating the concrete with an aqueous solution of gadolinium nitrate, neutron radiography, with either a gadolinium or gadolinium oxy sulphide intensifying screen, was found to be more effective than X–radiography at detecting the cracks. It was also suggested (115) that the extent of microcracking could be quantified using digital image analysis techniques.

An extension of neutron radiography is Real Time Neutron Radiography (RTNR) which is currently being used (116) in the study of aqueous fluid flow and in a variety of other areas. Using a gadolinium oxy–sulphide intensifying screen and two alternative image systems, good results have been obtained for the analysis of lubricant and spray systems inside metalic structures. A real time image processing system, based on an IBM 9002 computer, was used to enlarge and enhance the reconstructed images. The images were further improved by the use of a mask to subtract out undesired detail from the real time images. Another use of RTNR of interest here is the study of the transport of water bound waste through soil in order to predict the movement of waste and toxic material to the water table.

CHAPTER 5 EXPERIMENTATION

5.1 Introduction

The experimental set–up has been devised to facilitate coupled liquid water flow to the cold end of a partially frozen soil. The coupled flow arises due to an applied temperature gradient, inducing a gradient of liquid pressure. Other gradients due to solute concentration or electrical potential are assumed negligible.

Suction and water content determinations are then used to facilitate determination of the transport characteristic, hydraulic conductivity.

5.2 Classification of the Matrix

Soil classification and compaction tests were carried out on the Snowcal (ground chalk) matrix material. The classification tests comprised particle size distribution and specific gravity determinations and evaluation of the dry density/moisture content relationship was obtained using a soil compaction test.

5.2.1 Grading

The hydrometer method, for fine grained soils (117), was used to determine the particle size distribution for Snowcal. The results are represented graphically in figure 19. The specific gravity of Snowcal is 2.75 +/– 0.005, which was determined using the pycnometer method for fine grained soils (118).

5.2.2 Compaction

The 2.5 Kg rammer method (119) was used to perform compaction tests to obtain the maximum dry density/optimum moisture content relationship for Snowcal. The results are:

Maximum dry density	=2.06 Mg/m^3
Optimum moisture content	=12.6 %

5.2.3 TRRL Frost Heave Test

The test is described in section 2.2.1. The Snowcal matrix was tested in the TRRL frost heave test self refrigerated unit.

The results are tabulated in table 2 and a graph showing the average heave plotted against time for the nine Snowcal specimens is given in figure 20

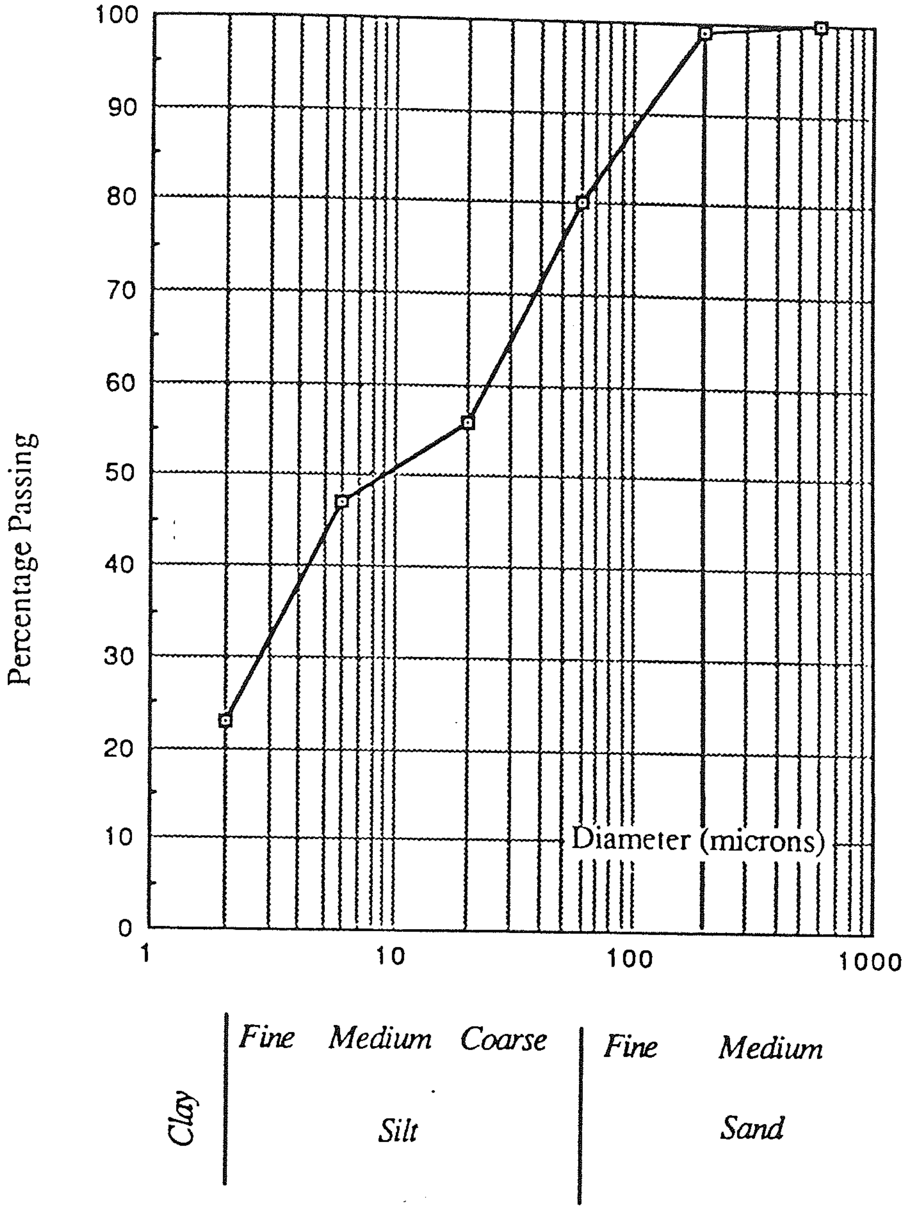

Figure 19 – Particle Size Distribution for Snowcal

Table 2. TRRL Frost Heave Test Results for Snowcal

Time (Hours)	Heave (mm) for Specimens 1–9									Average
	1	2	3	4	5	6	7	8	9	
0	0	0	0	0	0	0	0	0	0	0
24	22	24	23	22	17	22	30	28	28	24
48	46	52	51	50	45	49	59	59	57	52
72	69	72	72	72	68	73	80	80	80	74
96	90	105	101	103	94	104	117	111	111	104

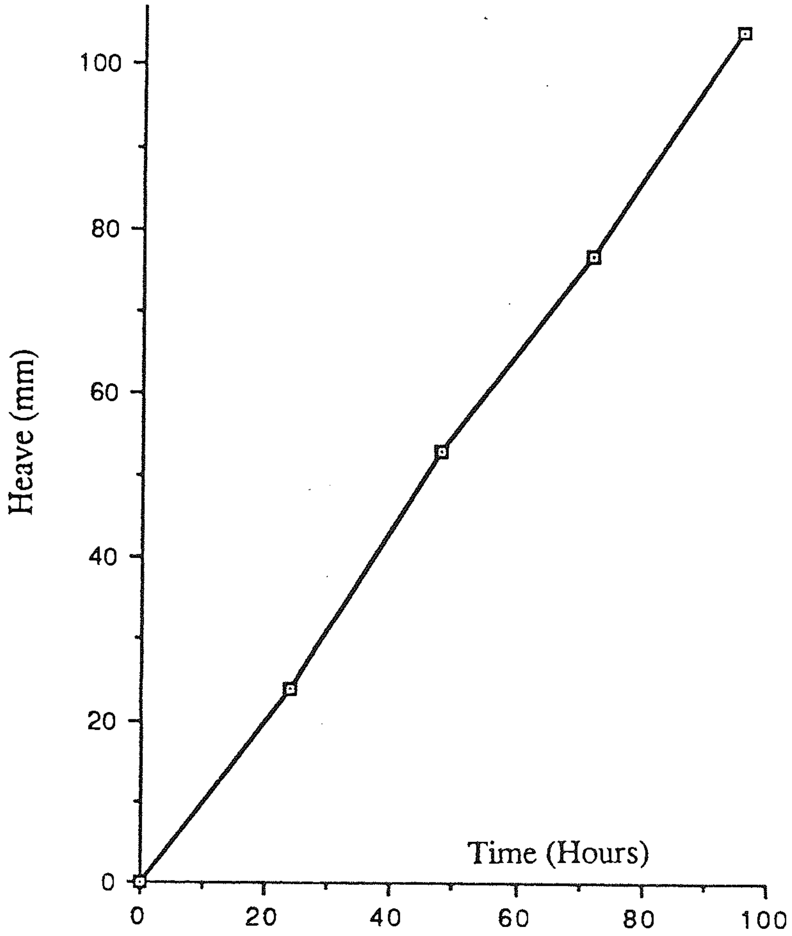

Figure 20. Average Heave Against Time Results for Snowcal

5.3 Development of a Neutron Beam Facility

5.3.1 Introduction

The following sections report the developments in the testing apparatus and experimental set–up. Initial experiments were carried out to assess the quality of the available neutron beam and to set a suitable exposure duration and reactor power. Subsequent tests were then performed with the test rig frequently modified to achieve improved results. Because the experiments were carried out in a nuclear reactor the usual freedoms on test duration and technique were somewhat restricted.

5.3.2 The Experimental Apparatus

The design of a suitable test rig was conditioned by the need to satisfy two basic considerations essential for the successful outcome of the investigation. The first was the need to obtain discernable, easily interpreted results and the second was the requirement for a thermal gradient through the soil matrix.

Table 3 – Properties of PTFE.

Mechanical			Thermal		Misc	
Tensile Strength at 23° C Kgf/cm^2	Modulus of Elast. at 23° C Kgf/cm^2	Coeff. Linear Thermal Expansion 30–100°C mm/mm/°C	Melting Point °C	Coeff. of Thermal Cond. Kcal/m.hr°C	Specific Gravity	Water Absorption 24 Hours %
105–245	3500–6300	100E–6 200E–6	327	0.22	2.1–2.3	0.02

For neutron radiography, aluminium, with its low neutron absorption coefficient, is the ideal construction material. However, to establish a thermal gradient in the soil an insulating material is required, and so aluminium with its high thermal conductivity was unsuitable. Most good thermal insulators have high hydrogen contents so their incorporation in the test rig would have obscured clear identification of water in the soil. PTFE provided a workable compromise, with its low thermal conductivity and neutron adsorption relative to hydrogen it was found to be an adequate construction material and was, hence, extensively used throughout the test rig. Aluminium was also used in the test rig to provide a basic framework and to give support to the PTFE components. Technical details on PTFE (120) are given in table 3.

To present a uniform thickness of soil to the beam to simplify interpretation of results the soil matrix was housed in a rectangular cross-section cell.

5.3.3 Neutron Detection

The neutron detector used for this investigation was a photosensitive film, which gives high spatial resolving power for low cost. The other advantage of using a film plate was that the results are presented pictorially, this provides comprehensive detail of the area covered and is generally regarded as the most effective method of displaying information. The technical details for the film and developing solutions are given in Appendix 1 of this report.

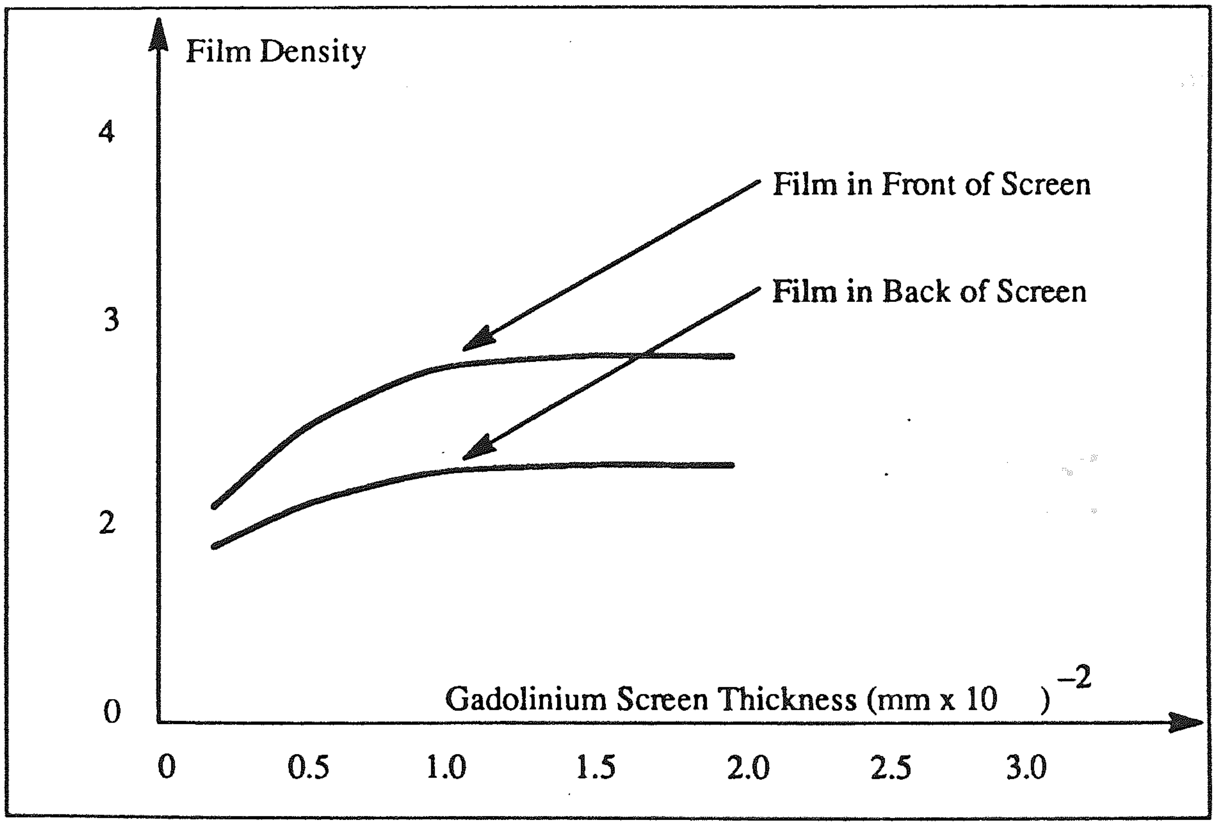

Figure 21 – Gadolinium Screen Speed Results for Direct Neutron Exposure.

The photosensitive emulsion of the selected film had a low neutron registration efficiency and therefore an intensifying screen was required to give discernable radiographs. A

0.025mm thick gadolinium foil screen was used in a direct method and was pressed against the film during exposure. The effect of gadolinium screen thickness and position, infront or behind the film, is shown in figure 21. The film plate and intensifying screen were housed in an aluminium light tight container and positioned as near to the test rig as possible during exposure.

To produce a high quality radiograph approximately 10^9 quanta or registrations per cm^2 are required although a recognisable image of many everyday objects can be produced with 10^4 registrations per cm^2. It was estimated that the image recorder used in these experiments, the photosensitive film and intensifying screen, has a thermal neutron registration efficiency of about 10%. It was therefore necessary to arrange for between 10^5 and 10^{10} n cm^{-2} to fall on the image plane in a reasonable time. The beam used for the initial experiments was formed in a 100mm x 100mm square cross–section, horizontal access hole with better than 1° collimation angle and gives a flux of approximately 10^6 n cm^{-2} s^{-1} at the radiographic position for a base flux of $1.4x10^{12}$ n cm^{-2} s^{-1}.

5.3.4 Preliminary Experiments

An initial experiment was performed to assess the distribution of neutrons in the cross–section of the beam and so determine a suitable exposure time and reactor power to give sufficient quanta at the image plane. Data for the distribution of neutrons in the beam cross–section were obtained using a fission chamber and a neutron counter located 30mm and 150mm from the beam outlet. Sand was used for the soil matrix as the mass adsorption coefficient for sand (silicon) is significantly different from that of hydrogen, as shown in figure 17. The sample was contained in a box, constructed from 5mm thick PTFE sheet, to give a sample thickness of 12.5mm.

This matrix was irradiated at increasing reactor powers and exposure durations until a radiograph of suitable clarity was obtained at a reactor power of 300Kw and an exposure period of 300s. To simulate water a collection of hollow high density plastic spheres, solid plastic beads and polystyrene half spheres and sheets were embedded in the matrix and irradiated for 300s at a reactor power of 300Kw. These regular shaped objects were chosen, instead of using water, so that the effect of the matrix on the image quality could be more easily seen.

5.3.5 Results from Preliminary Experiments

The distribution of neutrons is shown in figure 22 for distances of up to 60mm either side of the centre line of the beam for positions 30mm and 150mm from the hole. Two radiographs were obtained with the rig positioned 100mm from the hole, one showing the lower portion of the matrix and the other showing the upper portion. Contact prints of these radiographs are given in plates 1 and 2.

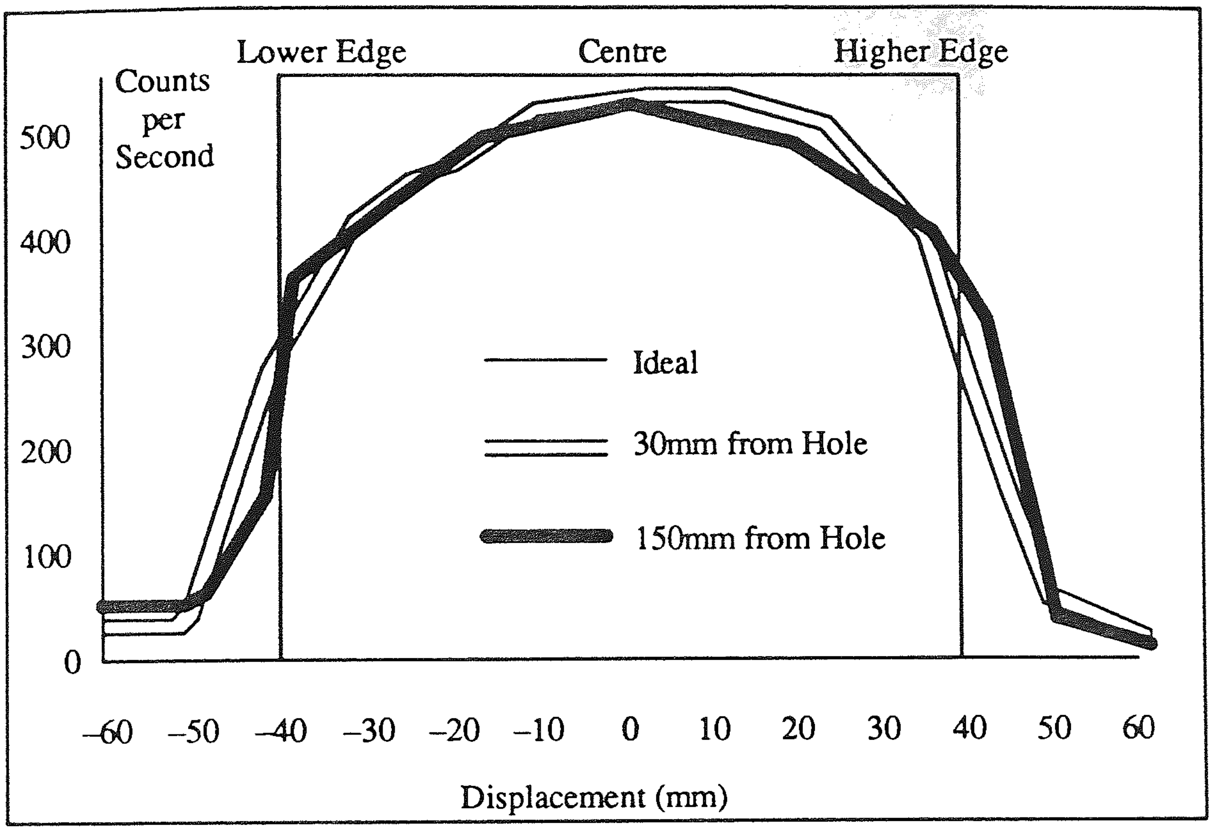

Figure 22 – Distribution of Neutrons around the 4" x 4" Reactor Hole.

The neutron distribution shows that there was a reduction in the intensity towards the edges of the beam. This is indicated on the radiographs by the circular blurring of the square outline of the beam. The plots obtained at 30mm and 150mm are however very similar indicating good beam collimation, and the images of the plastic and polystyrene inclusions are remarkably clear indicating an acceptably low level of interfering gamma radiation. Having found the results encouraging it was decided to persevere with the beam to examine a Snowcal, (powdered chalk) matrix under freezing conditions, again employing a reactor power of 300Kw and an exposure time of 300s.

It was decided to correct for variations in the beam intensity at the radiograph analysis stage of the experiment rather than modify the beam by inserting a graphite moderator, of pre-determined thickness, into the collimator. To limit any geometric unsharpness effects the light tight container was kept pressed against the cell, containing the soil matrix, during exposure.

5.3.6 Test Rig and Specimen Preparation

Table 4 illustrates the beam characteristics. A schematic diagram of the neutron flight tube and experimental set up is given in figure 23.

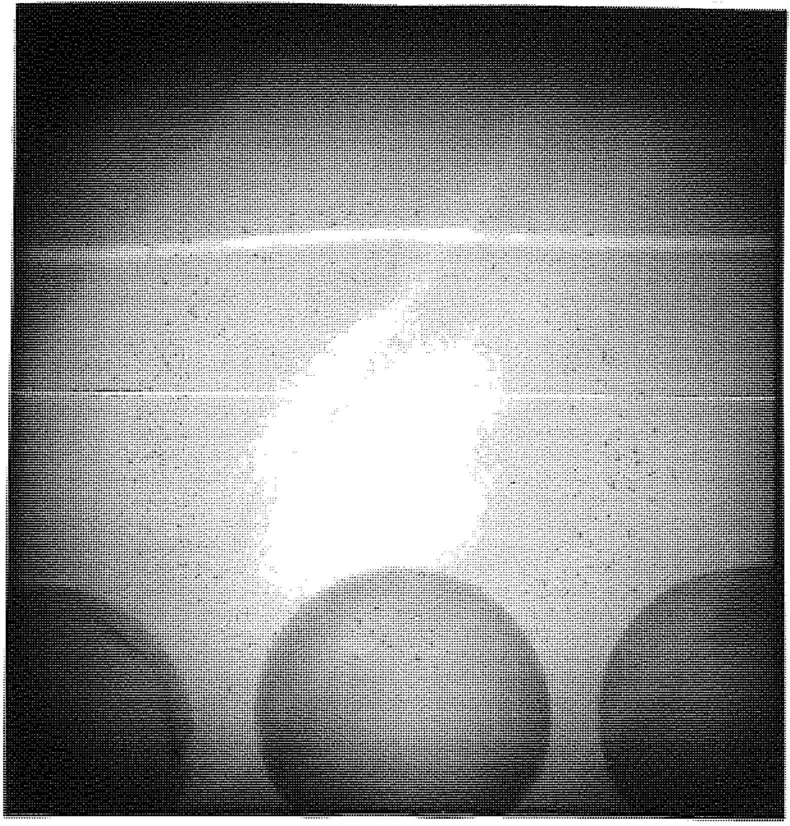

Plate 1 – Upper Portion of Matrix

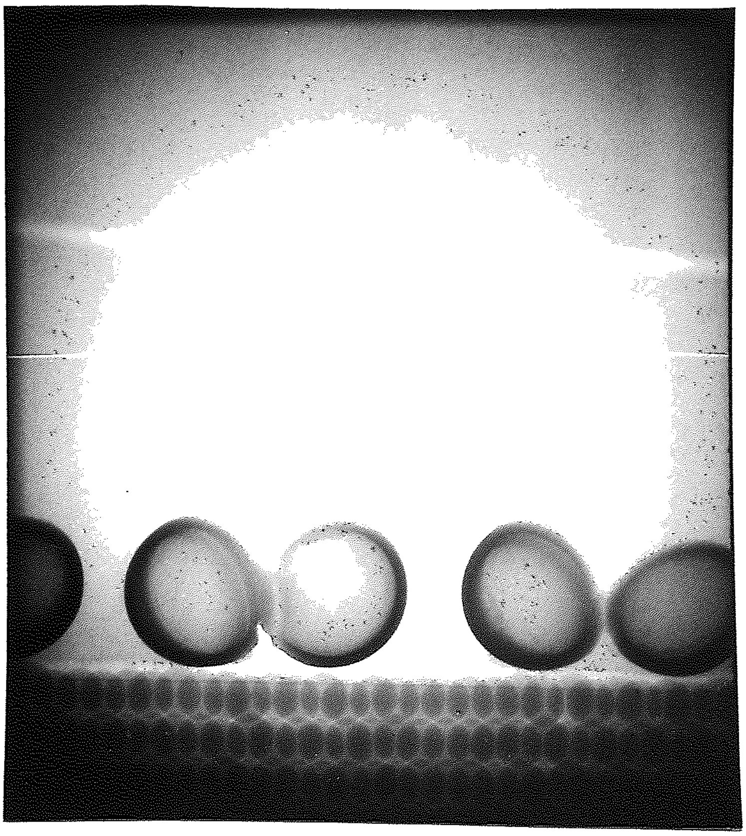

Plate 2 – Lower Portion of Matrix

Table 4 Comparison of the Characteristics of Neutron Beams.

Characteristics	Diagonal Beam	Horizontal Beam
Neutron Flux at Radiographic Position (n cm^{-2} s^{-1})	6	7.5 x 10^{7}
Exposure Time for Radiograph (s)	300	18
Reactor Power (KW)	300	100
Cross–sectional Area of Beam Tube (inches)	4 x 4	8 x 4
Beam Collimation (Degrees)	1	1

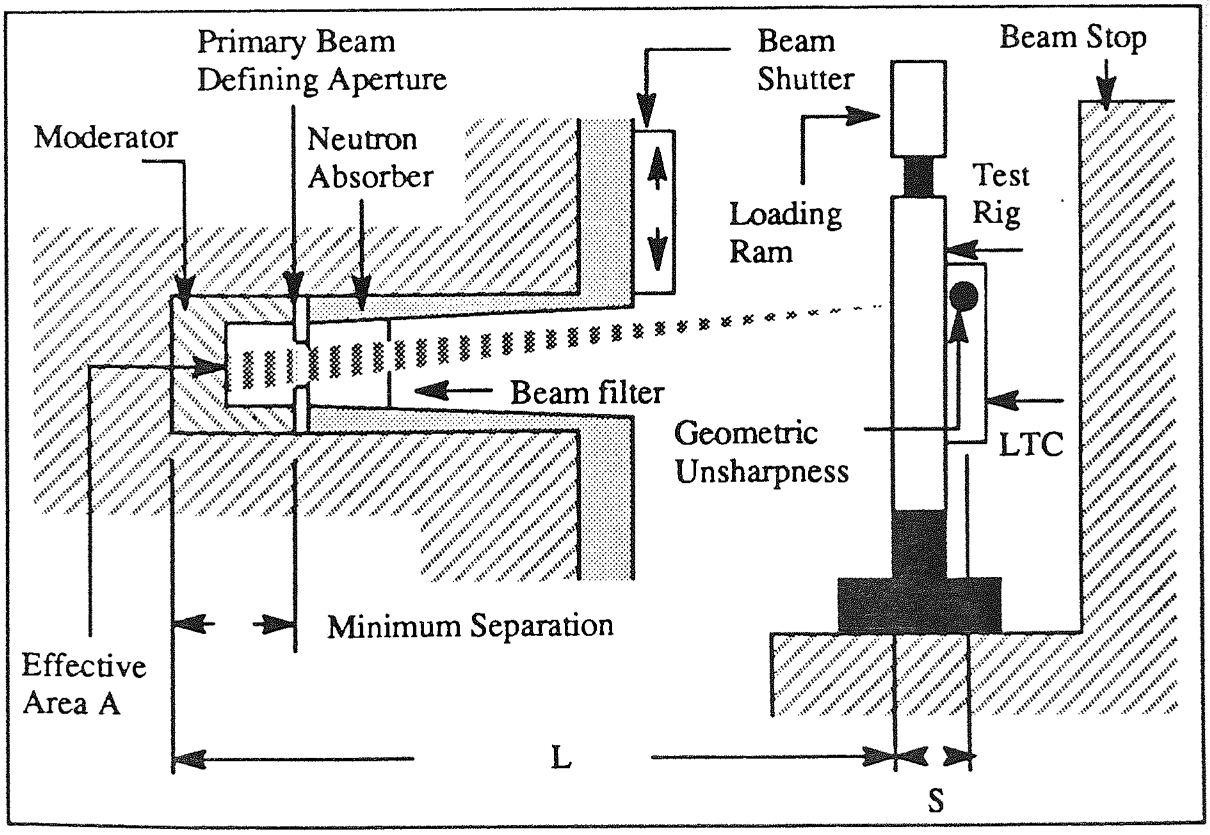

Figure 23 – Neutron Flight Tube and Experimental Setup.

The test rig was designed to facilitate freezing the specimen from the top down, with water uptake from the bottom. It was necessary to allow heave to develop unrestricted and, when required, to be able to restrict heave through the application of an overburden pressure. The apparatus comprised a rigid aluminium frame in which the specimen cell was located. The cell was manufactured from 5mm thick PTFE sheets, joined with aluminium screws. At the lower end of the cell it was connected to an aluminium water bath, via a porous brass cover. An outer aluminium jacket was glued to the water bath, and by circulating cooled water through this jacket the temperature of water in the water bath could be controlled. The water supply to the bath was from a mariotte vessel (3). A freezing head, constructed from 1mm thick aluminium sheet was used to chill the top of the specimen, refrigerant from a thermostatically controlled bath being recirculated through the freezing head. The head was able to move freely in and out of the top of the cell so that the specimen movement was not restricted. The head was connected by a rigid bar to a Bellofram compressed air loading ram and this permitted the application of a controlled overburden pressure to the test specimen. The freezing head thus acted as a piston allowing the soil to expand or provided an overburden pressure to restrict such movement, a technique used to effect by other researchers (78,82). The test rig is shown in figure 24.

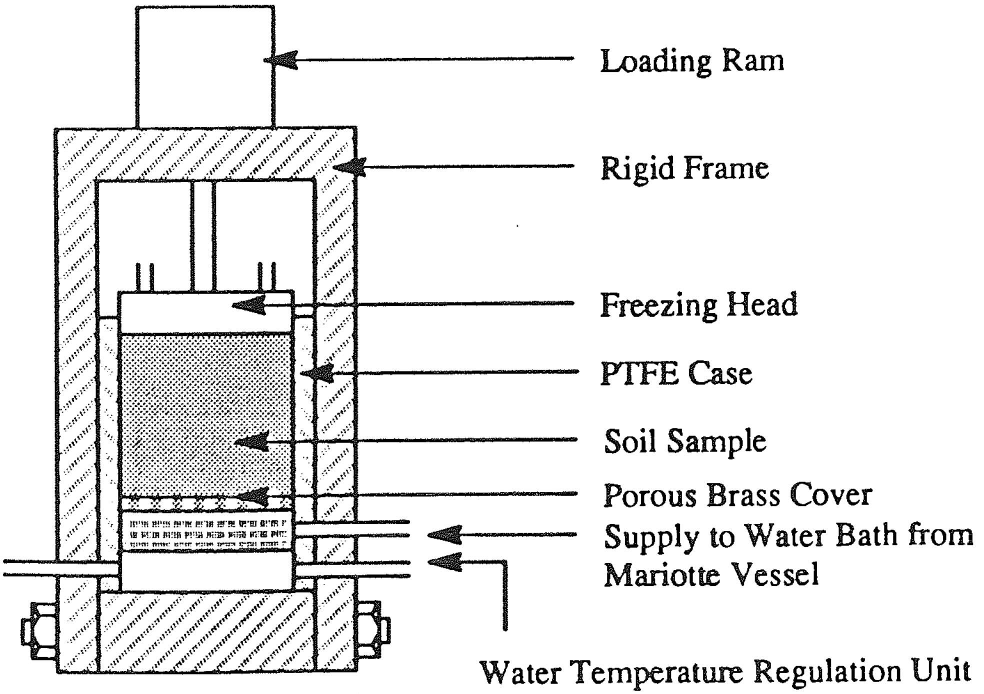

Figure 24 – Test Rig.

A linear motion potentiometer was also attached to the freezing head so that the movement of the head could be displayed on a chart recorder. Water uptake by the specimen and heave during freezing were continuously recorded on a chart recorder. Copper/constantan thermocouples, located at 10mm intervals along the length of the specimen, enabled the temperature profile to be determined throughout the test. This type of thermocouple at this spacing has been considered desirable for temperature profile determinations by many researchers (78,82). The temperatures of the freezing head and water temperature regulation unit were maintained by passing cooled ethylene glycol and water mixture through them via Churchill circulators.

The dimensions of the cell were controlled by the availability of appropriately sized X–ray photosensitive film, rather than by the cross–sectional area of the neutron beam. It was envisaged that the use of a larger cross–sectional beam was a future possibility and it was therefore decided to optimise the size of the soil matrix and perform the initial trial experiments with the 100mm x 100mm cross–section beam. As only part of the soil matrix would be shown in any radiograph, Image Quality Indicators (IQI's) were omitted from the initial rig design. With a larger cross–sectional beam IQIs would be included as standard sized sections of a given material, positioned around the rig so that variations in beam intensity would appear as variations in the exposure of the IQIs.

Two experiments were conducted using this test rig design with the neutron beam. These were primarily concerned with the preparation and compaction of uniform specimens. In both experiments a matrix of Snowcal at the pre–determined optimum moisture content of 12.6% was compacted into the PTFE cell. As the cell dimensions were not compatible with those of the standard compaction mould (21) and owing to the high plastic deformation of PTFE, it was necessary to develop an appropiate compaction procedure to achieve uniformity in the test specimen. After a process of trial and error a suitable method of compaction was standardised. Initially the sample was divided into ten equal layers and each layer was compacted with the blunt end of a knitting needle. This method proved inadequate as upon capillary up take of water the matrix underwent cavitation. The resulting void development is clearly depicted in the sequence of radiographs obtained during the test. Contact prints of the radiographs are given in plates 3–6.

For the second experiment minor alterations were made to the cell. The front and back faces of the cell were milled down to 4mm thickness over the area occupied by the soil matrix. The recess so formed was used to accommodate aluminium plates which, when bolted together, stiffened the cell. With the cell strengthened in this way it was possible to increase the degree of compaction of the sample by dropping a 150 gm brass bar a distance of 100mm, 25 times on each of the ten, previously scarified, layers.

The results of the experiment are, however, also unsatisfactory. The degree of compaction was adequate (1.65 Mg/m^3) and although a temperature of –1 °C was attained beneath the freezing head, a lack of fit between the head and the soil matrix resulted in ice

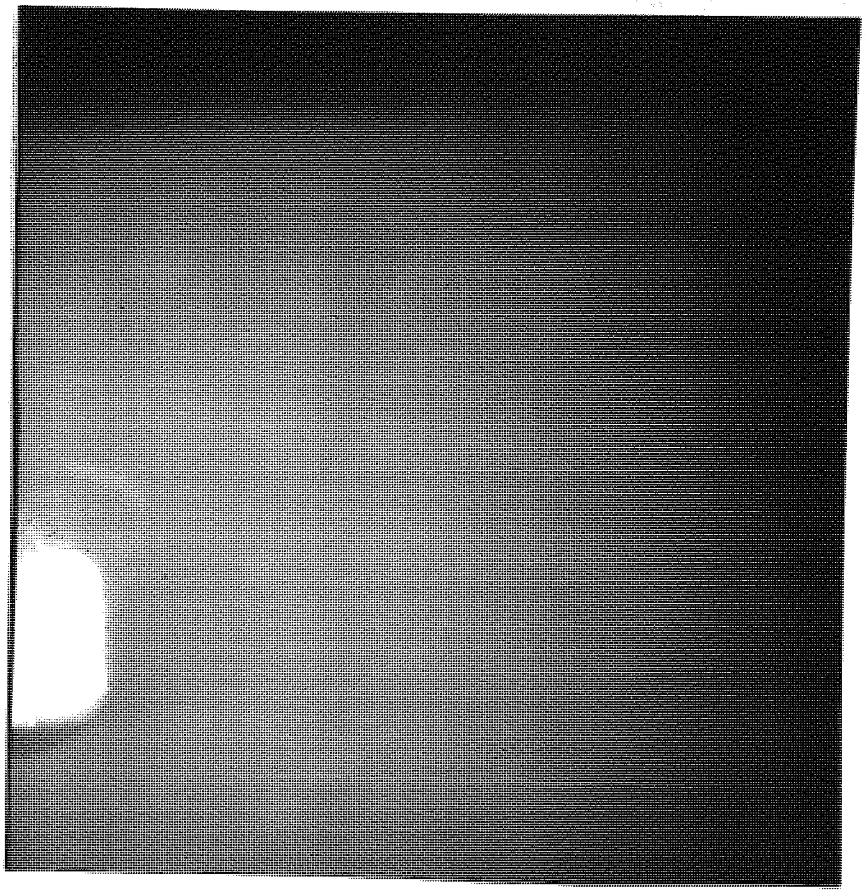

Plate 3 – Void Development: Stage 1

Plate 4 – Void Development: Stage 2

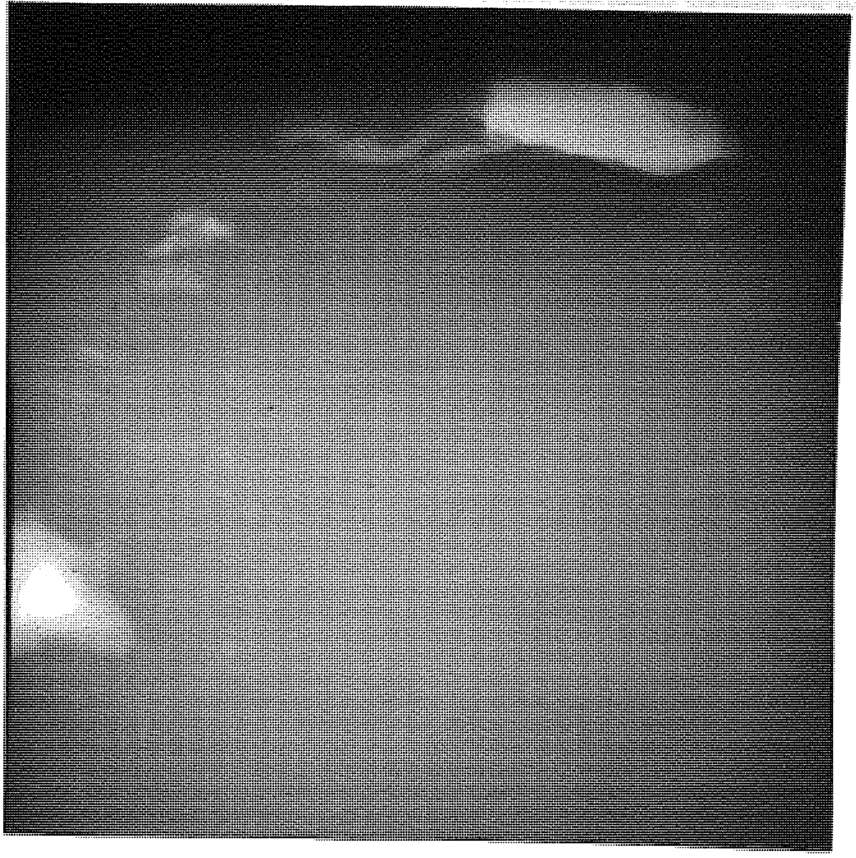

Plate 5 – Void Development: Stage 3

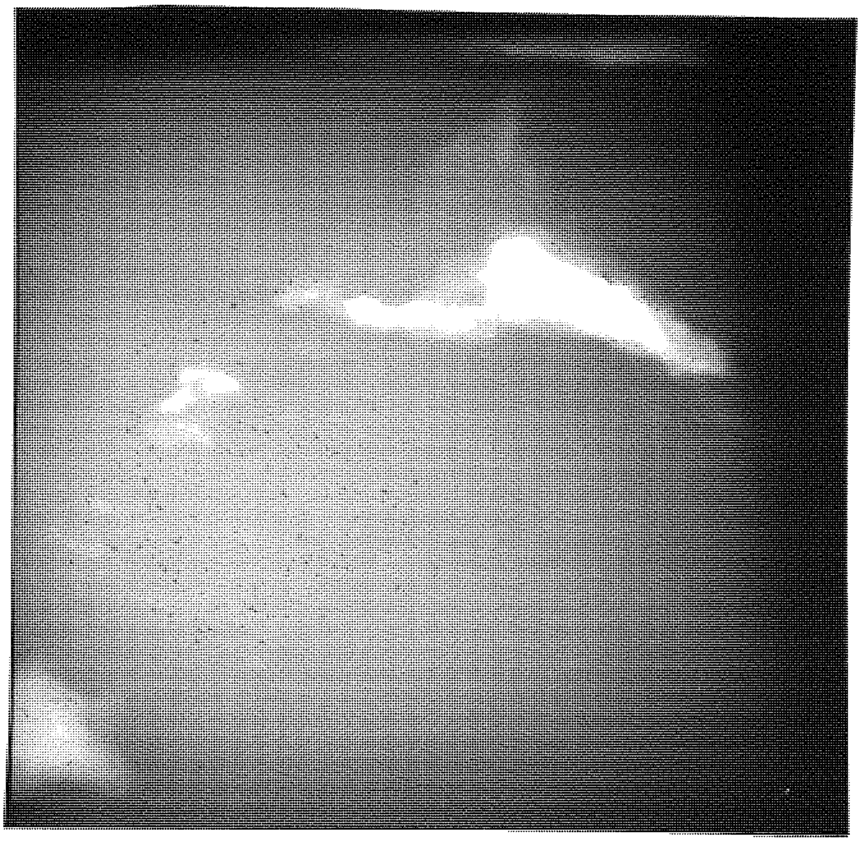

Plate 6 – Void Development: Stage 4

accumulating below the head with no zero isotherm penetration into the matrix. This is shown in contact prints of a selection of radiographs obtained during the test, which are given in plates 7–8.

5.3.7 Modifications to Test Rig

Following the initial tests, the test rig and experimental set up were completely re–designed to incorporate the improvements listed below:

1. Increase uniformity of matrix compaction
2. Stabilised and reduced air and matrix temperature.
3. Better contact between the freezing head and matrix.
4. Reduce side wall restraint between the matrix and test rig.
5. Inclusion of IQIs and soil moisture content references.

A diagram of the test rig is given in figure 25 and a schematic diagram of the experimental set up is given in figure 26.

The apparatus has been designed in three sections. The top section, housing the freezing head, the middle section, with the sample and the lower section, incorporating the water bath and water temperature regulation unit. Each section comprised a machined PTFE sleeve with aluminium stiffening faces front and back. To prevent condensation between the stiffening faces and the PTFE sleeves of each section, the faces were smeared with silicon grease and slid onto the PTFE sleeves before tightening down. The silicon has a mass adsorption coefficient sufficiently different to that of hydrogen. The sleeves beyond the aluminium faces were recessed to enable the sections to slot together by means of aluminium runners. Once in position the sections were secured by tightening down screws through plates at the tops of the runners.

The water bath and water temperature regulation unit were milled from one piece of aluminium plate to ensure good thermal conductivity for accurate temperature control. Once located the water bath, with scintered brass cover, protruded from the PTFE sleeve. A rubber 'O' ring, forced over the water bath, made the seal between the lower and middle sections. The water temperature regulation unit and freezing head were cooled by ethylene glycol and water, at reduced temperature, being circulated through them using Churchill circulators. The water bath was connected to a marriotte vessel to provide a constant head of water to the specimen.

The specimen was compacted in six PTFE rectangular cross–section rings 1.5mm thick which slid in the PTFE sleeve. The rings were intended to reduce side wall resistance and so allow the specimen to heave during freezing. For conditions consistent with the application of the Clausius–Clapeyron equation the soil should be unconstrained. If constrained the distribution of stress between soil solids, ice and liquid water, must be

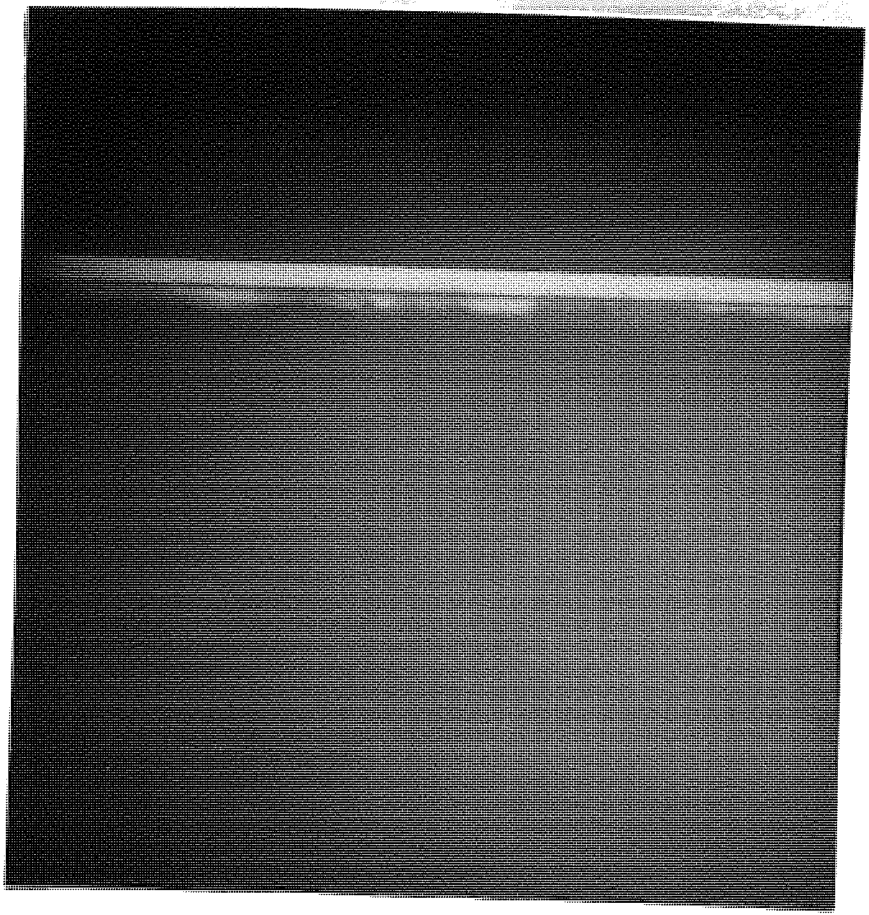

Plate 7 – Lack of Fit Between the Freezing Head and The Soil Matrix: Stage 1

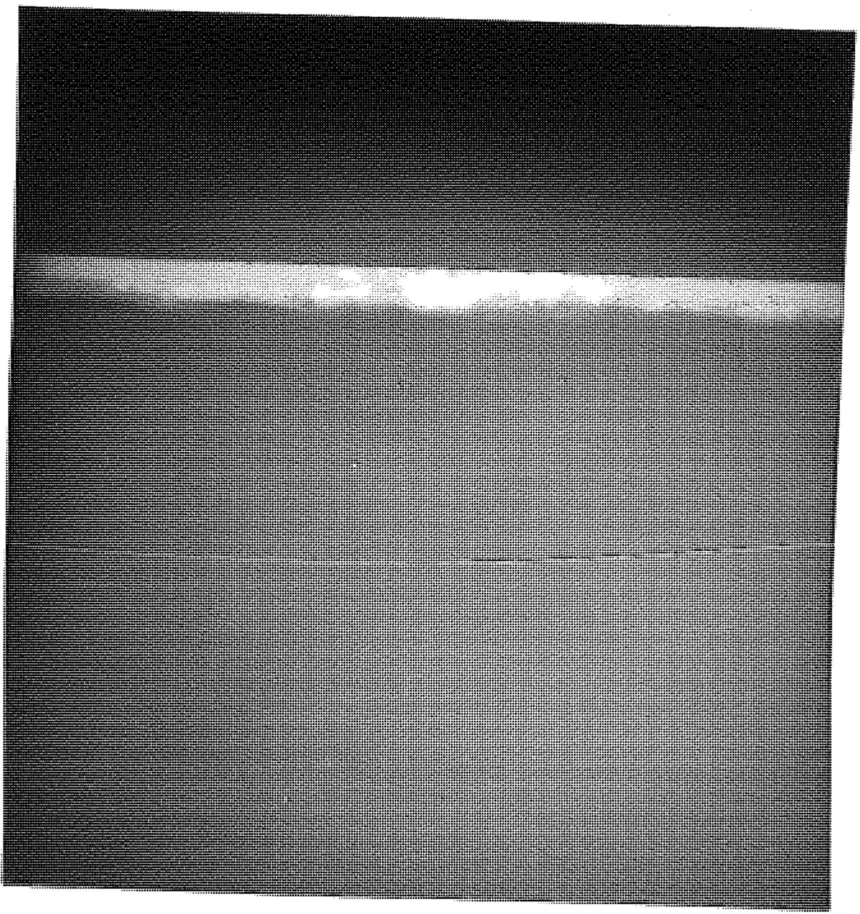

Plate 8 – Lack of Fit Between the Freezing Head and the Soil Matrix: Stage 2

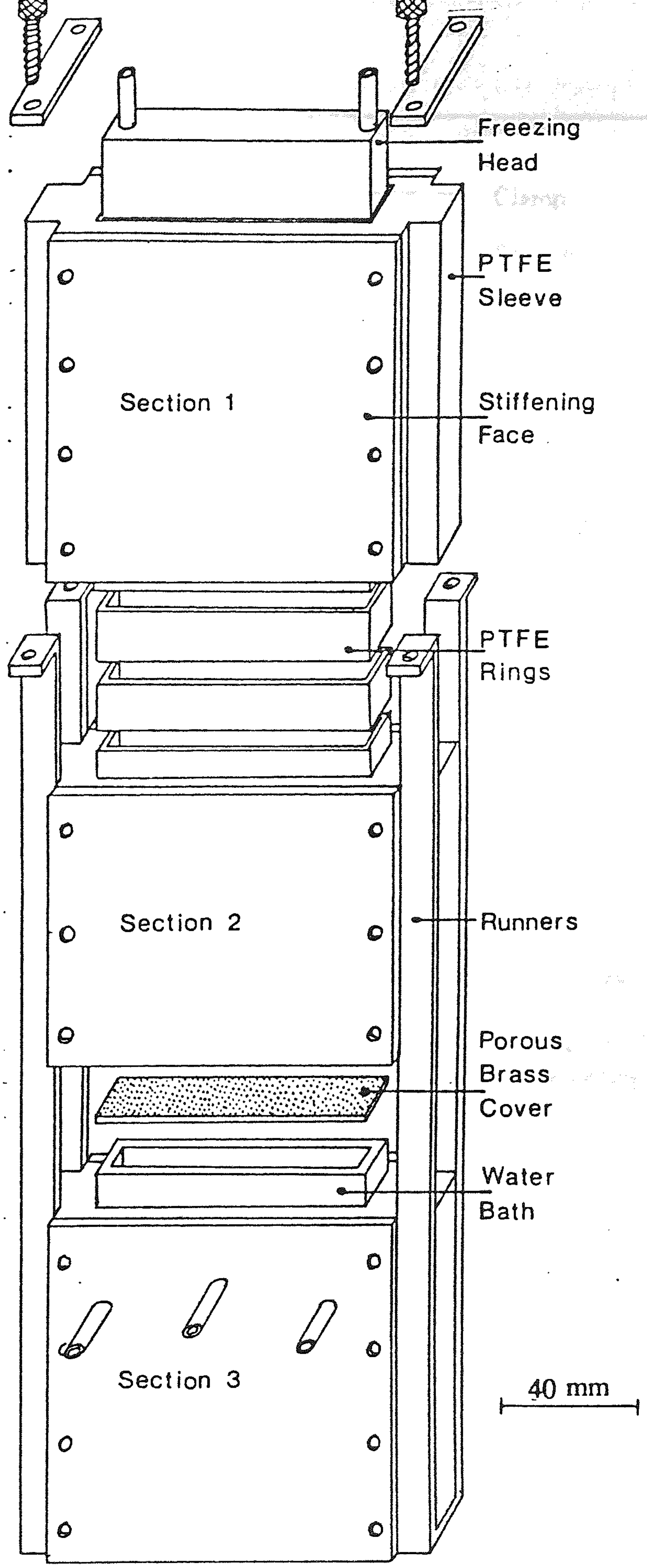

Figure 25a – Modified Test Rig.

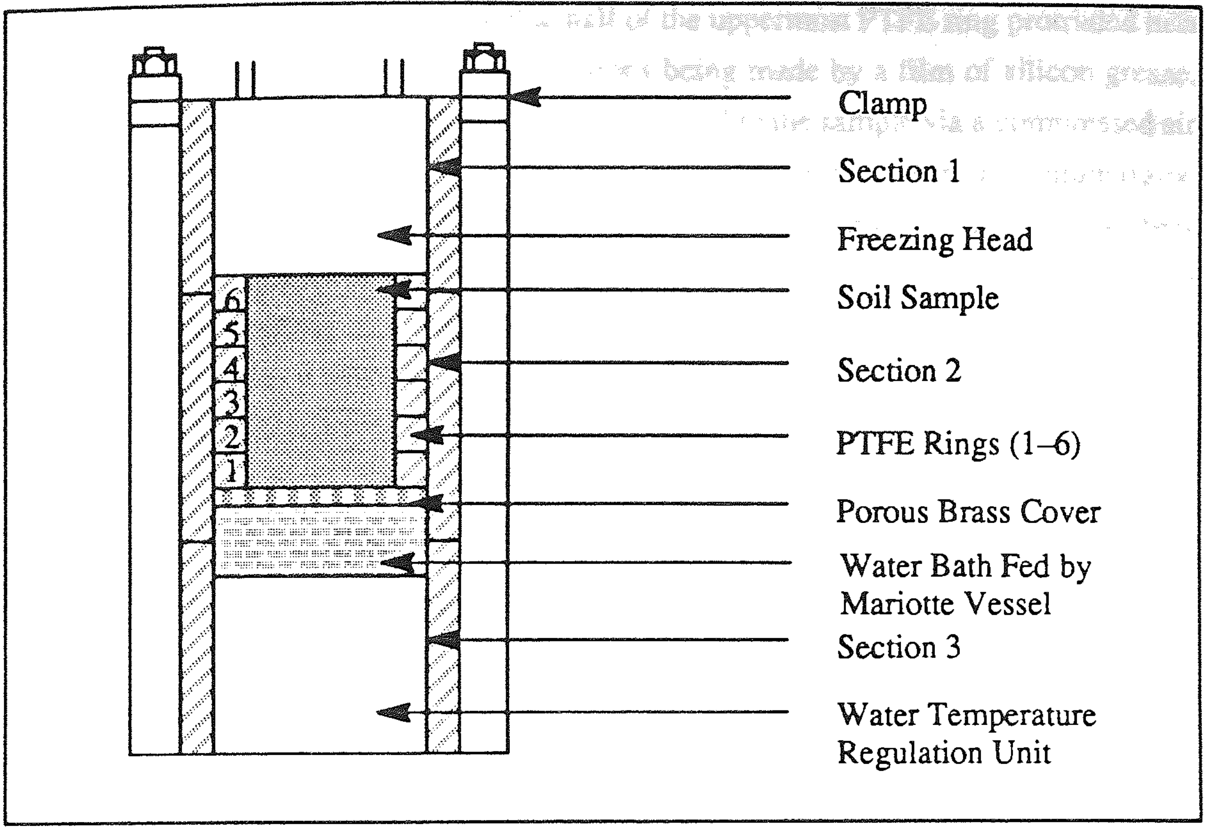

Figure 25b – Modified Test Rig.

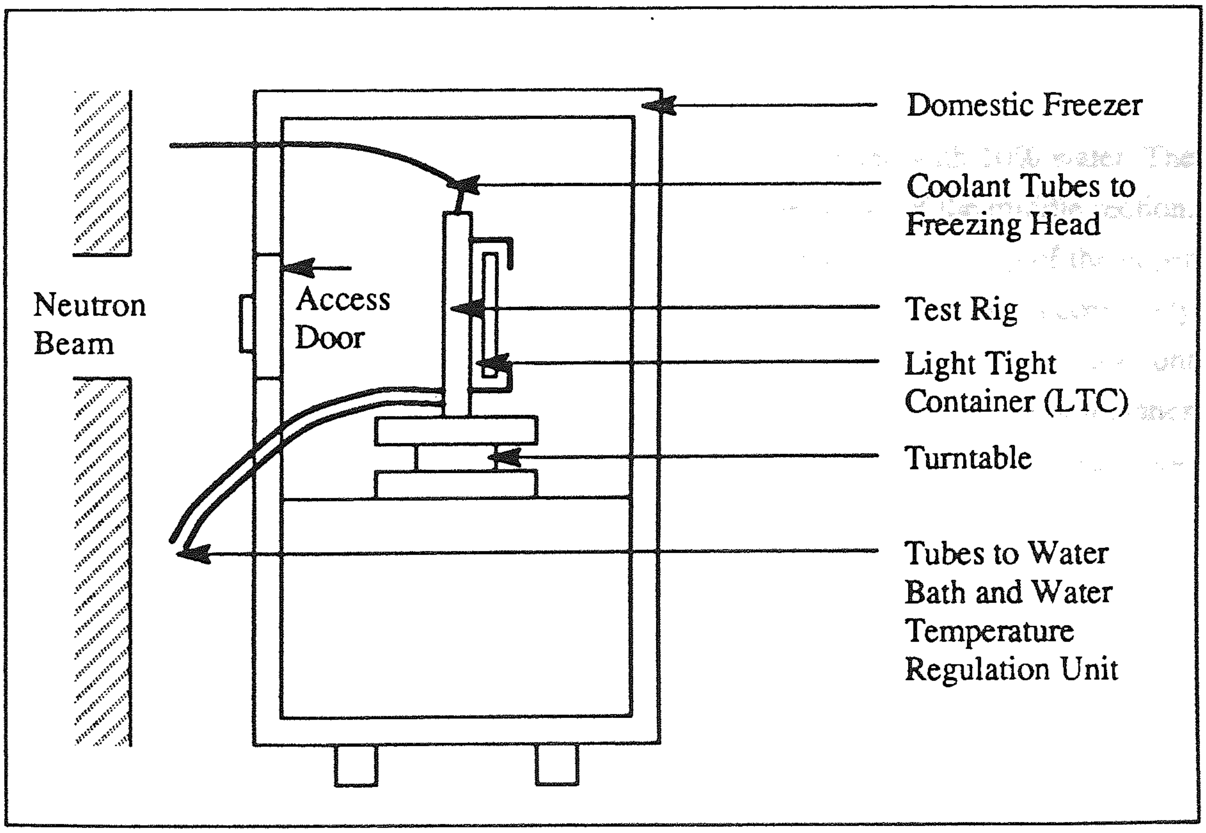

Figure 26 – Schematic Diagram of Experimental Set–up.

determined (88). When locating the middle section onto the lower section, the water bath penetrated into the middle section so that half of the uppermost PTFE ring protruded into the top section, the seal between these sections being made by a film of silicon grease. When required, overburden pressure could be applied to the sample via a compressed air loading ram. The three sections and a reference cell were mounted in an aluminium frame by means of two horizontal aluminium channels. The reference cell had three chambers and was identical in cross–section to the middle section. Each chamber contained a sample of matrix of known water content so that each radiograph had a permanent standard, independent of developing techniques or slight beam alterations. The frame also supported the loading ram and was positioned on a turntable so that the whole apparatus could be rotated through 90° to facilitate access to the back of the apparatus.

To provide an environment at constant temperature, the apparatus and turntable were installed in a domestic upright freezer. The freezer was fitted with an insulated door into which a small removable door was slotted to allow the neutron beam access to the apparatus. The film and intensifying screen were housed in a light tight aluminium case. During irradiation of the sample the aluminium case slotted into horizontal channels which positioned it behind the middle section. Access to the light tight container was achieved, through the removable door, by rotating the apparatus through 90° with the turntable.

5.3.8 Standardised Test Procedure

These tests were performed on a sample matrix of Snowcal mixed with 10% water. The material was compacted into the PTFE rings, located in the sleeve of the middle section. Compaction involved dropping a 150 gm brass rod from a fixed height (top of the upper section when in place on the middle section). The number of tamps were successively increased, by one tamp for each layer, from 10 tamps/layer to19 tamps/layer to account for decreasing dropping distance. The ten layers were chosen so that compaction planes did not coincide with the ring intersections. Finally the top surface was levelled to provide a flat face for the freezing head.

The domestic freezer was operated to provide an air temperature of +5 °C, both for pre–test conditions and throughout the test, with the freezing head and water bath being maintained at –4 °C and +4 °C respectively throughout the test. Radiographs were taken at 30 minute intervals from commencement of freezing to the completion of the test each with an exposure time of 300 seconds.

An initial radiograph was obtained by the following sequence of operations. The access door to the freezer was removed, so that the test rig could be rotated through 90° on the turntable, and the light tight container, complete with X–ray film and intensifying screen, was inserted. The test rig was returned to its original position and the freezer, mounted on a wheeled platform, was positioned in line with the neutron flight tube. The concrete block shielding the flight tube was removed and replaced when the exposure time of 300 seconds had elapsed. The freezer was wheeled out of poisition and the access door replaced. After radiation levels in the freezer had decayed to an acceptable level the light tight container was removed and the X–ray film developed using the techniques and equipment detailed in Appendix 1. Lowering of temperature was initiated by setting the circulator supplying the freezing head to –4 °C and the circulator supplying the water temperature regulation unit to +4 °C. Radiographs were then taken, using the previously reported procedure, at 30 minute intervals throughout the 4.5 hour test. The test was limited to 4.5 hours because reactor limitations on test durations prevented testing into the evening and over night. Water uptake by the specimen during freezing was recorded on a chart recorder by means of a linear motion potentiometer, fixed in the mariotte vessel and attached to a polystyrene float which rested on the water. The temperature below the freezing head and the air temperature in the freezer were recorded using copper/constanton thermocouples.

5.3.9 Standardised Test, Radiographs

Contact prints of the radiographs are given in plates 9–18.

5.3.9.1 Discussion of Radiographs

The radiographs show the freezing front penetrating into the soil with bands of ice clearly visible, as darker lines in the frozen section, towards the end of the test. The soil did not, however, take up water and consequently any ice accumulation was due to the relatively small quantity of water in the soil redistributing.

Associated with the accumulation of ice was a certain amount of heave depicted by the separation of the upper and second PTFE ring. The results were encouraging and consequently the basic test rig design was unaltered for subsequent tests. The beam, however, was of insufficient cross–sectional area to cover both the main cell and the reference cell, and the associated low power of the beam meant long exposure times were required.

5.3.10 Improved Beam Facility

The experimental set up was altered to permit the use of a larger cross–section beam of greater intensity, to cover the whole of the apparatus (main cell and reference cell).

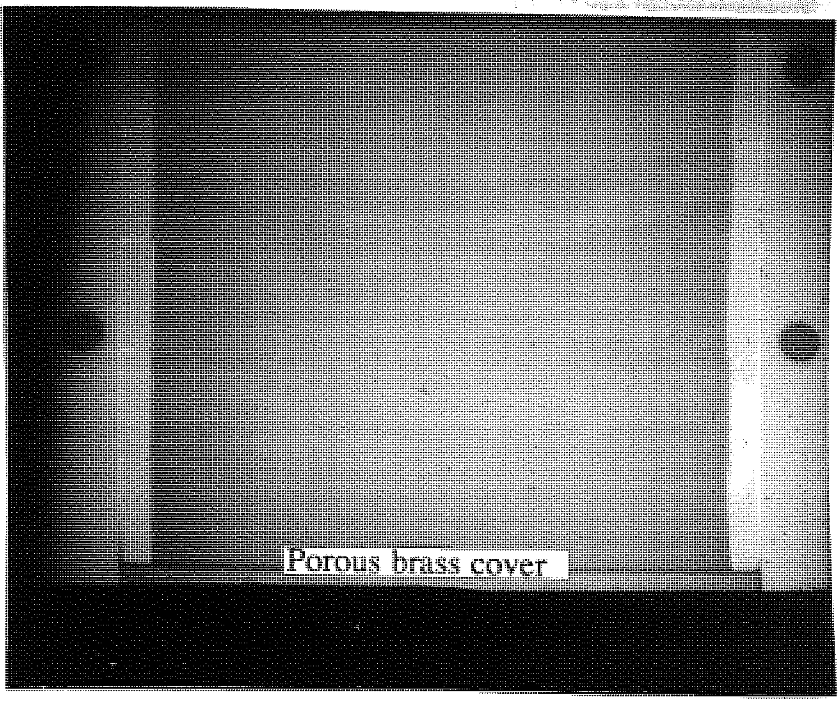

Plate 9 – Standardised Test (Time: 0 min., Heave: 0 mm, Temp.: 5.2 degrees C)

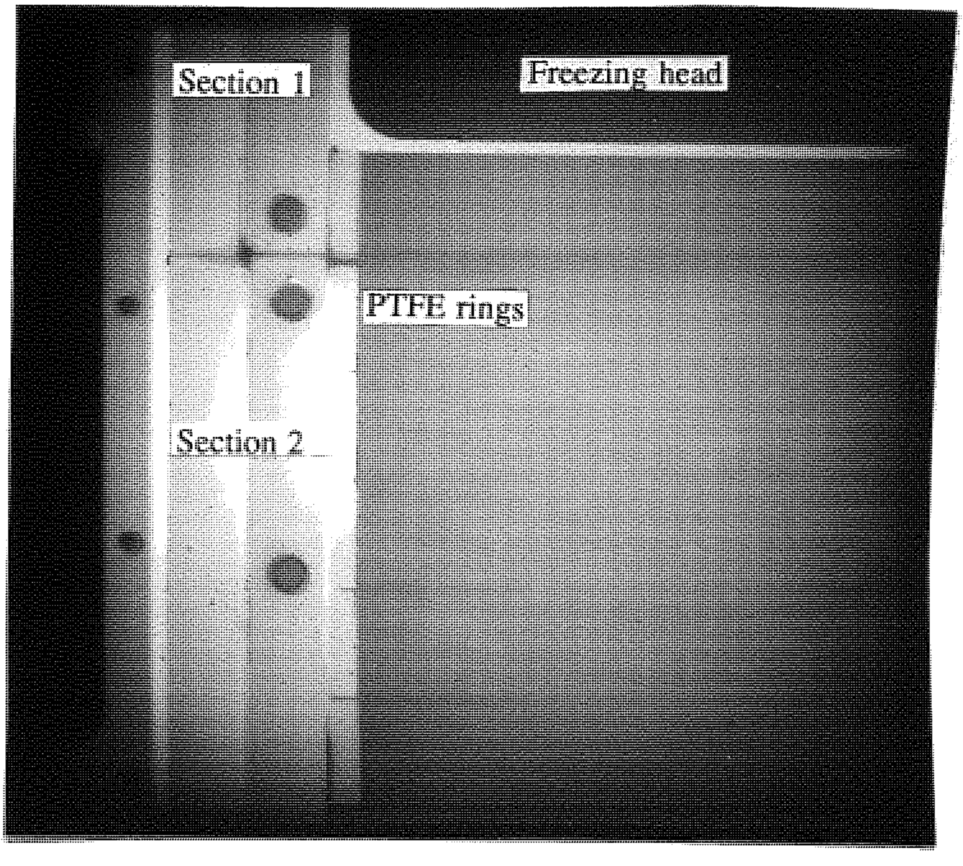

Plate 10 – Standardised Test (Time: 30 min., Heave: 0 mm, Temp.: 0.3 degrees C)

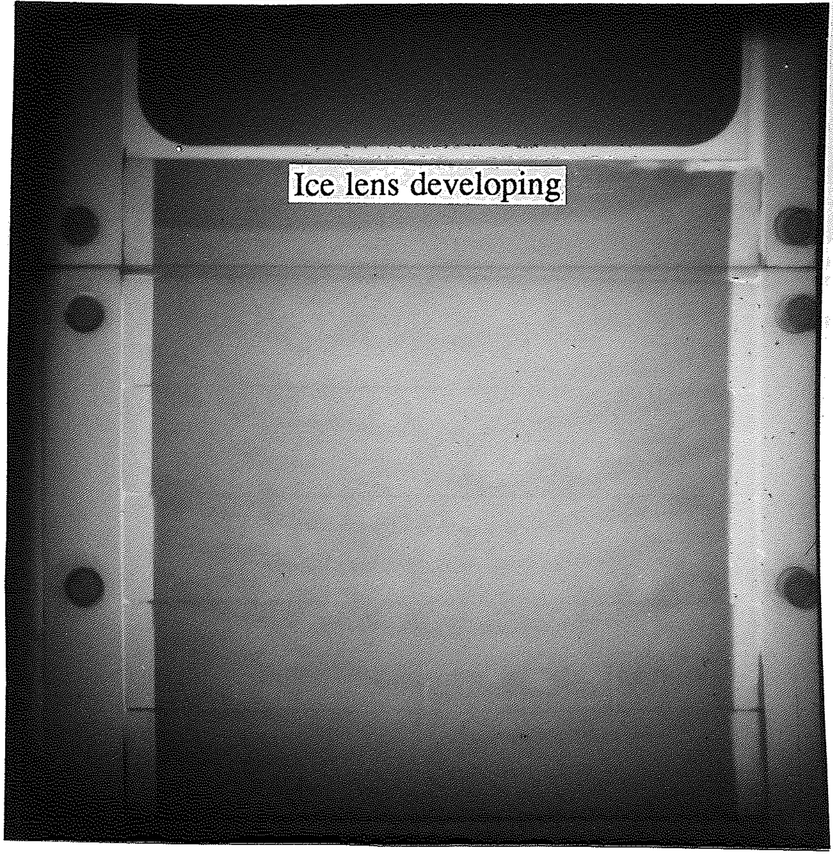

Plate 11 – Standardised Test (Time: 60 min., Heave: 0 mm, Temp.: –2.5 degrees C)

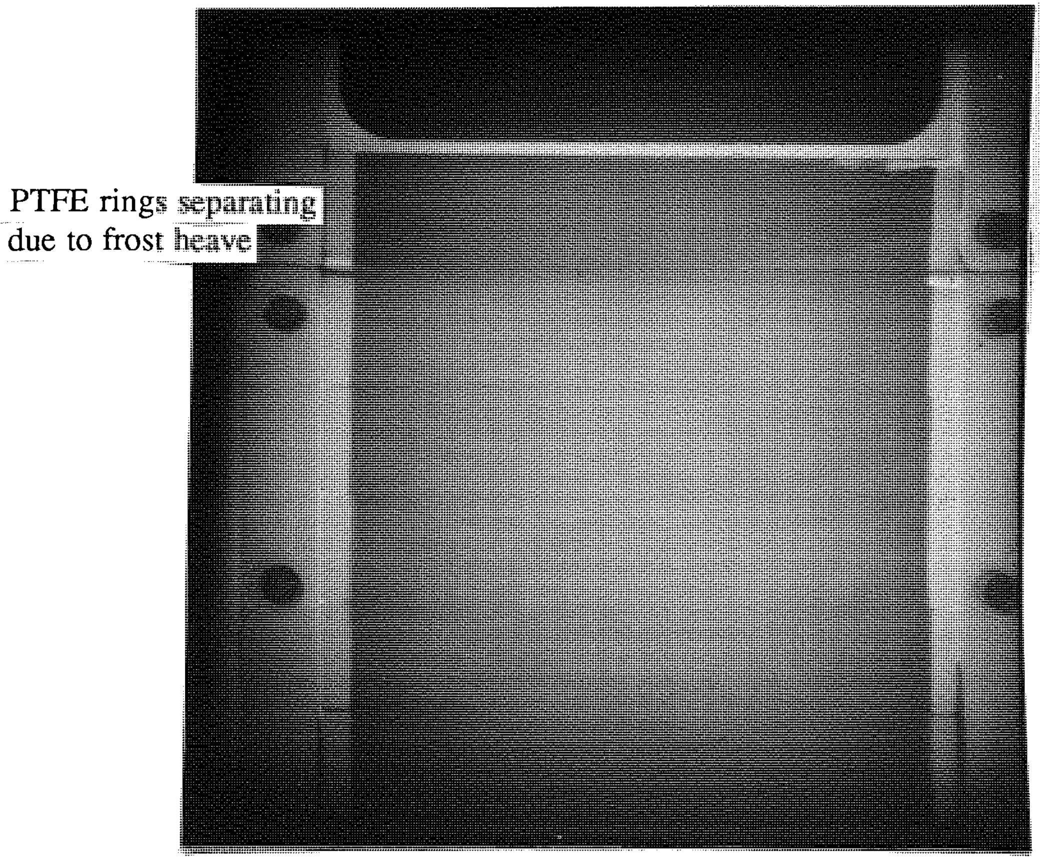

Plate 12 – Standardised Test (Time: 90 min., Heave: 0.6 mm, Temp.: –4.3 degrees C)

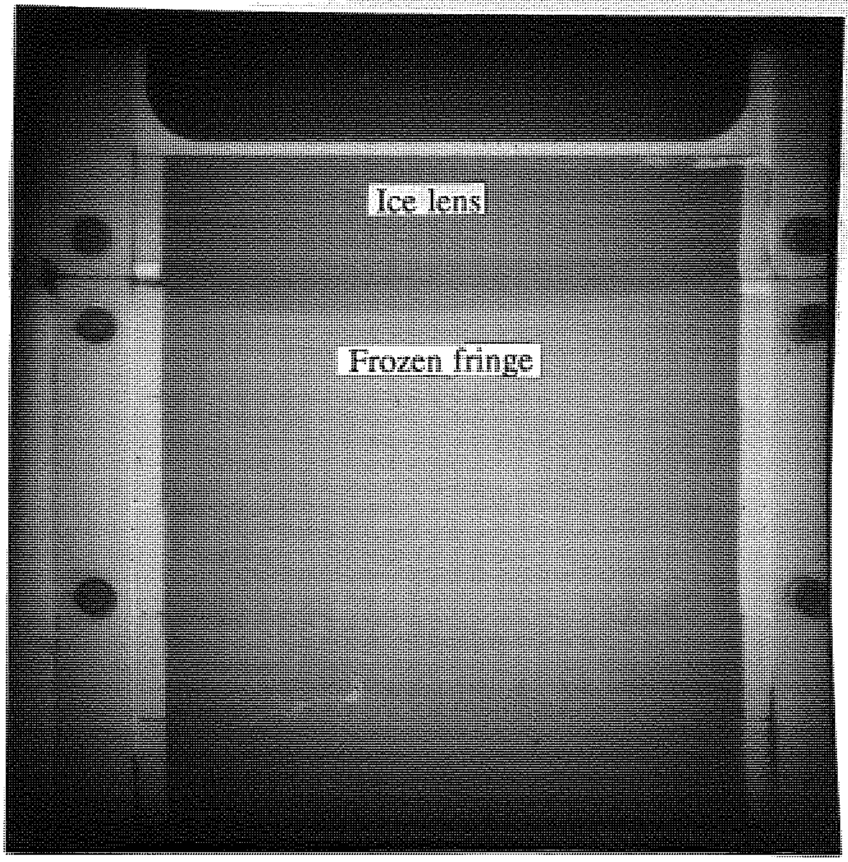

Plate 13 – Standardised Test (Time: 120 min, Heave: 1.1 mm, Temp.: –3.9 degrees C)

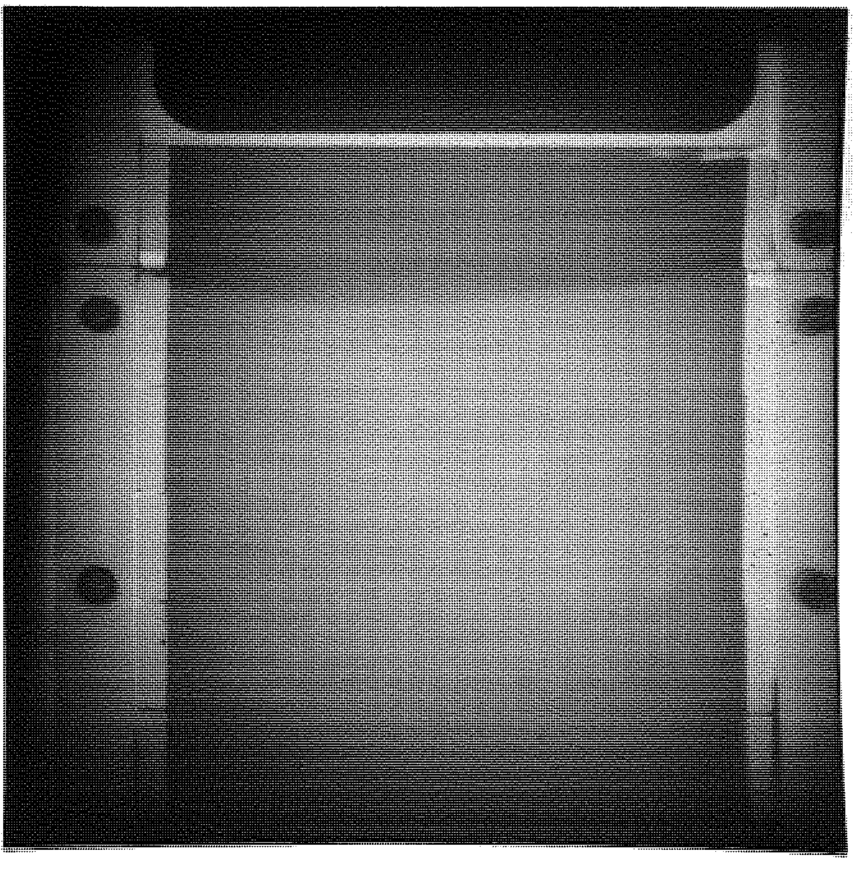

Plate 14 – Standardised Test (Time: 150 min., Heave: 1.9 mm, Temp.: –4.1 degrees C)

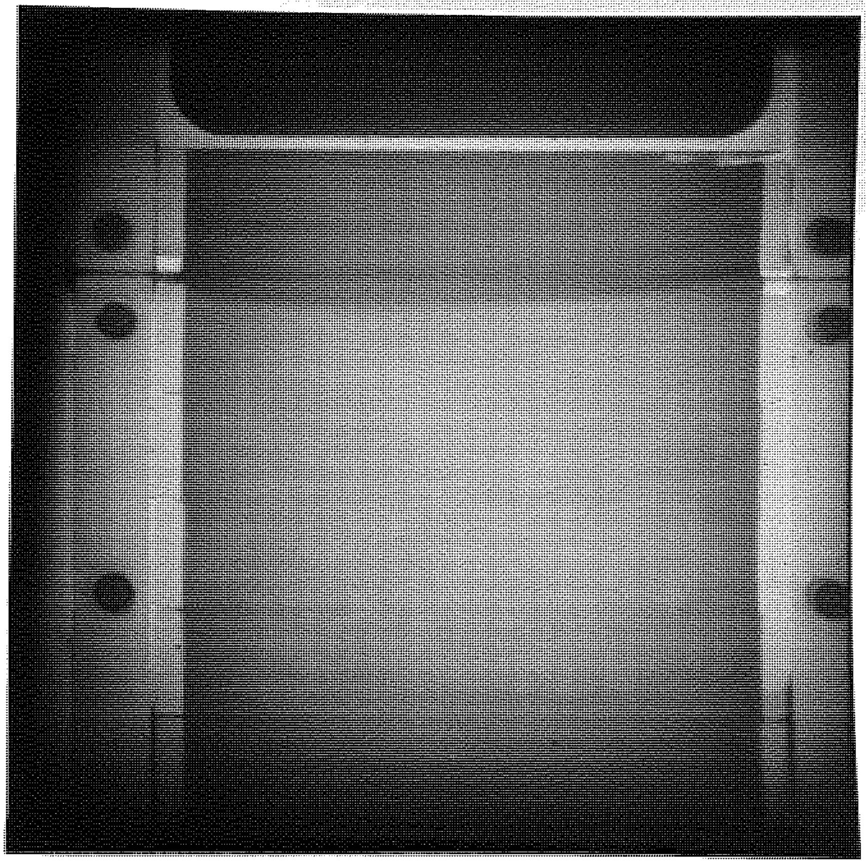

Plate 15 – Standardised Test (Time: 180 min., Heave: 2.0 mm, Temp.: –4.1 degrees C)

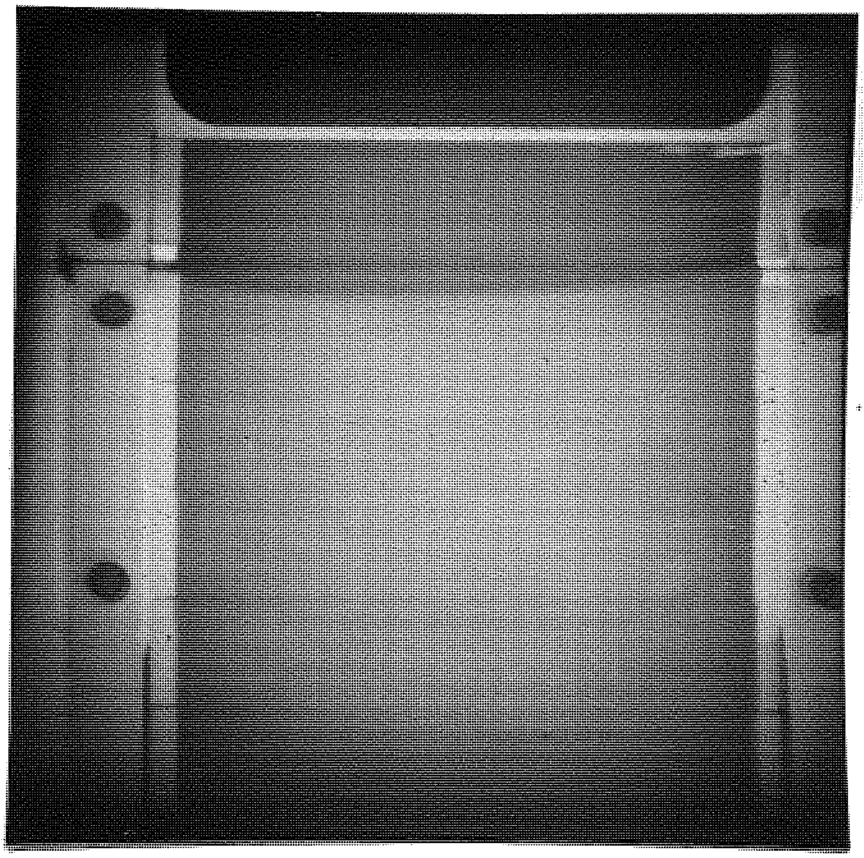

Plate 16 – Standardised Test (Time: 210 min., Heave: 2.1 mm, Temp.: –3.8 degrees C)

Plate 17 – Standardised Test (Time: 240 min., Heave: 2.1 mm, Temp.: –3.9 degrees C)

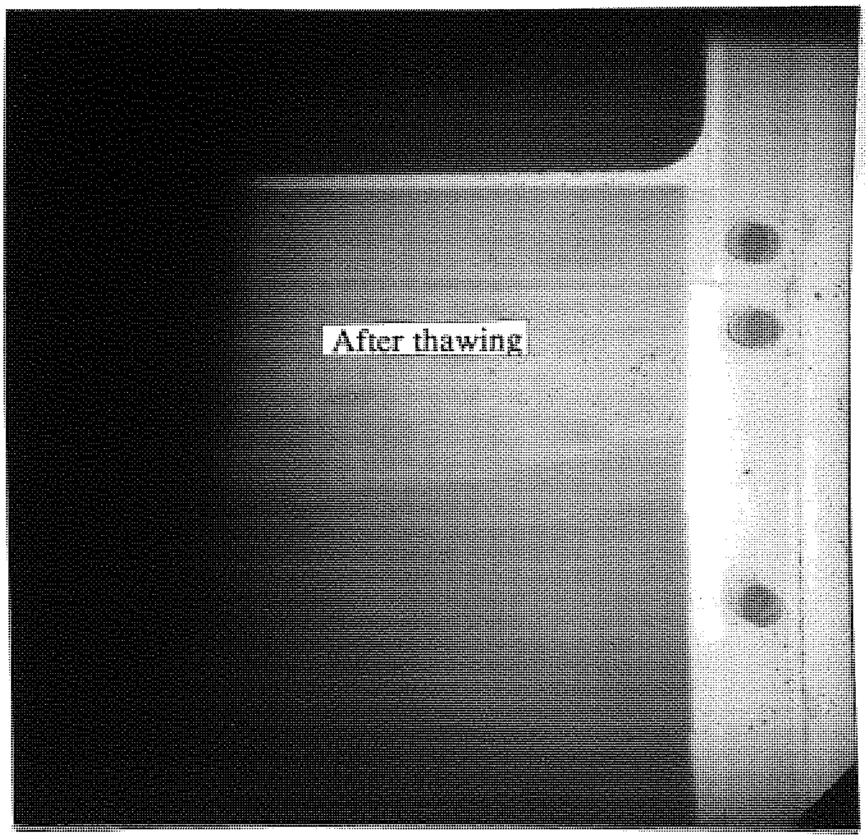

Plate 18 – Standardised Test (Time: 270 min., Heave: 0 mm, Temp.: 2.0 degrees C)

The beam used in the initial experiments was of diagonal orientation, in plan, in the reactor and penetrated the removable concrete shielding but did not enter the core of the reactor. This proved adequate, to give discernable radiographs of ice forming in the matrix, provided large reactor powers and exposure times were used. An additional limitation was that the cross-sectional area of the beam was too small to accommodate both the main cell and reference cell on one X-ray plate. The improved beam was obtained from a horizontal, through beam tube which passed through the reactor via the main and secondary thermal columns, as shown in figure 18. The cross-sectional area of the beam was compatible with the X-ray plate and the much higher neutron intensity enabled the exposure time to be greatly reduced. Table 4 gives a comparison of the two beams.

Gold foils, attached to carriers, were radiated at the anticipated specimen location to give the distribution of neutrons across the beam. Readings were taken across the beam at 25mm intervals at the beam centre and 75mm above and below it. The results are given in figure 27. Referring to figure 27, the shape of the plateau region of the graph was probably due to the shape of neutron flux in the graphite moderator. There was no apparent variation in the vertical direction over a distance of 150mm but the full intensity of the beam covered a width of only 100mm.

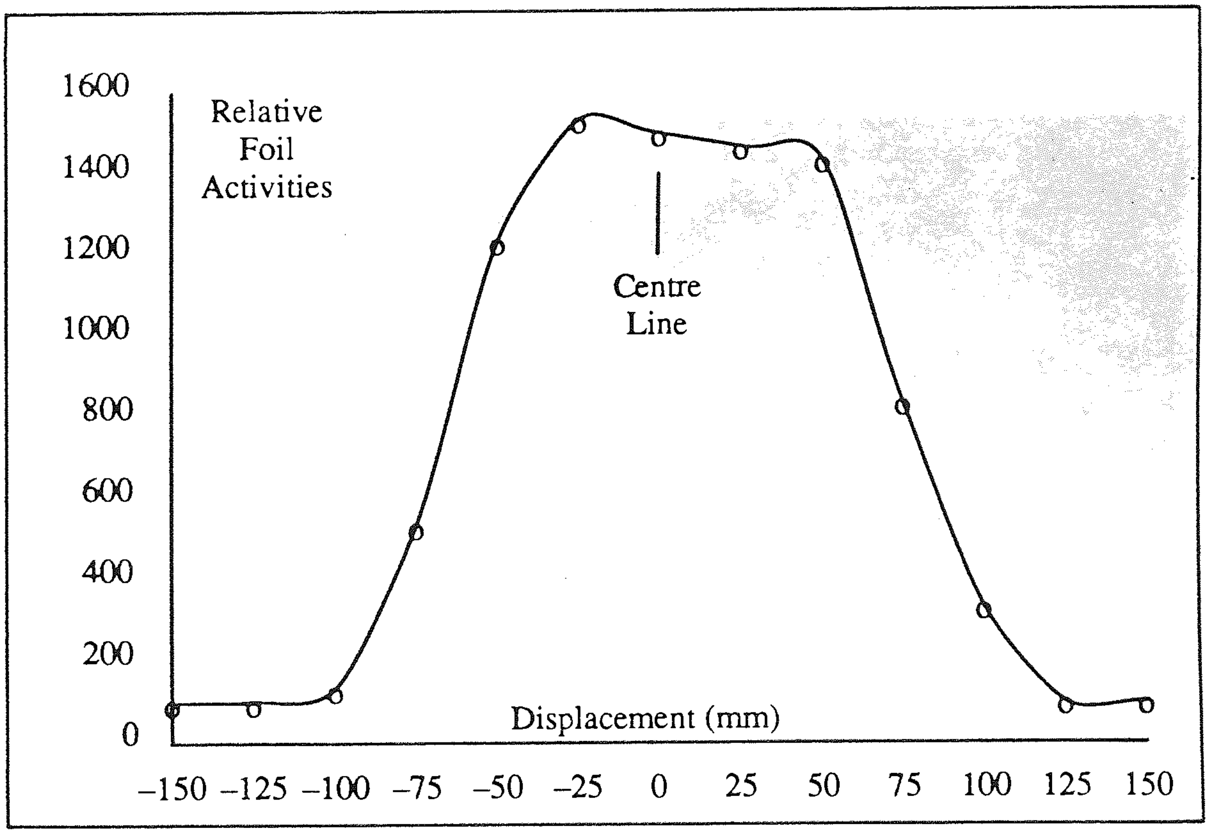

Figure 27 – Neutron Distribution – Beam 2.

Examples of radiographs produced with the two beams at the reactor powers, exposure times and neutron fluxes given in table 4 are shown in plates 19 and 20.. The overall

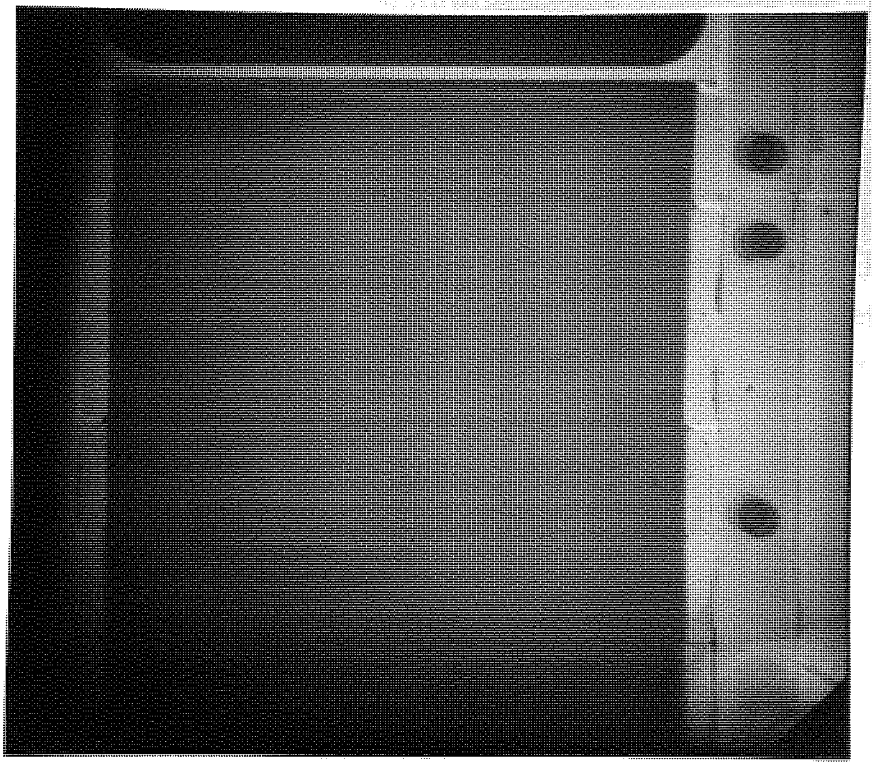

Plate 19 – Diagonal Beam – Radiograph

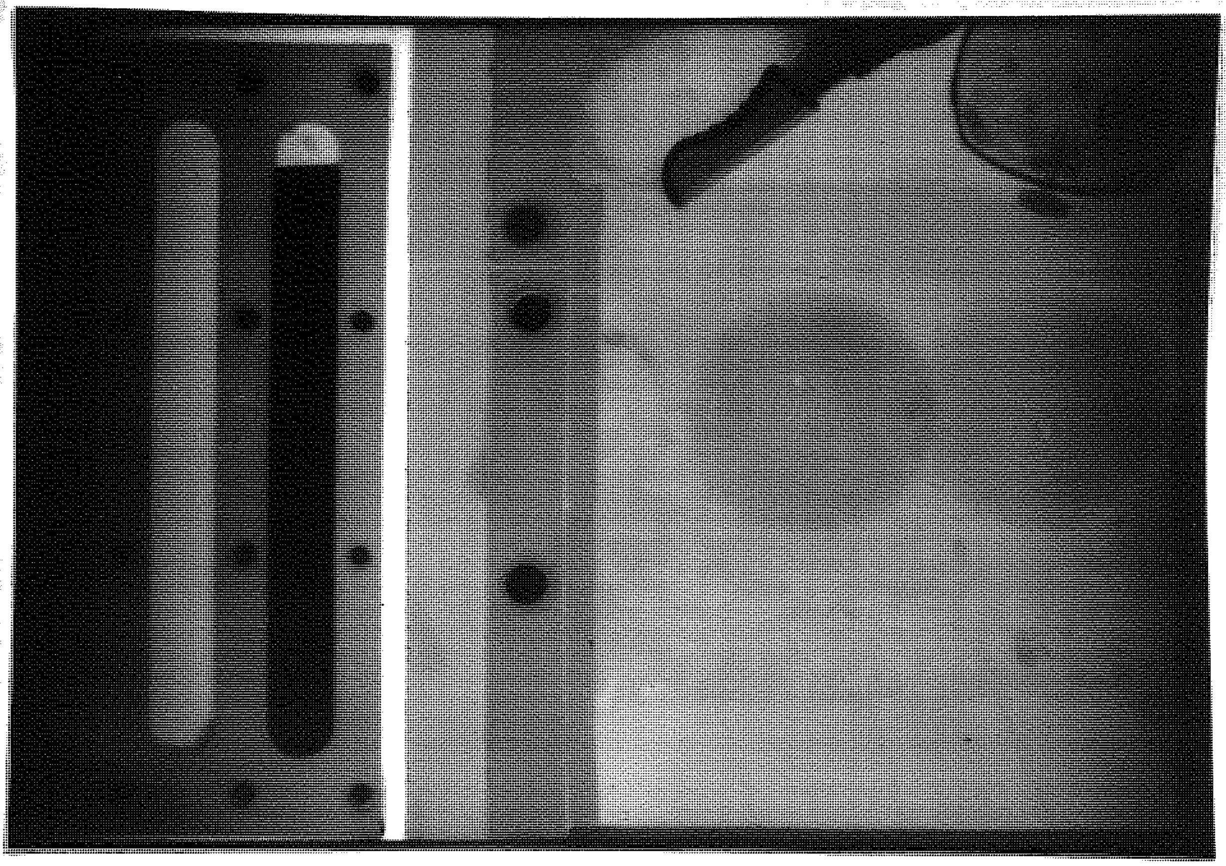

Plate 20 – Horizontal Beam – Radiograph

quality of the images compare well but plate 20 (result obtained with the horizontal beam) was produced with a much reduced exposure time and a lower reactor power. The surprising narrowness of the horizontal beam resulted in a blurring of the edges of the radiograph, an allowance was made for this effect in the subsequent analysis of the radiographs. Plate 19 (result obtained with the diagonal beam) illustrates the limitation of the cross–sectional area of the beam. Only half of the main cell and reference cell appeared on the radiograph compared with all of both cells in plate 20. The reference cell was identical for each beam and the main cell was filled with a matrix of snowcal and 10% water for the diagonal beam test and dry snowcal with two polystyrene hemispheres, to represent approximately 2% water content, for the horizontal beam test.The freezing head was removed for the test with the horizontal beam and, in its place, half a plastic clothes peg and a wrist watch were installed. The relevance of these everyday objects is discussed in section 5.3.10.2.

5.3.10.1 Modifications to Experimental set–up

The horizontal beam was of higher intensity and therefore required more radiation shielding. To accommodate this need, it was necessary to re–design the test set up.

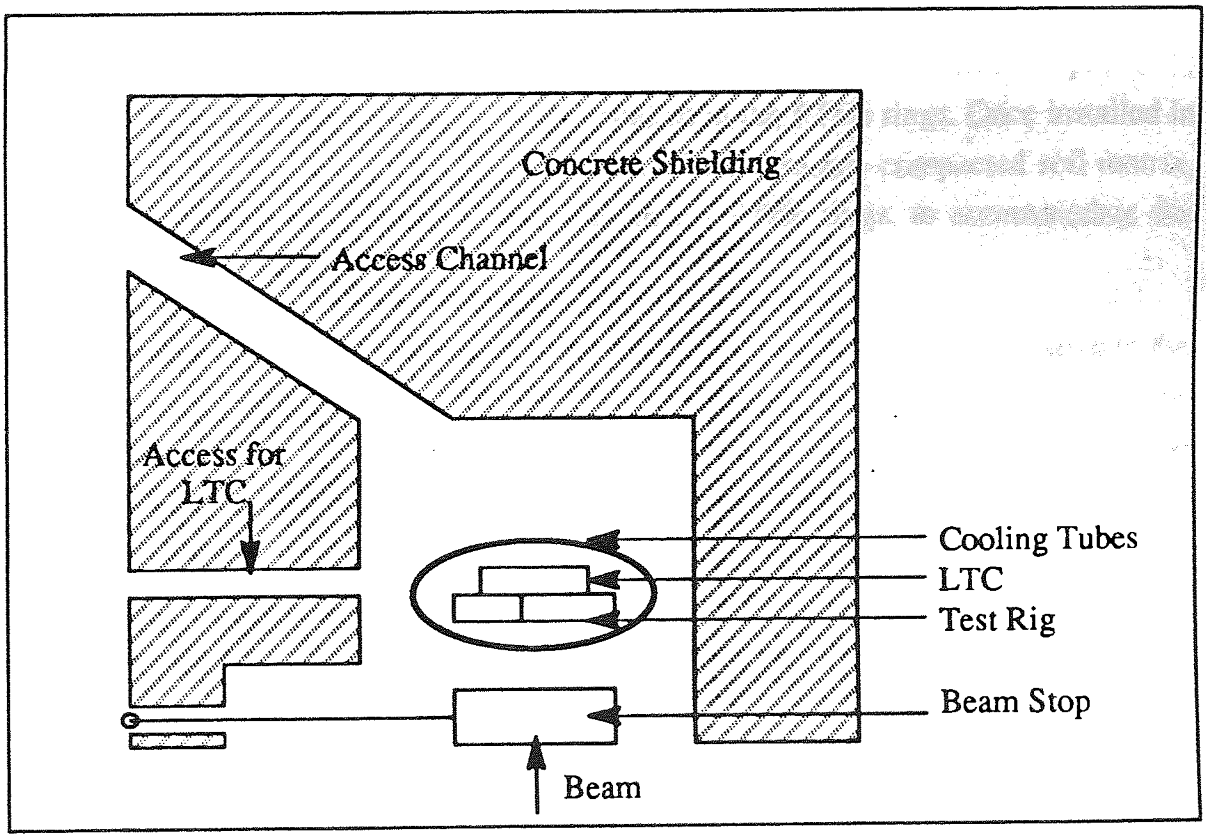

Figure 28 – Plan View of Cavity, Experimental Rig and Shielding.

The method of maintaining the cell at a constant temperature by installation in an upright fridge and the system of sliding the fridge, containing the cell and photographic plate, into the line of the beam were dispensed with. The cell was permanently positioned in the line of the beam and surrounded with concrete radiation shielding. The cavity, formed by the shielding, acted as thermal insulation for the cell. The air temperature in the cavity was lowered by circulating ethylene glycol/water mixture through a network of pipes surrounding the cell, and arranged to avoid covering the faces of the test cells. A slot, formed in a section of the concrete shielding, enabled the light tight (LTC) container, with X–ray plate and intensifying screen, to be located behind the cell and removed after irradiation. Suspended from the slot were rubber strips, set so that the LTC disturbed the strips which then fell back into place to thermally seal the passage. Another channel, formed in the shielding, carried the instrumentation leads and cooling tubes to the test rig and was thermally sealed using expanded foam spray sealant. Precise exposure times were achieved by the use of a beam stop, as depicted in figure 28 which gives a plan view of the cavity, experimental rig and shielding. Stages in constructing the test rig and positioning it in the cavity are shown in plates 21–26.

5.3.10.2 Modifications to Test Rig

To locate the psychrometer/thermocouple probes in the soil matrix the central and upper portions of the main cell had slots cut in the PTFE insulation to coincide with holes drilled in the PTFE rings, as shown in figure 29 and plate 27. The slots enabled the probes to move freely in the vertical direction when installed in the PTFE rings. Once installed in the rings the sensing part of the probes protruded into the pre–compacted soil matrix, which had small holes drilled, via the holes in the PTFE rings, to accommodate the sensing part of the probes.

The half a plastic peg and wrist watch, referred to in Section 5.3.10 were installed in the rig for the test radiograph so that the degree to which they absorbed neutrons might be visually assessed. It can be seen in plate 20 that the metal mechanisms inside the wrist watch contrast well with the thick rim of the plastic peg. This contrast was put to good effect in the rig by installing a pocket watch, on which the hands and hours were marked by 5mm lengths of 2mm diameter plastic tube so that the time when each radiograph was taken was permanently recorded on the radiograph.

5.3.10.3 Instrumentation

The water supply to the matrix was from a marriotte vessel. Within the vessel a polystyrene float, connected to a linear motion potentiometer, rested on the water. In this way any water uptake by the matrix was represented by a movement of the float which was registered by the potentiometer and recorded on a chart recorder.

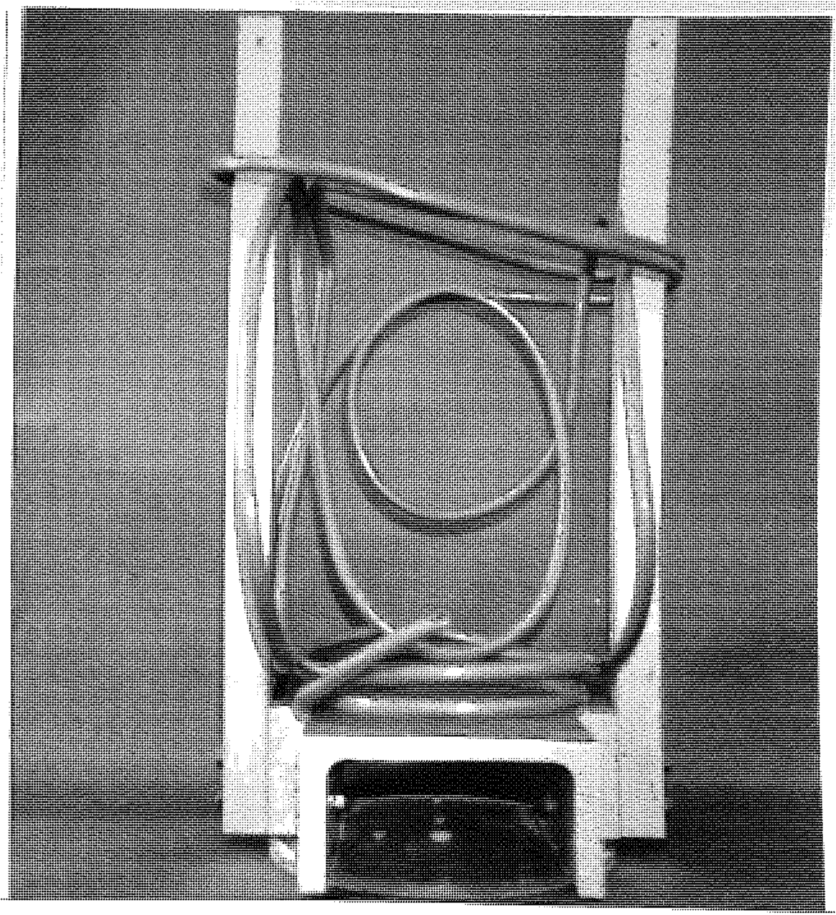

Plate 21 – Test Rig Frame and Cooling Tubes

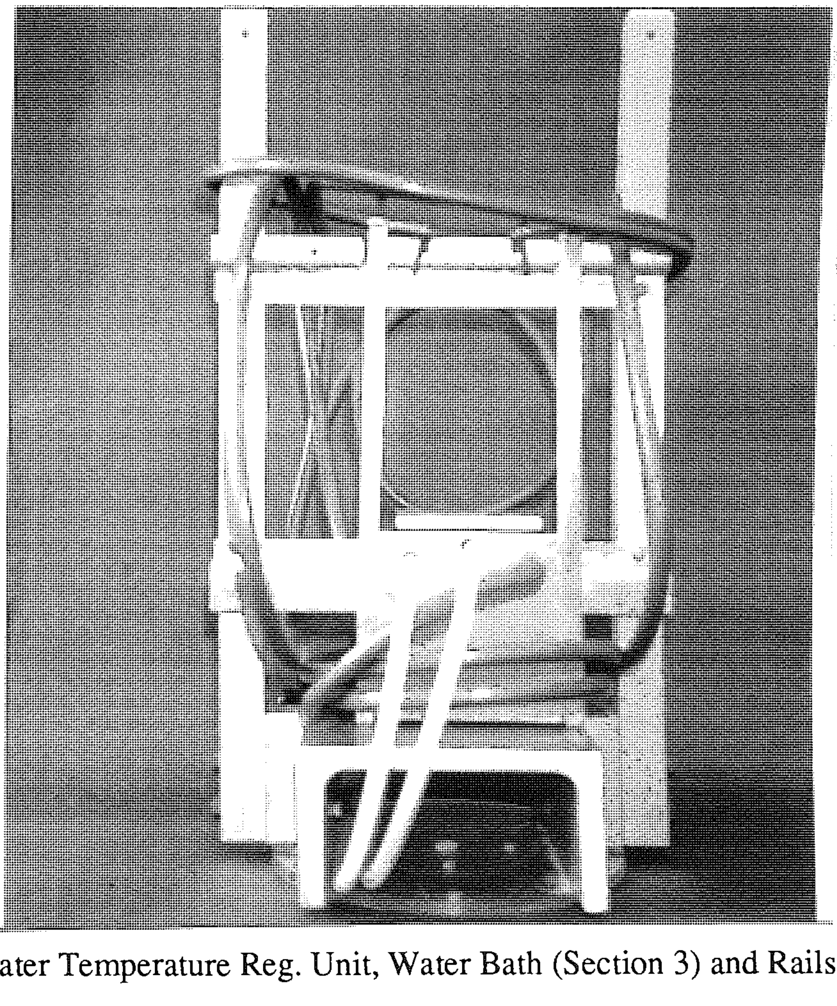

Plate 22 – Water Temperature Reg. Unit, Water Bath (Section 3) and Rails Positioned.

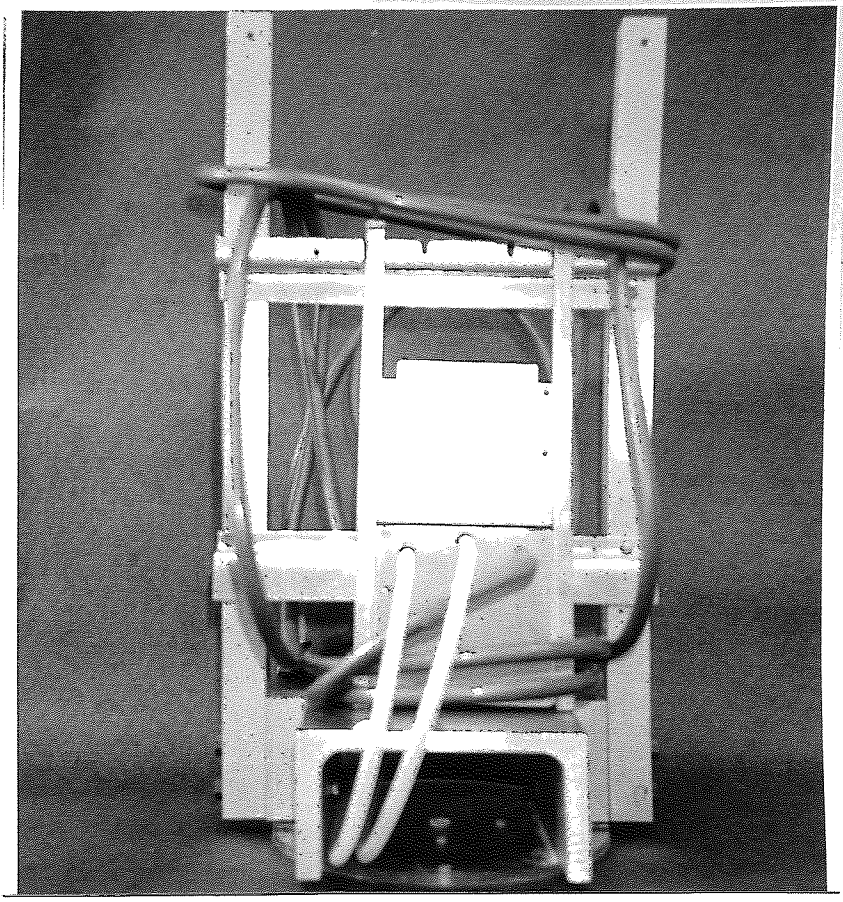

Plate 23 – Section 2 Positioned

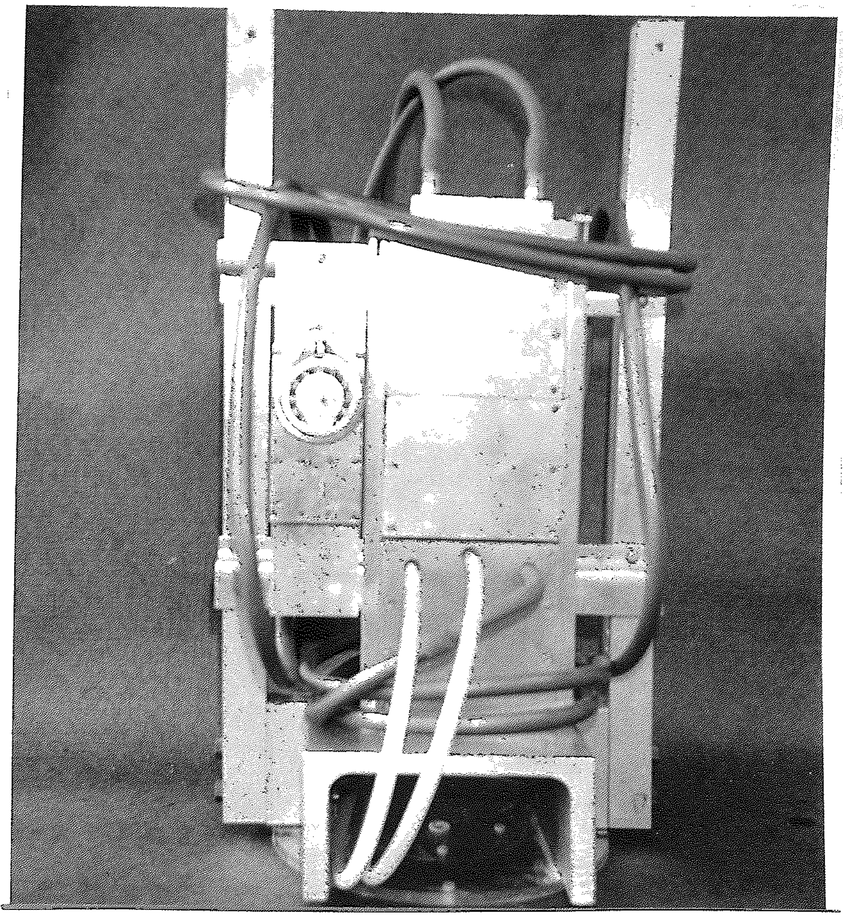

Plate 24 – Section 1 and Reference Cell Positioned

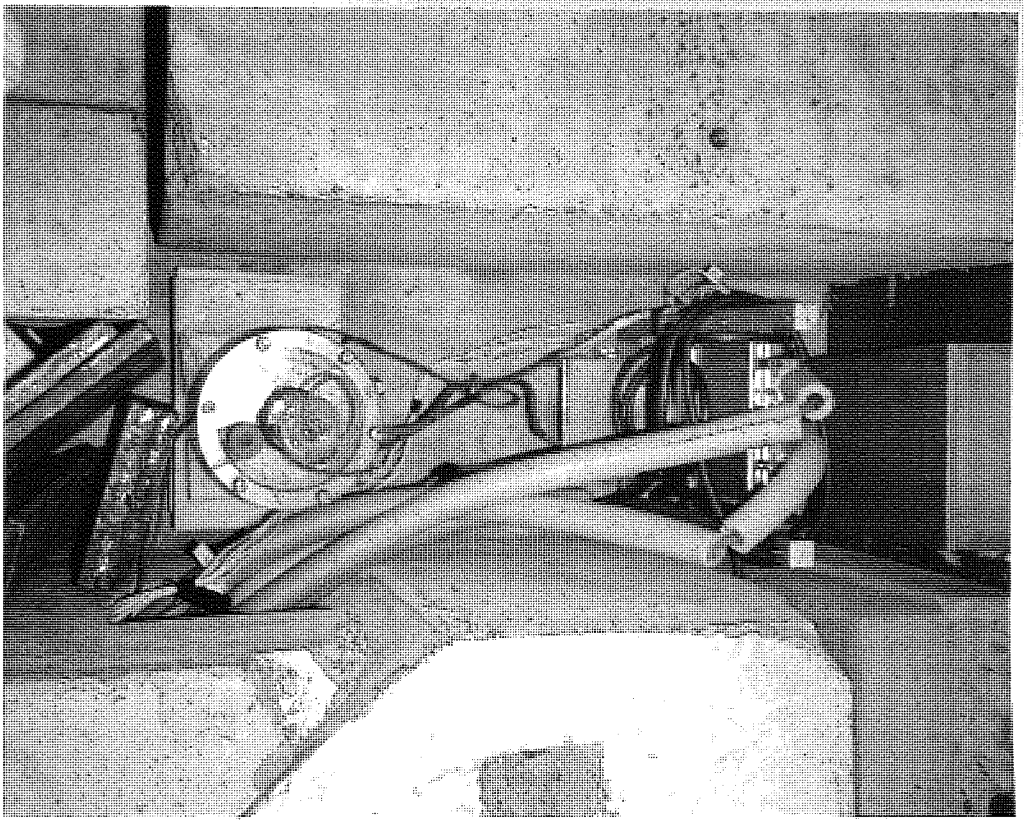

Plate 25 – Cavity and Test Rig

Plate 26 – Concrete Shielding to Cavity

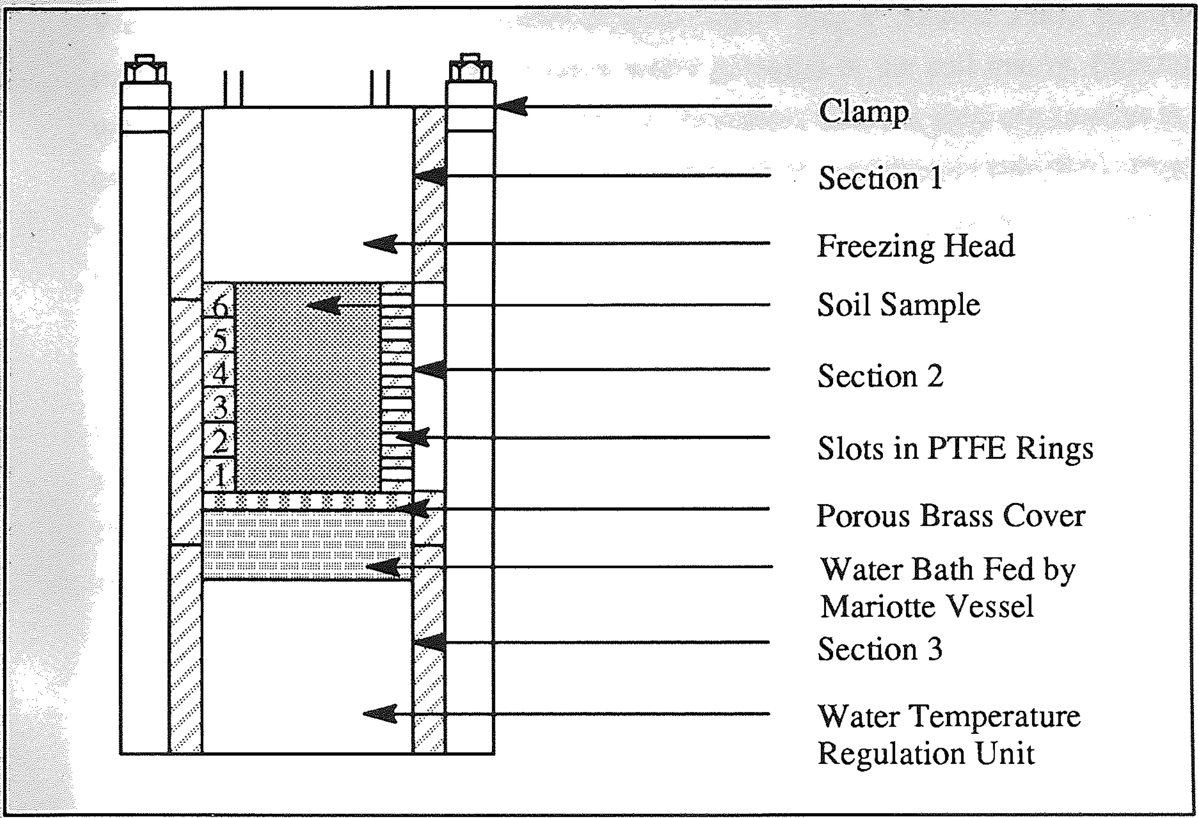

Figure 29 – Test Rig with Slots for Psychrometer Probes

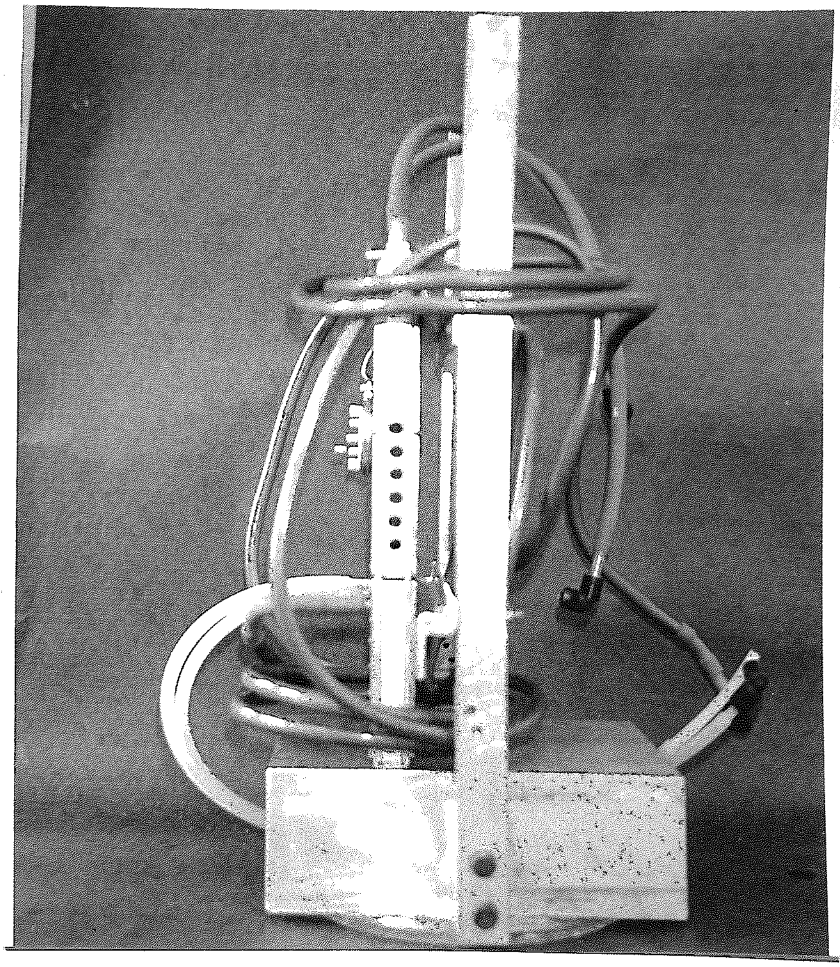

Plate 27 – Side View of Test Rig

Wescor PST 55–30 psychrometer/thermocouples and a Wescor PR55 psychrometric microvoltmeter were used to measure water potential in the soil matrix. Psychrometers were chosen in preference to soil water tensiometers because they are smaller in size, so causing less disruption to the soil, and are capable of operation at sub–zero temperatures without the problems of semi–permeable membranes associated with tensiometers containing ethylene glycol–water solution, discussed in 3.4.2. The psychrometers incorporated a small chromel/constantan thermocouple concentrically mounted in the centre of a hollow cylindrical stainless steel bulb, shown in figure 30. This design was selected as it minimised the effects of temperature gradients which could adversely affect the suction readings. Measurement of relative vapour pressure in snow using thermocouple psychrometers (121) orientated horizontally has shown a 200μm mesh stainless steel shield to be ideal for low temperature work. The single junction thermocouple permitted measurement of the local thermal gradients to enable correction of the suction readings. A calibration model for this type of psychrometer/thermocouple has been developed (52) and a modified computer program from the model, given in Appendix 2, has been used in these experiments to determine the appropriate suction values.

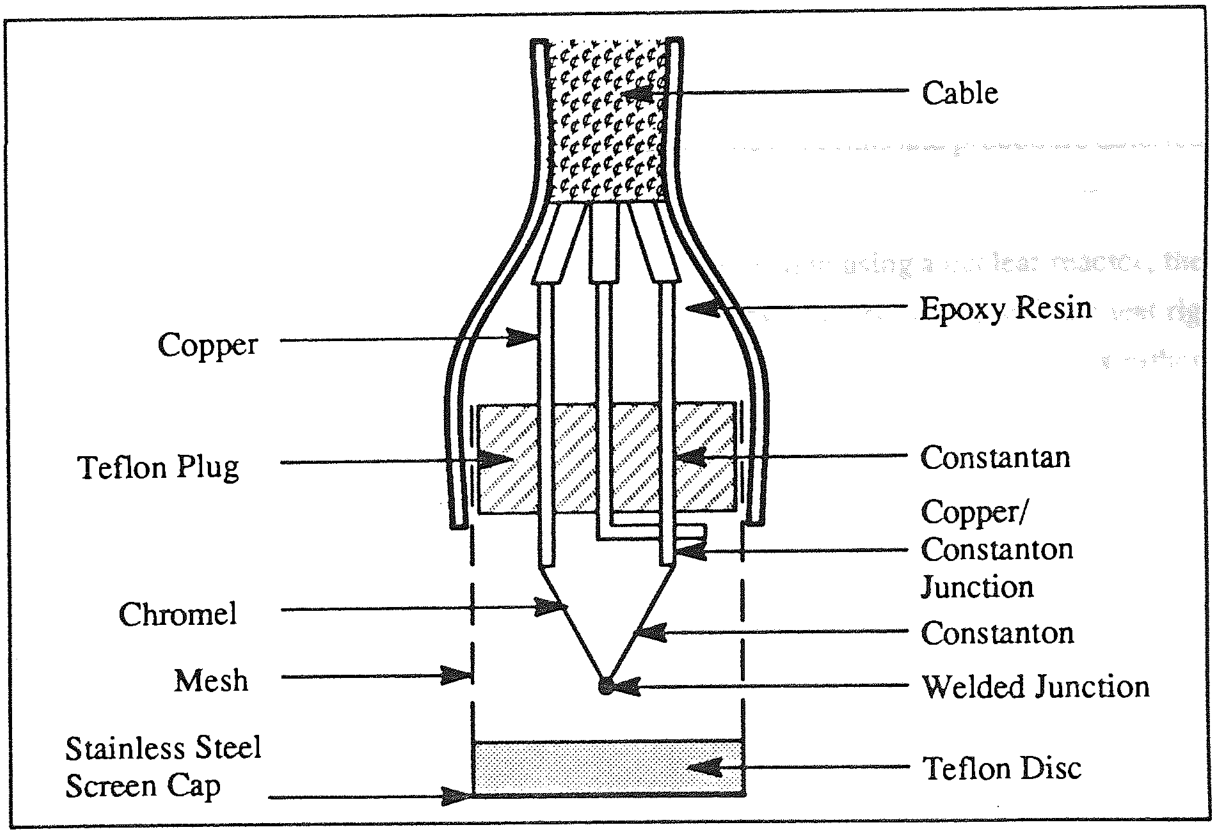

Figure 30 – Screen–caged Single Junction Peltier Thermocouple Psychrometer

The psychrometers utilised the peltier effect to measure water potentials. Water from the matrix was conducted through the bulb to the inner surface where it evaporated until the humidity reached 100%. An electric current was passed through the thermocouple for fifteen seconds which cooled the sensing junction slightly below ambient temperature so that water from the atmosphere condensed on the thermocouple. A cool time of 30–40 seconds has been used to good effect by other research workers (121) but reducing the time to 15 seconds, which is also a commonly used cool time (52), had little adverse effect on the readings. After cooling the condensed water evaporated which again cooled the junction. This time however the cooling was a function of the rate of evaporation which is related, via the vapour pressure of the atmosphere, to the water potential of the matrix. Copper/constantan thermocouples were located alongside the psychrometers to record the matrix potential throughout the test. The electrical resistance of the soil between the psychrometer probes was determined throughout the test to identify ice in the matrix. This was achieved through connections to the stainless steel shields of the psychrometers. The shields were insulated from the rest of the probe by a plastic casing and from each other by the PTFE rings which housed them.

5.3.10.4 Test 1

The test procedure was unchanged from that described in Section 5.3.8. To obtain radiographs the LTC was initially positioned behind the cell, the beam stop was then removed, so that the neutron beam fell on the cell, and replaced after the selected exposure time of 18 seconds had elapsed. After the LTC had, radioactively cooled down, it was removed and the photographic plate developed using the materials and procedure detailed in Appendix 1.

Because of the economic and physical constraints involved in using a nuclear reactor, the test was limited to two 3 hour periods where radiographs could be taken, with the test rig left running overnight. Ideally the test should have been allowed to run for days rather than hours so that the amount of heave, and the associated water uptake, could be related to that recorded in TRRL frost heave tests.

5.3.10.5 Results

Psychrometer readings, electrical resistance readings and temperature readings are given in table form in Appendix 3. The radiographs are shown in Appendix 4.

5.3.10.6 Discussion of Results

The radiographs depict the freezing front penetrating into the soil with an associated small amount of heave. The reactor authorities were concerned about unmonitored leakage from the rig overnight and, therefore, the water supply was disconnected but the cooling arrangements were left unaltered. The test duration can, hence, be thought of as two three hour periods.

As the soil temperature decreased the suction increased until zero–offset readings, which are a measure of temperature gradients within the probes, exceeded a value of 60, at which point values were no longer considered realistic. Work by other researchers (52) has shown that internal temperature gradients, which give zero–offset readings in excess of 60 can result in inaccurate suction readings. To avoid this problem the freezing process would have to be performed at a much lower rate, so that equilibriation periods for the psychrometers would be more acceptable. Increasing the cooling time for the probes from 15 seconds to 45 seconds did not make any appreciable difference to the readings.

Once the temperature gradient was established in the soil the psychrometer readings remained consistent throughout the test. Values for electrical resistance in the soil increased dramatically in the frozen zone and were also consistent throughout the test.

The temperature gradient was non–linear, due to inadequate insulation on the front and back faces of the test cells. This situation was, however, unavoidable as to insulate the faces would have restricted access for the neutron beam to the sample

5.3.11 Improved Rig Design (Test 2)

To obtain a more uniform temperature gradient in the soil matrix the test rig, with cooling pipework was encased in a 340mm x 340mm x 480mm insulated box, shown in figure 31. To reduce the effects of radiation scatter within the box, and to provide insulation, the sides of the box were fashioned out of plywood sections filled with parafin wax. At the front of the box a 5mm PTFE window provided access for the neutron beam. The LTC was able to pass in and out of the box by means of a vertical slot, aligned with the channel formed in the shielding. A hollow polystyrene sleeve formed a thermal seal between the box and shielding, through which the LTC could pass. Despite this modification the experimental procedure remained unchanged.

5.3.11.1 Results with Improved Rig design

Psychrometer readings, electrical resistance readings and temperature readings are given in table form in Appendix 3. The radiographs are shown in Appendix 4.

5.3.11.2 Discussion of Results

The cooling pipework enabled a more uniform temperature gradient to be established in the soil. The psychrometer readings, as in test 1, were considered unrealistic when zero–offset values exceeded 60 and , once the temperature gradient was established, were consistent and agreed closely with readings in test 1. Electrical resistance readings increased dramatically in the frozen zone and were also consistent with test 1.

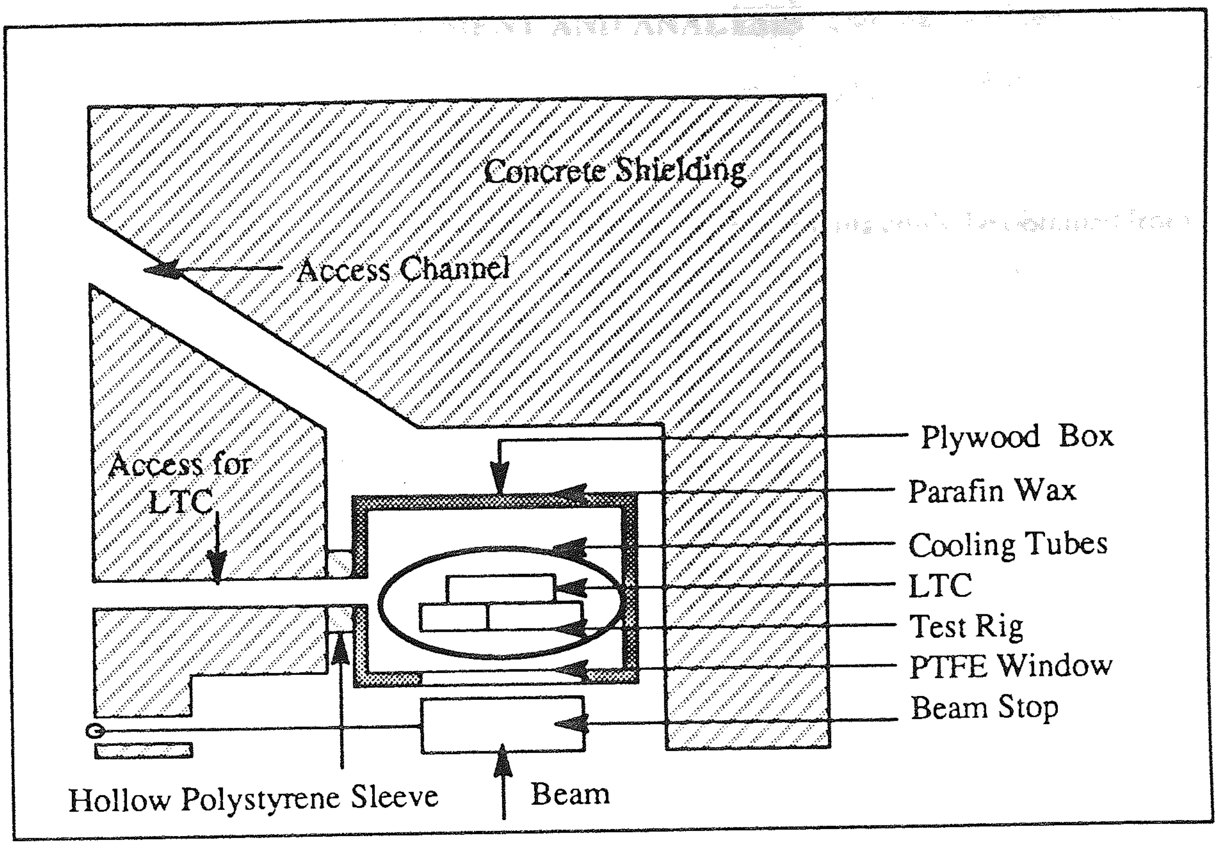

Figure 31 – Improved Test Rig.

6 RADIOGRAPH ENHANCEMENT AND ANALYSIS

6.1 Introduction

In order that a systematic and reliable evaluation of water contents could be obtained from the radiographs, the images were digitised, reformed using image analysis computing software and enhanced to accentuate variations in water content throughout the matrix. The matrix, depicted on the images, was then divided into 263 compartments each compartment representing 10 x 10 spatially ordered picture elements (pixels) and a number corresponding to the grey level allocated to each compartment. The data was then evaluated numerically to give the water contents. Given that only six psychrometers could be used in the matrix, the division of the matrix into 263 compartments was considered adequate to provide suitable data for the water contents corresponding to each psychrometer location.

6.2 Digitising

Contact prints were made of the radiographs (negatives) and 35mm slides (transparancies) made of these prints. The transparencies were scanned in a System P–1000 high speed, digital, photoscan microdensitometer (122). A schematic diagram of the densitometer is given in figure 32. The transparencies were mounted over a square opening in the rotating drum of the scanner. The transparency was then fully scanned by a combined movement of the source / receiver assembly (Y direction) over the rotating drum (Xdirection). The size of the soil matrix on the original matrix was 72.5mm x 84mm and on the 35 mm slides this was reduced to 15mm x 17.5mm. The 35mm slides were scanned with a spot size of100 μm (0.1mm) and hence the soil matrix area was covered by 150 x 175 pixels. Thus each pixel represents an area of 0.5 mm x 0.5 mm on the original negative.

The receiver in the densitometer is a photomultiplier which responds electronically to the component of the illuminating beam transmitted through the image. Information for each pixel is passed from the photomultiplier to an electronic system which performs an analog to digital conversion on the information received. The scanner uses a light density measurement range of 0 –3, and through the analog to digital conversion, the density data is recorded on magnetic tape in binary form and is expressed as 256 integer grey levels. White on the negative was set to 0 and black to 255. Therefore the reference cell with 100% water content had higher digital count values than those of the 0% water reference cell. From the scanned data, stored on magnetic tape, the images were entered for analysis on an International Imaging Systems (I2S), system 575 software, digital imaging processing system (version 3.1) (123).

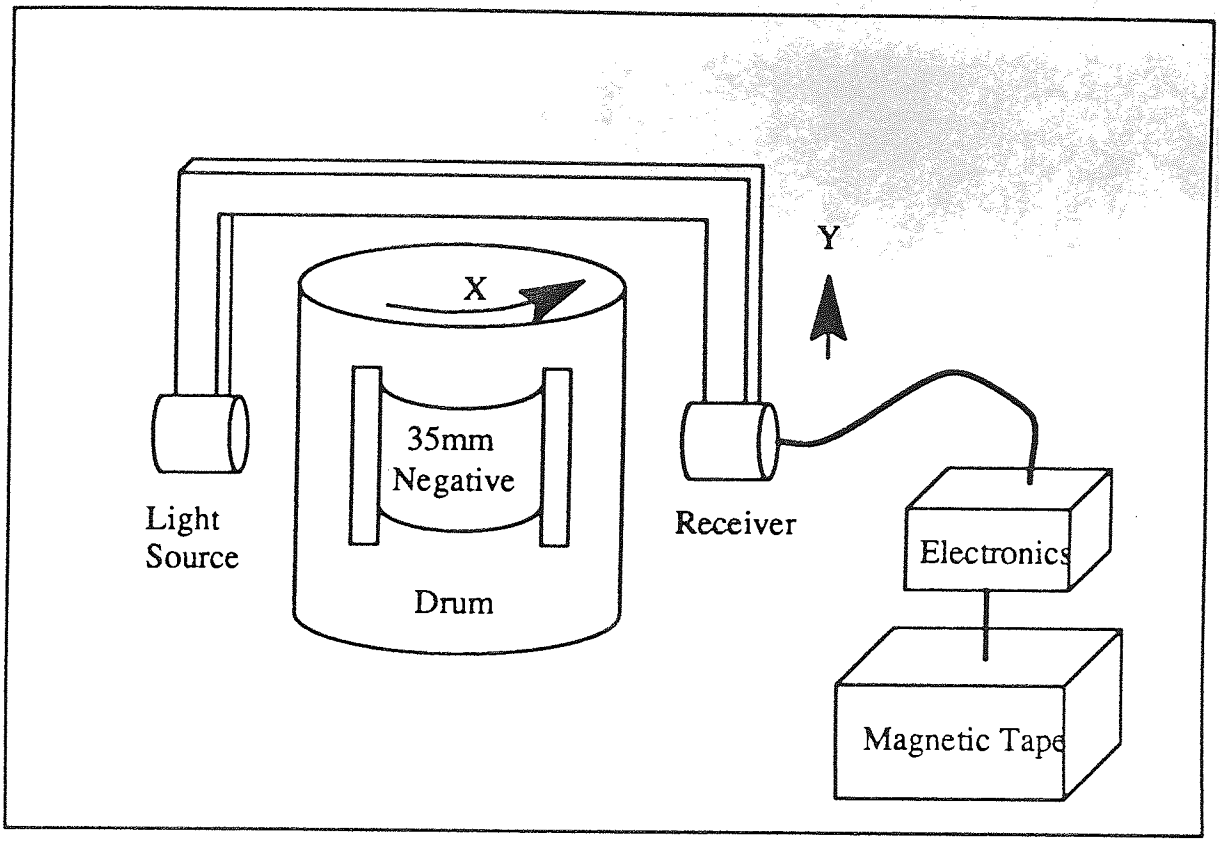

Figure 32 – Schematic Diagram of a Densitometer.

6.3 Normalising

To account for any differences in exposure, printing and scanning the frames were individually normalised. The first stage in the process was to geometrically register all the displayed images relative to the first image, which has been obtained from equilibrium matrix conditions before freezing had been initiated. This was achieved by invoking the 'Warp' routine available on the imaging system.

The rectangular images produced using the rectangular neutron beam tube are blurred at the edges due to the narrowness of the neutron beam, radiographs for which are given in Appendix 4. With the images geometrically aligned, this effect could be corrected by numerically dividing the values in subsequent images by the values in the first (mask) image to give an effect consistent with a uniform radiation exposure across the beam. The initial series of radiographs are given in plates 28–42 and the normalised images in plates 43–56.

6.4 Enhancement

To utilise the full range of display tones available (0 to 255) the range of image values was uniformly expanded. For any one frame the digital counts less than those within the 0% water reference cell were set to zero (black) and those within the 100% water reference

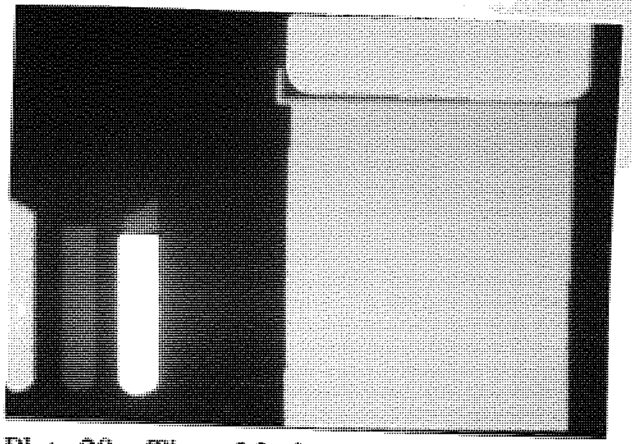

Plate 28 – Time: Mask

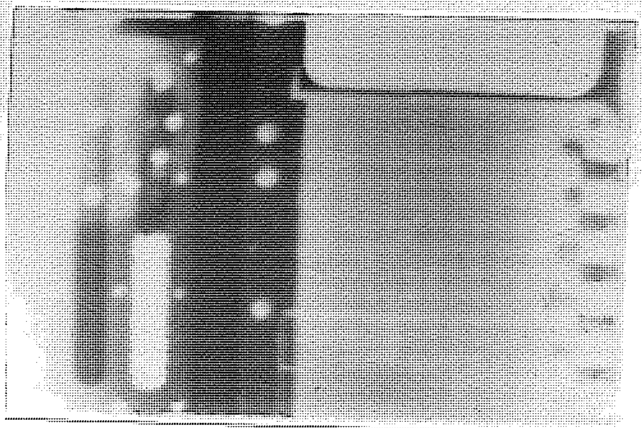

Plate 29 – Time: 0 minutes

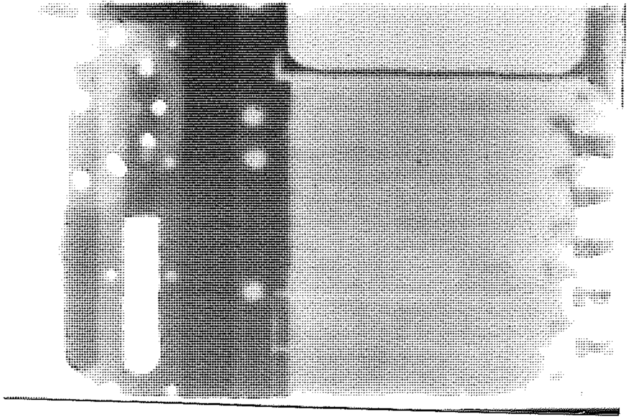

Plate 30 – Time: 15 minutes

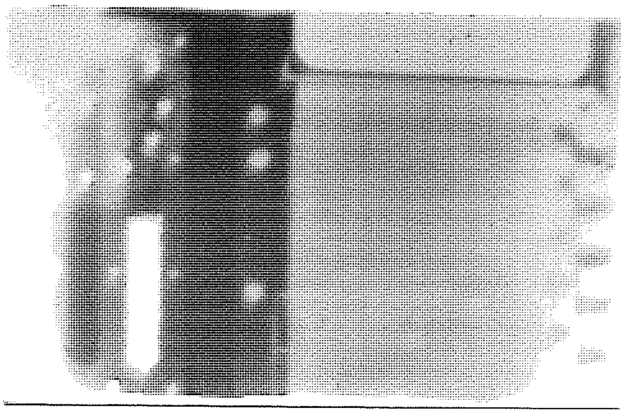

Plate 31 – Time: 30 minutes

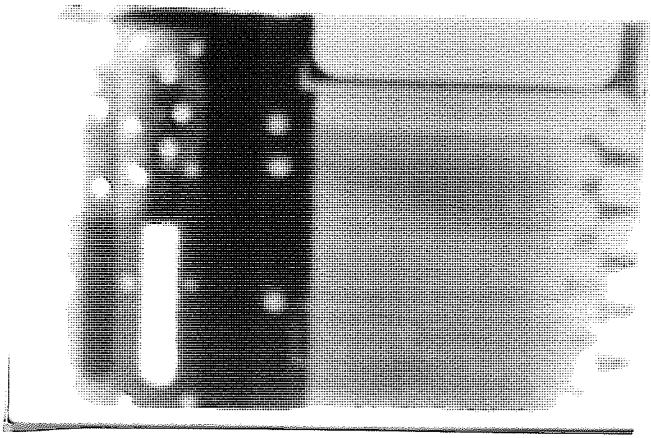

Plate 32 – Time: 54 minutes

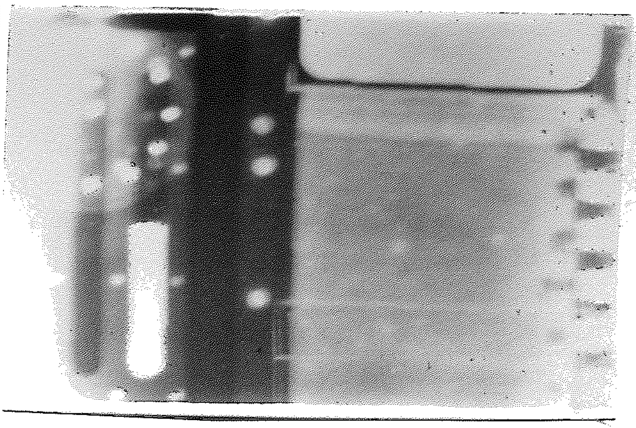

Plate 33 – Time: 85 minutes

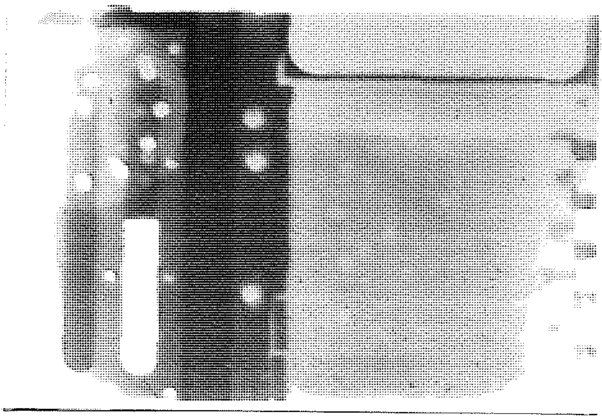

Plate 34 – Time: 130 minutes

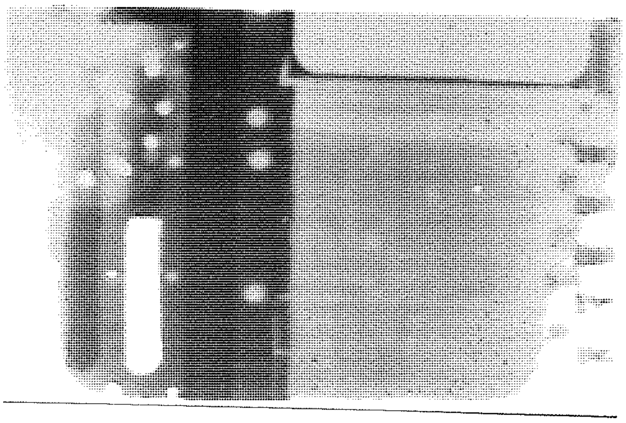

Plate 35 – Time: 167 minutes

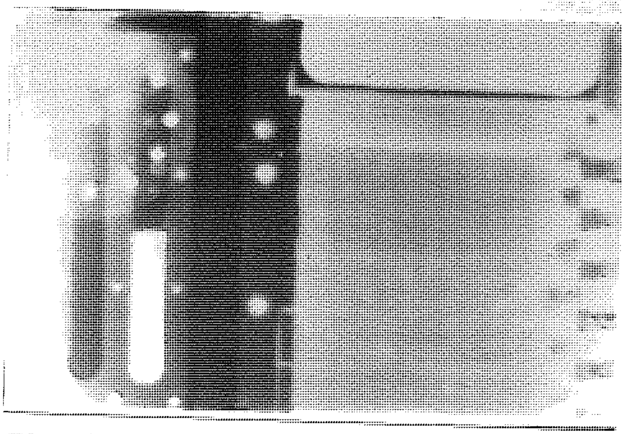

Plate 36 – Time: 219 minutes

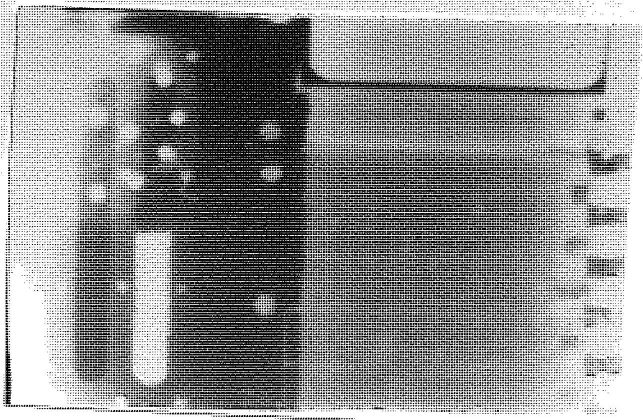

Plate 37 – Time: 1155 minutes

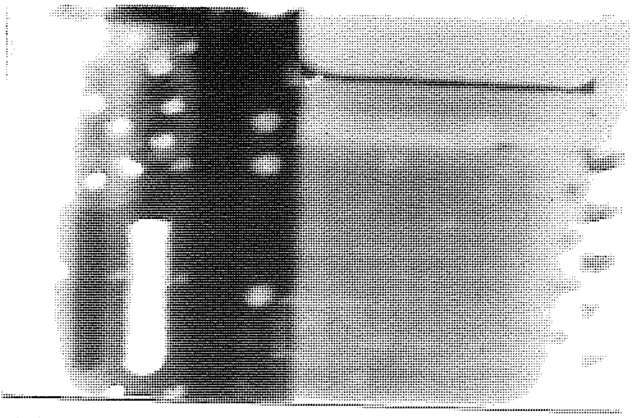

Plate 38 – Time 1218 minutes

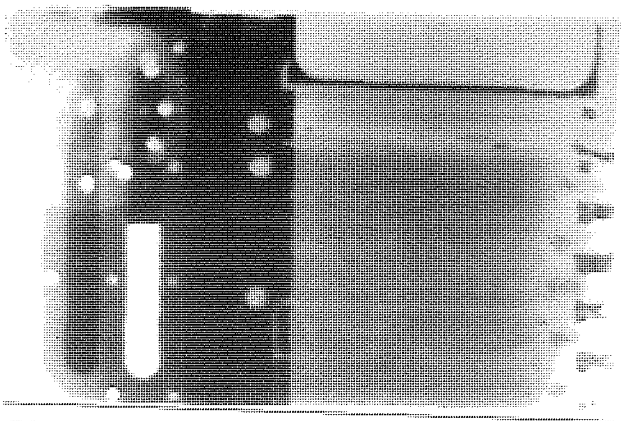

Plate 39 – Time: 1241 minutes

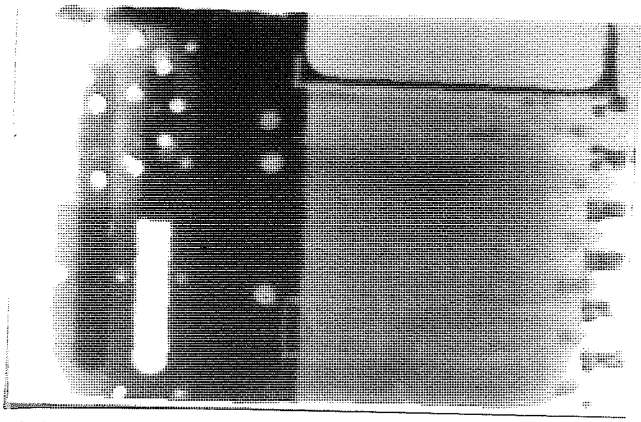

Plate 40 – Time: 1267 minutes

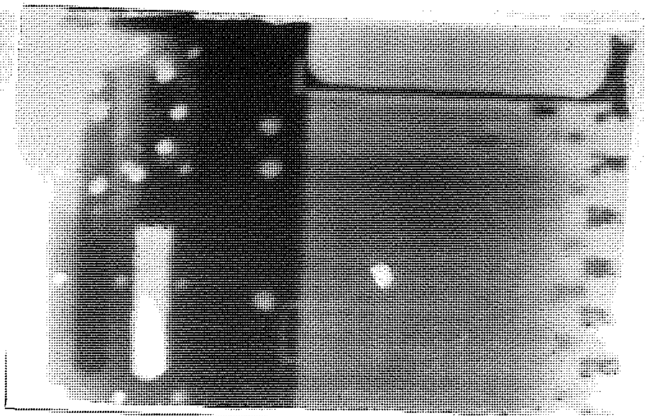

Plate 41 – Time: 1301 minutes

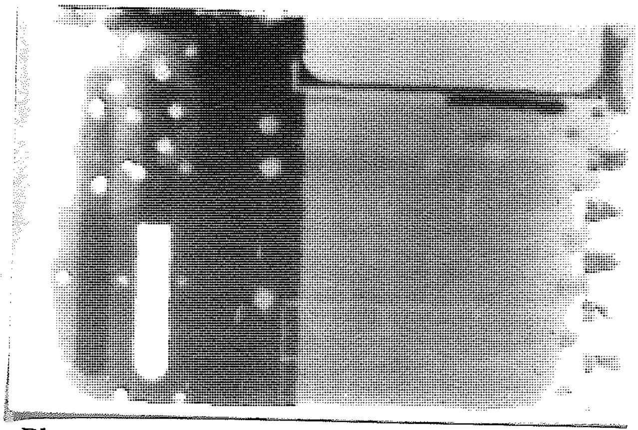

Plate 42 – Time: 1391 minutes

Plate 43 – Normalised, Time: 0 minutes

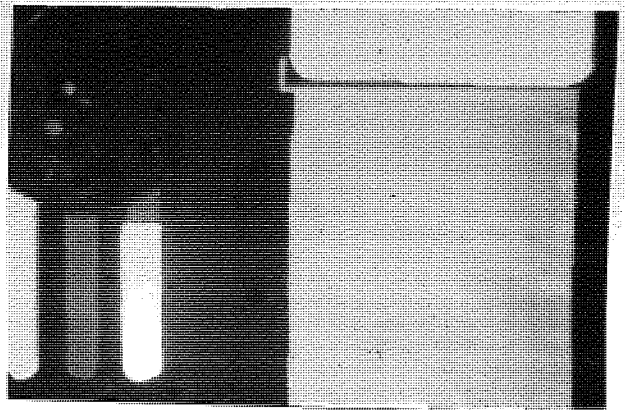

Plate 44 – Normalised, Time: 15 minutes

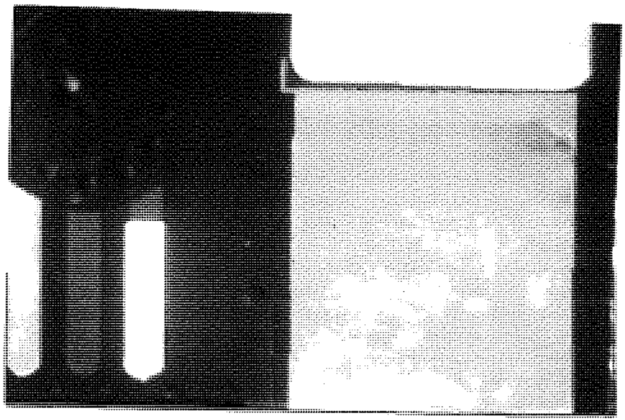

Plate 45 – Normalised, Time: 30 minutes

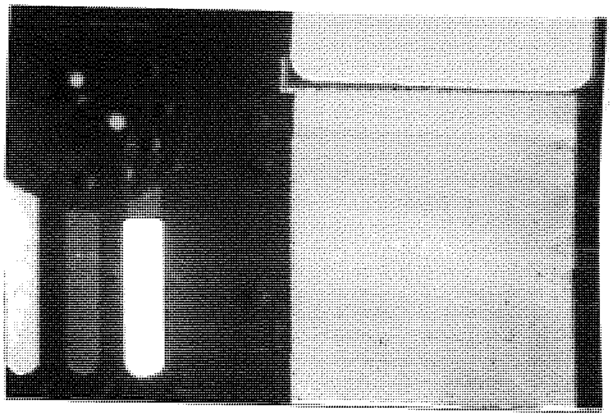

Plate 46 – Normalised, Time: 54 minutes

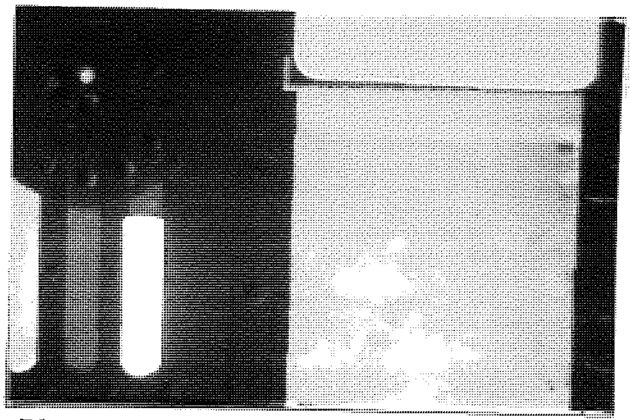

Plate 47 – Normalised, Time: 85 minutes

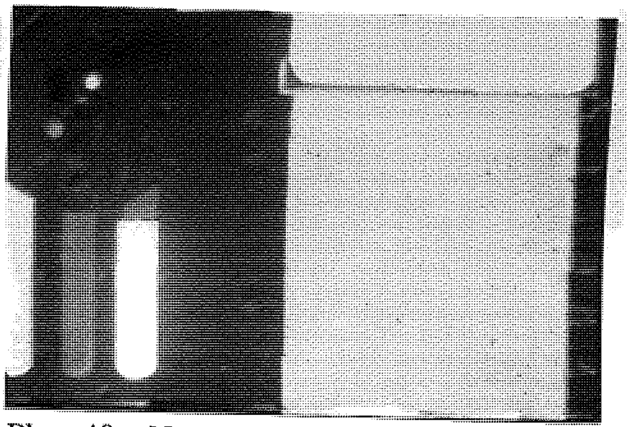

Plate 48 – Normalised, Time: 130 minutes

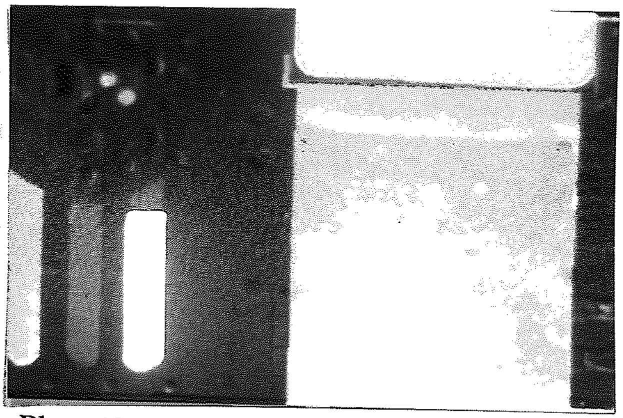

Plate 49 – Normalised, Time: 167 minutes

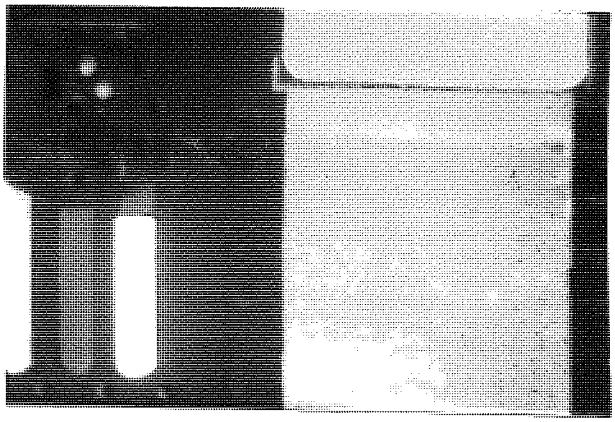

Plate 50 – Normalised, Time: 219 minutes

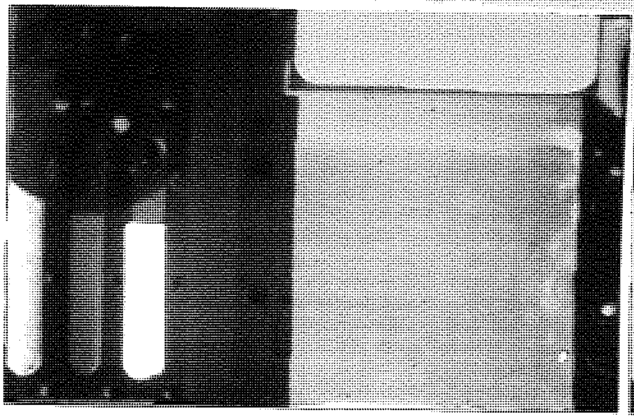

Plate 51 – Normalised, Time: 1155 minutes

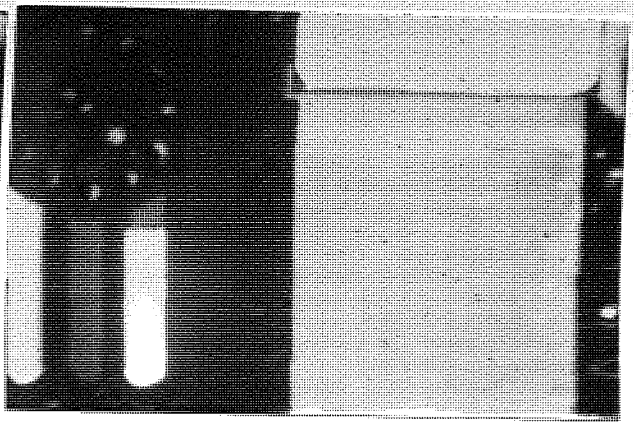

Plate 52 – Normalised, Time: 1218 minutes

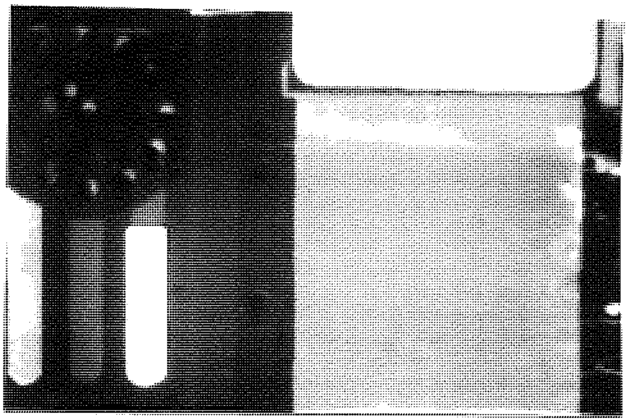

Plate 53 – Normalised, Time: 1241 minutes

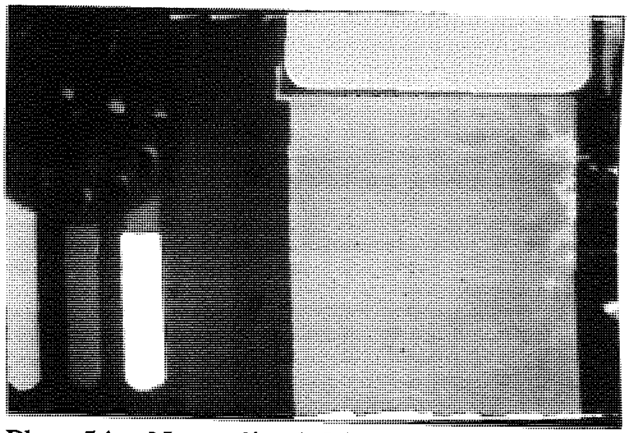

Plate 54 – Normalised, Time: 1267 minutes

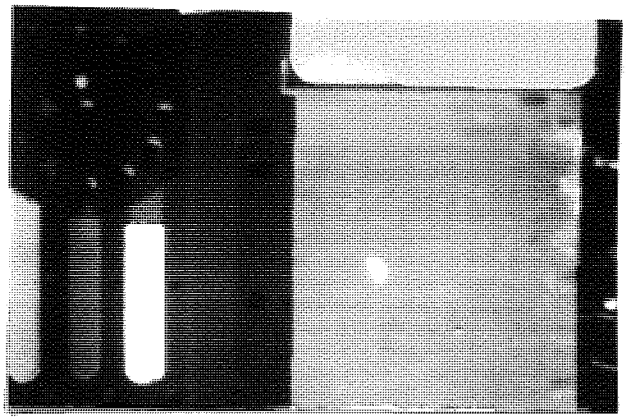

Plate 55 – Normalised, Time: 1301 minutes

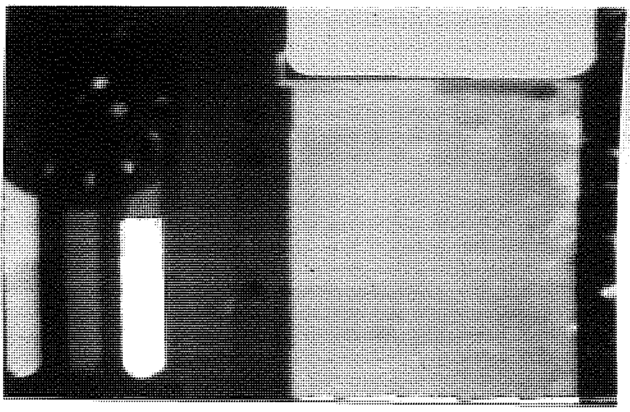

Plate 56 – Normalised, Time: 1391 minutes

cell was set to 255 (white) to produce an enhanced black and white image. Any values which lay within these extremes were then linearly stretched in accordance with equation 37 so that the new linear count became:

$$Xn = ((X - X0)/(X100 - X0)) \times 255 \quad \text{.......(37)}$$

where:

Xn = New, normalised digital count.
X = Old digital count.
X100 = Digital counts of 100% water reference cell.
X0 = Digital counts of the 0% water reference cell.

The enhanced images are given in plates 57–70. In this way the soil matrix areas with water contents of 0% to 100% were enhanced to give a possible range of 256 grey levels.

6.5 Visual Enhancement

The human eye can discriminate many more shades of colour than it can tones of grey. Therefore, in order that the water content variations could be more easily seen , the frames were density sliced in colour to give false colour images. Different colours were assigned to steps of 25 digital counts, ranging from red for levels 0–25 inclusive and blue for levels 225–255 inclusive.

As there were slight variations in the exposure and developing with each image, the water content values were represented by slightly different digital counts in each image. To counter this effect the water content reference cells were used to adjust each image so that water contents were accurately depicted by given digital counts and hence, in the density sliced images, by given colours.

The density sliced images are given in plates 71–84.

6.6 Data Output

Data counts from the normalised and enhanced images were averaged for each compartment over the radiograph area. Averaged values for the matrix and reference cells included values from the test rig, at the edges, and hence these values were discarded. The remaining matrix area was then sectioned according to the psychrometer locations and the values averaged to provide one value of water content per psychrometer per radiograph.

The water content values for the matrix and reference cells are given in the tables of Appendix 3.

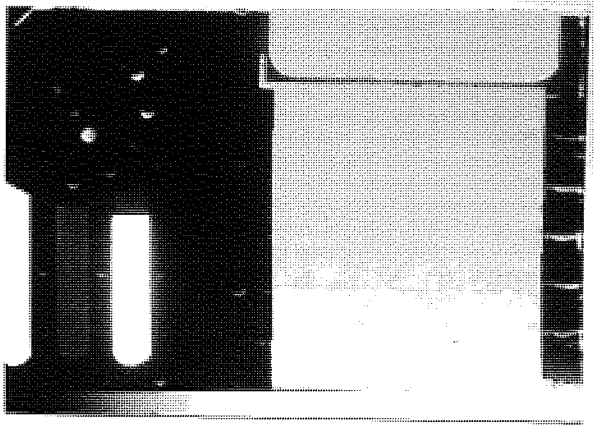

Plate 57 – Enhanced, Time: 0 minutes

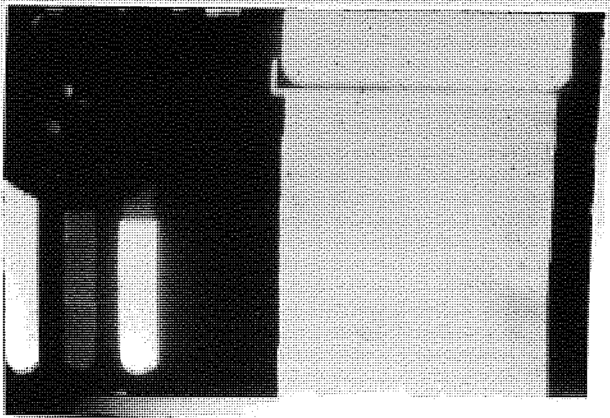

Plate 58 – Enhanced, Time: 15 minutes

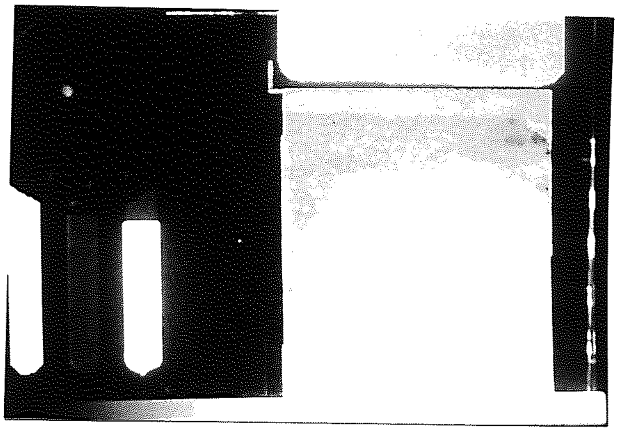

Plate 59 – Enhanced, Time: 30 minutes

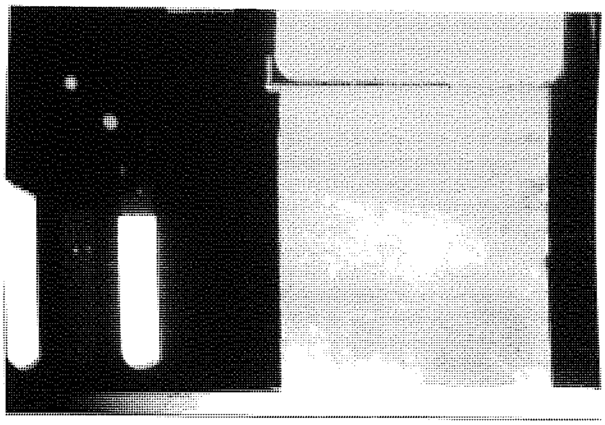

Plate 60 – Enhanced, Time: 54 minutes

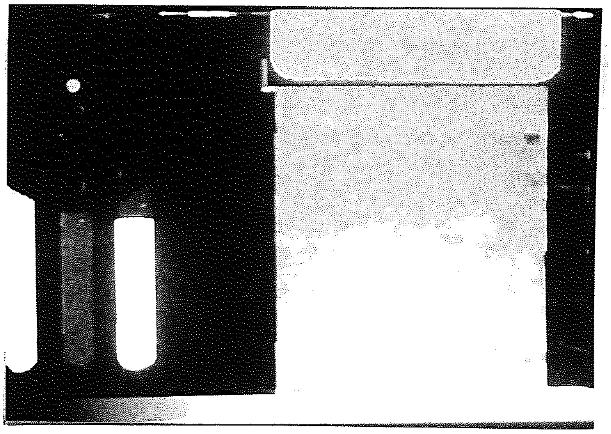

Plate 61 – Enhanced, Time: 85 minutes

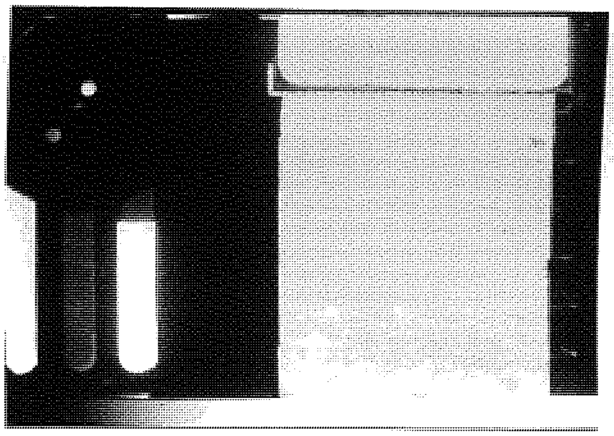

Plate 62 – Enhanced, Time: 130 minutes

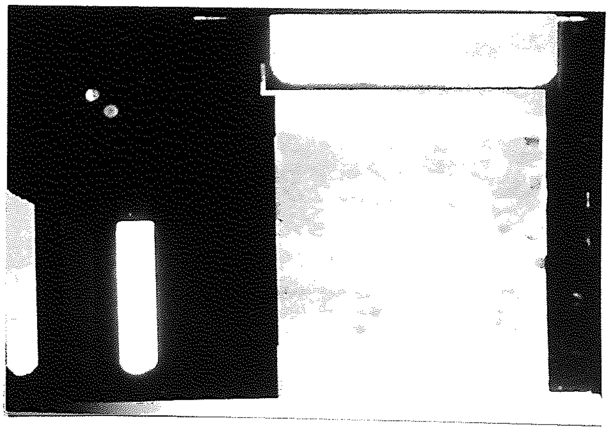

Plate 63 – Enhanced, Time:167 minutes

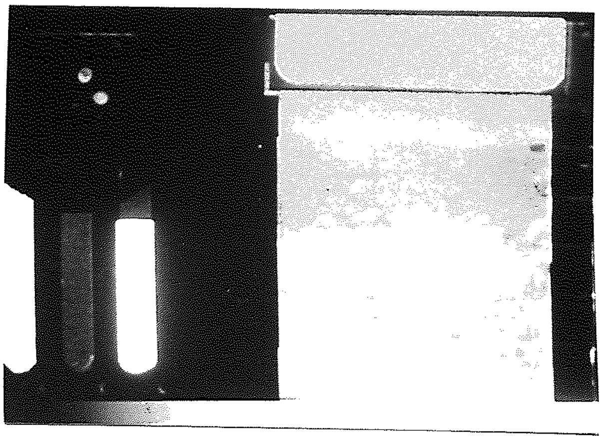

Plate 64 – Enhanced, Time: 219 minutes

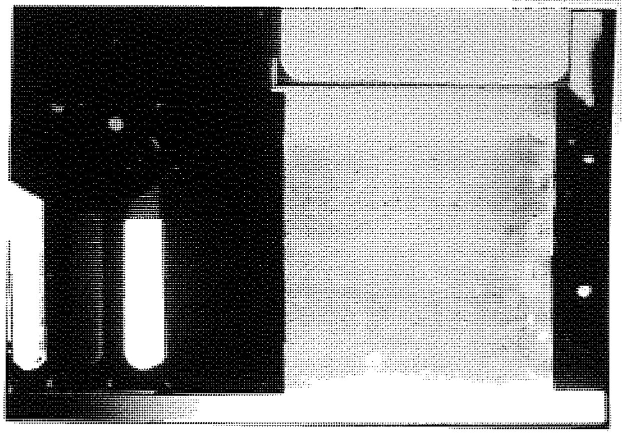

Plate 65 – Enhanced, Time: 1155 minutes

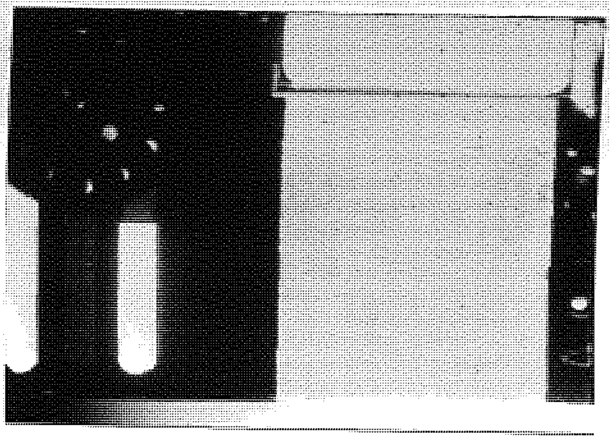

Plate 66 – Enhanced, Time:1218 minutes

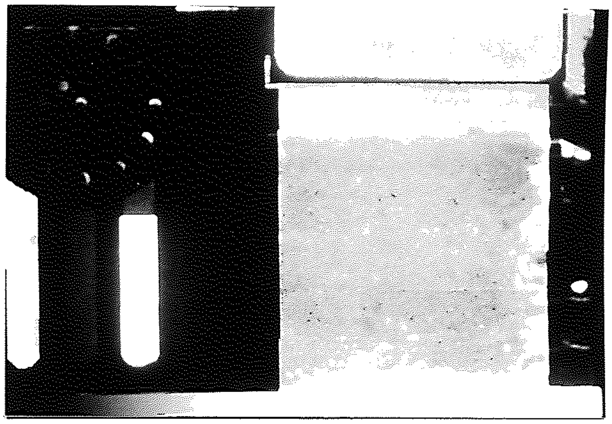

Plate 67 – Enhanced, Time: 1241 minutes

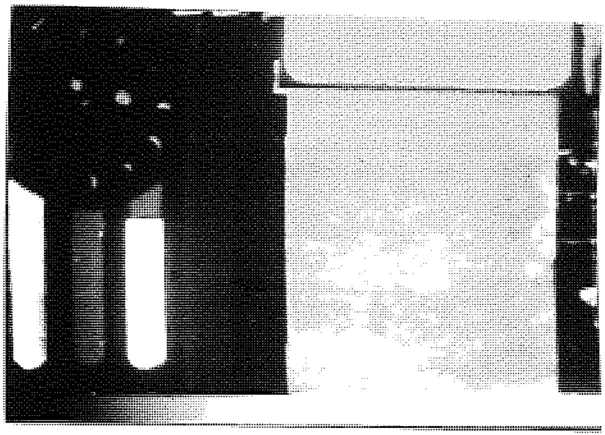

Plate 68 – Enhanced, Time: 1267 minutes

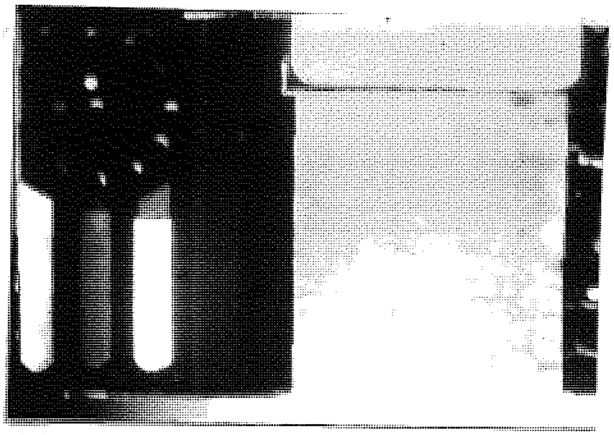

Plate 69 – Enhanced, Time: 1301 minutes

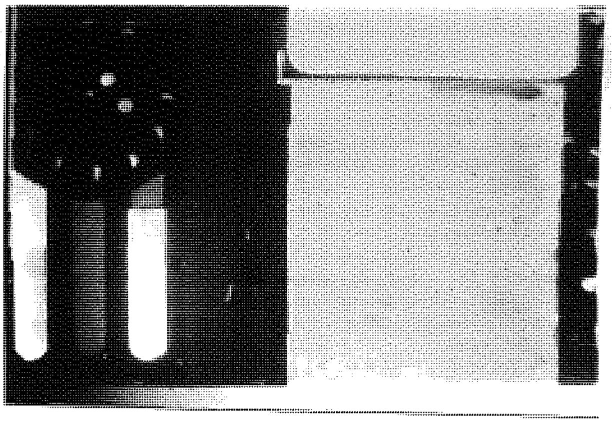

Plate 70 – Enhanced, Time: 1391 minutes

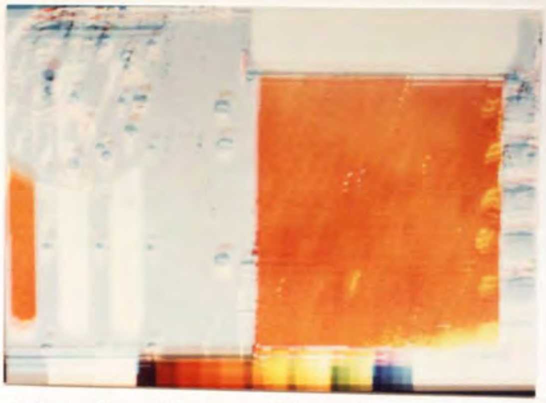

Plate 71 – Colour, Time: 0 minutes

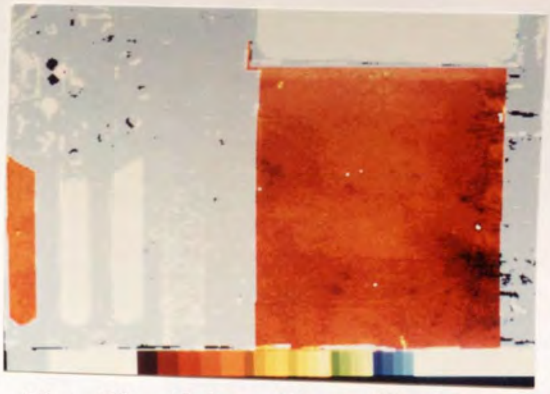

Plate 72 – Colour, Time: 15 minutes

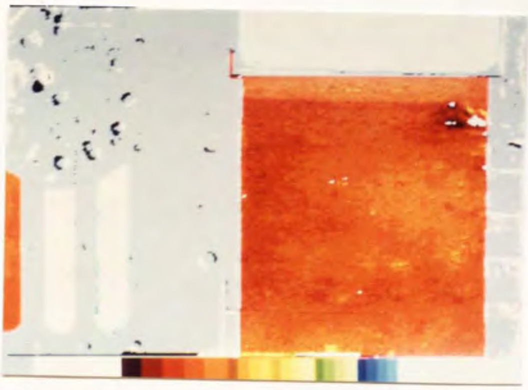

Plate 73 – Colour, Time: 30 minutes

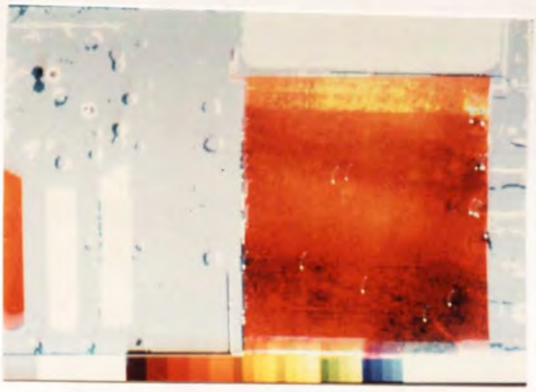

Plate 74 – Colour, Time: 54 minutes

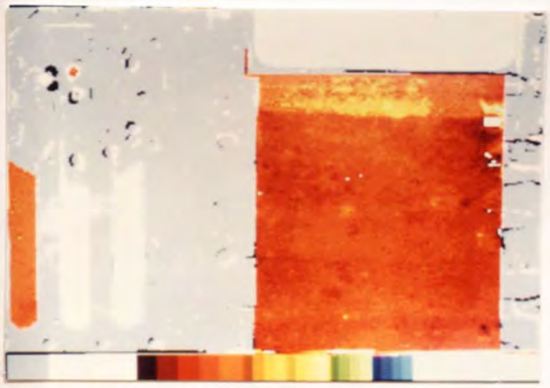

Plate 75 – Colour, Time: 85 minutes

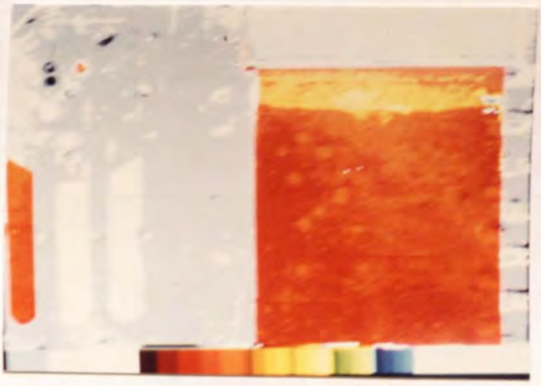

Plate 76 – Colour, Time: 130 minutes

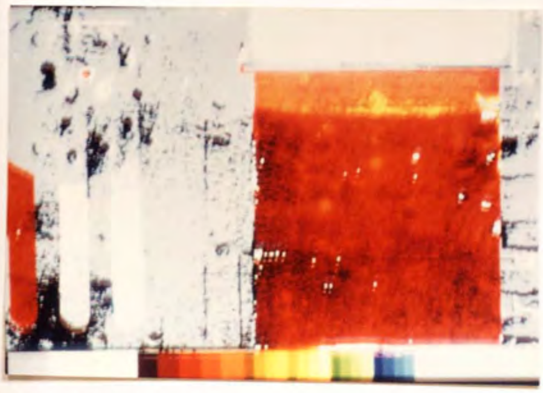

Plate 77 – Colour, Time: 167 minutes

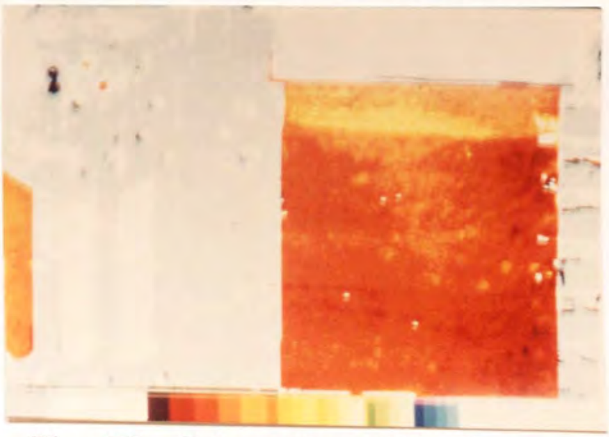

Plate 78 – Colour, Time: 219 minutes

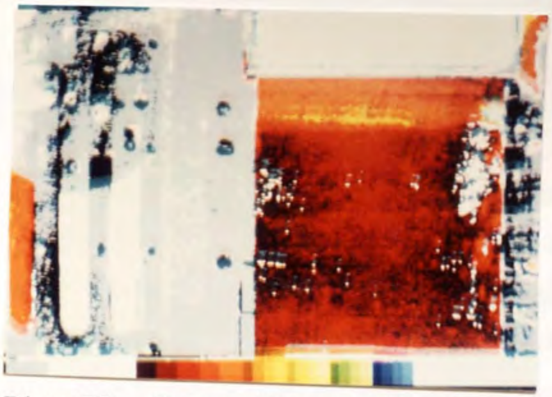

Plate 79 – Colour, Time: 1155 minutes

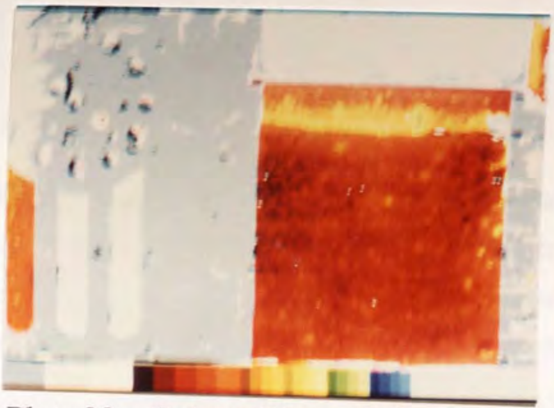

Plate 80 – Colour, Time: 1218 minutes

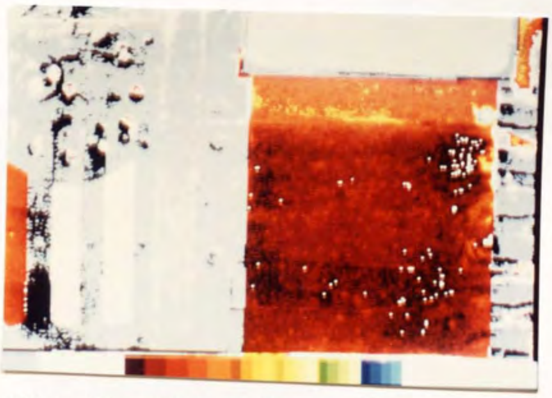

Plate 81 – Colour, Time: 1241 minutes

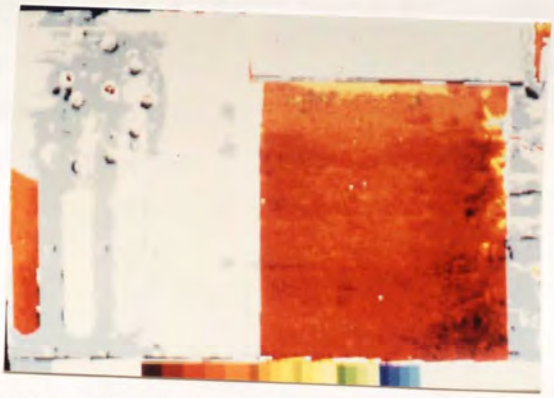

Plate 82 – Colour, Time: 1267 minutes

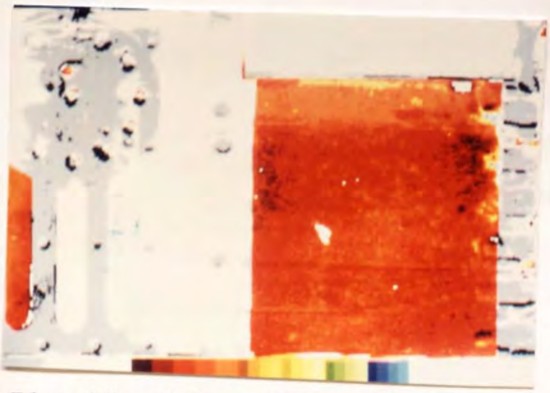

Plate 83 – Colour, Time: 1301 minutes

Plate 84 – Colour, Time: 1391 minutes

CHAPTER 7 RESULTS AND ANALYSIS

7.1 Introduction

The digital information on water contents from the enhanced radiographic images was combined with suction measurements, taken throughout the matrix during the tests, to provide the basis for hydraulic conductivity determinations. Mathematical models have been employed to make these determinations and the theory and inherent assumptions are explained. A computer program (52) (Appendix 2) has been used to make necessary corrections, for horizontal temperature gradients in the probes, to the suction measurements and again the relevant theory and assumptions are explained. Results using the psycrometer manufacturer's correction technique are also given. Additional information on temperatures, electrical resistance, water uptake and heave in the matrix is related to radiographs at critical times throughout the tests.

7.2 Results

The values for electrical resistance are of use in distinguishing ice from water in the matrix and are intended for comparison rather than for the quantative evaluation of ice content, and so the recorded instrument readings are used without calibration. The temperature profiles were obtained using copper/constantan thermocouples which had been calibrated prior to experimentation using an ice cell and therefore the recorded values can be input directly to the model. The readings obtained using the thermocouple/psychrometers require correction for the temperature gradient across the sensing junction which was recorded as a zero offset. The values for moisture content in the matrix are related to the reference cells and averaged to give a single value for water content at each psychrometer location.

7.2.1 Corrections to Psychrometer Readings

Each of the psycrometers used in the experiments was supplied with an individual calibration curve. These calibration curves were checked using 0.5514 molar NaCl solution by immersing the psychrometers in the solution, which was shielded from thermal fluctuations using insulation material, and allowing up to 1 hour for equilibrium to be achieved. After calibration the thermocouple and shield were carefully washed to remove any remaining NaCl residue.

The psychrometer readings were corrected using the manufacturer's suggested method and a method developed by Brown and Bartos (52).

7.2.1.1 Manufacturer's Correction Method

The millivolt output (mv) from the psychrometer was adjusted for psychrometer temperature (T) using the formula:

Corrected Reading (Bars) = $(mv/(0.325+0.027T))/0.47$ ....(38)

7.2.1.2 Brown and Bartos Calibration Model

The model takes account of the effect of zero–offset readings (omv) on the measured potentials. It is suggested (52) that zero–offsets affect water potentials in a predictable manner and that they can be used to correct estimates of water potential made under thermal gradients.

In the reported experiments every effort was made to minimise thermal gradients along the axis of the psychrometer. As suggested (52) the probes were installed in the sample horizontally so as to be normal to the established temperature gradient throughout the length of the soil. It was not possible, however, to insulate the rig on the front and back faces as obstructing material, in the path of the neutron beam, was reduced to a minimum to facilitate good image production. Therefore, slight temperature gradients along the probe were inevitable, particularly at the start of the test, when cooling of the specimen was initiated.

From observations on psychrometers in the field (52) the acceptable range of zero offset is –60 to +60 microvolts and consequently this range was chosen as the limiting range for the reported experiments. The model determines the error in psychrometer output caused by temperature gradients, as measured by zero–offsets, at varing psychrometer temperature and water potential.

The model program and sample output are given in Appendix 2 and both manufacturer corrected results and Brown and Bartos corrected results are given in Appendix 3.

7.2.2 Corrections to Water Content Readings

The reference cells containing saturated matrix material (100% cell) and dry matrix material (0% cell) were used to correct the values for moisture content in the sample. The averaged values of data counts in each reference cell were used to correct the averaged data counts for each psychrometer location (mc) using the following equation:

Corrected Moisture Content (cm^3/cm^3) = $(mc-0\%)/(100\%-0\%)$.................................(39)

7.2.3 Graphical Representation of Results

Hydraulic potential, moisture content, electrical resistance and temperature plots against time are given for each psychrometer location throughout tests 1 and 2 in Appendix 5.

7.2.4 Radiographs

Standard, normalised, enhanced and colour images are given in plates 85–100 for times T=0,15,54 and 219 minutes of test 1. The corresponding hydraulic potential, moisture content, electrical resistance and temperature profiles are given in figures 33–36.

Profiles for test 2 are shown in figures 37–40 for times T=0,62 and 315 minutes.

7.3 Analysis of Results

7.3.1 Introduction

In soils exposed to freezing, the most widely adopted approach for determining the hydraulic conductivity (coefficients) uses water migration data and a form of the Clausius–Clapeyron equation to convert temperature gradients to effective pressure gradients in the frozen and partially frozen soil (42,87). Knowing the temperature gradient throughout the length of the soil the effective pressure gradient can be calculated using the Clausius–Clapeyron equation of the form:

$H = L / Tg \, dT$ ....(17)

Hydraulic conductivities are then found by solving a form of Darcy's Law, where:

$Q = -KA \ dH/dL$ ....(25)

This approach assumes stable temperature conditions with a uniform temperature gradient and negligible heat flow normal to the temperature gradient. Owing to the arrangement of the experimental set up and the problems associated with insulating the cell containing the soil matrix, total elimination of heat flow normal to the temperature gradient and development of a linear temperature profile were not possible. It was, therefore, not appropriate to use the Clausius–Clapeyron and Darcy equations for the analysis of the experimental data.

It was decided to base the determination of the hydraulic conductivities on the soil moisture–suction relationships, assuming their independence from temperature gradients. The method of analysis is limited to one initially developed by Childs and Collis–George (62) which is based on the creation of a moisture characteristic for the soil which forms the input to permeability determinations from probability laws for pore size distribution. The analysis can be considered in three stages. The initial stage involves an examination of the relationship between the degree of saturation and the corresponding suction to form a moisture–suction curve or moisture characteristic for the medium. From this a cumulative pore size distribution curve (degree of saturation vs pore radius) is

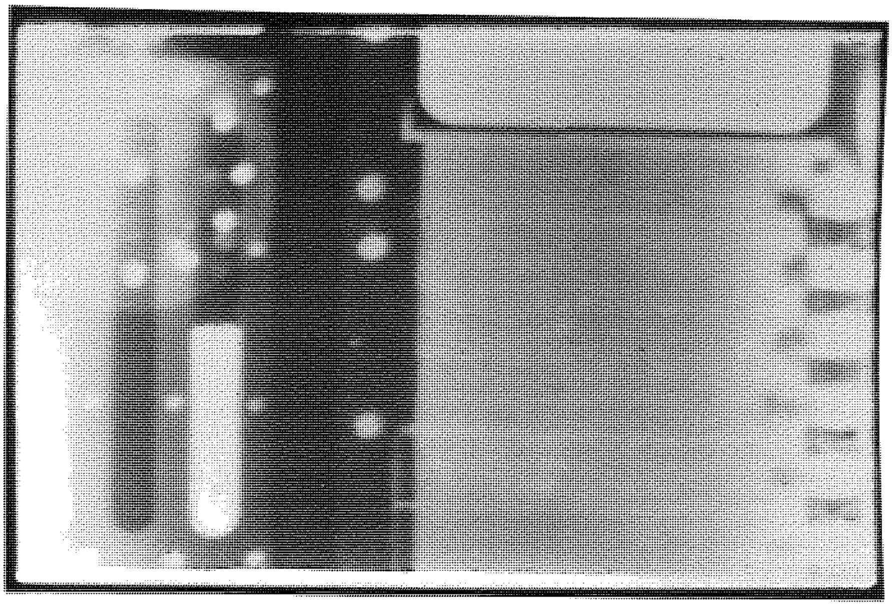

Plate 85 – Standard Image, Time: 0 minutes

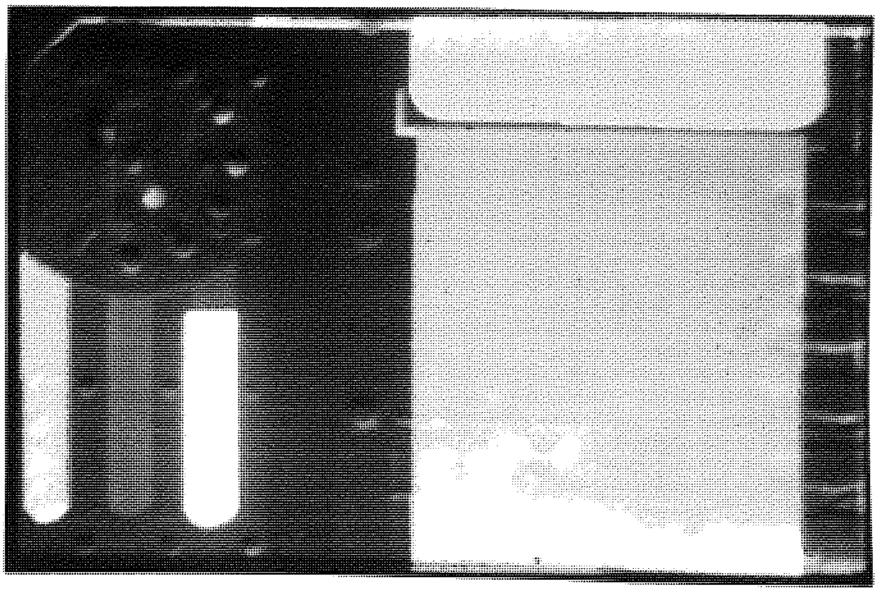

Plate 86 – Normalised Image, Time: 0 minutes

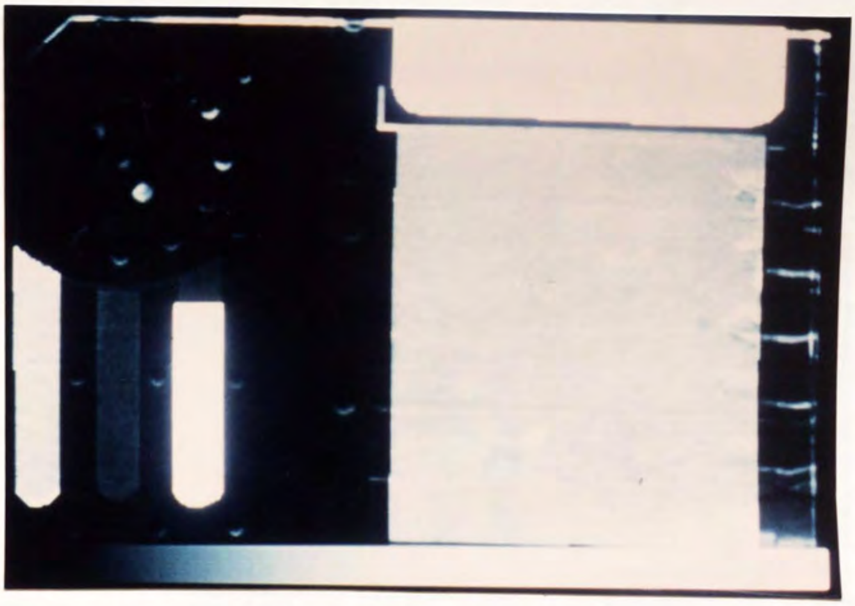

Plate 87 – Enhanced Image, Time: 0 minutes

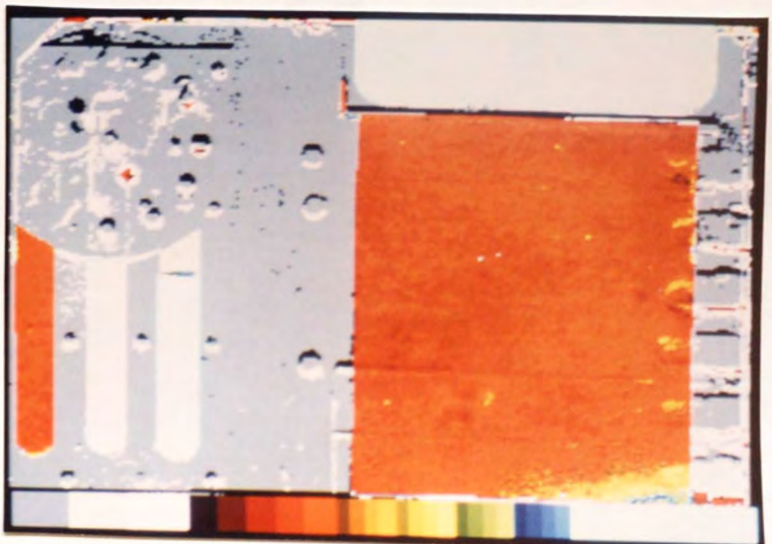

Plate 88 – Colour Image, Time: 0 minutes

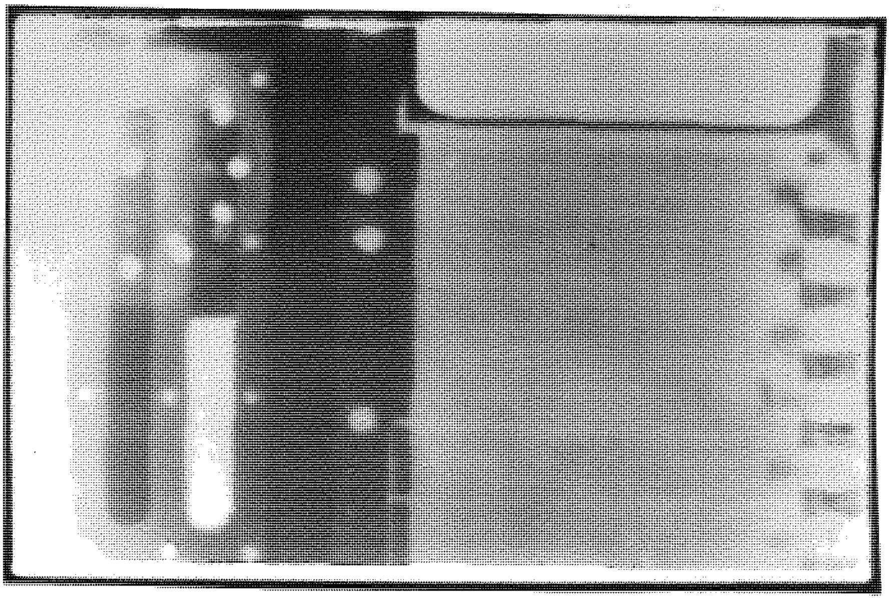

Plate 89 – Standard Image, Time: 15 minutes

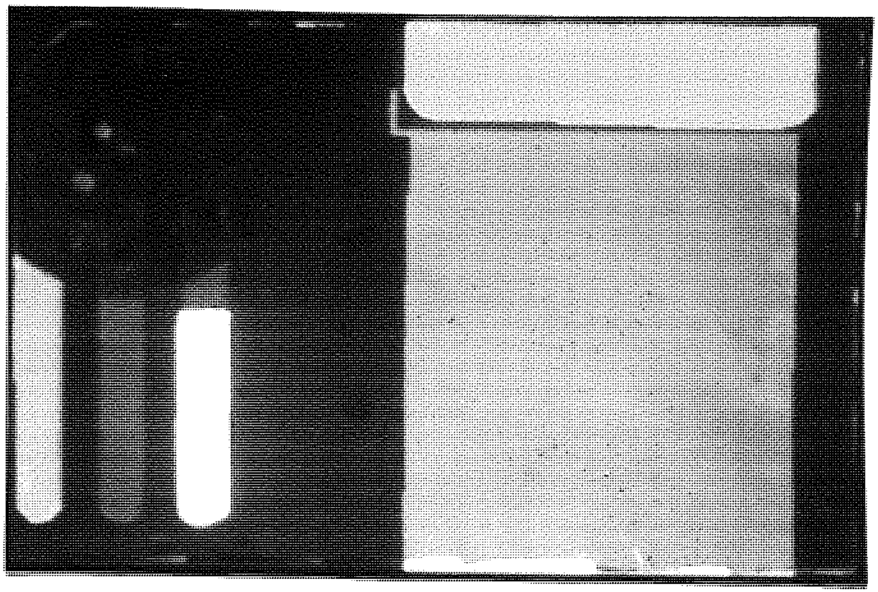

Plate 90 – Normalised Image, Time: 15 minutes

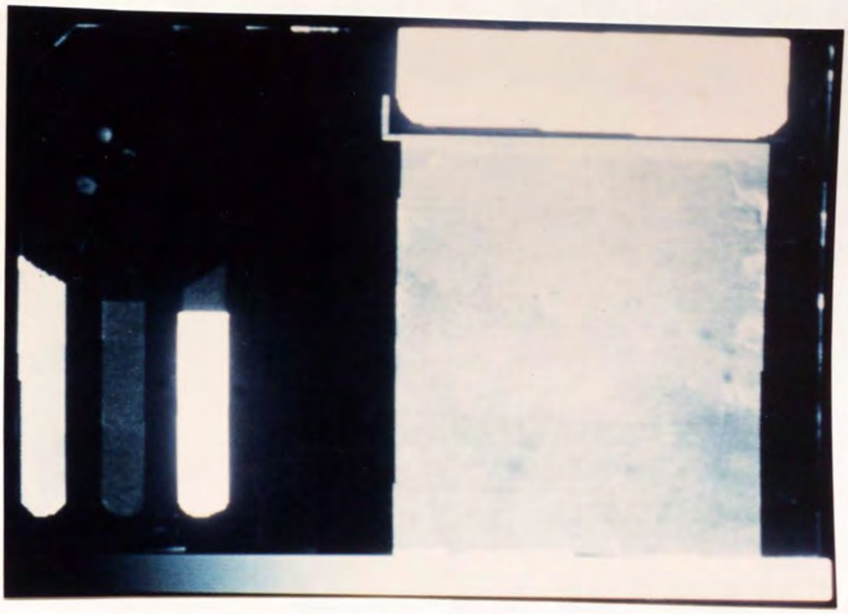

Plate 91 – Enhanced Image, Time: 15 minutes

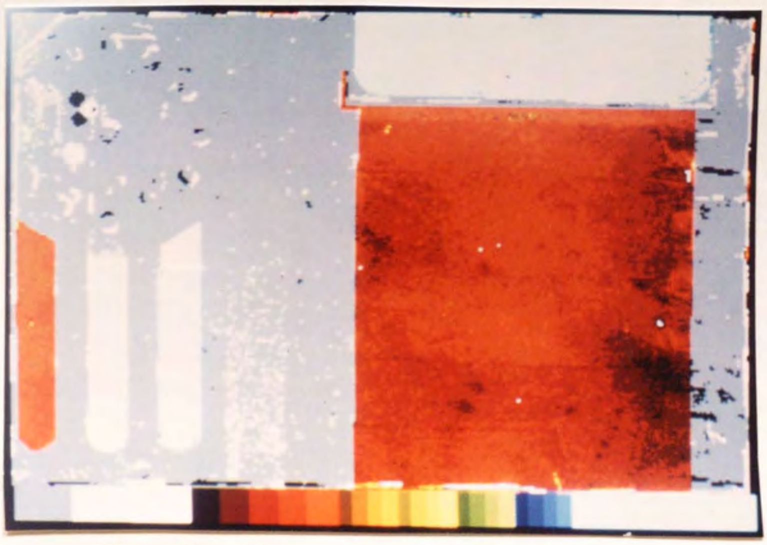

Plate 92 – Colour Image, Time: 15 minutes

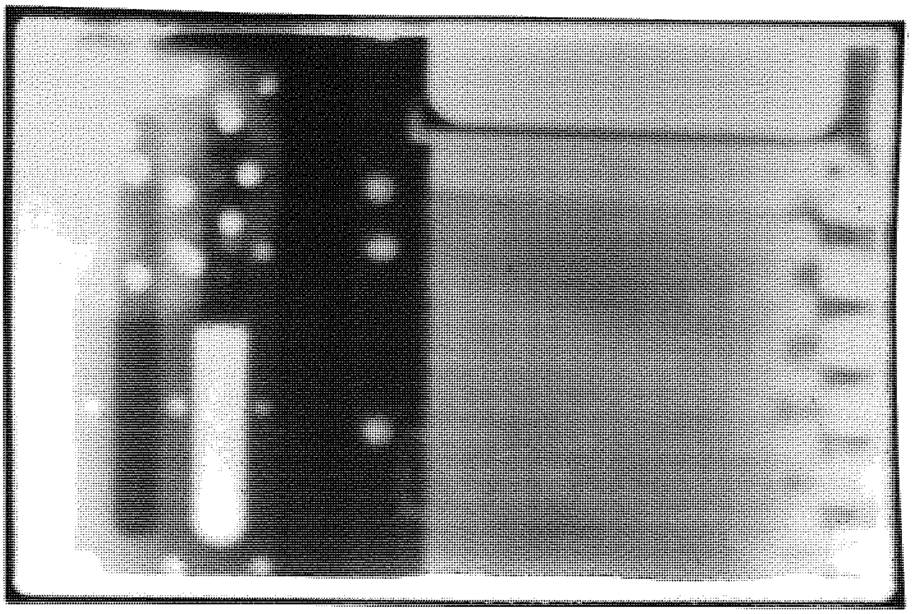

Plate 93 – Standard Image, Time: 54 minutes

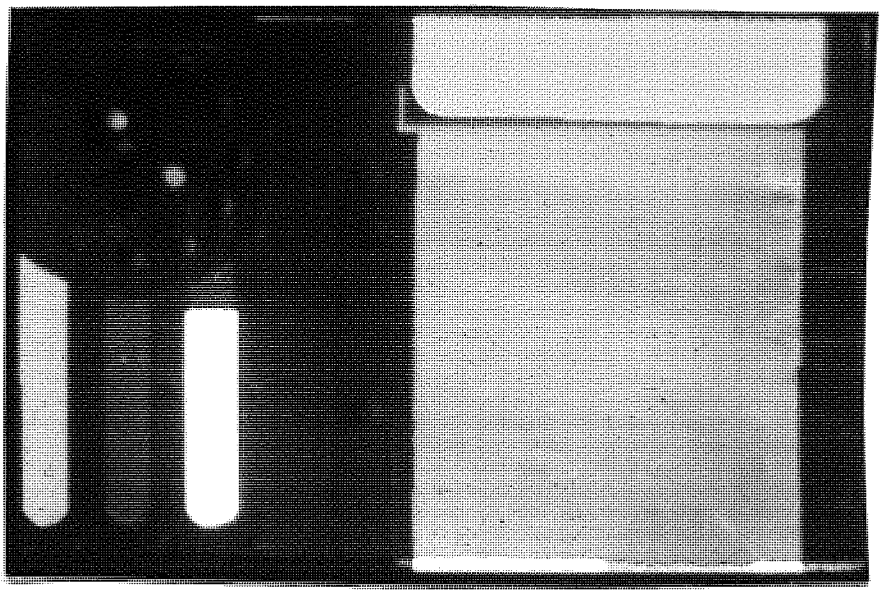

Plate 94 – Normalised Image, Time: 54 minutes

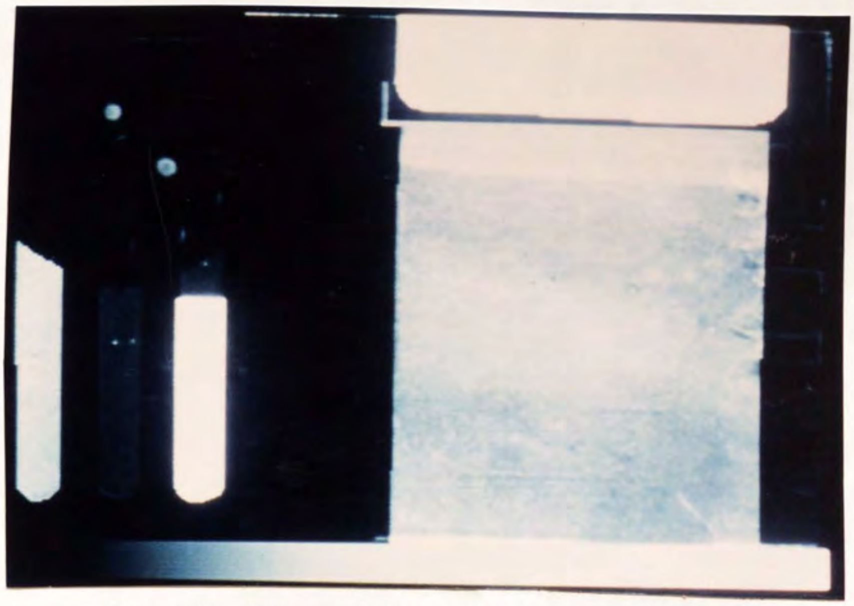

Plate 95 – Enhanced Image, Time: 54 minutes

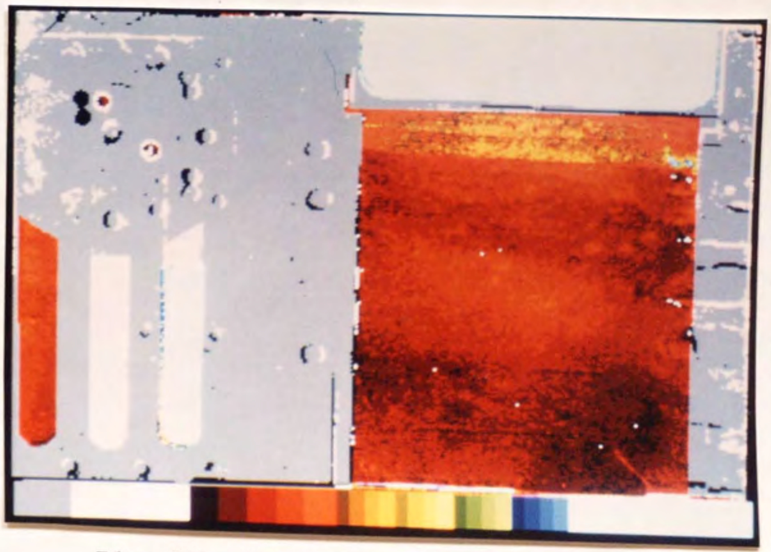

Plate 96 – Colour Image, Time: 54 minutes

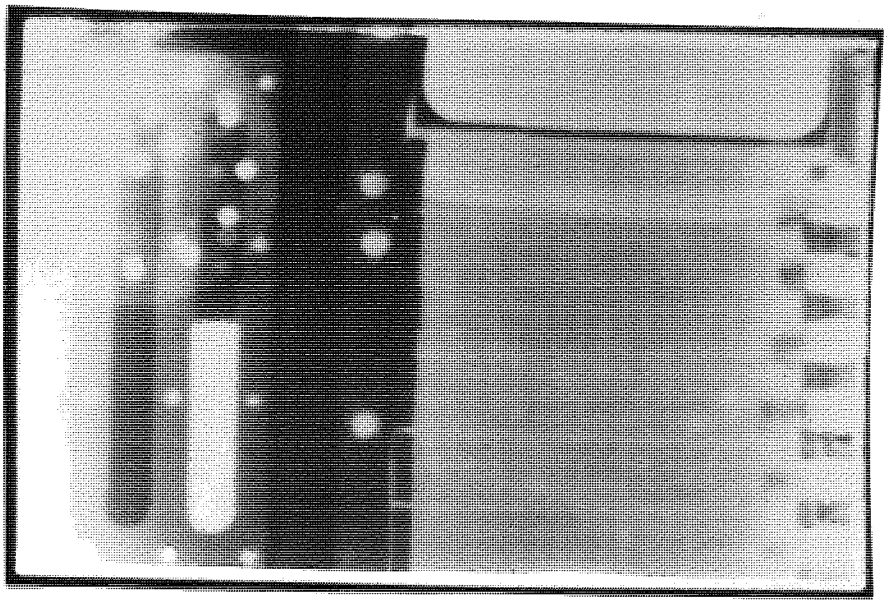

Plate 97 – Standard Image, Time: 219 minutes

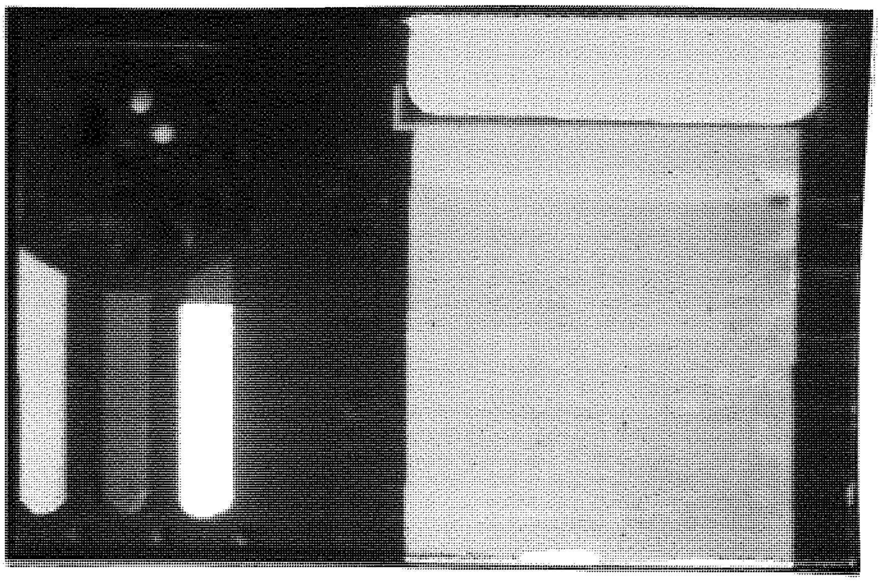

Plate 98 – Normalised Image, Time: 219 minutes

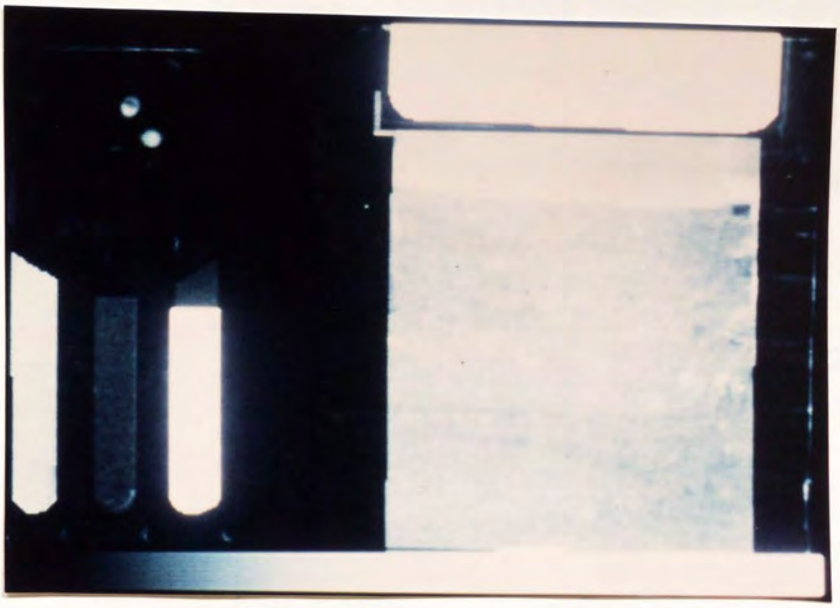

Plate 99 – Enhanced Image, Time: 219 minutes

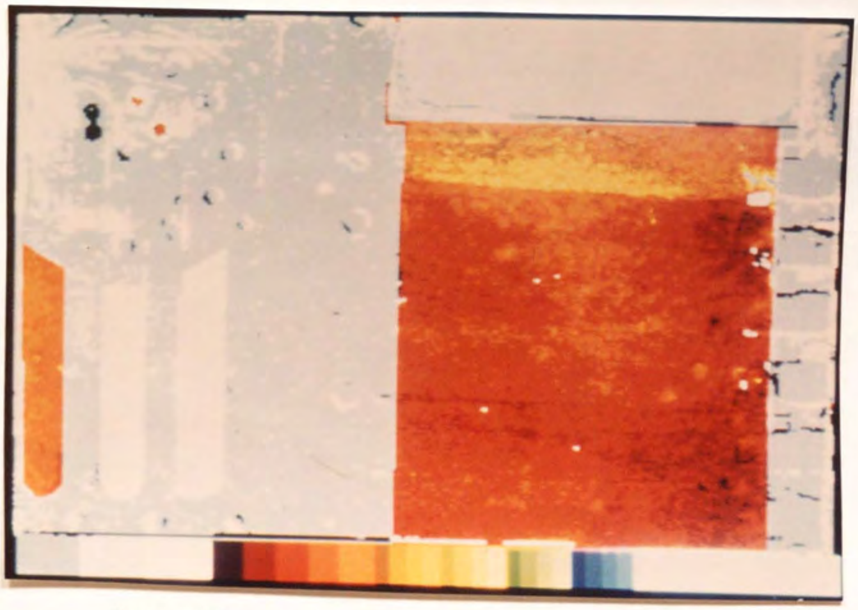

Plate 100 – Colour Image, Time: 219 minutes

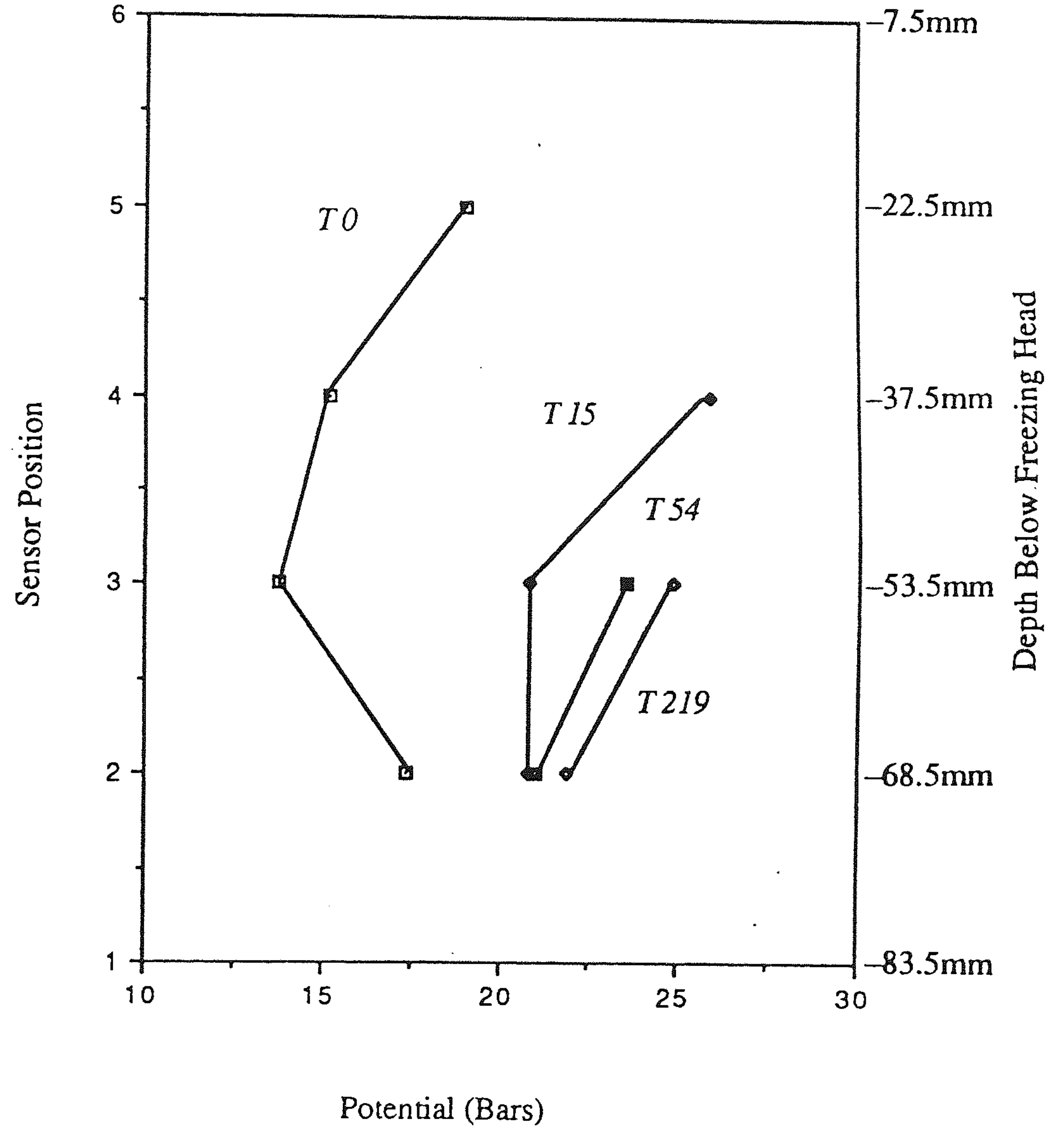

Figure 33 – Hydraulic Potential Profile (Test 1)

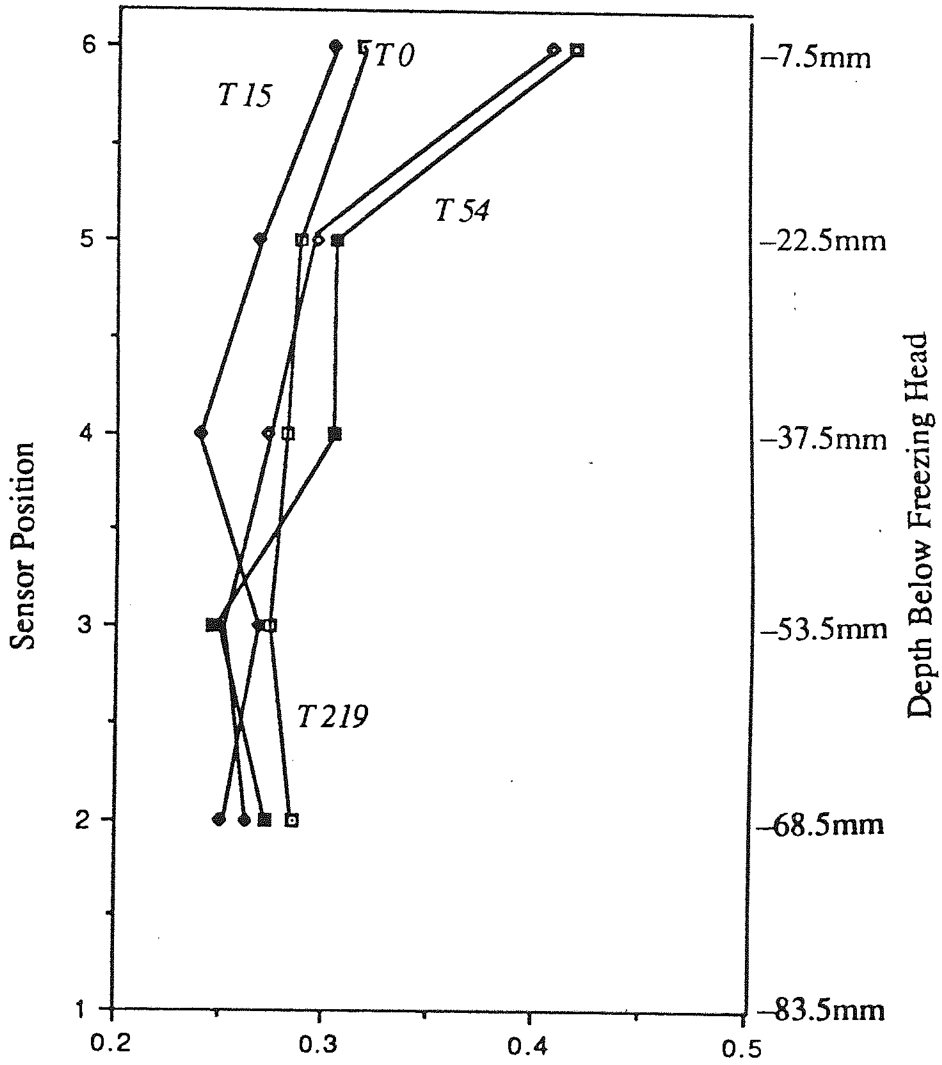

Figure 34 – Moisture Content Profile (Test 1)

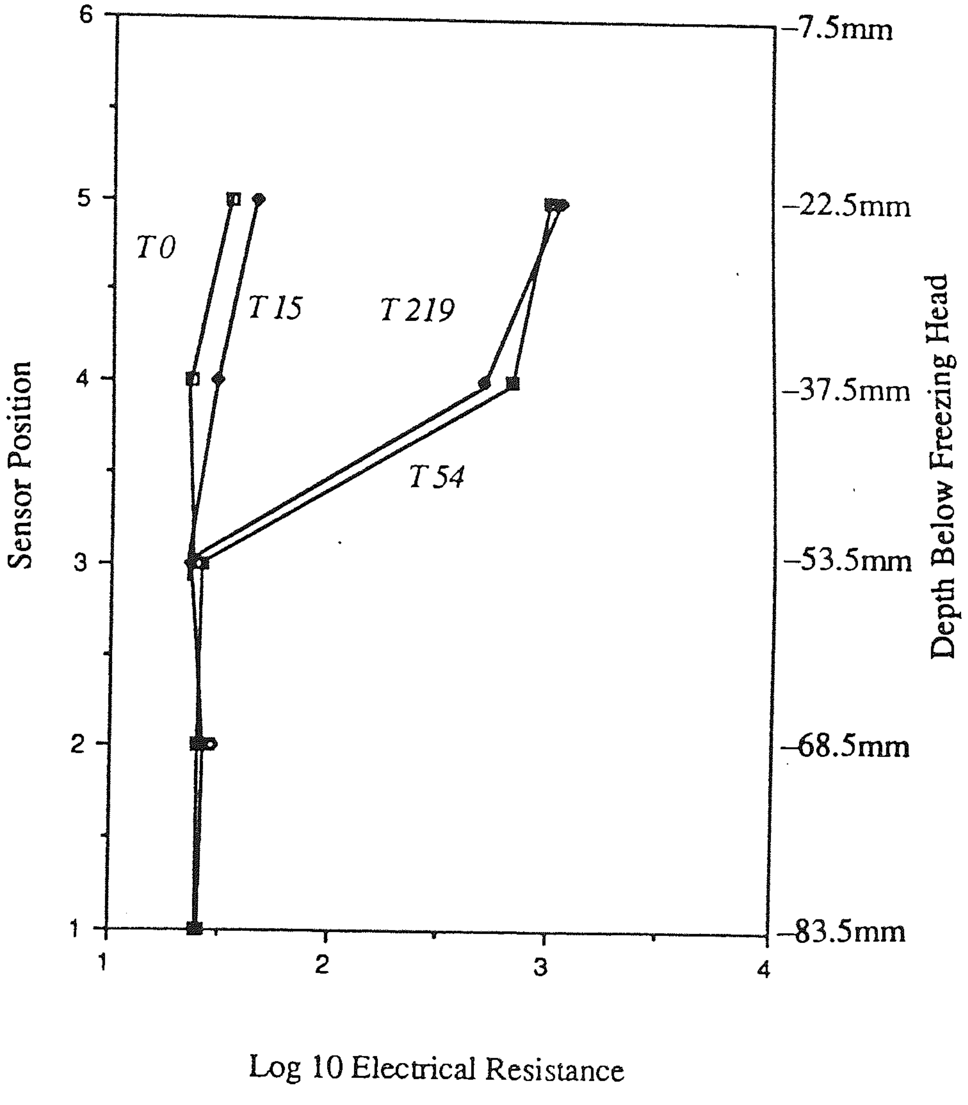

Figure 35 – Electrical Resistance Profile (Test 1)

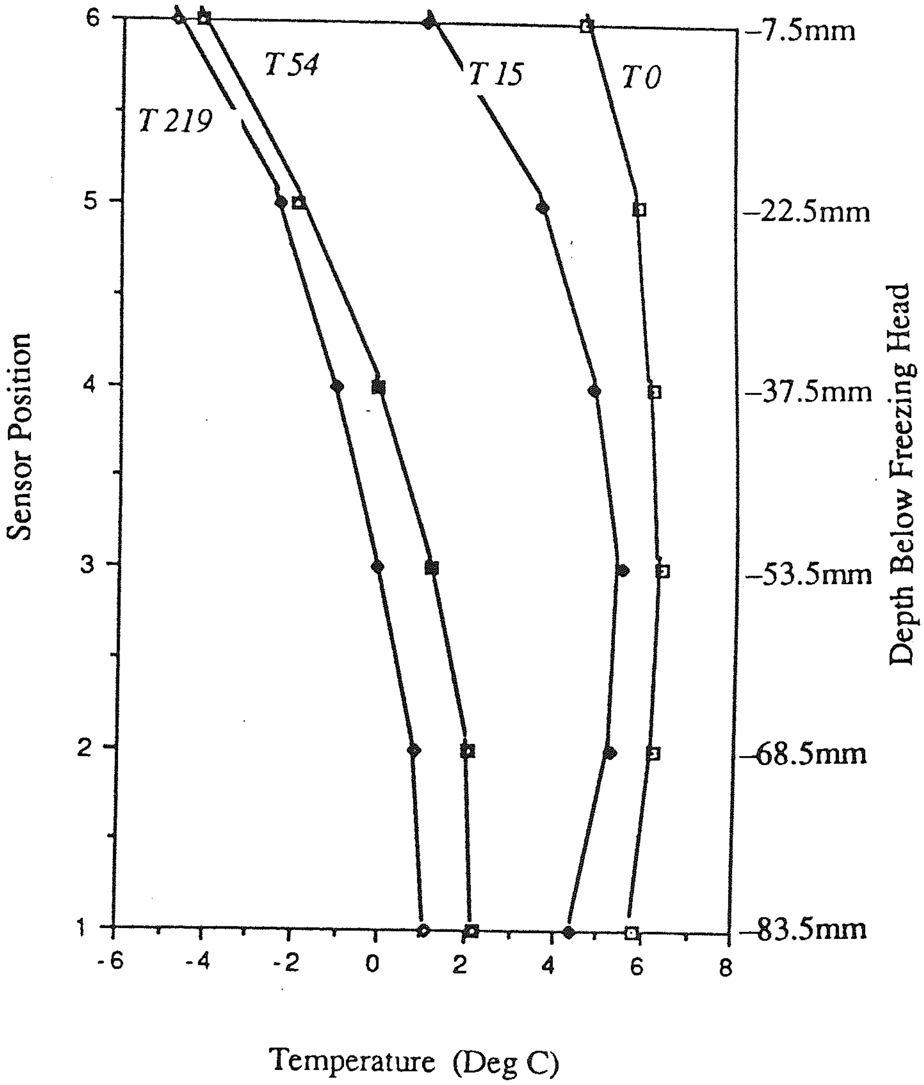

Figure 36 – Temperature Profile (Test 1)

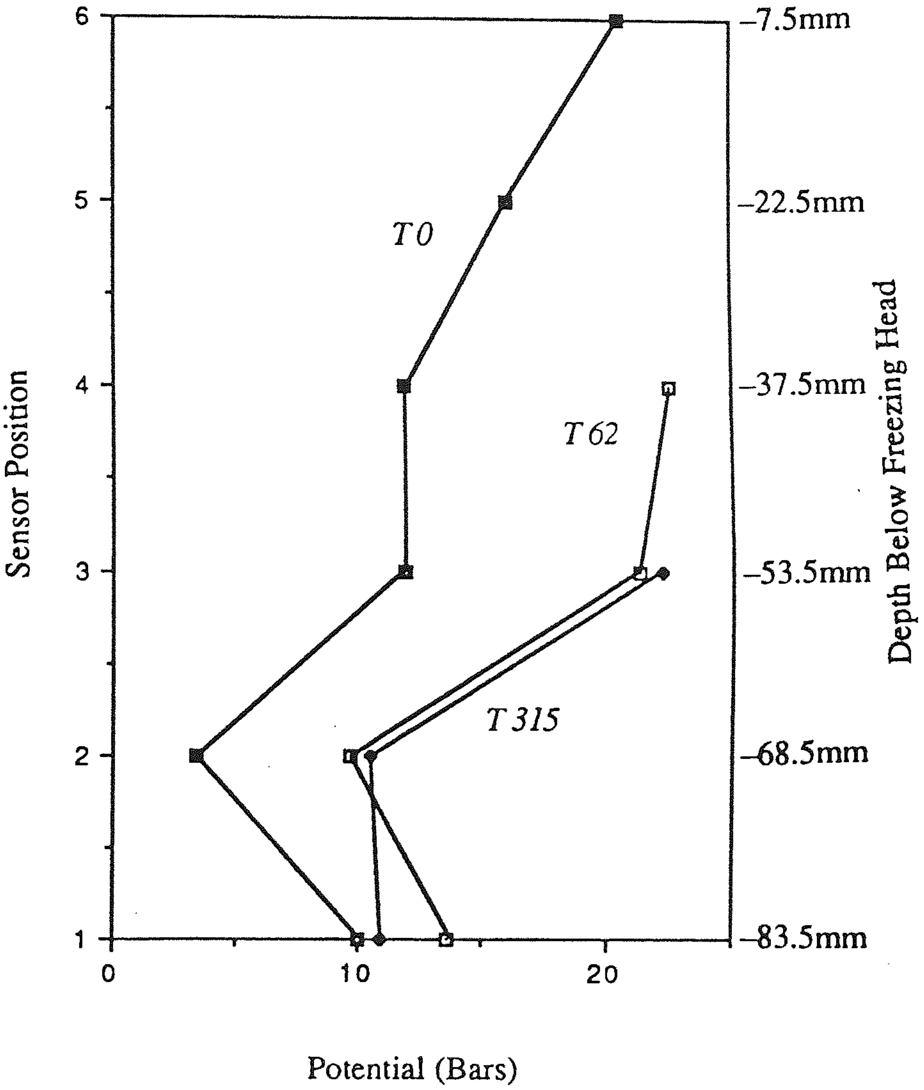

Figure 37 – Hydraulic Potential (Test 2)

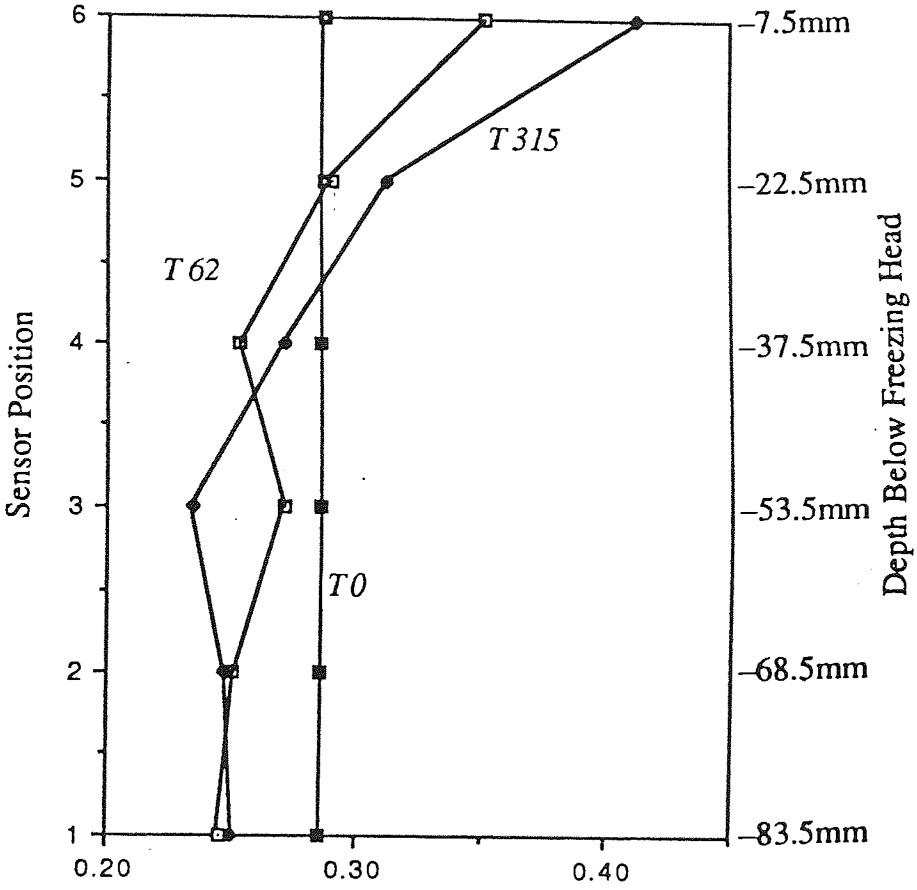

Figure 38 – Moisture Content Profile (Test 2)

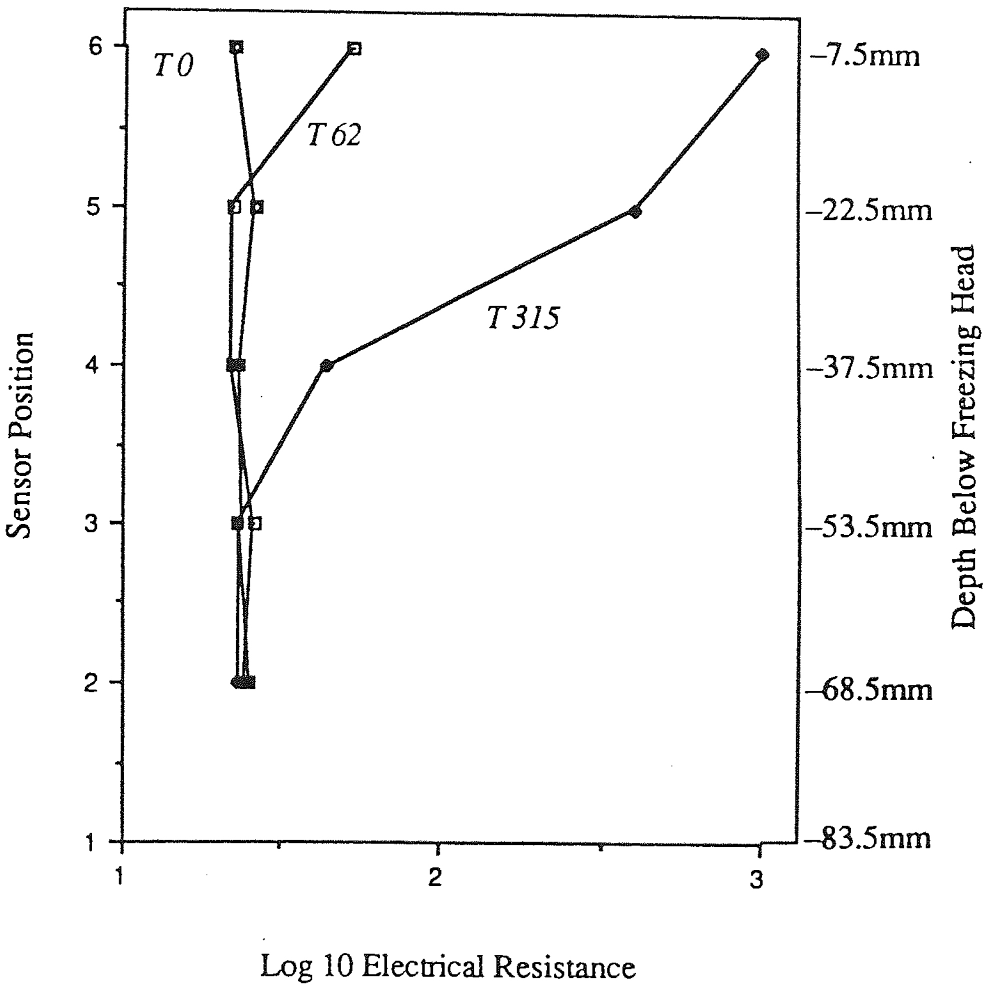

Figure 39 – Electrical Resistance Profile (Test 2)

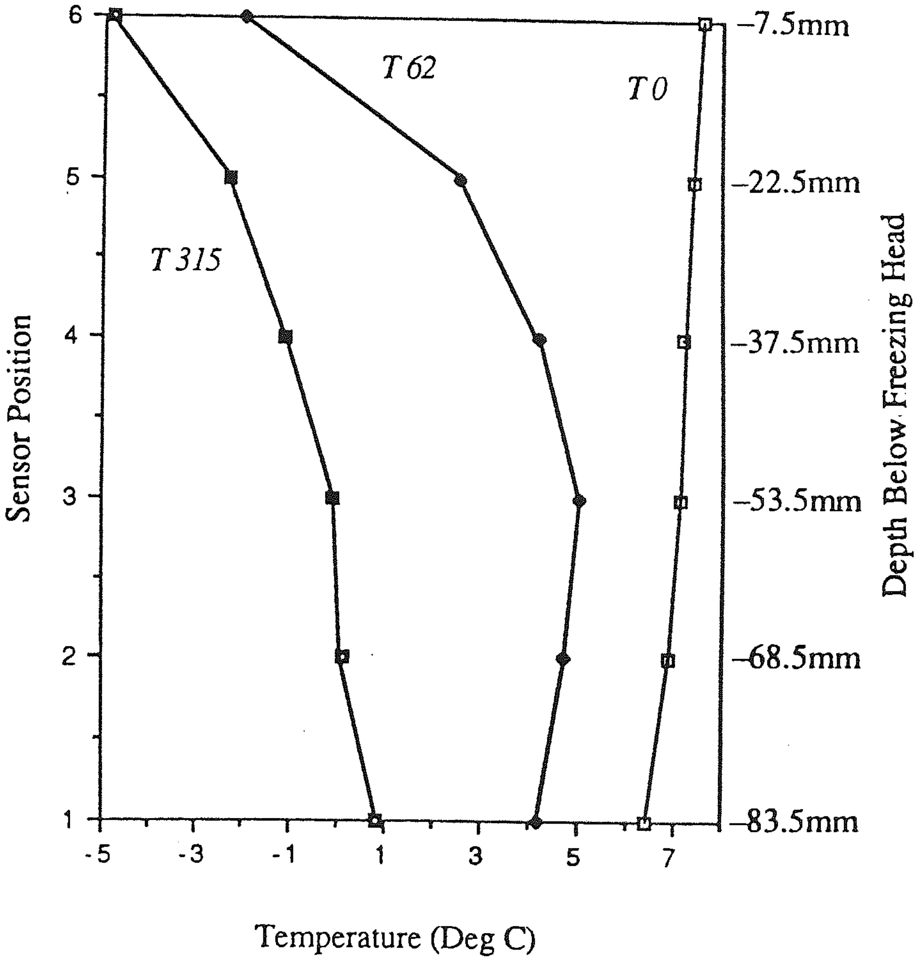

Figure 40 – Temperature Profile (Test 2)

deduced. In the second stage, a series–parallel model is employed to develop an equation for the permeability of an unsaturated medium. Finally, the permeability function determined in the previous stage is integrated numerically (using Simpsons Rule) for the probability density function determined in the first stage.

7.3.2 Analysis Theory

7.3.2.1 Stage 1

It has been stated by Brutsaert (124) that: "With a given moisture content or degree of saturation one can, neglecting hysteresis phenomena, always associate a unique moisture suction. The relationship between the degree of saturation and the suction may be referred to as the moisture–suction curve or moisture characteristic of the medium."

Laplace's equation for the pressure drop across the concave interface between water and air in a pore can be written as:

$$dP = \sigma(1/r_1 + 1/r_2) \cos \theta \qquad (40)$$

where:

dP = pressure drop across the interface.
σ = surface tension.
θ = water–solid contact angle.
r_1 & r_2 = minor and major radius of curvature of the interface.

If r_1 and r_2 are replaced by a mean radius r and the assumption made that the contact angle between the water/air interface and the pore wall is extremely small then the equation can be written as:

$$dP = 2\sigma/r \qquad (41)$$

or:

$$h = 2\sigma/g(\rho_w-\rho_a)r \qquad (42)$$

where:

h = pressure expressed as cm water.
g = gravitational acceleration (9.81 m/s^2).
ρ_w= density of water (998 Kg/m^3).
ρ_a = density of air (1.293 Kg/m^3).
σ = surface tension (72.75 mN/m at 20 °C).

hence by substituting quantities in equation 42:

$h = 0.149/r$ ....(43)

but since the surface tension is effected by temperature, with the value at 0 °C becoming 75.7 mN/m the equation must be modified for soil water temperature and so becomes:

$h = 0.155/r$ ....(44)

The degree of saturation corresponding to a given moisture suction, h, is also the pore volume fraction occupied by pores of radius equal to or less than r. Hence with the moisture–suction curve, obtained experimentally, the cumulative pore size distribution curve (degree of saturation S vs pore radius r) can be determined using $r = 0.155/h$. The technique does, however, have two limitations. Very large suctions are required to reduce the moisture content to zero and so determination of the exact shape of the distribution at the lower end is virtually impossible and the validity of the capillary model (on which $r = 0.155/h$ is based) breaks down at very small r (ie a clayey soil). To overcome these problems the following linear transformation can be used:

$Se = (S-Sr)/(1-Sr)$ ....(45)

where:

S = degree of saturation (volume of water /total pore volume)
Sr = residual saturation (relating to the pore volume which does not contribute to the flow of water).
Se = effective saturation.

However if Sr is chosen judiciously a plot of log Se vs. log h approaches a negatively sloping straight line. The following equation has been proposed (125) to overcome the problem:

$Se = A/h^B$ ....(46)

where:

A & B = characteristic constants of the medium.

A better fit is obtained, however, if the following equation is used:

$Se = a/(a+h^b)$ ....(47)

a & b = characteristic constants of the medium.

Substituting for h from equation 47 this becomes:

$Se = r^b/((0.155^b/a)+r^b)$ ....(48)

The effective pore size density function $se(r) = dSe/dr$ is then given by:

$se(r) = bdr^{b-1}/(d+r^{b})^{2}$ ....(49)

where:

$d = 0.155^{b}/a$

7.3.2.2 Stage 2

A series–parallel model has been proposed (62) to calculate the relative permeability of a porous medium for water. The theoretical basis for the model assumes that the porous medium is equivalent to a set of independent parellel pores of different permeabilities which are fractured normally to the direction of flow and then rejoined after random rearrangement. In this way account is taken of the random variation of pore sizes of the medium in the plane normal to the direction of flow and the variation along the direction of flow.

The discharge in each single pore, which is now two sections in series, is assumed to be governed by the section of smaller diameter. It is also assumed (126) that in an homogeneous, isotropic and liquid saturated porous medium the discharge/unit cross–sectional area equals the average velocity in the pores normal to the area times the pososity (fo). Hence it is assumed that fo.s(r).dr is the area/unit area occupied by openings whose sizes are between r–dr/2 and r+dr/2 which is equivalent to the probability of a point in any cross section through the medium being found in a pore with size between r–dr/2 and r+dr/2.

The fraction of area of section occupied by the sequence of pores, with size between x–dx/2 and x+dx/2 of the first surface with pores with size between y–dy/2 and y+dy/2 of the second surface is equal to:

$(fo(1-Sr))^{2}.se(x).se(y).dx.dy$ ....(50)

It is assumed that in a pore with size parameter r the average velocity is given by a law similar to Poiseuille's:

$Vs = -(r^{2}\Psi/G\mu)(dh/ds)$ ....(51)

where:

Ψ = specific weight of the liquid.
μ = viscosity.
dh/ds = gradient of the hydraulic head (expressed as energy/unit weight).
G = geometric constant depending on the shape and arrangement of grains, which is very closely equal to 8.

If it is assumed that the flow between two pores is controlled by the smallest (size x) then the rate of flow that takes place through a fraction of the cross–sectional area, occupied by the sequences of pores with size between x–dx/2 and x+dx/2 that are in contact with the pores with size between y –dy/2 and y+dy/2 is:

$$-[fo(1-Sr)]^2(\Psi/G\mu)(dh/ds).[se(x)\int_0^x se(y)y^2dydx + se(x)x^2\int_x^\infty se(y)dydx] \quad\text{.................(52)}$$

The first term gives the flow from pores of the first surface with size between x–dx/2 and x+dx/2 into all the pores of the second surface that are smaller than x.

The second term gives the flow into the pores of the second surface that are larger than x. Integration over x yields, finally, the total discharge/unit cross–sectional area of the porous medium.

Therefore intrinsic permeability K', where $K' = K\mu/\Psi$, is for a saturated medium:

$$K' = [fo^2(1-Sr)^2/G] . [\int_0^\infty Se(x)\int_0^x Se(y)y^2dydx + \int_0^\infty Se(x)x^2\int_x^\infty Se(y)dydx] \quad\text{...............(53)}$$

To extend the result to partially saturated medium, the upper limit of integration is changed from infinity to the size of the largest pores that are available for flow at a given degree of saturation. Hence, for an unsaturated medium:

$$K' = [fo^2(1-Sr)^2/G].R \quad\text{...(54)}$$

where R is:

$$R = \int_0^r se(x)\int_0^x se(y)y^2dydx + \int_0^r se(x)x^2\int_x^r se(y)dydx] \quad\text{.......................................(55)}$$

7.3.2.3 Stage 3

The function R determined in Stage 2 can now be integrated for the specific probability density function determined in Stage 1. In the pore size distribution function (effective saturation relationship):

$$Se = r^b/(d+r^b) \quad\text{...(56)}$$

the parameters d and b are determined from the experimentally established relationship between moisture suction and degree of saturation by means of equation 44 and by use of the least squares estimate of the moisture content characteristics equation, given in Appendix 2.

By substituting $U = r^b/d$ in equation 56:

$$Se = U/(1+U) \qquad (57)$$

Differentiating Se with respect to r produces the density function:

$$se(r) = (dbr^{b-1})/(d+r^b)^2 \qquad (58)$$

Combining this with the final equation 58 of Stage 2 the R function is:

$$R = d^{2/b} . \left[\int_0^U 1/(1+x)^2 . \int_0^x y^{2/b}/(1+y)^2 \, dydx \right] + \left[\int_0^U x^{2/b}/(1+x)^2 . \int_x^\infty 1/(1+y)^2 \, dydx \right] \qquad (59)$$

Substituting equation 57 into equation 59 gives:

$$R = 2d^{2/b} . [Se \int_0^\infty x^{2/b}.(1-x)^{-2/b} dx - \int_0^\infty x^{(2+b)/b}.(1-x)^{-2/b} dx] \qquad (60)$$

This is then integrated numerically using Simpsons Rule.

7.3.3 Analysis of Results

The corrected psychrometer readings, determined using the Brown and Bartos technique and using the manufacturer's technique are given together with the corrected moisture content values in Appendix 3 for both tests.

A plot of moisture content against suction for all the results from tests 1 and 2 is given in figure 41 and a moisture content against log suction plot is given in figure 42. data points from the curve in figure 42 are used as input data for the least squares program of Appendix 2. The program evaluates constants A and B for the equation of the line:

$$\theta = (\theta res/\theta sat) + A((1-\theta res/\theta sat)/(A+\psi^B)) \qquad (61)$$

where:

θ = moisture content (cm^3/cm^3)
θres = residual moisture content, determined from figure 42 as 0.24 cm^3/cm^3
θsat = saturation moisture content, determined form figure 42 as 0.41 cm^3/cm^3
ψ = suction (cm H_2O)
A = 1186795 $cm^{1.659}$ (in cm H_2O suction)
B = 1.659

The effective saturation (Se), given by equation 48, and the effective pore size density function se(r), given by equation 49, are shown in table 5 for a range of suctions from

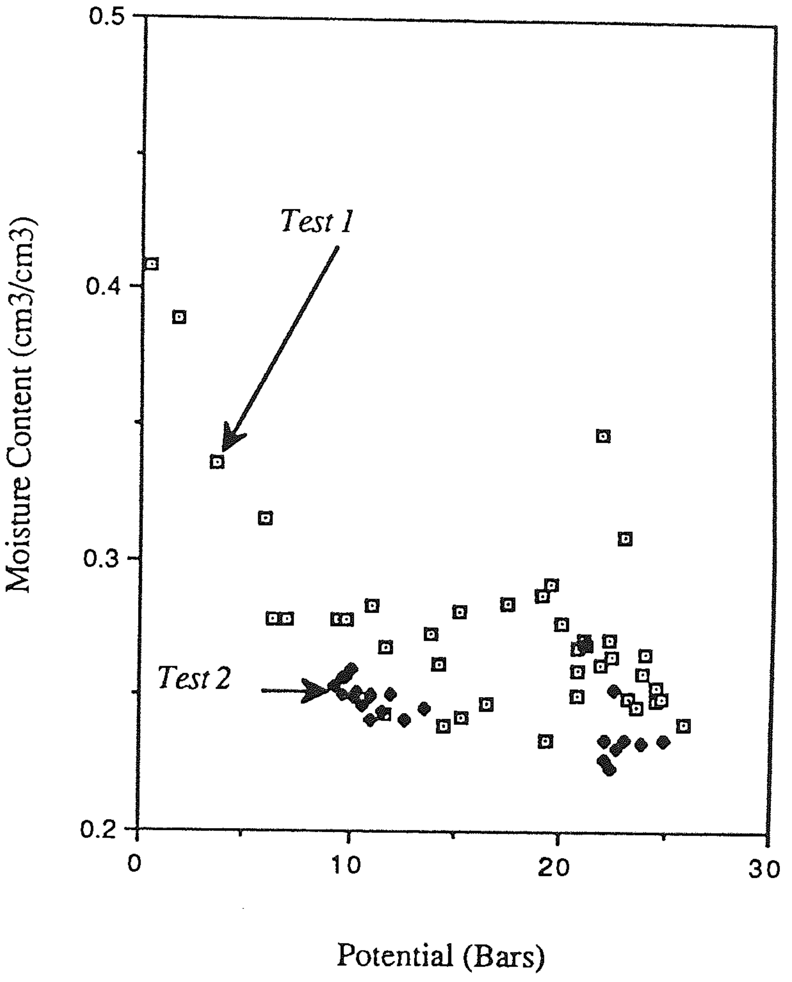

Figure 41 – Moisture Content Against Suction (Tests 1 and 2)

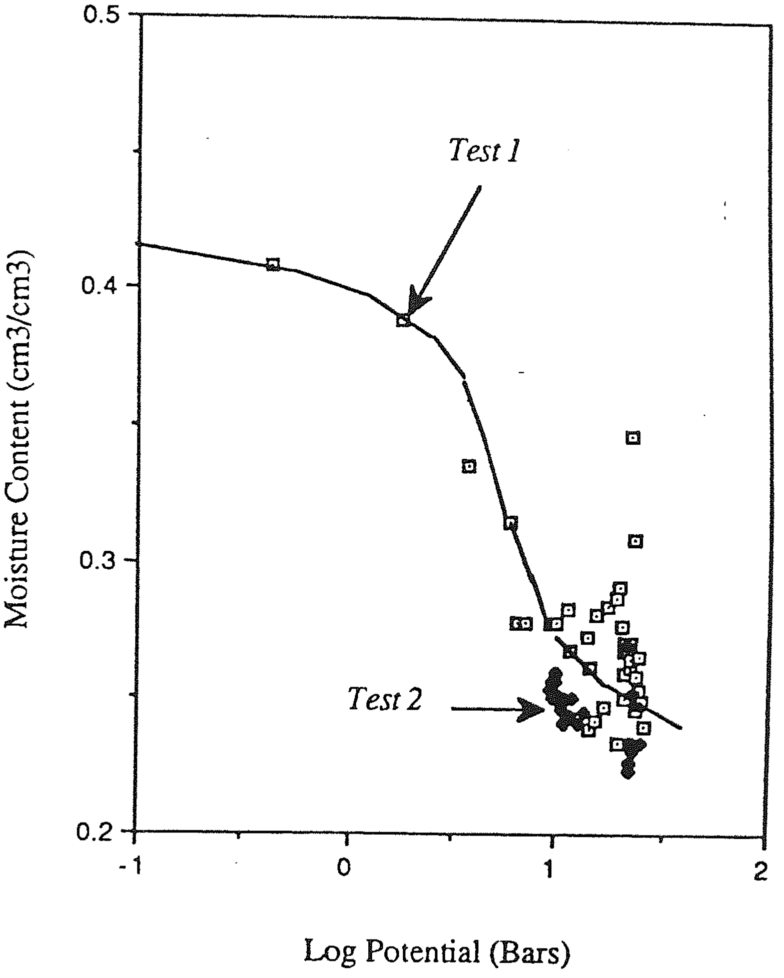

Figure 42 – Moisture Content Against Log10 Suction (Tests 1 and 2)

5–32000cm of water. The effective pore size density function is shown graphically in figure 43.

Values for the R function are also given in figure 46 along with the hydraulic conductivity (K) obtained using:

$$K = ((f_0^2(1-Sr)^2/G).R).c \ldots\ldots\ldots\ldots (62)$$

where:

Sr = residual saturation, estimated as $\theta res/\theta sat = 0.59$
f_0 = porosity = $(G_s\rho\omega - \rho_d)/G_s\rho\omega = 0.40$
where: G_s = specific gravity for Snowcal = 2.75
ρ_w = density of water = 1 Mg/m^3
ρ_d = dry density of the matrix = 1.65 Mg/m^3
c = conversion factor cm^2 to cm/s at 0 °C = 5.6×10^4

Table 5 – Table of Results

Suction (h)(cm)	Effective Saturation (Se)	Pore Radius (r)(cm)	Effective Pore Size Density Function (Se(r))	R Function	Hydraulic Conductivity (K)(cm/s)
5	0.999	0.031	0.0006	1.43E-9	2.86E-7
100	0.998	1.55E-3	1.8690	1.39E-9	2.79E-7
500	0.975	3.10E-4	128.823	1.08E-9	2.16E-7
1000	0.926	1.55E-4	733.433	7.50E-10	1.49E-7
5000	0.464	3.10E-5	13310.624	3.93E-11	7.85E-9
8000	0.284	1.94E-5	17417.974	6.97E-12	1.39E-9
16000	0.112	9.69E-6	17000.899	3.08E-13	6.14E-11
20000	0.080	7.75E-6	15744.944	1.03E-13	2.04E-11
25000	0.057	6.20E-6	14289.982	3.34E-14	6.68E-12
30000	0.043	5.17E-6	13059.432	1.32E-14	2.64E-12
32000	0.038	4.84E-6	12614.902	9.45E-15	1.89E-12

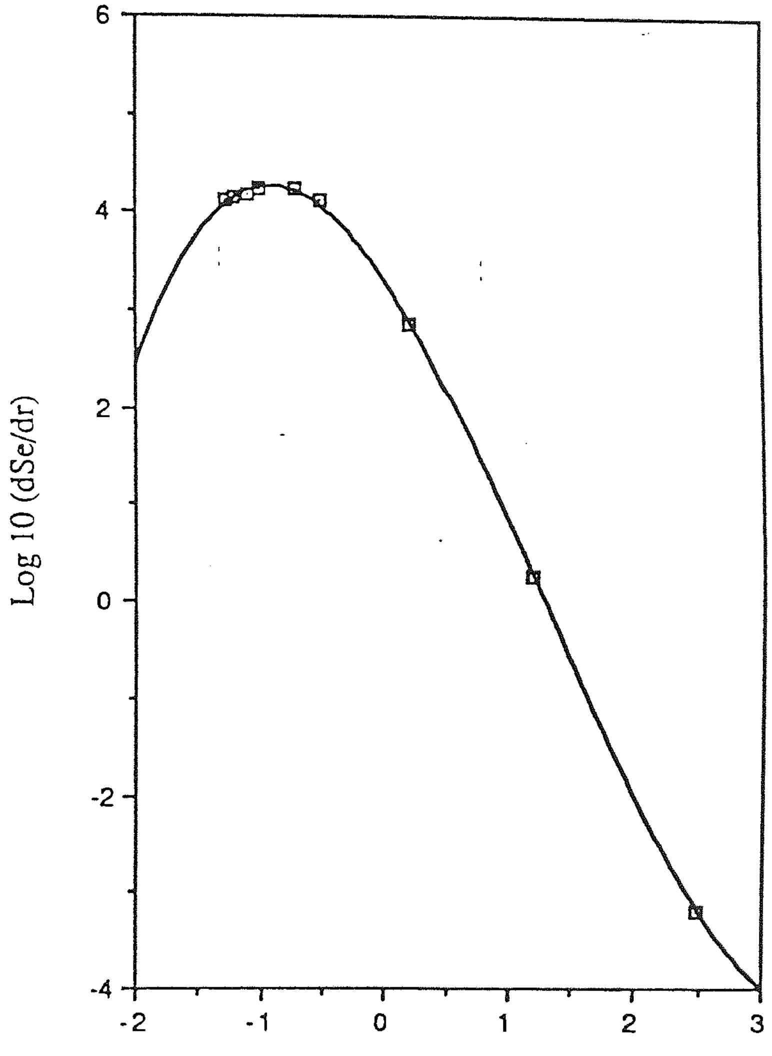

Figure 43 – Effective Pore Size Density Function

CHAPTER 8 COMPARISON AND DISCUSSION OF RESULTS

The hydraulic conductivities, determined in Chapter 7, are compared with other experimentally determined results for frozen, partially frozen and unfrozen silty soils.

The hydraulic conductivity in the saturated unfrozen region of the soil is comparable with Falling Head Permeameter results for the saturated soil (3) and with the established range of saturated permeabilities for a silt (10^{-5} to 10^{-7} cm/s) (127).

As the degree of saturation decreases towards the frost line the soil suction increases and the hydraulic conductivity decreases. This expected relationship is represented in figures 44 and 45, which show hydraulic conductivity plotted against soil suction and degree of saturation for a silty sand (128), a silty clay (128) and the research material, Snowcal. The relationship for Snowcal falls between those of the silty clay and the silty sand which is as expected as the particle size distribution for Snowcal, figure 19, indicates that it conforms to that of a silt.

Once into the frozen zone, large reductions in hydraulic conductivity are recorded for relatively small sub–zero temperatures. A silt at 28% saturation has been reported (75) to vary in hydraulic conductivity between 10^{-4} cm/s at 0 °C and 10^{-9} cm/s at –0.4 °C.

Comparisons of recent hydraulic conductivity determinations for various silty soils, at or around 0 °C are given in table 6. The temperature profile, obtained for the freezing experiments on Snowcal, was achieved using thermocouples positioned below the psychrometers and held in place by the frictional resistance of the psychrometer probe in it's locating hole. As a result of this technique, the profile for temperature is displaced slightly from that of suction and consequently, when comparing temperature to suction, and therefore hydraulic conductivity, the temperature readings have slightly higher absolute values. In addition, the temperature gradient was liable to small fluctuations, due to the unavoidable lack of insulation on the front and back faces of the cell. The value of hydraulic conductivity for Snowcal is, therefore, given for the temperature range –0.2 and 1.0 °C.

The suction values using the psychrometer thermocouples in the experiments were high, but comparable with established values for silt at low volumetric moisture contents (58). The values were consistent between both tests 1 and 2. Two methods were used to correct the psychrometer readings for temperature, the manufacturer's technique and that suggested by Brown and Bartos (52), both of which have been explained in Chapter 7. Values obtained using both methods are given in Appendix 3 and a comparative plot of

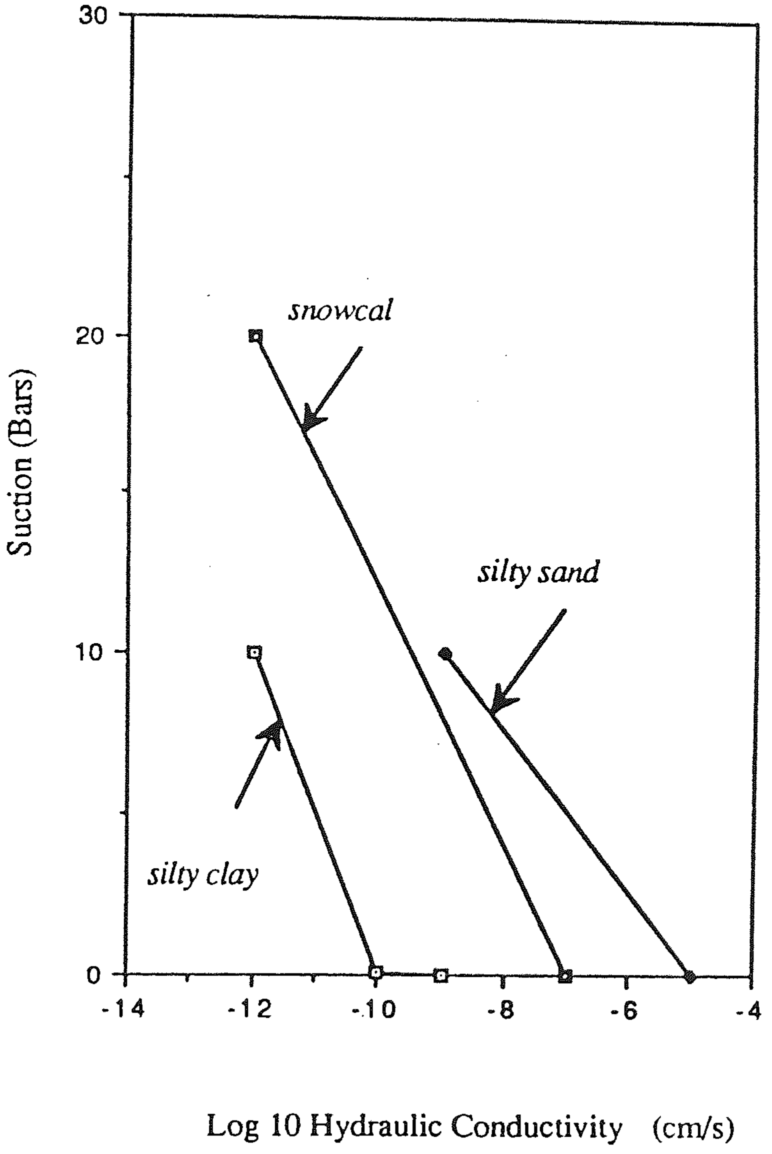

Figure 44 – Hydraulic Conductivity against Soil Suction

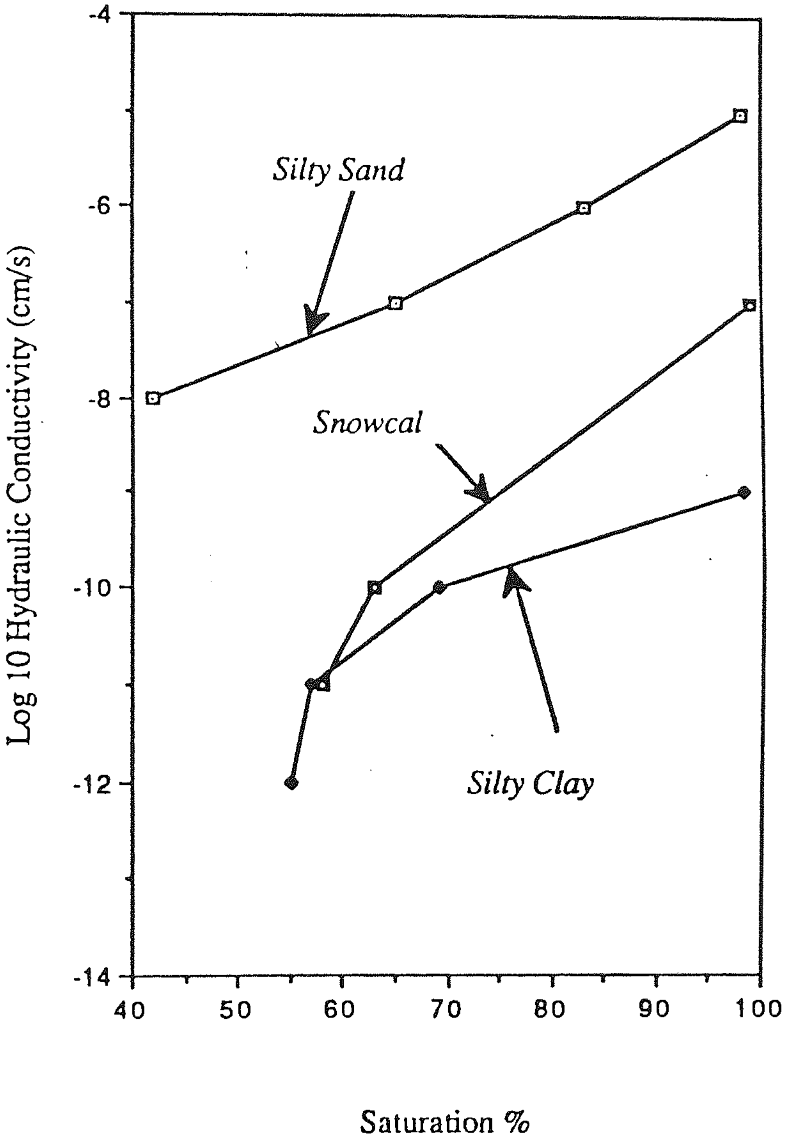

Figure 45 – Hydraulic Conductivity against Degree of Saturation

Table 6. Hydraulic Conductivities for Silty Soils at or arround 0°C.

SOIL TYPE	HYD. COND. (cm/s)	TEMP. (°C)	SAT. (%)	REFERENCE
Carleton Silt	1×10^{-4}	0	–	Burt & Williams (76)
	1×10^{-8}	-0.2	–	" "
Slims Valley Silt	1×10^{-5}	0	–	Burt & Williams (76)
	1×10^{-5}	0	–	Aguirre–Puente et al (78)
	1×10^{-8}	-0.5	–	" "
Manchester Silt	1×10^{-6}	0	–	Horiguchi & Miller (73)
	1×10^{-11}	-0.3	–	" "
Silt Fraction 4–8μm	2×10^{-6}	0	–	" "
	1×10^{-10}	-0.2	–	" "
Chena Silt	1×10^{-6}	0	–	" "
	1×10^{-10}	-0.2	–	" "
NWA Silt	1×10^{-6}	0	–	" "
	1×10^{-11}	-0.2	–	" "
Calgary Silt	1×10^{-7}	0	–	" "
	1×10^{-10}	-0.2	–	" "
Fairbanks Silt Loam	4×10^{-6}	0	–	Kane & Stein (129)
Silty Clay	7×10^{-7}	>0	–	Smith (94)
	4.5×10^{-9}	-0.2	–	" "
AASHO A–4 Soil (sand 62%, silt 20%, clay 18%)	2.7×10^{-10}		30	Elzeftawy&Dempsey (130)
N. W. Silt (Alaska)	2.8×10^{-8}		40	Ingersoll (131)
Silver Sand	1×10^{-9}	0	–	Van Loon et al (132)
	1.1×10^{-9}	-0.1	–	" "
Snowcal	1×10^{-11}	-0.2..1°C		Thesis

the two sets of corrected values is given in figure 46. The values corresponded well over the whole range of suctions and it was therefore decided to use the manufacturer's values in all relevant calculations, as psychrometers were also found to compare well with the individual cxalibration curves, supplied with each probe, when tested with the suggested salt solution.

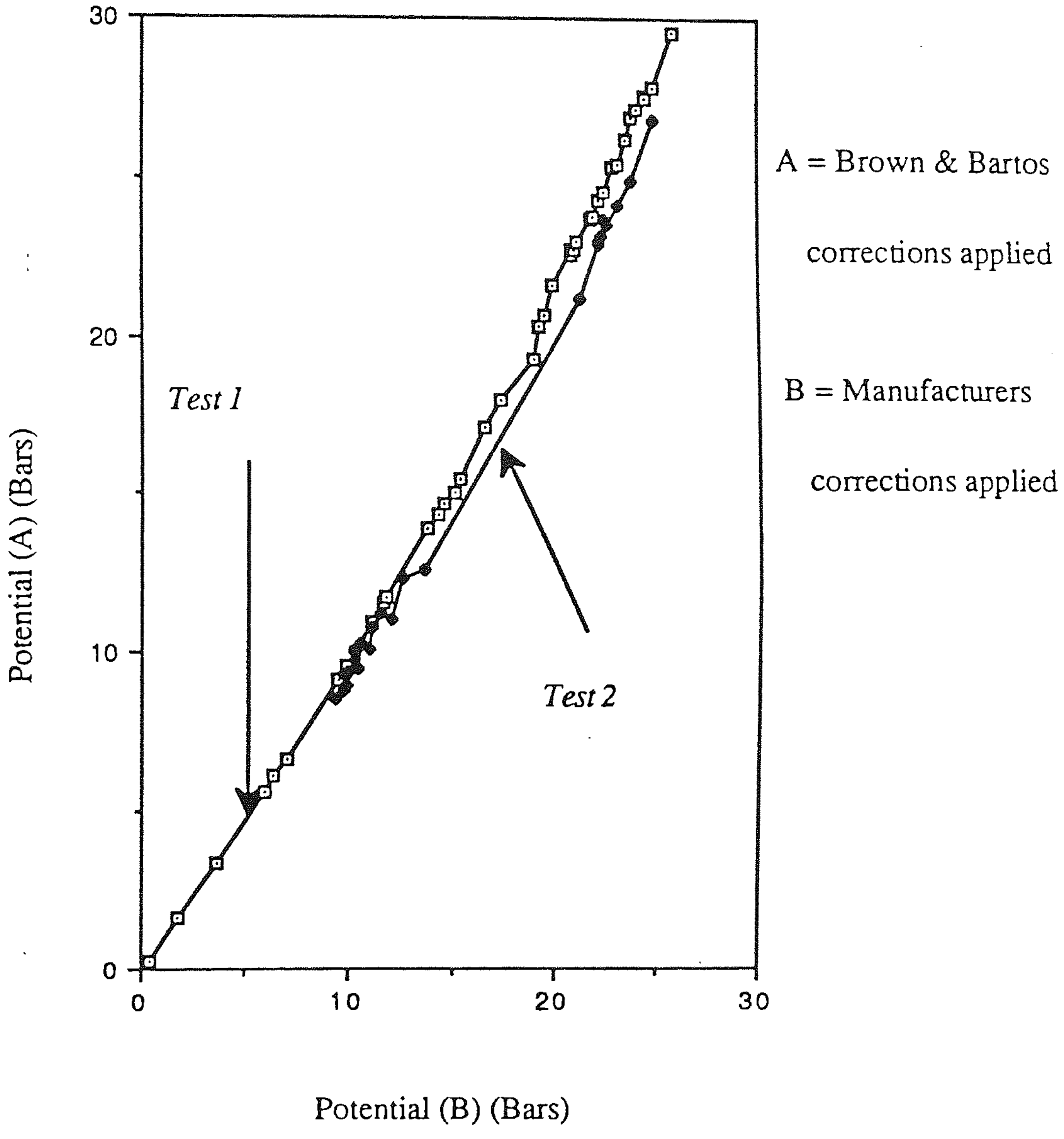

Figure 46 – Potential Values Corrected Using Information Supplied by Wescor (A) and Brown and Bartos (B)

CHAPTER 9. CONCLUSIONS

This application of neutron radiography has lead to the development of an experimental technique which utilises recent developments in a number of related fields. Thermocouple psychrometers, widely used by plant and soil scientists, provided reliable information on the soil water suctions and were much more suitable for the experimental system than more traditional tensiometers . The techniques used in remote sensing were adopted for enhancement of the images obtained from the thermal neutron beam. The technique has been shown to produce realistic and reproducible values for hydraulic conductivities in an artificial silt soil subject to freezing conditions. It relies on the determination of volumetric water contents from the digital analysis of neutron radiographs and evaluation of suctions throughout the specimen by the use of psychrometer probes. The method used to determine moisture contents from the radiographs involved an enhancement of the image to provide greater contrast and subsequent digitising of the image, from which values for the soil water were obtained and corrected using the reference cell values.

Following the initial work, a more powerful beam became available but, unfortunately, there was a distinct tailing off in intensity at the extremities, which was clearly discernable in the blurring of the images at the edges. To correct for this the images were normalised, an added analysis stage, which would have been unnecessary with a beam of more uniform intensity. Despite this the technique proved successful and reliable because each image had its own reference section, making analysis independent of both variations in neutron beam intensity and in the developing of the images.

A major benefit of the technique is that it is non–intrusive, in that determinations of water content can be made at any time throughout the test without the soil having to be sectioned for gravimetric determinations of water content. Furthermore the method can be used with any soil provided the elements present in the soil have neutron absorption coefficients that are significantly different to that of hydrogen and so enable water to be clearly distinguished from the soil.

In these experiments Snowcal was chosen as the soil material because it has been shown, in the tests reported in Chapter 5 and elsewhere (3), to be susceptible to frost action. However, the test duration was limited to only a few hours compared to several days in traditional freezing experiments and, although fully developed ice lenses were not achieved, heave values of 1–2mm were obtained. The data in Chapter 5 indicates that, following similar freezing periods, the heaves obtained from Snowcal specimens, subjected to the TRRL frost heave test, were of similar magnitude.

The rectangular cross section specimen used throughout the experiments has resulted in some problems. The major problems arose from the expansive forces of the growing ice phase, which led to non–uniform expansion in the thin section PTFE rings. This expansion served to restrict the movement of the rings in the PTFE linings of the cells, despite lubrication of the rings with a silicon based grease. A way of limiting the problem would be to use circular cross–section rings as used by McCabe (3) to prevent uni–directional expansion. The use of a circular cross–section specimen was originally discounted because of envisaged problems with interpretation of data from the radiographs, however with the sophisticated image analysis computing software available this difficulty could now be overcome.

Experiments carried out with the cold neutron facility at Harwell Research Reactor demonstrated that a specimen thickness greater than 12.5mm prevented acceptable contrast between water and the soil and therefore a circular cross–section sample would have to be restricted to 12.5mm diameter. This is not unreasonable as both Miller (71) and Aguirre–Puente (78) used comparable sized specimens in their work. Problems would be encountered, however, in incorporating the large size psychrometer/thermocouples into the soil for inevitably this would produce unacceptable disruption to the integrity of the soil. For the experiments at Harwell a specimen of Snowcal was prepared in accordance with TRRL LR90 Frost Heave Test (21). A commercial freezer was used to house this specimen, as depicted in figure 47.

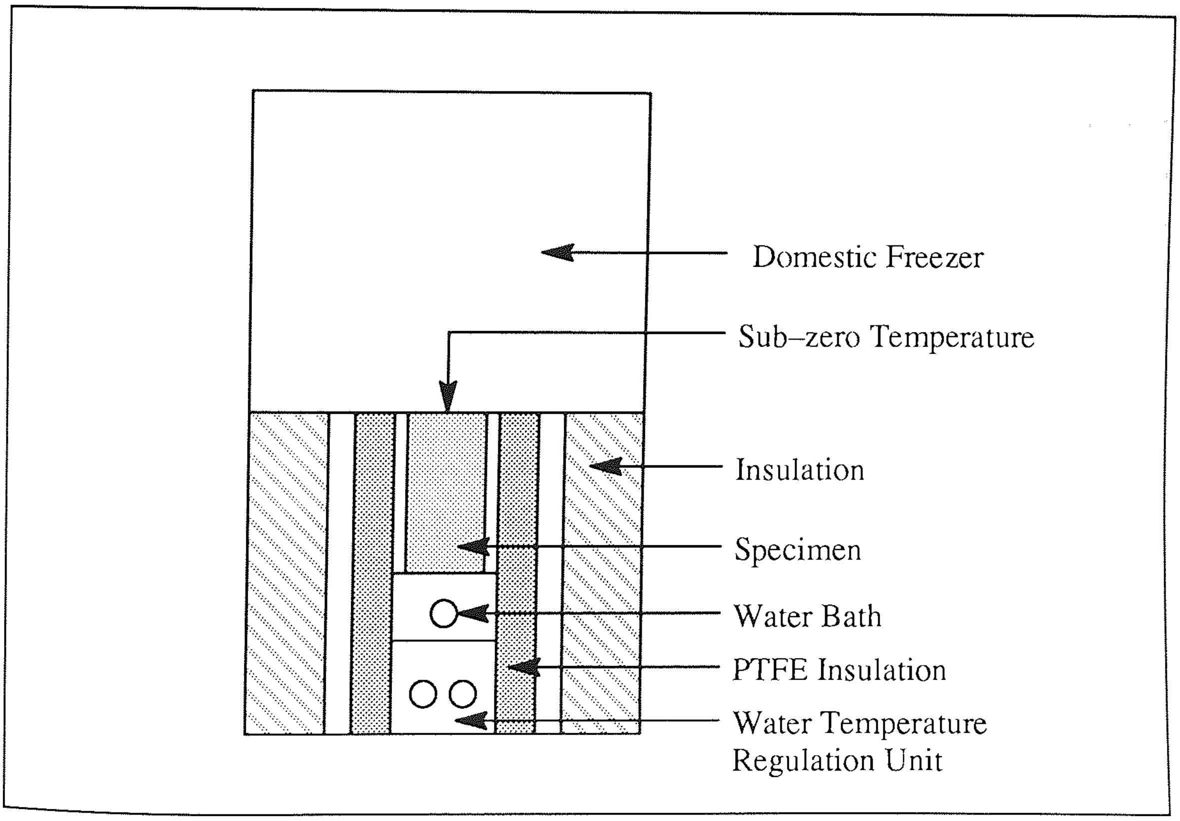

Figure 47 – Cold Neutron Beam – Experimental Set–up.

The specimen was positioned on a water bath located on a water temperature regulation unit and the surrounding space filled with PTFE loose insulation (PTFE swarf) to the top of the specimen. The top of the specimen was subjected to the air temperature in the freezer which was maintained at –4°C for 48 hours. During freezing a series of radiographs of the specimen were obtained using a variety of films and intensifying screens. No ice lens formation or water movement could be discerned on the radiographs. To demonstrate that the thickness of the specimen was preventing the observation of any ice lenses, the frozen section of the specimen was sliced vertically into 12mm sections which were individually radiographed using the cold neutron beam with a Kodak CX x–ray film and gadolinium intensifying screen. Contact prints of the images are given in plates 101 and 102 and clearly show ice lensing in the soil. The quantity of water in the 100mm diameter specimen was therefore to great to permit contrasts in exposure of the photographic plate, but with the 12mm sections (as used in previous experiments with thermal neutron beams) the ice lenses formed in the soil were depicted in detail on the radiograph.

The experimental work reported in this thesis has shown that the technique can be used to obtain hydraulic conductivity values for soils under freezing conditions and that the values for hydraulic conductivity conform to those of other researchers and hence help to validate their methods. Of major importance, however, is the capability of the technique to actually show ice lenses forming in the soil. The tests carried out using the thermal neutron beams show clearly the formation of an ice lens and the subsequent development of a frozen fringe of soil beneath the ice lens. The initial freezing process is considered to correspond with the Capillary Theory and this is supported by the movement of moisture through the soil to the growing ice lens at the freezing front. The long term development of ice lens formation is evidenced by the formation of a frozen fringe below the ice lens and this observation supports the mechanism associated with secondary heave. The use of false colour images has been particularly useful in depicting the development of the ice lens and frozen fringe and hence the use of image enhancement is considered to be of fundamental importance to this technique.

The dynamic nature of ice lens formation in freezing soils suggests the use of real time neutron radiography (RTNR). The I2S image analysis system used in this research permitted a sequential projection of images at various time separations and hence it was possible, by speeding up the sequence, to show the ice phase forming. Logically the use of RTNR would smooth out the sequence as the provision of images at discrete time separations would lead to a real visual presentation of the processes occurring in the soil as it freezes and takes up water. As previously reported in Chapter 4 Lindsay et al (116) have obtained good results with RTNR in a number of other applications.

Plate 101. Iced Lensed Soil Section

Plate 102. Iced Lensed Soil Section

The technique does, however, have serious drawbacks when applied to the study of freezing soils. The use of a neutron facility at a nuclear reactor is very expensive, costs to industry can run into thousands of pounds for fairly limited use, and so economic considerations are likely to preclude future use of nuclear reactors for this type of study. There are also safety matters which must be considered. The test involves the use of apparatus to supply the freezing head and water bath temperature regulation unit with cooling fluid. These circulators have to be positioned outside the concrete shielding as the cavity containing the test rig is of limited size. This means that circulating fluid, irradiated by the neutron beam in the cavity, is brought outside the shielding, through the operation of these circulators, where it may prove a danger to health. Total shielding of all equipment used in the experimental work would prevent access for temperature adjustment etc. and so limit the versatility of the test and would, again, increase the costs.

The technique of neutron radiography is not, however, restricted to studies of freezing soils, the range of applications is rapidly increasing covering everything from growing plants (114) to concrete (115). The sensitivity of neutron radiography, compared with x–radiography, for distinguishing water, has made it the ideal choice for the experiments reported here and further development of the work has lead to an analysis of porous building materials. This has evolved into the analysis of the structural and aesthetic breakdown of clay bricks during deterimental weathering conditions. The disfigurement of brick masonry by discolouration is a major concern to the building industry. Efflorescence depends on the chemical composition, particularly the salts present in the bricks, the pore structure of bricks, the moisture content and the rate of moisture evaporation. By obtaining information on the pore structure of bricks and combining this with data obtained by neutron radiography on the quantity and movement of water in the bricks, the mechanisms involved in efflorescence could be better understood and techniques could be developed for its control.

The proposed experiment would involve the use of a cold neutron beam to examine bricks under simulated severe weathering conditions to obtain information on water movements and ice formation. The constituent atoms in clay bricks are low neutron absorbers and so fairly transparent to a neutron beam. Consequently a series of radiographs taken at frequent intervals during a freeze–thaw cycle, or the use of RTNR, should depict the movement of water and the formation of ice within the brick, and therefore provide information on the failure mechanism.

An investigative study was comissioned by Ibstock, brick manufacturers of Bristol, the tests being undertaken on the facilities at Harwell Research Laboratories, which were donated free of charge as Harwell has an interest in the subject. To date preliminary tests have been carried out on a variety of dry bricks to determine their responce to neutrons. The bricks have cadmium markers, in the form of letters A and B, positioned at the front and back of the brick. The clarity of the markers provides a good indication of the relative transparency of the bricks to neutrons. Contact prints of two radiographs of the bricks are given in plates 103 and 104. These were obtained with the cold neutron beam facility at Harwell, using a Kodak CX x–ray film and gadolinium intensifying screen. The radiographs clearly depict the differences in structure between the hand made brick and the machine made brick and on both bricks the cadmium markers are clearly visible. Continuing work at Harwell is investigating the moisture flows in clays to assess nuclear leakage problems and the ingress of water into materials, particularly concrete, is being examined using a combination of water (H_2O) and deuterated water (D_2O) (Deuterium is a heavy isotope of hydrogen with a mass roughly double that of hydrogen and consequently its mass adsorption coefficient for neutrons is markedly different to that for hydrogen). The image analyses reported in this thesis are now being adopted for these studies to enhance the images produced from neutron radiography.

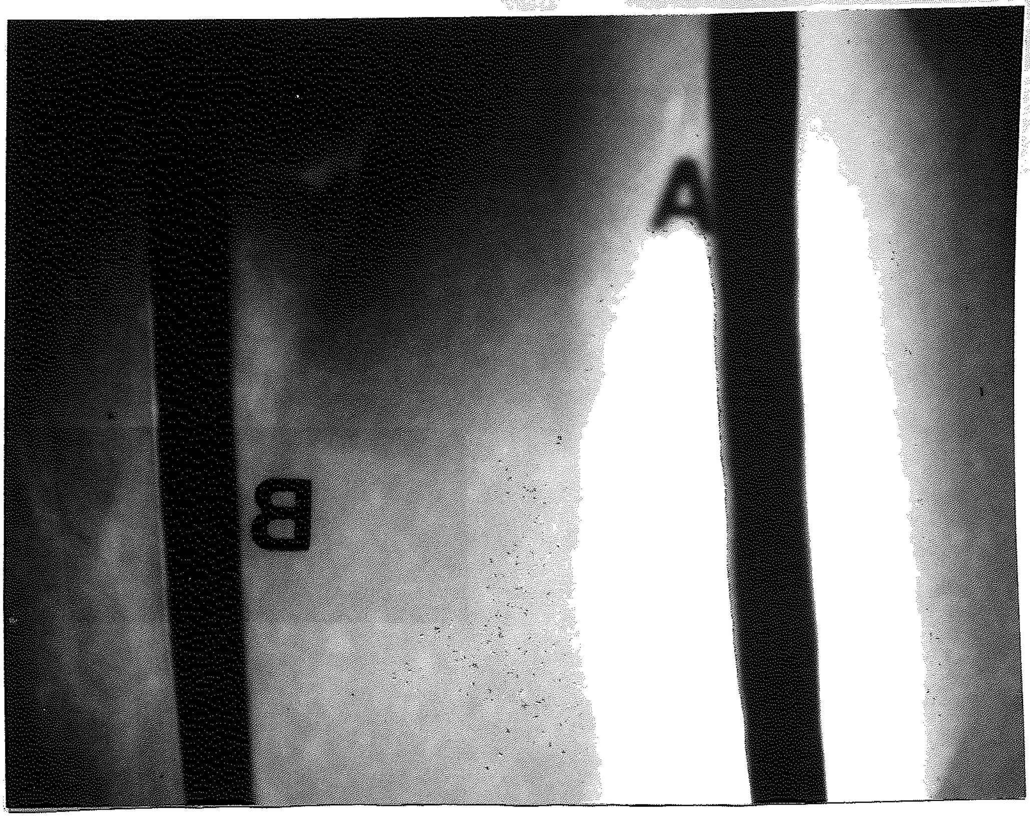

Plate 103. Hand Made Brick Section

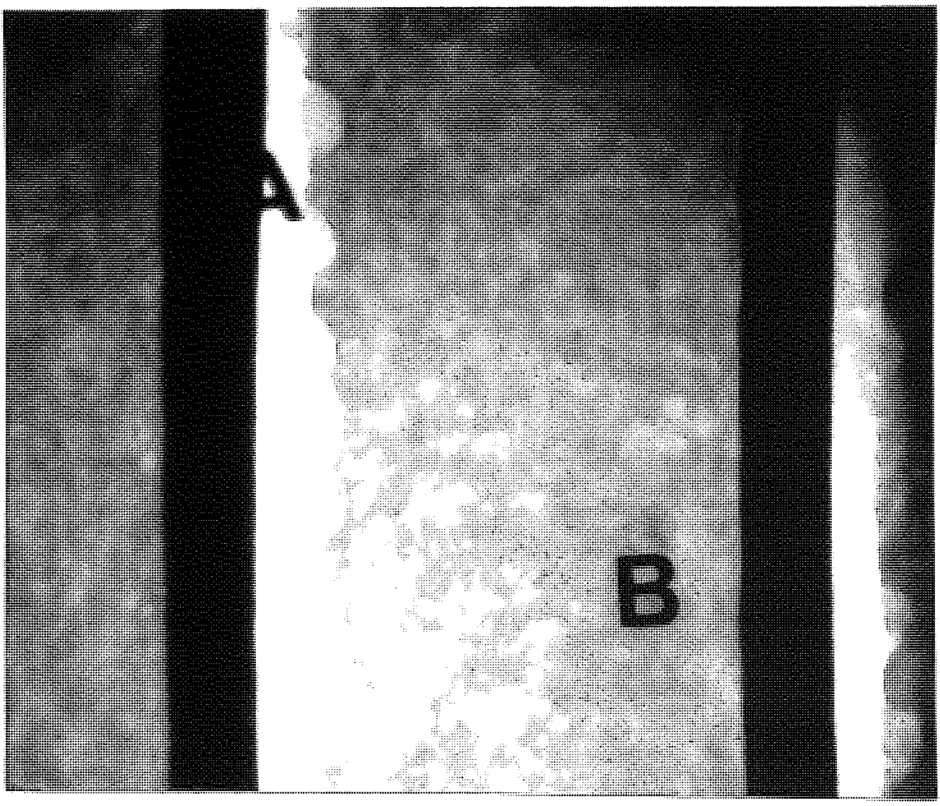

Plate 104. Machine Made Brick Section

REFERENCES

1. Taber S. Frost Heaving. Journal of Geology, Vol. 37 No. 5 1929, pp 428–461.

2. Miller R.D .Freezing Phenoma in Soils. Chapter 11 in Applications of Soil Physics, Hillel, Academic Press, N.Y. 1980

3. McCabe E.Y. Frost Action in Granular Materials. Ph.D Thesis, Aston University, 1982.

4. Everett D.H. The Thermodynamics of Frost Damage to Porous Solids. Transactions of the Faraday Society, Vol. 57, 1961, pp 1541–1551.

5. Holden J.T. Approximate Solutions for Millers Theory of Secondary Heave. Proceedings 4th Int. Conf. on Permafrost, Fairbanks, Alaska, July 1983.

6. Takagi S. The Absorption Force Theory of Frost Heaving. Cold Regions Science and Technology, Vol. 3, 1980, pp 57–81.

7. Konrad J.M. and Morgenstern N.R. A Mechanistic Theory of Ice Lens Formation in Fine–Grained Soils. Can. Geo. Journal, Vol. 17, 1980, pp 473–486.

8. Konrad J.M. and Morgenstern N.R. The Segregation Potential of a Freezing Soil. Can. Geo. Journal, Vol. 18, 1981, pp 482–491.

9. Konrad J.M. and Morgenstern N.R. Prediction of Frost Heave in the Laboratory During Transient Freezing. Can. Geo. Journal, Vol. 19, pp 250–259.

10. Mageau D.W. and Sherman M.B. Frost Cell Design and Operation. Proceedings 4th Int. Conf. on Permafrost, Fairbanks, Alaska, 1983, pp 767–772.

11. Mahoney J.P. and Vinson T.S. A Mechanistic Approach to Pavement Design in Cold Regions. Proceedings 4th Int. Conf. on Permafrost, Fairbanks, Alaska, 1983, pp 779–782.

12. Konrad J.M. and Morgenstern N.R. Frost Susceptibility of Soils in Terms of their Segregation Potential. Proceedings 4th Int. Conf. on Permafrost, Fairbanks, Alaska, 1983, pp 660–665.

13. Konrad J.M. and Morgenstern N.R. Frost Heave Prediction of Chilled Pipelines Burried in Unfrozen Soils. Can. Geo. Journal, Vol. 21, 1984, pp 100–115

14. Jones R.H. Developments and Applications of Frost Susceptibility Testing. Engineering Geology, Vol. 18, 1981, pp 269–280.

15. Taber S. Freezing and Thawing of Soils as Factors in the Destruction of Road Pavements. Public Roads, Vol. 11 No. 6, 1930, pp 113–132.

16. Jones R.H. and Dudek S.J.M. Comparison of a Precise Freezing Cell with other Facilities for Frost Heave Testing. Trans. Res. Rec. 1979, 705 pp 63–71.

17. Croney D. and Jacobs J.C. The Frost Susceptability of Soils and Road Materials. RRL. Report LR90, Crowthorne, England 1967.

18. Kaplar C.W. Freezing Test for Evaluating Relative Frost Susceptibility of Various Soils. USA CRREL, Tech. Rep. 1974, 250, 36pp.

19. Jones R.H. and Hurt K.G. Improving the Repeatability of Frost Heave Tests. Highways and Road Construction July/August 1975, pp 8–13.

20. Transport and Road Research Laboratory. Research on the Frost Susceptibility of Road Making Materials. TRRL Leaflet 611, Crowthorne, 1977, 2pp.

21. The LR90 Frost Heave Test– Interim Specification for use with Granular Materials. TRRL 1977 Crowthorne, England, Sup. Rep. 318:16pp. Updated to SR829.

22. MM 64. Materials Memorandum TRRL (1981), 42pp.

23. Sutherland H.B. and Gaskin P.N. A Comparison of the TRRL and CRREL Tests for Frost Susceptibility of Soils. Can. Geo. Journal, Vol. 10 No. 3, 1973, pp 553–555.

24. Chamberlain E.J. Frost Susceptability of Soil– A Review of Index Tests. CRREL Monograph 81–2. US Army Corps of Engineers. Cold Regions Research and Engineering Laboratory, Hanover, New Hampshire, Dec. 1981, pp 110.

25. Casagrande A. Discussion on Frost Heaving. Proc. Highways Research Board, Vol. 11, pt. 1, 1931, pp 168–172.

26. Kettle R.J. and McCabe E. Heaving Pressures as a Means of Assessing Frost Susceptibility. Proc. of Seminar on the Prediction of Frost Heave, 9th April 1981. Nottingham University.

27. Williams P.J. Thermodynamic Conditions for Ice Accumulation in Freezing Soils. Frost Action in Soils Vol. 1, International Symposium, University of Lulea, Sweden. Feb. 16th–18th 1977.

28. Konrad J.M. and Morgenstern N.R. Effects of Applied Pressure on Freezing Soils. Can. Geo. Journal, Vol. 19 1982, pp 494–505.

29. McCabe E. and Kettle R.J. The Influence of Surcharge Loads on Frost Susceptability. Preceedings of the 4th International Conference on Permafrost, 1983, pp 816–820.

30. O'Neil K. The Physics of Mathematical Frost heave Models: A Review. Cold Regions Science and Technology, Vol. 6, 1983, pp 275–291.

31. Guyman G.L. ; Hromadka T.V. and Berg R.L. A One–Dimensional Frost Heave Model, Based Upon Simulation of Simultaneous Heat and Water Flux. Cold Regions Science and Technology, Vol. 3, 1980, pp 253–262.

32. Guyman G.L.; Berg R.L and Hromadka T.V. Field Tests of a Frost Heave Model. Permafrost: 4th Int. Conf., Proceedings. National Academy Press, Washington, D.C., U.S.A. 1983, pp 409–414.

33. Hopke S.W. A Model for Frost Heave Including Overburden. Cold Regions Science and Technology, Vol. 3, 1980, pp 111–127.

34. Gori F. A Theoretical Model for Predicting the Effective Thermal Conductivity of Unsaturated Frozen Soils. Proceedings 4th Int. Conf. on Permafrost, Fairbanks, Alaska, 1983, pp 363–368.

35. Penner E. Soil Moisture Movements During Ice Segregation. Highways Research Board Bulletin 135, 1956, pp 109–118.

36. Williams P.J. Suction and its Effects in Unfrozen Water of Frozen Soils. Proceedings First International Permafrost Conference, Nat. Acad. Sci. –N.R.C. Publ. 1287, 1963, pp 225–229.

37. Kinosita S. Soil Water Movement and Heat Flux in Freezing Ground. Proceedings 1st Conf. on Soil–Water Problems in Cold Regions, Calgery, Alberta, (American Geophysical Union) pp 33–41.

38. McCabe E.Y. Thermal Aspects of Frost Action. Proceedings 4th Int. Conf. on Ground Freezing, Sapporo, Japan, 1985, Vol ii, pp 47–54.

39. Osterkamp T.E. Structure and Properties of Ice Lenses in Frozen Ground. Proc. Conf. on Soil–Water Problems in Cold Regions, Calgary, Alberta, Canada, pp 89–111.

40. Arvidson W.D. and Morgenstern N.R. Water Flows Induced by Soil Freezing. Can. Geo. Journal, Vol. 14, 1977, pp 237–245.

41. Nerseova Z.A. and Tsytovich N.A. Unfrozen Water in Frozen Soils. Proceedings of Int. Conf. on Permafrost, Washington D.C, National Academy of Sciences, 1966, pp 230–234.

42. Williams P.J. and Perfect E. Investigation of Thermally Actuated Water Migration in Frozen Soils. Final Report to the Dept. of Energy, Mines and Resources, Earth Physics Branch. April 1980.

43. Takagi S. Segregation Freezing as the Cause of Suction Force for Ice Lens Formation. Report 78–6, US Army Cold Regions Research and Engineering Laboratory, Hanover, N.H.

44. Corte A.E. Vertical Migration of Particles in Front of a Moving Freezing Plane. Journal of Geological Research, Vol. 67, No. 3, 1962, pp 1085–1090.

45. Hoekstra P. The Physics and Chemistry of Frozen Soils. Highways Research Board– Special Report 103, 1969, pp 78–90.

46. Burt T.P. A Study of Hydraulic Conductivity in Frozen Soils. M. A Thesis, Carleton University, Ottawa, Canada, 1974.

47. Taylor D.W. Fundamentals of Soil Mechanics. Wiley, New York, 1949, pp 700.

48. Schofield R.K. Suction in Swollen Clays. Pore Pressure and Suction in Soils, 1961, Butterworths pp 59–60.

49. Gardner W.R. Soil Suction and Water Movement. Pore Pressure and Suction in Soils, 1961, Butterworths pp 137–140.

50. Williams P.J. Pressure Membrane Apparatus for the Investigation of High Suctions in Soils. Building Research Note No. 45, 1964, Division of Building Research, National Research Council, Ottawa, Canada.

51. Hodnett M. Soil Water Physics in the Field. Soil Water Physics Group Meeting. Rothamsted Experimental Station, Harpenden, 18th Feb. 1987.

52. Brown R.W. and Bartos D.L. A Calibration Model for Screen–Caged Peltier Thermocouple Psychrometers. United States Department of Agriculture, Forest Service. Research Paper INT–293, July 1982.

53. Waldron L.J. and Mambein T. Soil Moisture Characteristics by Osmosis with Polyethylene Glycol. A Simple System with Osmotic Data and Some Results. Soil Sci. 110, 1970, pp 401–404.

54. Williams P.J. Measurement of Suction Pressures Developed on Freezing of Soils. Proceedings 5th Western Canadian Conference on Heat Transfer, Ottawa, 1972, pp 56–59.

55. Jones R.H and Hurt K.G. An Osmotic Method for Determining Rock and Aggregate Suction Characteristics with Applications to Frost Heave Studies. Quarterly Journal Eng. Geo. Vol. 11, 1978, pp 245–252.

56. McKim H., Berg R.L., McGaw R., Atkins R. and Ingersoll J.W. Development of a Remote Reading Tensiometer Transducer System for Use in Subfreezing Temperature. Proc. 2nd Conf. on Soil Water Problems in Cold Regions. Edmonton, Canada, 1976.

57. McGaw R., Berg R.L., and Ingersoll J.W. An Investigation of Transient Processes in an Advancing Zone of Freezing. Proc. 4th Int. Conf. Permafrost. Fairbanks, Alaska, 1983, pp 821–825.

58. Thompson J.D. Subgrade Effects on the Frost Heave of Roads. Ph.D Thesis, University of Nottingham, 1981.

59. Richards L.A. Capillary Conductivity of Liquids Through Porous Mediums. Physics, Vol. 1, 1931, pp 318–333.

60. Richards L.A. and Moore D.C. Influence of Capillary Conductivity and Depth of Wetting on Moisture Retention. Trans. Am. Geophys. 33.4, 1952.

61. Moore R.E. Water Conduction from Shallow Water Tables. Hilgardia, Vol. 12, 1939, pp 383–426.

62. Childs E.C.J. and Collis–George N.C. The Permeability of Porous Materials. Proc. Roy. Soc. (London) A201, 1950, pp 392–405.

63. Nielsen D.R.; Kirkham D. and Perrier E.R. Soil Capillary Conduction, Comparison of Measured and Calculated Values. Soil Sci. Soc. Am. Journal, Vol. 24, 1960, pp 157–160.

64. Richards S.J. and Weeks L.V. Capillary Conductivity Values from Moisture Yield and Tension Measurements in Soil Columns. Soil Sci. Soc. Am. Journal, Vol. 35, 1953, pp 3–8.

65. Gurr C.G. Use of Gamma–Rays in Measuring Water Content and Permeability in Unsaturated Columns of Soil. Soil Sci. Vol. 94 No. 4, 1962, pp 224–229.

66. Visalingham M. and Tandy J.D. The Neutron method for Measuring Soil Moisture Content: A Review. Journal of Soil Science, Vol. 243 No. 4, 1972, pp 499–511.

67. Gardner W.R. Some Steady State Solutions of the Unsaturated Moisture Flow Equation with Application to Evaporation from a Water Table. Journal of Soil Science Society of America, Vol. 85, 1958, pp 228–232.

68. Miller R.D and Elric D.E. Dynamic Determination of Capillary Conductivity Extended from Non–negligable Membrane Impedance. Soil Sci. Soc. Am. Journal, Vol. 22, 1958, pp 483–486.

69. Kunze R.J. and Kirkham D. Simplified Accounts of Membrane Impedance in Capillary Conductivity Determinations. Soil Sci. Soc. Am. Journal, Vol. 26, 1962, pp 421–426.

70. Richards B.G. Determination of the Unsaturated Permeability and Diffusivity Functions from Pressure Plate Outflow Data with Non–negligable Membrane Impedance. In Moisture Equilibria and Moisture Changes in Soils Beneath Covered Areas. pp 47–54, 1965, Butterworths, Australia.

71. Miller R.D. Ice Sandwich: Functional Semipermeable Membrane. Science, Vol. 169, 1970, pp 584–585.

72. Sahin T. Transport of Water in Frozen Soil. M.S Thesis, Cornell University, Ithaca, N.Y, 1973.

73. Horriguchi K. and Miller R.D. Experimental Studies with Frozen Soils in an Ice Sandwich Permeameter. Cold Regions Science and Technology, Vol. 3, 1980, pp 177–183.

74. Horriguchi K. and Miller R.D. Hydraulic Conductivity Functions of Frozen Materials. Proceedings of 4th International Conference on Permafrost, Fairbanks, Alaska, 1983.

75. Williams P.J. and Burt T.P. Measurement of Hydraulic Conductivity of Frozen Soils. Can. Geo. Journal, Vol. 11, 1974, pp 647–650.

76. Burt T.P. and Williams P.J. Hydraulic Conductivity in Frozen Soils. Earth Surface Processes, Vol. 1, 1976, pp 349–360.

77. Perfect E. and Williams P.J. Thermally Induced Water Migration in Frozen Soils. Cold Regions Science and Technology, Vol. 3, 1980, pp 101–109.

78. Aguirre–Puente J. and Gruson J. Measurements of Permeabilities of Frozen Soils. Proceedings of 4th International Conference on Permafrost, Fairbanks, Alaska, 1983.

79. Yoneyama K.; Ishizki T. and Nishio N. Water Re–distribution Measurements in Partially Frozen Soil by X–Ray Technique. Proceedings of 4th International Conference on Permafrost, Fairbanks, Alaska, 1983.

80. McKim H.L; Walsh J.E. and Avion D.N. Review of Techniques for Measuring Soil Moisture in Situ. Special Report 80–31. US Army Cold Regions Research and Engineering Laboratory, Hanover, New Hampshire 03755, August 1980.

81. Hoekstra P. Moisture Movements in Soils Under Temperature Gradients with the Cold Side Temperature Below Freezing. Water Resources Research, Vol. 2 No. 2, 1966, pp 241–250.

82. Loch J.P.G. and Kay B.D. Water Redistribution in Partially Frozen, Saturated Silt, Under Several Temperature Gradients and Overburden Loads. Soil Sci. Soc. Am. Journal, Vol. 42, 1978, pp 400–406.

83. Fukuda M.; Orhun A. and Luthin J.N. Experimental Studies of Coupled Heat and Moisture Transfer in Soils During Freezing. Cold Regions Science and Technology, Vol. 3, 1980, pp 223–232.

84. Ayorinde O.A. Application of Dual–Energy Gamma–Ray Technique for Non–destructive Soil Moisture and Density Measurement During Freezing. Transactions of the American Society of Mechanical Engineers. Published in Journal of Energy Resources Technology, Vol. 105, 1983, pp 38–42.

85. Ducros P. and Dupont M. A Nuclear Magnetic Resonance Study of Water in Clays in Magnetic and Electrical Resonance and Relaxation. C.R. XIe Colloque Ampere Eindhoven, 1962.

86. Tice A.R.; Burrows C.M. and Anderson D.M. Determination of Unfrozen Water in Frozen Soils by Pulced Nuclear Magnetic Resonance. Proceedings of the 3rd Int. Conf. on Permafrost, Edmonton, Alberta, Canada, 1978, pp150–153.

87. Oliphant J.L; Trice A.R and Nakanos Y. Water Migration Due to Temperature Gradient in Frozen Soil. Proceedings of the 4th Int. Conf. on Permafrost, Fairbanks, Alaska, 1983, pp 951–956.

88. Kay B.D. and Perfect E. State of the Art: Heat and Mass Transfer in Freezing Soils. Proceedings of 5th Int. Symposium on Ground Freezing, Nottingham, 1988, pp 3–22. Edited by Jones R.H. and Holden J.T. published by Bulkema.

89. Oliphant J.L and Tice A.R Comparison of Unfrozen Water Contents Measured by DSC and NMR. Proceedings 3rd Int. Symp. on Ground Freezing. Hanover, New Hampshire. CRREL Special Report 82–16, 1982, pp 115–123.

90. Xu Xiaozu, Oliphant J.L and Tice A.R. Experimental Study of Factors Affecting Water Migration in Frozen Morin Clay. 4th Int. Symposium on Ground Freezing. Sapporo, Japan. Vol. 1, 1985, pp 123–128.

91. Patterson D.E. and Smith M.W. The Measurement of Unfrozen Water Content by Time Domain Reflectometry: Results from Laboratory Tests. Can. Geo. Journal, Vol. 18 No. 1, 1981, pp 131–144.

92. Topp G.C.; Davis J.L and Annan A.P. Electromagnetic Determination of Soil Water Content: Measurements in Coaxial Transmission Lines. Water Resources Research, Vol. 16 No. 3, June 1980, pp 574–582.

93. Patterson D.E. and Smith M.W. The Use of Time Domain reflectometry for the Measurement of Unfrozen Water in Frozen Soils. Cold Regions Science and Technology, Vol. 3, 1980, pp 205–210.

94. Smith M.W. Observations of Soil Freezing at Invik, Northwest Territories, Canada. Can. Journal of Earth Sciences, Vol. 22, 1985, pp 283–290.

95. Stein J. and Kane D.L. Monitoring the Unfrozen Water Content of Soil and Snow using Time Domain Reflectometry. Water Resources Research, Vol. 19 No. 6, 1983, pp 1573–1584.

96. Oliphant J.L A Model for Dielectric Constants of Frozen Soils. Freezing and Thawing of Soil–Water Systems. Am. Soc. Civil Engineers. New York, 1985, pp 46–57.

97. Bouyoucos G.J. Classification and Measurement of the Different Forms of Water in Soil by means of the Dilatometer Method. Michigan Agricultural Experiment Station Bulletin 36, 1917, pp 48.

98. Mageau D.W. and Morgenstern N.R. Observations on Moisture Migrations in Frozen Soils. Can. Geo. Journal, Vol. 17, 1980, pp 54–60.

99. Anderson D.M.; Trice A.R. and McKim H.L. The Unfrozen Water and the Apparent Specific Heat Capacity of Frozen Ground. Proc. 2nd Int. Conf. on Permafrost, Washington, 1973, pp 289–294.

100. Williams P.J. Specific Heats and Unfrozen Water Content of Frozen Soils. Proceedings 1st Canadian Conference on Permafrost (National Research Council, Associate Committee on Soil and Snow Mechanisms– Technical Memorandum 76)

101. Harlan R.L. Analysis of Coupled Heat–Fluid Transport in Partially Frozen Soil. Water Resources Research, Vol. 9 No. 5, 1973, pp 1314–1322.

102. Nakano Y.; Trice A.R.; Oliphant and Jenkins T.F. Soil–Water Diffusivity of Unsaturated Soils at Sub–Zero Temperatures. Proceedings of 4th International Conference on Permafrost, Fairbanks, Alaska, 1983, pp 889–893.

103. Faltings V. and Harteck P. Der Tritiumgehalt der Atmosphaire. Z Naturforsch. 5 A, 1950, pp 438–439.

104. Grosse A.V.; Johnson W.H.; Wolfgang R.L. and Libby W.F. Tritium in Nature. Science, Vol. 113, 1951, pp 1–2.

105. Schmalz B.L. and Polzer W.L. Tritiated Water Distribution in Unsaturated Soil. Soil Science, Vol. 108 No. 1, 1968, pp 43–47.

106. Vogel J.C.; Thilo L. and van Duken M. Determination of Groundwater Recharge with Tritium. Journal of Hydrology, Vol. 23, pp 131–140.

107. Allison G.B and Hughes M.W. The use of Environmental Tritium to Estimate the Recharge to a South–Australian Aquifer. Journal of Hydrology (NL), Vol. 26 No. 3/4, pp 245–254, 1974.

108. Chizhov A.B.; Chizhova N.I.; Morkovkina I.K. and Romanov V.V. Tritium in Permafrost and in Ground Ice. Proceedings 4th Int. Conf. on Permafrost, Fairbanks, Alaska, 1983, pp 147–150.

109. Sir J. Chadwick. Radioactivity and Radioactive Substances. 4th Ed., Published by Sir Isaac Pitman and Sons Ltd. Revised and Supplemented by Prof. J.Rotdat, 1953.

110. Hawkesworth M.R. Neutron Radiography: Equipment and Methods. Atomic Energy Review, Vol. 15 No. 2, pp 169–220, 1977.

111. Hawkesworth M.R. and Walker J. Cold Neutron Radiography Applied to the Study of Hydrogen in Palladium. Proceedings of the 1st World Conference on Neutron Radiography, 1982. San Diego California USA.

112. Veenema J.J.; Mesman D. and Leefland H.P. Neutron Radiography Exercises at Low Flux Reactors. Proceedings of the 1st World Conference on Neutron Radiography, 1982. San Diego California USA.

113. Kartashev E.R Neutron Radiography Facilities Using Neutron Beams from Nuclear Reactors. Proceedings of the 1st World Conference on Neutron Radiography, 1982. San Diego California USA.

114. Roland G. A Neutron Radiography Technique for Studying Young Roots Growing in Soil. Proceedings of the 1st World Conference on Neutron Radiography, 1982. San Diego California USA.

115. Aderhold H.C.; Hover K.C. and Najjar W.S. The Cornell Neutron Radiography Facility and its Applications to the Study of the Internal Structure and Microcracking of Concrete. Proceedings of the 2nd World Conference on Neutron Radiography, Paris 16–19 June 1986.

116. Lindsay J.T.; Jones J.D. and Kauffman C.W. Real Time Neutron Radiography and its Application to the Study of Internal Combustion Engines and Fluid Flow. Proceedings of the 2nd World Conference on Neutron Radiography, Paris 16–19 June 1986.

117. Bs 1377: 1975, Methods of Test for Soils for Civil Engineering Purposes. Section 2: Soil Classification Tests:
2.7 Test 7 Determination of Particle Size Distribution.
2.7.4 Test 7(D) Subsidary Method for Fine – Grained Soils (Hydrometer Method).

118. Bs 1377: 1975, Methods of Test for Soils for Civil Engineering Purposes. Section 2: Soil Classification Tests:
2.6 Test 6 Determination of the Specific Gravity of Soil Particles.
2.6.2 Test 6(B) Method for Fine–Grained Soils.

119. Bs 1377: 1975, Methods of Test for Soils for Civil Engineering Purposes. Section 4: Soil Compaction Tests:
4.1 Test 12 Determination of the Dry Density/Moisture Content Relationships(2.5Kg Method).

120. 'Polypenco' Engineering Plastics Materials. Polypenco Ltd., PO Box 56, Welwyn Garden City, Herts AL71BR, 1985.

121. van Haveren B.P. Measurements of the Relative Vapour Pressure in Snow with Thermocouple Psychrometers. A Contribution of the Interdisciplinary Study Group on Snow, Utah State University, 1971.

122. System P–1000 Photoscan. Bulletin 1600, 1978. Optronics International, inc., 7 Stuart Road, Chelmsford, Mass. 01824 USA.

123. Users Manual, System 500, Digital Image Processing System (Version 3.1). International Imaging Systems, 1981.

124. Brutsaert W. Probability Laws for Pore–Size Distributions. Soil Science, Vol. 101 No. 2, Feb. 1966.

125. Brooks R.H. and Corey A.T. Hydraulic Properties of Porous Media. Colorado State University (Fort Collins), Hydrology Paper 3, 1964.

126. Dupuit J. Etudes Theoriques et Pratiques sur le Mouvement des Eaux dans les Cannaux Decouverts et a Travers les Terrains Permeables, Deuxieme ed. Dunod, Editeur, Paris, 1863.

127. Schroeder W.L. Soils in Construction (3rd Ed.). Published by John Wiley and Sons, pp 62.

128. Daniel D.E. Permeability Test for Unsaturated Soil. Geotechnical Testing Journal, GTJODJ, Vol. 16 No. 2, June 1983, pp 81–86.

129. Kane D.L. and Stein J. Water Movements into Seasonally Frozen Soils. Water Resources Research, Vol. 19 No. 6, December 1883, pp 81–86.

130. Elzeftawy A. and Dempsey B.J. Unsaturated Transient and Steady–State Flow of Moisture in Subgrade Soil. Transportation Research Record, 1976, pp 56–61.

131. Ingersoll J. Hydraulic Properties of Various Soils Using the Pressure Cell Permeameter. Informal, Unofficial Memorandum for Limited Distribution Only. Technical Note – Corps of Engineers, US Army Cold Regions Research and Engineering Laboratory, Hanover, New Hampshire.

132. van Loon W.K.P.; van Haneghem I.A. and Boshoven H.P.A. Thermal and Hydraulic Conductivity of Unsaturated Frozen Soils. Proceedings of the 5th International Symposium on Ground Freezing (Jones and Holden Ed.), 1988 Balkema, Rotterdam. ISBN 90 6191 8243, pp 81–90.

APPENDIX 1. RADIOGRAPHIC MATERIALS

FILM: Kodak Industrex CX, medium speed, fine grain, high contrast, direct exposure film.

DEVELOPER: Kodak LX 24 X–Ray developer. Solution: 0.3L water mixed with 0.2L developer, topped up with 0.635L water and stirred.
Duration: 6 minutes.

STOP BATH: Kodak indicator stop bath. Solution: 0.02L stop bath mixed with 1.0L water.
Duration: 30 seconds.

FIXER AND HARDENER: Kodak FX–40 X–Ray liquid fixer and Kodak HX–40 X–Ray hardener. Solution: 0.5L water mixed with 0.1L fixer and 0.15L hardener.
Duration: 4 minutes, followed by a wash in a water bath(2L water with 2 drops of detergent).

APPENDIX 2. COMPUTER PROGRAMS

The Brown and Bartos calibration program and the Least Squares program are given, together with sample output, in the following pages.

Aston University

Content has been removed for copyright reasons

Aston University

Content has been removed for copyright reasons

Aston University

Content has been removed for copyright reasons

Aston University

Content has been removed for copyright reasons

Aston University

Content has been removed for copyright reasons

APPENDIX 3. RESULTS TABLES (TESTS 1 AND 2)

KEY:

PSYCHROMETER VARIABLES:

mv: Psychrometer reading (milivolts).
omv: zero–offset reading (milivolts).
T: temperature (Deg. C).
Sec: cool time (seconds).

TEST 1

Time (m)	Position	*Psychrometer Variables* *mv*	*omv*	*T*	*Sec*	Potential *BB* Bars	M	*Moisture Content Data*	*Reference 100% / 0%*	Moisture Content cm3/cm3	Electrical Resistance	Temp. Deg C
Mask	6	*0.5*	*-6.6*	*11.3*	*15*	*1.55*	1.69	*50.00*	*100.00*	0.289	33	8.1
	5	*2.3*	*-11.0*	*11.3*	*15*	*7.37*	7.77	*50.00*	*30.00*	0.289	28	7.5
	4	*3.2*	*-15.2*	*11.2*	*15*	*10.57*	10.85	*50.00*		0.289	24	7.4
	3	*3.0*	*-20.3*	*11.1*	*15*	*10.18*	10.22	*50.00*		0.289	26	7.1
	2	*3.7*	*-23.0*	*10.5*	*15*	*13.10*	12.94	*50.00*		0.289	24	6.8
	1	*0.0*	*-53.0*	*9.8*	*15*	*	*	*50.00*		0.289		6.7
0	6	*	*	*10.5*	*15*	*	*	*51.76*	*97.71*	0.319	35	4.6
	5	*5.6*	*-19.3*	*11.2*	*15*	*19.30*	18.99	*49.62*	*30.26*	0.287	23	5.8
	4	*4.4*	*-17.3*	*10.9*	*15*	*15.00*	15.12	*49.22*		0.281	25	6.1
	3	*4.0*	*-22.0*	*10.9*	*15*	*13.92*	13.74	*48.68*		0.273	25	6.3
	2	*4.9*	*-25.0*	*10.2*	*15*	*17.94*	17.36	*49.42*		0.284	25	6.2
	1	*0.0*	*-53.0*	*9.5*	*15*	*	*	*		*		5.8
15	6	*	*	*6.7*	*15*	*	*	*51.33*	*100.00*	0.304	45	1.0
	5	*	*	*8.3*	*15*	*	*	*48.79*	*30.05*	0.268	30	3.6
	4	*6.8*	*-41.0*	*8.7*	*15*	*29.60*	25.84	*46.81*		0.240	23	4.8
	3	*5.5*	*-36.0*	*8.8*	*15*	*22.76*	20.80	*48.77*		0.268	26	5.4
	2	*5.4*	*-36.0*	*8.4*	*15*	*22.70*	20.82	*47.55*		0.250	25	5.2
	1	*0.0*	*-47.0*	*7.9*	*15*	*	*	*		*		4.4

TEST 1

Time (m)	Position	Psychrometer Variables				Potential Bars		Moisture Content Data	Reference 100% / 0%	Moisture Content cm3/cm3	Electrical Resistance	Temp. Deg C
		mv	omv	T	Sec	BB	M					
Mask	6	0.5	-6.6	11.3	15	1.55	1.69	50.00	100.00	0.289	33	8.1
	5	2.3	-11.0	11.3	15	7.37	7.77	50.00	30.00	0.289	28	7.5
	4	3.2	-15.2	11.2	15	10.57	10.85	50.00		0.289	24	7.4
	3	3.0	-20.3	11.1	15	10.18	10.22	50.00		0.289	26	7.1
	2	3.7	-23.0	10.5	15	13.10	12.94	50.00		0.289	24	6.8
	1	0.0	-53.0	9.8	15	*	*	50.00		0.289		6.7
0	6	*	*	10.5	15	*	*	51.76	97.71	0.319	35	4.6
	5	5.6	-19.3	11.2	15	19.30	18.99	49.62	30.26	0.287	23	5.8
	4	4.4	-17.3	10.9	15	15.00	15.12	49.22		0.281	25	6.1
	3	4.0	-22.0	10.9	15	13.92	13.74	48.68		0.273	25	6.3
	2	4.9	-25.0	10.2	15	17.94	17.36	49.42		0.284	25	6.2
	1	0.0	-53.0	9.5	15	*	*	*		*		5.8
15	6	*	*	6.7	15	*	*	51.33	100.00	0.304	45	1.0
	5	*	*	8.3	15	*	*	48.79	30.05	0.268	30	3.6
	4	6.8	-41.0	8.7	15	29.60	25.84	46.81		0.240	23	4.8
	3	5.5	-36.0	8.8	15	22.76	20.80	48.77		0.268	26	5.4
	2	5.4	-36.0	8.4	15	22.70	20.82	47.55		0.250	25	5.2
	1	0.0	-47.0	7.9	15	*	*	*		*		4.4

TEST 1

Time (m)	Position	*Psychrometer Variables*				Potential		*Moisture Content Data*	*Reference 100% / 0%*	Moisture Content cm3/cm3	Electrical Resistance	Temp. Deg C
		mv	*omv*	*T*	*Sec*	*BB* Bars	M Bars					
30	6	*	*	*5.5*	*15*	*	*	*54.71*	*97.33*	0.366	89	-1.1
	5	*	*	*7.4*	*15*	*	*	*50.50*	*30.15*	0.303	31	1.1
	4	*	*	*7.8*	*15*	*	*	*51.00*		0.310	26	2.9
	3	*5.8*	*-38.0*	*7.9*	*15*	*25.32*	22.92	*50.90*		0.309	27	3.9
	2	*5.3*	*-37.0*	*7.1*	*15*	*23.70*	21.82	*53.48*		0.347	25	4.0
	1	*0.0*	*-44.0*	*7.3*	*15*	*	*	*		*		3.4
54	6	*	*	*4.8*	*15*	*	*	*56.48*	*93.89*	0.419	1000	-4.2
	5	*	*	*6.8*	*15*	*	*	*49.18*	*29.55*	0.305	647	-2.0
	4	*	*	*7.2*	*15*	*	*	*49.12*		0.304	26	-0.1
	3	*5.8*	*-40.0*	*7.4*	*15*	*26.19*	23.51	*45.39*		0.246	28	1.1
	2	*5.1*	*-37.0*	*7.1*	*15*	*22.73*	21.00	*47.00*		0.271	26	2.0
	1	*0.0*	*-41.0*	*7.0*	*15*	*	*	*		*		2.2
85	6	*	*	*4.5*	*15*	*	*	*55.29*	*98.39*	0.373	1200	-4.9
	5	*	*	*6.7*	*15*	*	*	*48.68*	*29.70*	0.276	570	-2.3
	4	*	*	*7.2*	*15*	*	*	*47.35*		0.257	29	-0.9
	3	*5.9*	*-42.0*	*7.5*	*15*	*26.87*	23.80	*47.49*		0.259	29	0.2
	2	*5.4*	*-38.0*	*7.1*	*15*	*24.30*	22.24	*48.29*		0.271	27	1.1
	1	*0.0*	*-42.0*	*7.0*	*15*	*	*	*		*		1.2

TEST 1

Time (m)	Position	Psychrometer Variables mv	omv	T	Sec	Potential Bars BB	M	Moisture Content Data	Reference 100% / 0%	Moisture Content cm3/cm3	Electrical Resistance	Temp. Deg C
130	6	*	*	4.3	15	*	*	59.89	98.94	0.432	1127	-4.7
	5	*	*	6.5	15	*	*	51.00	30.15	0.303	526	-2.3
	4	*	*	7.1	15	*	*	49.21		0.277	29	-1.0
	3	5.9	-42.0	7.3	15	27.11	24.04	48.44		0.266	30	0.1
	2	5.1	-38.0	7.0	15	22.96	21.11	48.63		0.289	25	1.1
	1	0.0	-41.0	6.9	15	*	*	*		*		1.3
167	6	*	*	4.3	15	*	*	55.81	94.17	0.397	1140	-4.8
	5	*	*	6.5	15	*	*	49.68	30.58	0.301	480	-2.3
	4	*	*	7.0	15	*	*	48.78		0.286	26	-1.0
	3	6.0	-42.0	7.3	15	27.61	24.45	46.71		0.254	29	0.0
	2	5.0	-38.0	6.9	15	22.58	20.81	47.12		0.260	26	1.0
	1	0.0	-41.0	6.8	15	*	*	*		*		1.2
219	6	*	*	4.2	15	*	*	57.75	98.11	0.408	1100	-4.8
	5	*	*	6.3	15	*	*	50.03	29.89	0.295	480	-2.4
	4	*	*	6.8	15	*	*	48.41		0.272	25	-1.1
	3	6.0	-41.0	7.0	15	27.84	24.84	46.88		0.249	29	-0.1
	2	5.2	-38.0	6.7	15	23.77	21.87	47.74		0.262	25	0.8
	1	0.0	-40.0	6.7	15	*	*	*		*		1.1

TEST 1

Time (m)	Position	Psychrometer Variables mv	omv	T	Sec	Potential BB Bars	M	Moisture Content Data	Reference 100% / 0%	Moisture Content cm3/cm3	Electrical Resistance	Temp. Deg C
1155	6	*	*	3.6	15	*	*	57.54	93.44	0.431	900	-4.7
	5	*	*	6.2	15	*	*	50.72	30.38	0.323	400	-2.2
	4	*	*	6.8	15	*	*	47.16		0.266	22	-1.0
	3	5.6	-38.0	7.0	15	25.40	23.18	46.13		0.250	28	-0.1
	2	4.8	-36.0	6.7	15	21.58	19.89	47.84		0.277	24	1.0
	1	0.0	-40.0	6.7	15	*	*	*		*		1.3
1218	6	*	*	3.9	15	*	*	61.16	106.17	0.407	1000	-4.7
	5	*	*	6.6	15	*	*	52.58	30.24	0.294	480	-2.1
	4	*	*	7.1	15	*	*	50.00		0.260	22	-1.1
	3	5.5	-38.0	7.3	15	24.57	22.41	50.31		0.264	27	-0.2
	2	4.7	-35.0	7.0	15	20.70	19.46	52.34		0.291	24	1.0
	1	0.0	-41.0	7.0	15	*	*	*		*		1.3
1241	6	*	*	5.4	15	*	*	55.54	95.50	0.391	550	-2.6
	5	*	*	7.3	15	*	*	47.67	29.89	0.271	300	-0.9
	4	6.3	-39.0	8.2	15	27.50	24.53	46.18		0.248	23	0.6
	3	5.0	-31.0	8.4	15	20.35	19.28	45.25		0.234	27	1.6
	2	4.2	-30.0	8.0	15	17.13	16.52	46.14		0.248	24	2.0
	1	0.0	-43.0	8.1	15	*	*	*		*		1.7

TEST 1

Time (m)	Position	Psychrometer Variables mv	omv	T	Sec	Potential Bars BB	M	*Moisture Content Data*	*Reference 100% / 0%*	Moisture Content cm3/cm3	Electrical Resistance	Temp. Deg C
1267	6	*0.0*	*-32.0*	*9.0*	*15*	*	*	*52.83*	*90.22*	0.378	18	0.2
	5	*3.2*	*-24.0*	*9.5*	*15*	*11.78*	11.71	*46.22*	*30.15*	0.268	22	0.2
	4	*4.2*	*-23.0*	*9.6*	*15*	*15.47*	15.30	*44.67*		0.242	21	1.4
	3	*3.9*	*-23.0*	*9.6*	*15*	*14.32*	14.20	*45.88*		0.262	26	2.0
	2	*3.9*	*-25.0*	*9.2*	*15*	*14.70*	14.47	*44.50*		0.239	23	2.0
	1	*0.0*	*-47.0*	*8.8*	*15*	*	*	*		*		1.7
1301	6	*0.5*	*-16.0*	*10.4*	*15*	*1.67*	1.76	*53.81*	*91.05*	0.390	18	0.8
	5	*1.7*	*-13.0*	*10.5*	*15*	*5.63*	5.94	*49.29*	*30.05*	0.315	22	0.8
	4	*2.7*	*-16.0*	*10.5*	*15*	*9.15*	9.44	*47.00*		0.278	21	1.0
	3	*2.8*	*-18.0*	*10.4*	*15*	*9.63*	9.83	*47.00*		0.278	25	2.1
	2	*3.1*	*-21.0*	*10.1*	*15*	*10.97*	11.04	*47.31*		0.283	24	2.5
	1	*0.0*	*-49.0*	*9.5*	*15*	*	*	*		*		2.3
1391	6	*0.1*	*-6.9*	*11.7*	*15*	*0.30*	0.42	*54.71*	*90.39*	0.408	18	4.2
	5	*1.1*	*-7.0*	*11.7*	*15*	*3.38*	3.65	*50.36*	*30.10*	0.336	21	2.7
	4	*2.1*	*-10.8*	*11.6*	*15*	*6.64*	7.00	*46.84*		0.278	21	2.9
	3	*1.9*	*-15.7*	*11.5*	*15*	*6.16*	6.36	*46.84*		0.278	25	3.0
	2	*3.4*	*-20.2*	*11.0*	*15*	*11.62*	11.63	*44.76*		0.243	23	3.1
	1	*0.0*	*-54.0*	*10.2*	*15*	*	*	*		*		3.0

TEST 2

Time (m) Position		Psychrometer Variables				Potential Bars		*Moisture Content Data*	*Reference 100% / 0%*	Moisture Content cm3/cm3	Electrical Resistance	Temp. Deg C
		mv	*omv*	*T*	*Sec*	*BB*	M					
Mask	6	*4.9*	*-8.4*	*6.9*	*15*	*19.05*	20.39	*50.00*	*100.00*	0.286	22	7.6
0	5	*3.8*	*-12.3*	*6.7*	*15*	*14.99*	15.98	*50.00*	*30.00*	0.286	26	7.4
	4	*2.8*	*-13.9*	*6.6*	*15*	*11.06*	11.84	*50.00*		0.286	23	7.2
	3	*2.8*	*-12.4*	*6.6*	*15*	*10.98*	11.84	*50.00*		0.286	23	7.1
	2	*0.8*	*-12.6*	*6.4*	*15*	*3.10*	3.42	*50.00*		0.286	25	6.9
	1	*2.3*	*-9.4*	*5.9*	*15*	*9.15*	10.10	*50.00*		0.286		6.4
62	6	*	*	*2.2*	*15*	*	*	*56.74*	*106.88*	0.352	52	-2.0
	5	*	*	*4.5*	*15*	*	*	*51.87*	*29.50*	0.289	22	2.5
	4	*4.7*	*-37.0*	*4.4*	*15*	*23.70*	22.53	*49.02*		0.252	22	4.2
	3	*4.5*	*-27.0*	*4.7*	*15*	*21.18*	21.19	*50.39*		0.270	26	5.0
	2	*2.0*	*-27.0*	*4.3*	*15*	*9.30*	9.65	*48.85*		0.250	24	4.7
	1	*2.8*	*-18.0*	*4.2*	*15*	*12.64*	13.59	*48.46*		0.245		4.2
93	6	*	*	*0.0*	*15*	*	*	*71.12*	*121.13*	0.437	1000	-4.5
	5	*	*	*1.8*	*15*	*	*	*59.01*	*32.27*	0.301	450	-1.6
	4	*	*	*2.2*	*15*	*	*	*54.24*		0.247	25	-0.7
	3	*4.0*	*-42.0*	*2.2*	*15*	*22.88*	22.14	*52.41*		0.227	25	0.5
	2	*2.3*	*-38.0*	*2.4*	*15*	*12.40*	12.55	*53.69*		0.241	25	0.6
	1	*2.2*	*-24.0*	*2.5*	*15*	*11.05*	11.93	*54.50*		0.250		1.2

TEST 2

Time (m) Position		*Psychrometer Variables*				Potential		*Moisture Content Data*	*Reference 100% / 0%*	Moisture Content cm3/cm3	Electrical Resistance	Temp. Deg C
		mv	*omv*	*T*	*Sec*	*BB* Bars	M					
128	6	*	*	*0.4*	*15*	*	*	*64.09*	*111.71*	0.413	1150	-3.5
	5	*	*	*1.8*	*15*	*	*	*55.94*	*30.55*	0.313	450	-1.5
	4	*	*	*2.4*	*15*	*	*	*53.09*		0.278	27	-0.7
	3	*4.1*	*-41.0*	*2.4*	*15*	*23.14*	22.38	*48.74*		0.224	27	0.6
	2	*2.1*	*-37.0*	*2.4*	*15*	*11.23*	11.46	*50.34*		0.244	23	0.7
	1	*1.8*	*-23.0*	*2.4*	*15*	*8.99*	9.83	*51.38*		0.257		1.3
160	6	*	*	*0.5*	*15*	*	*	*78.30*	*137.75*	0.399	980	-3.3
	5	*	*	*2.0*	*15*	*	*	*69.26*	*38.82*	0.308	460	-1.4
	4	*	*	*2.5*	*15*	*	*	*65.25*		0.267	27	-0.6
	3	*4.2*	*-41.0*	*2.6*	*15*	*23.50*	22.61	*61.68*		0.231	27	0.6
	2	*1.9*	*-37.0*	*2.6*	*15*	*10.03*	10.23	*63.44*		0.249	24	0.7
	1	*1.8*	*-23.0*	*2.7*	*15*	*8.86*	9.62	*64.20*		0.257		1.3
213	6	*	*	*-0.1*	*15*	*	*	*107.84*	*194.54*	0.417	1100	-4.3
	5	*	*	*1.6*	*15*	*	*	*91.24*	*45.80*	0.306	450	-1.9
	4	*	*	*2.3*	*15*	*	*	*85.29*		0.266	25	-0.7
	3	*4.6*	*-46.0*	*2.5*	*15*	*26.76*	24.94	*80.65*		0.234	23	0.8
	2	*1.9*	*-38.0*	*2.6*	*15*	*10.08*	10.23	*82.84*		0.249	21	0.9
	1	*1.9*	*-27.0*	*2.9*	*15*	*9.44*	10.02	*84.34*		0.259		1.5

TEST 2

Time (m) Position		Psychrometer Variables mv	omv	T	Sec	Potential Bars BB	M	*Moisture Content Data*	*Reference 100% / 0%*	Moisture Content cm3/cm3	Electrical Resistance	Temp. Deg C
248	6	*	*	0.0	15	*	*	59.80	101.25	0.422	1100	-4.9
	5	*	*	1.6	15	*	*	52.28	29.54	0.317	400	-2.3
	4	*	*	2.2	15	*	*	48.98		0.271	50	-1.0
	3	4.2	-43.0	2.3	15	24.11	23.08	46.35		0.234	23	0.0
	2	2.0	-38.0	2.3	15	10.78	10.99	47.45		0.250	21	0.1
	1	1.9	-24.0	2.5	15	9.50	10.30	47.54		0.251		0.9
280	6	*	*	0.0	15	*	*	85.35		0.405	1000	-4.7
	5	*	*	1.5	15	*	*	74.87		0.309	380	-2.2
	4	*	*	2.1	15	*	*	70.88		0.272	40	-1.0
	3	4.3	-43.0	2.2	15	24.86	23.80	66.64		0.233	23	0.1
	2	2.0	-39.0	2.3	15	10.84	10.99	67.45		0.241	23	0.3
	1	1.7	-25.0	2.4	15	8.56	9.28	68.80		0.253		1.0
315	6	*	*	-0.1	15	*	*	81.69	140.92	0.413	990	-4.8
	5	*	*	1.5	15	*	*	71.49	40.00	0.312	400	-2.3
	4	*	*	2.0	15	*	*	67.22		0.270	43	-1.1
	3	4.0	-43.0	2.2	15	22.99	22.14	63.55		0.233	23	-0.1
	2	1.9	-39.0	2.2	15	10.33	10.52	64.88		0.247	23	0.1
	1	2.0	-25.0	2.4	15	10.11	10.92	65.23		0.250		0.8

APPENDIX 4. RADIOGRAPHS (TESTS 1 AND 2)

TEST 1. Time Mask

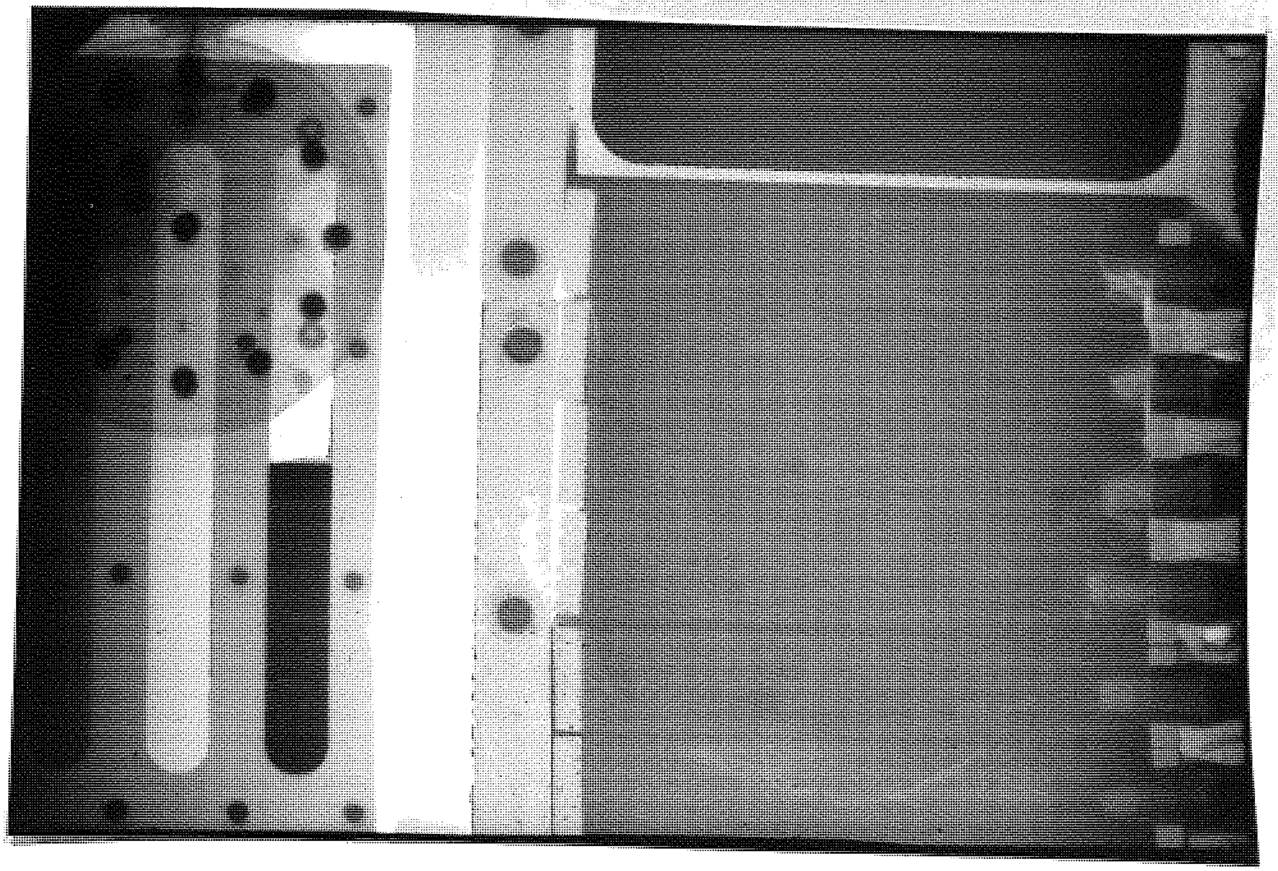

TEST 1. Time 0 minutes

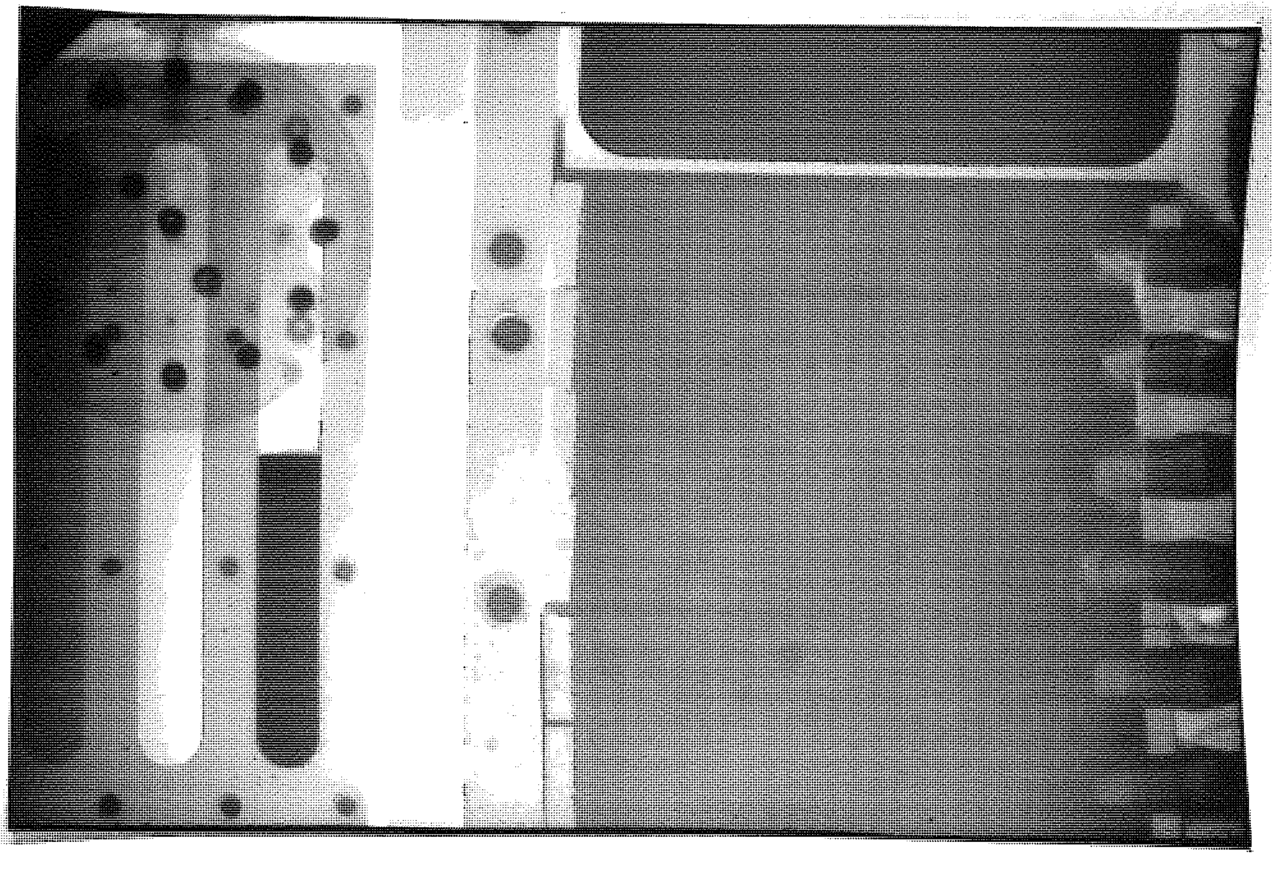

TEST 1. Time 15 minutes

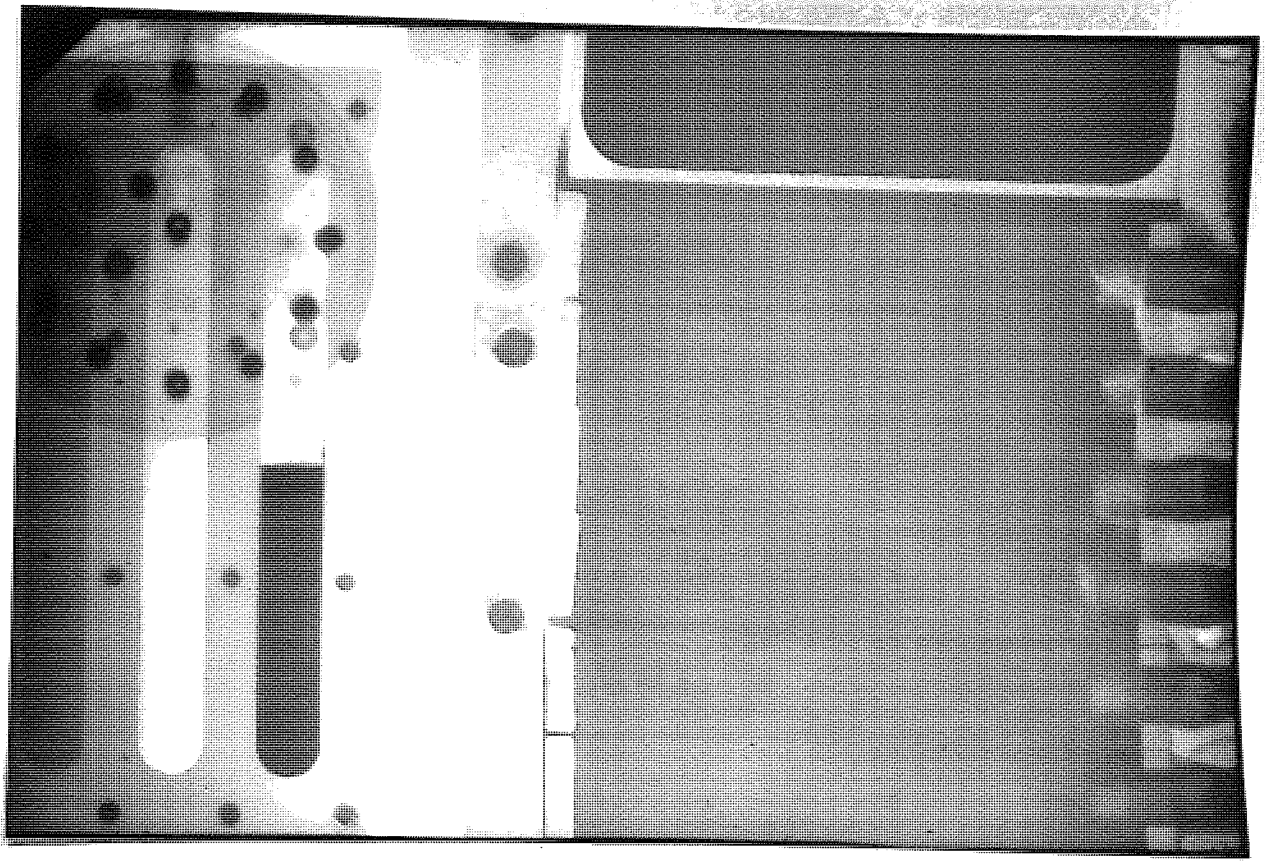

TEST 1. Time 30 minutes

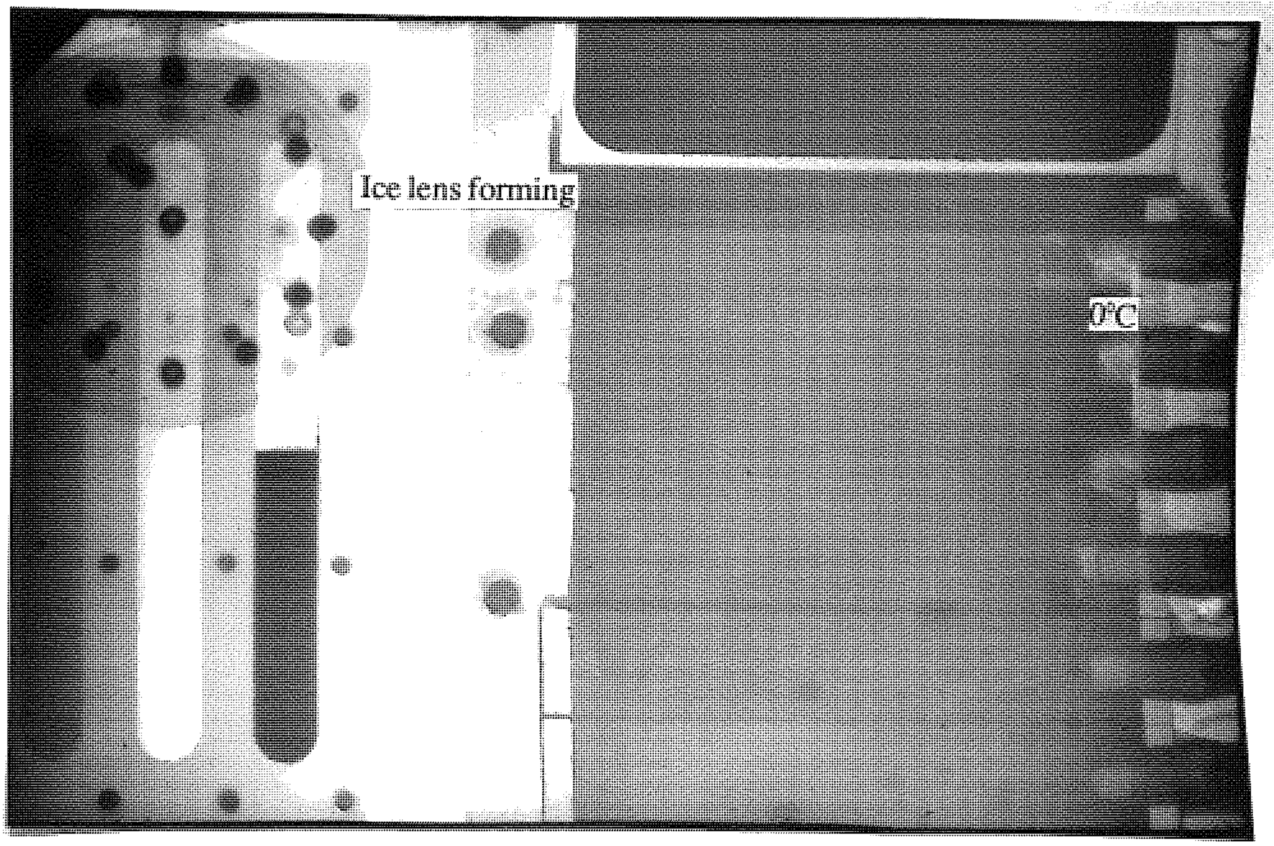

TEST 1. Time 54 minutes

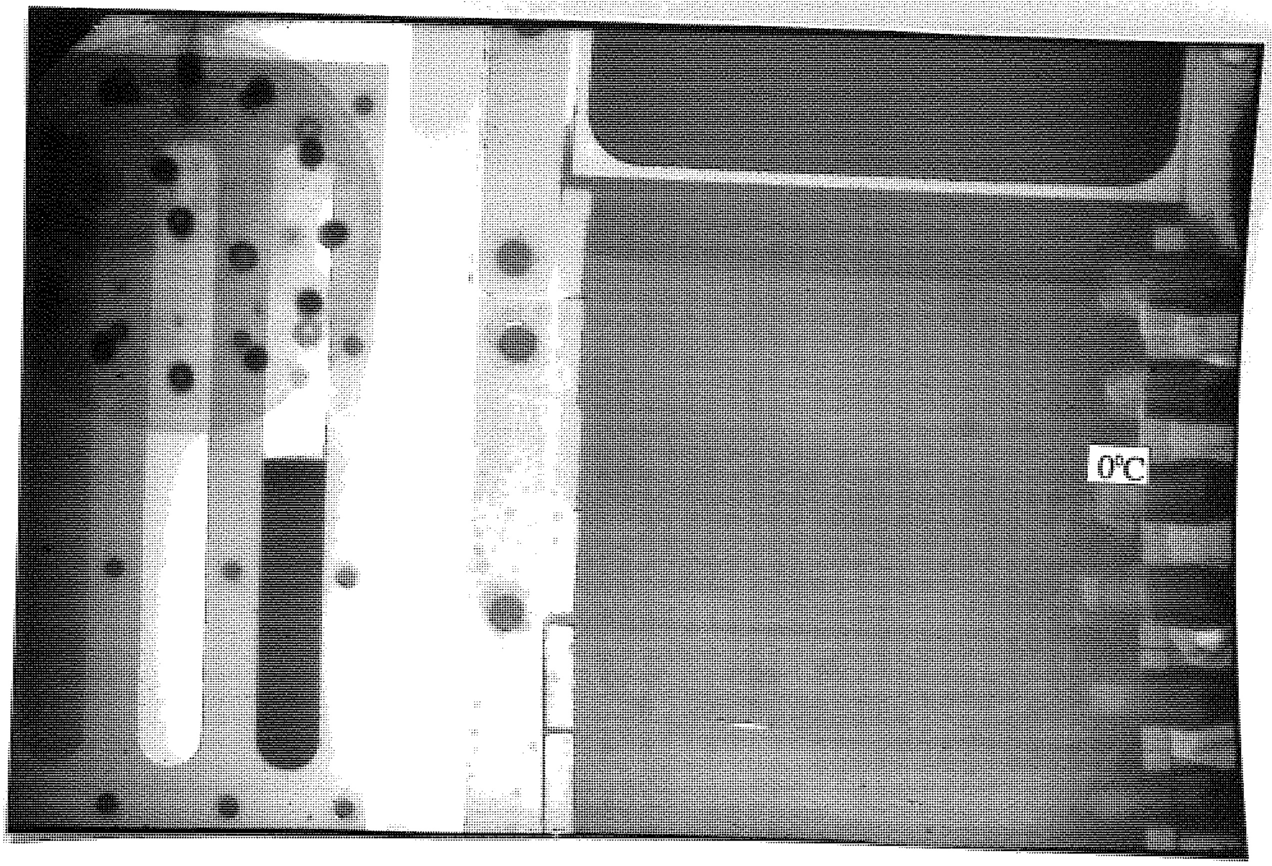

TEST 1. Time 85 minutes

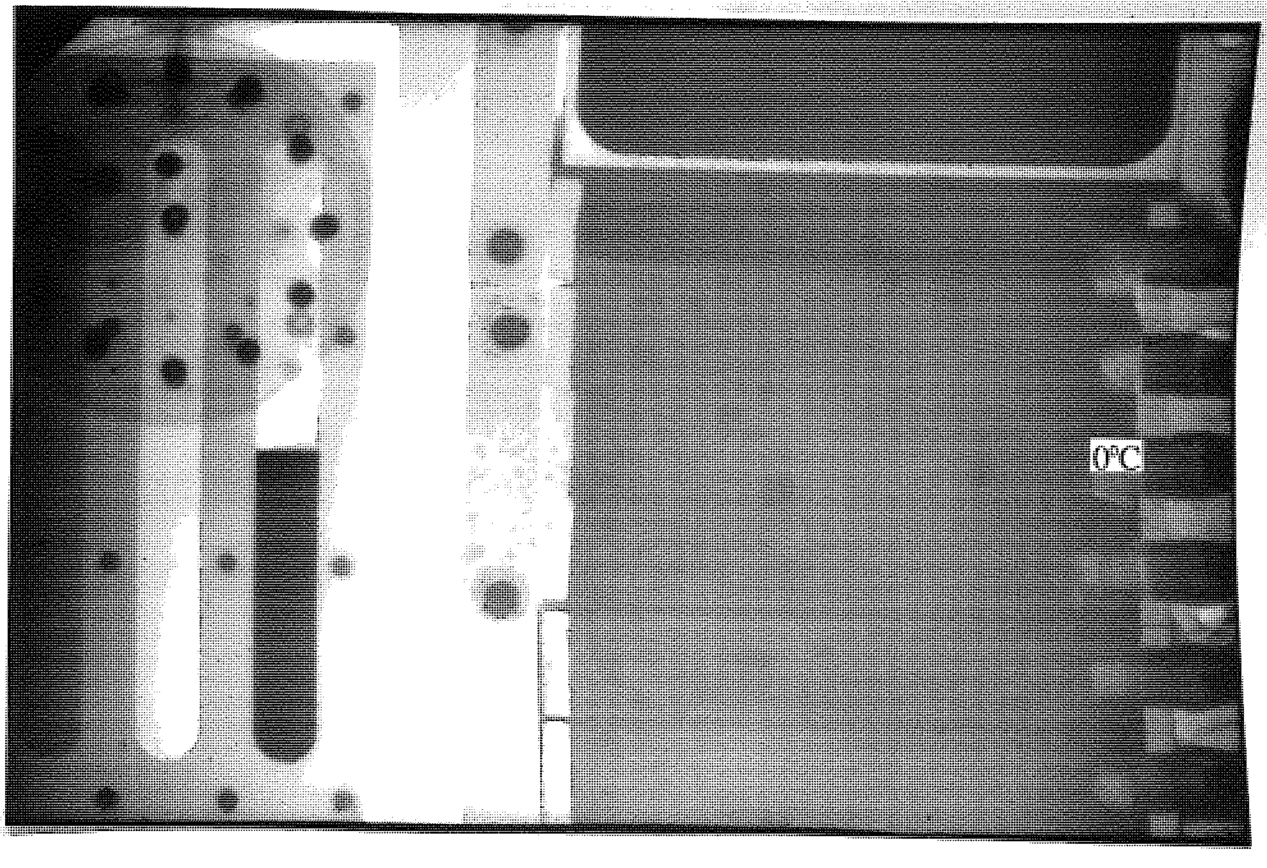

TEST 1. Time 130 minutes

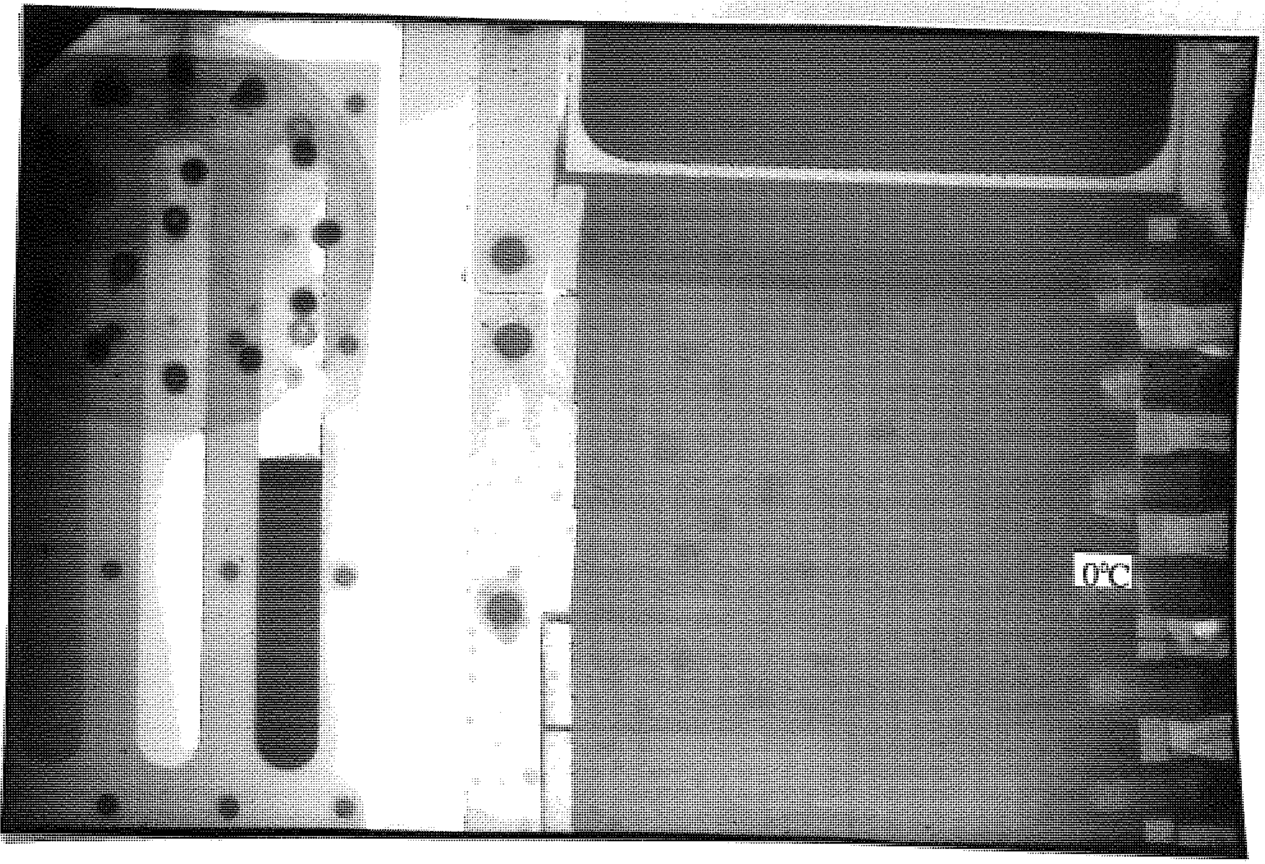

TEST 1. Time 167 minutes

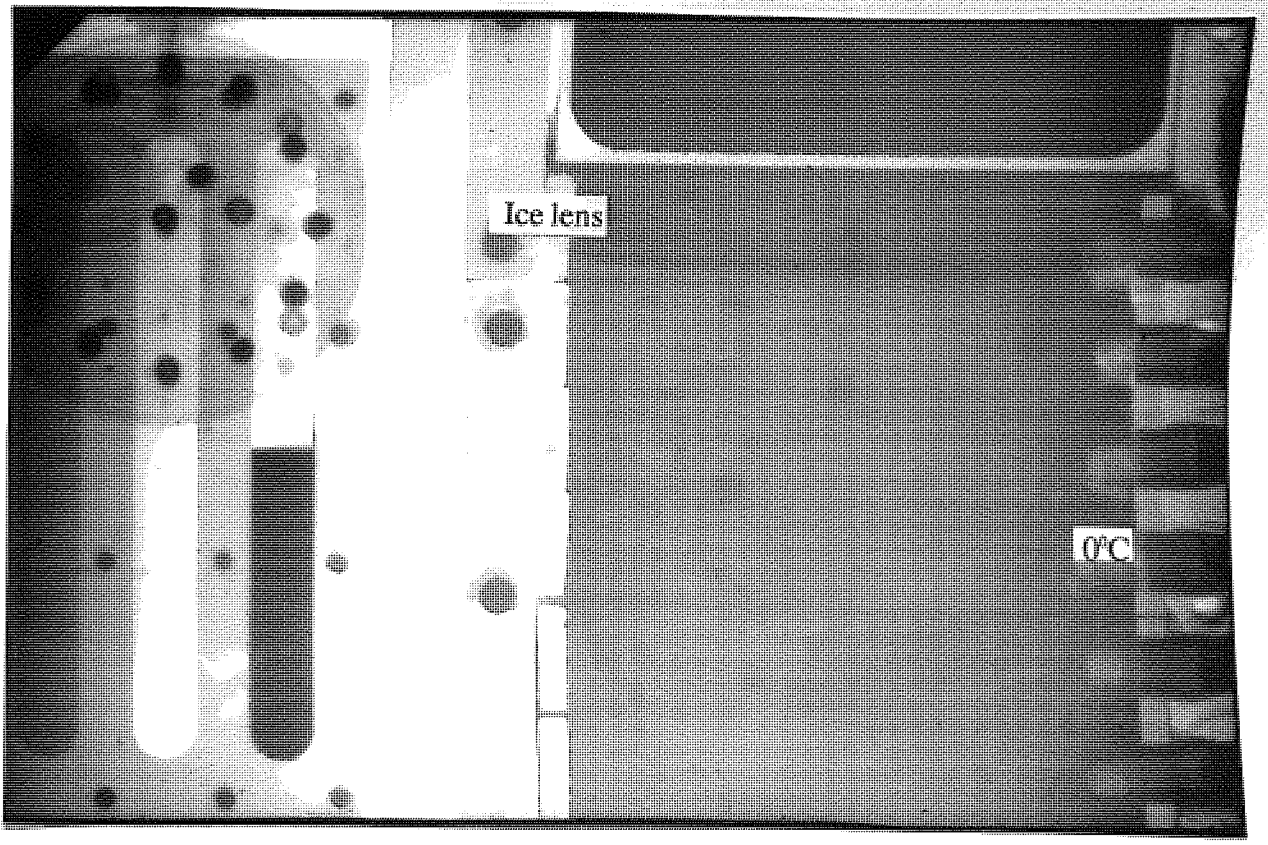

TEST 1. Time 219 minutes

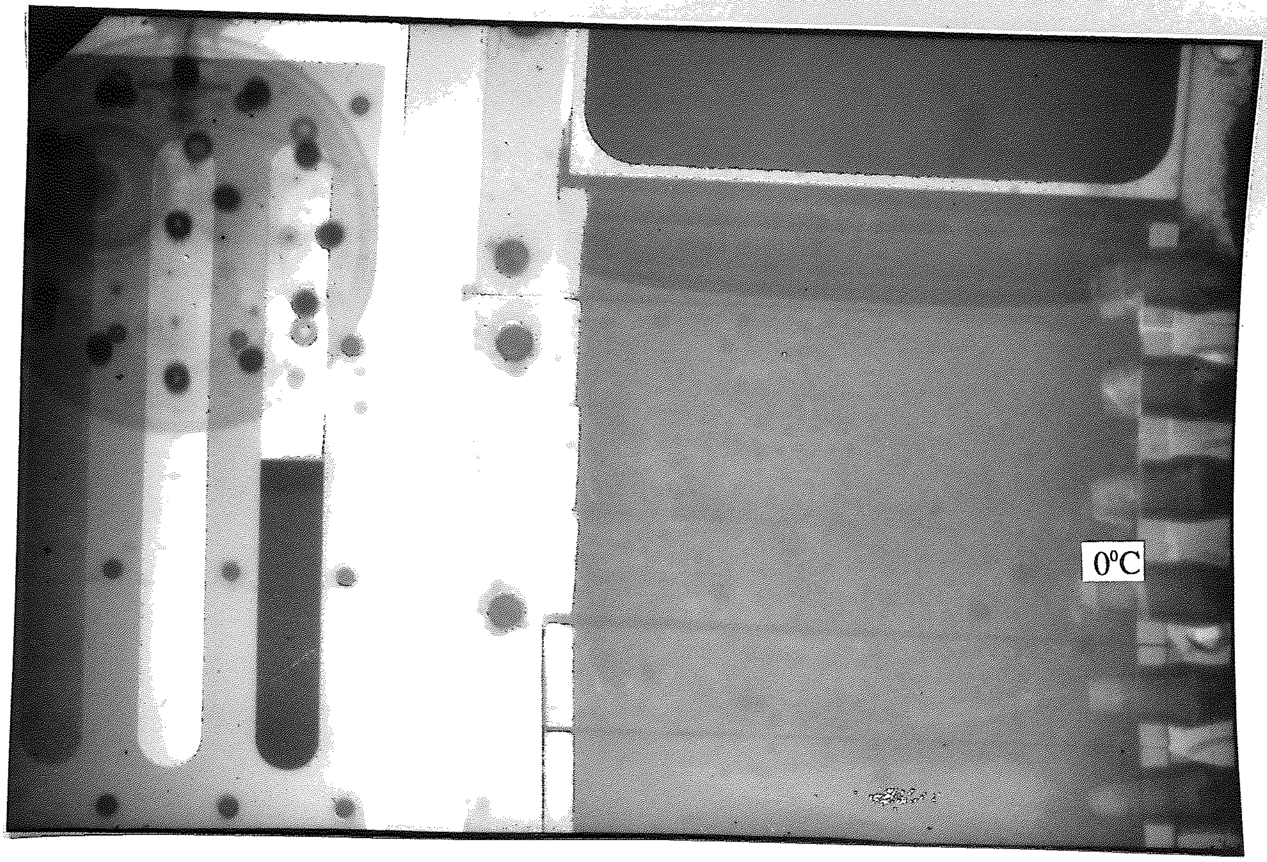

TEST 1. Time 1155 minutes

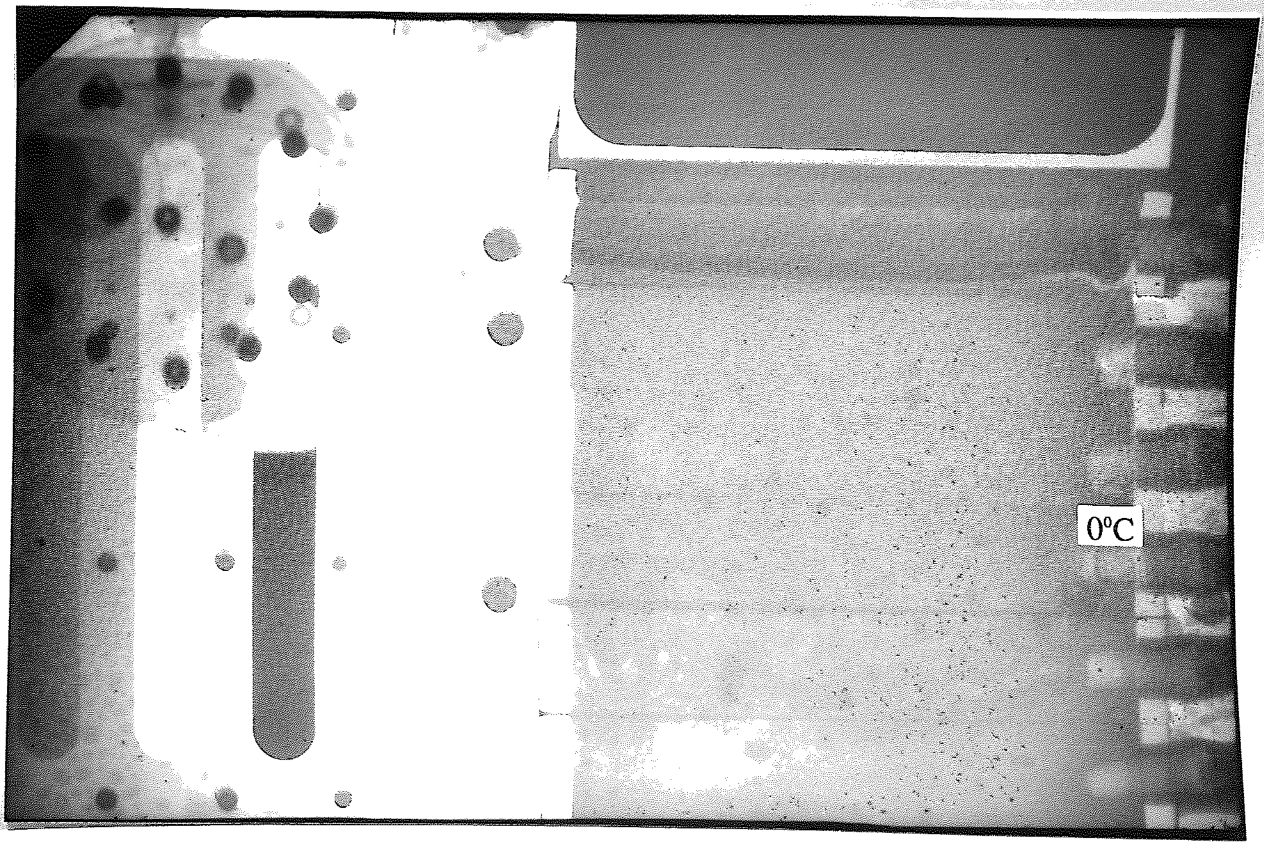

TEST 1. Time 1218 minutes

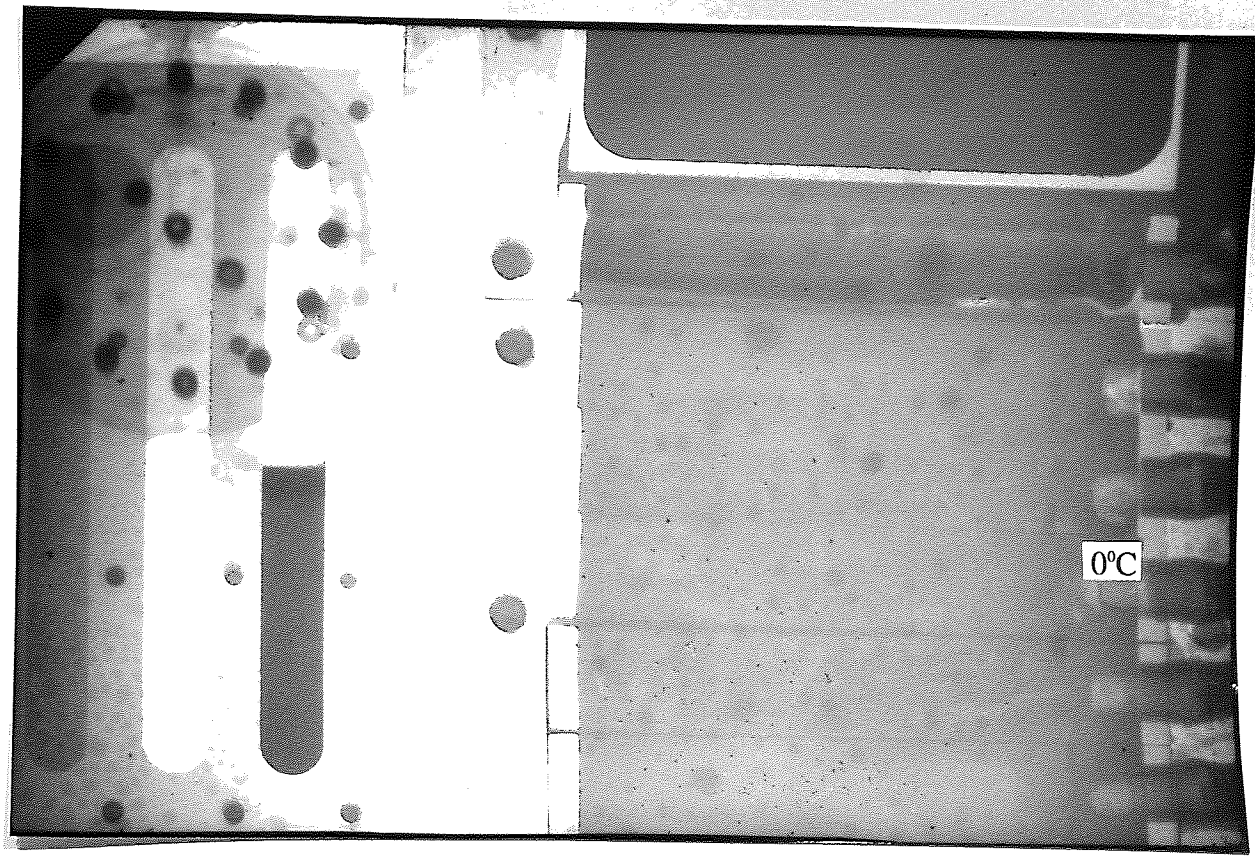

TEST 1. Time 1241 minutes

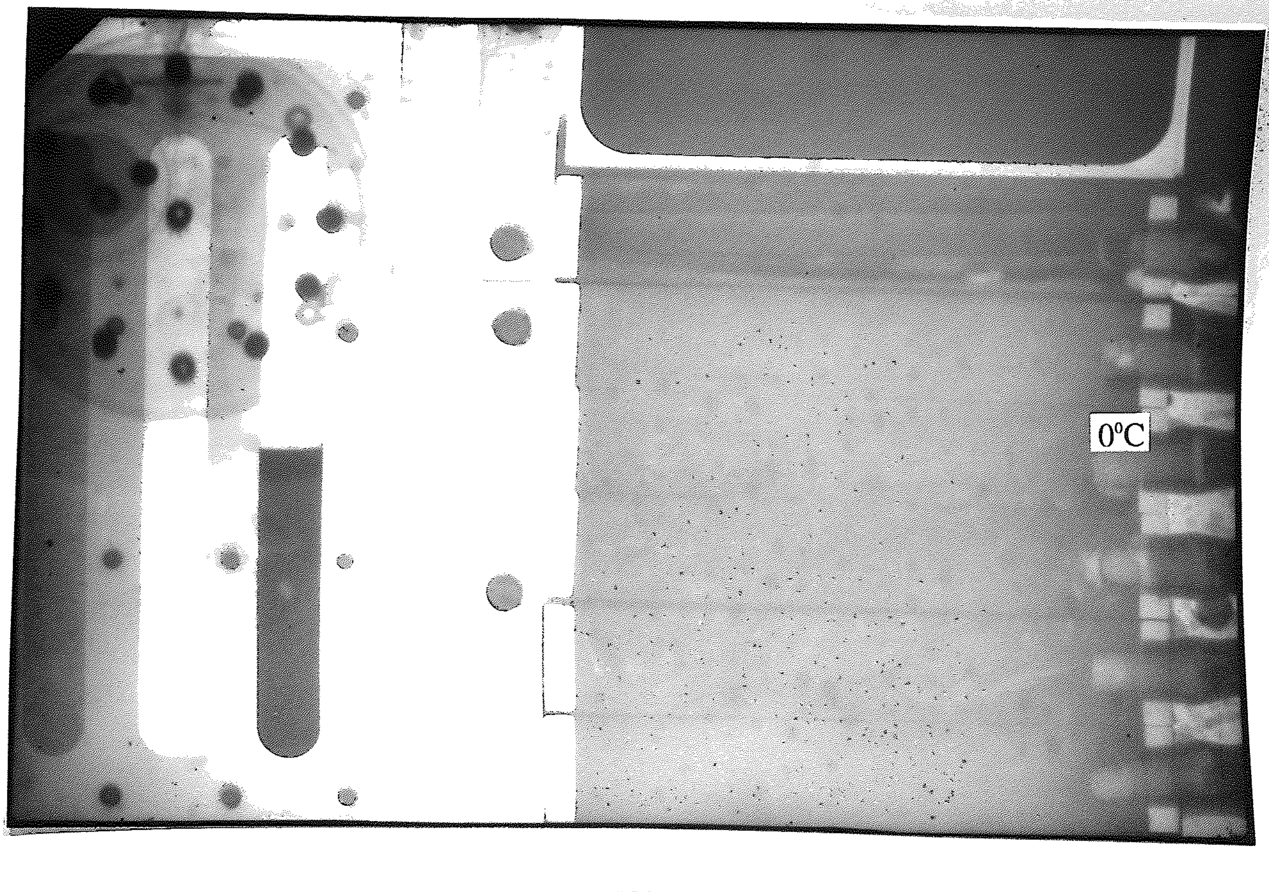

TEST 1. Time 1267 minutes

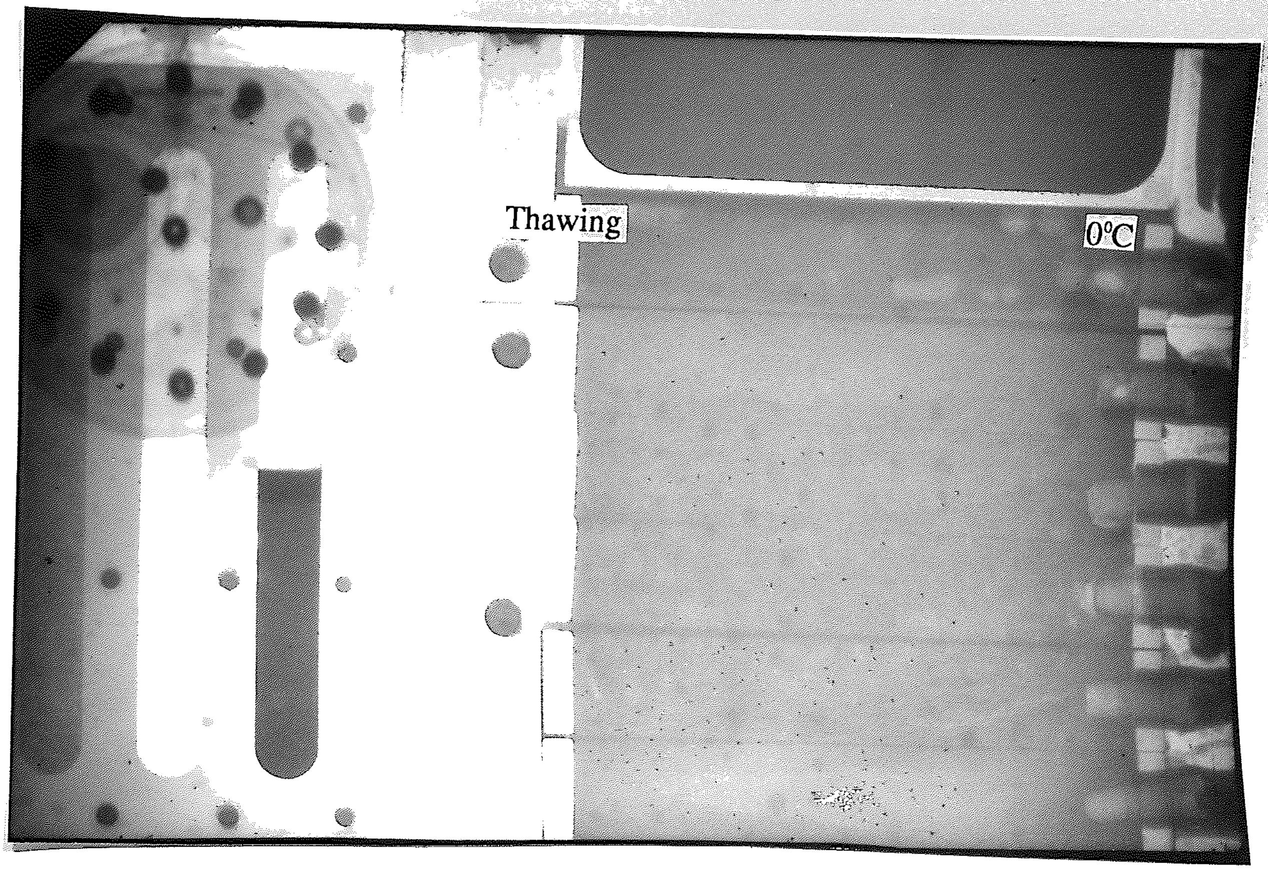

TEST 1. Time 1301 minutes

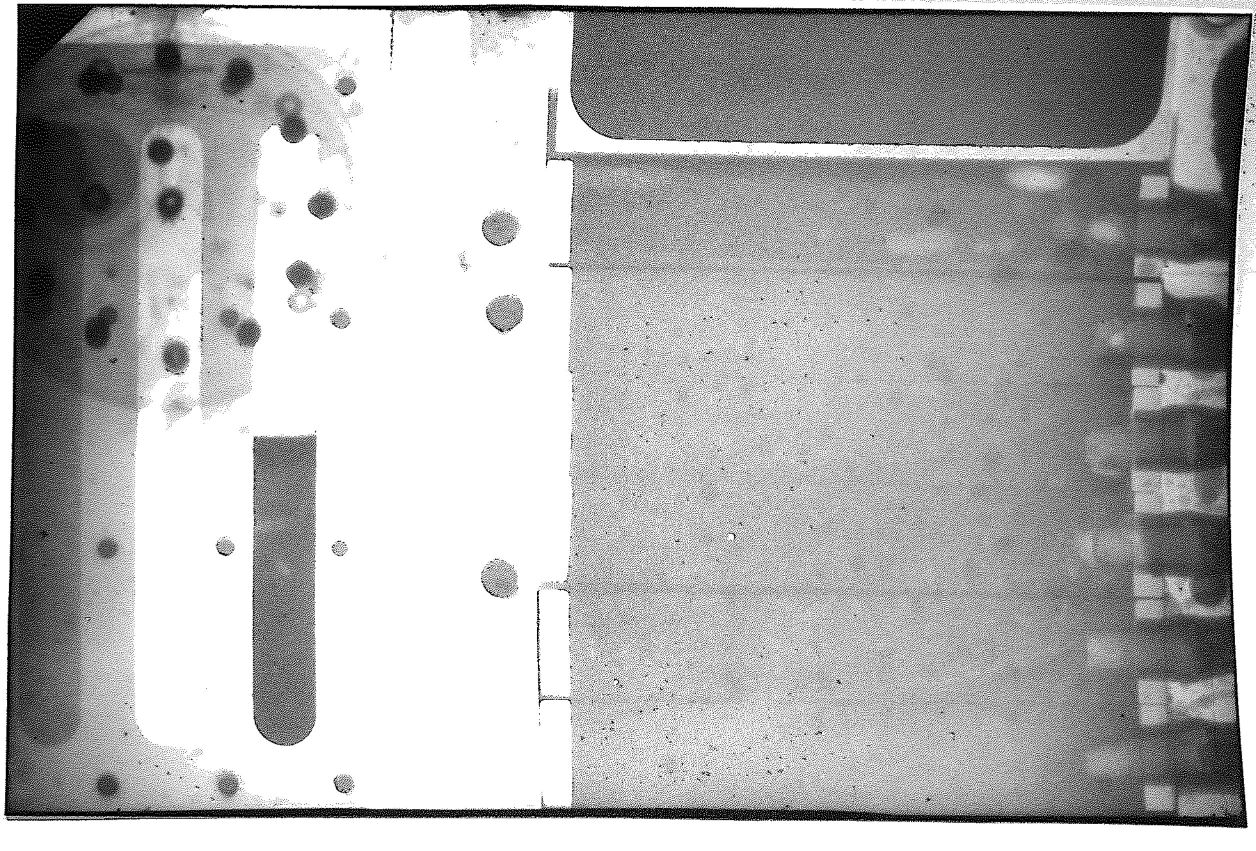

TEST 1. Time 1391 minutes

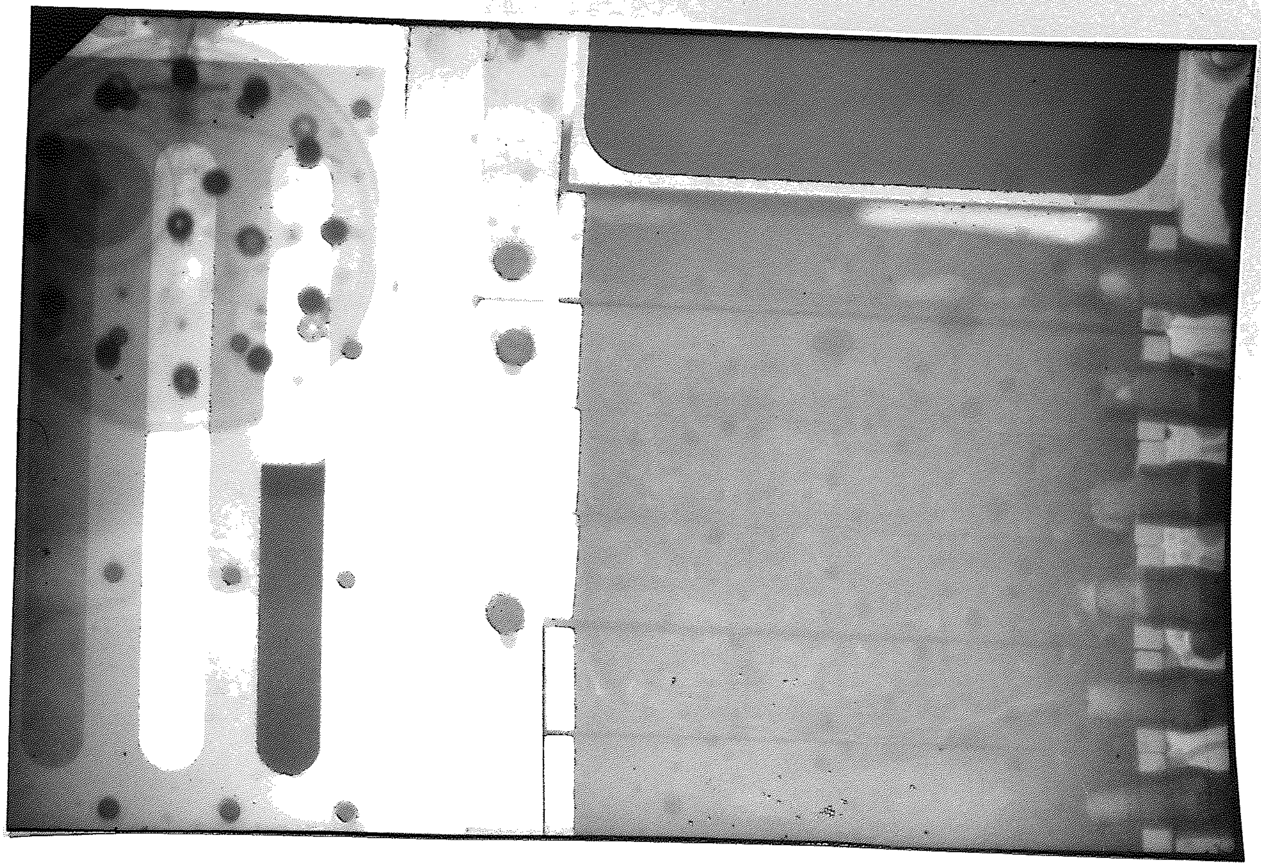

TEST 2. Time Mask

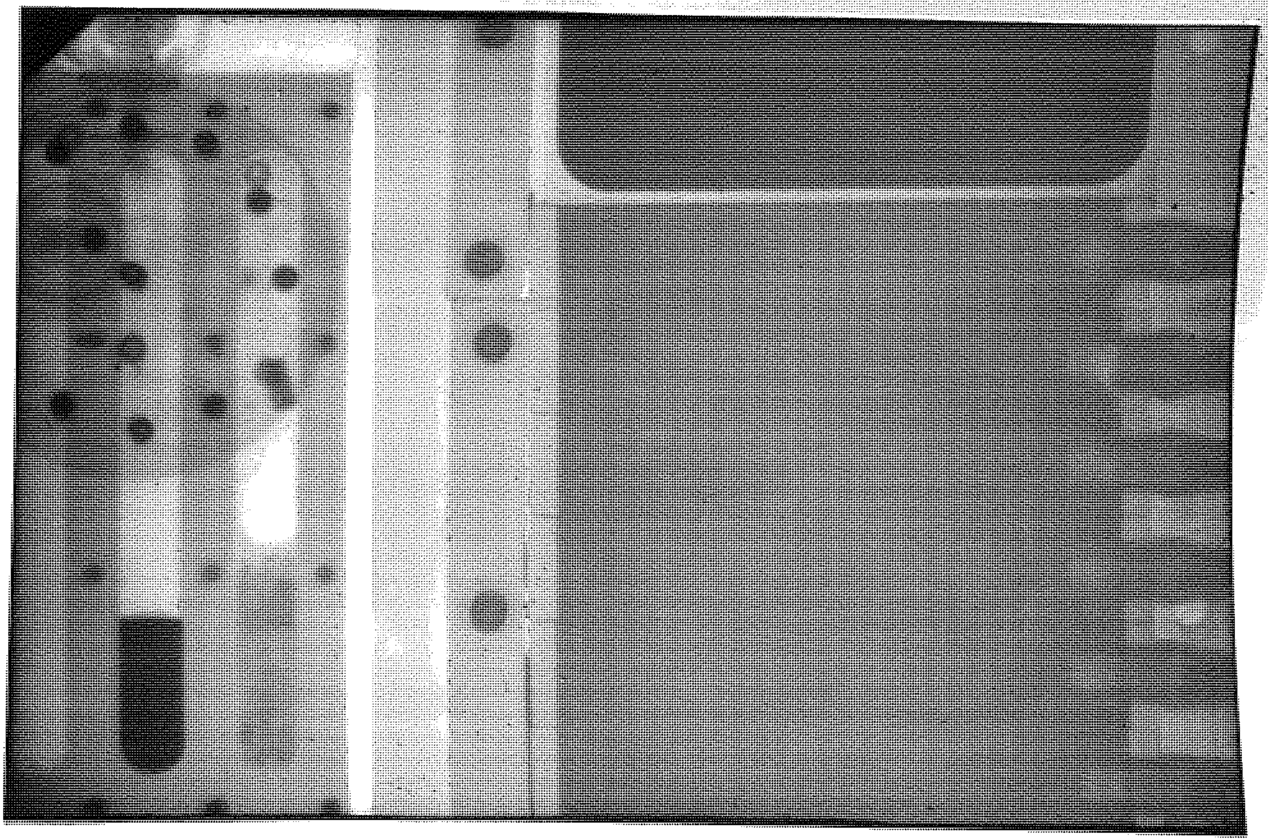

TEST 2. Time 62 minutes

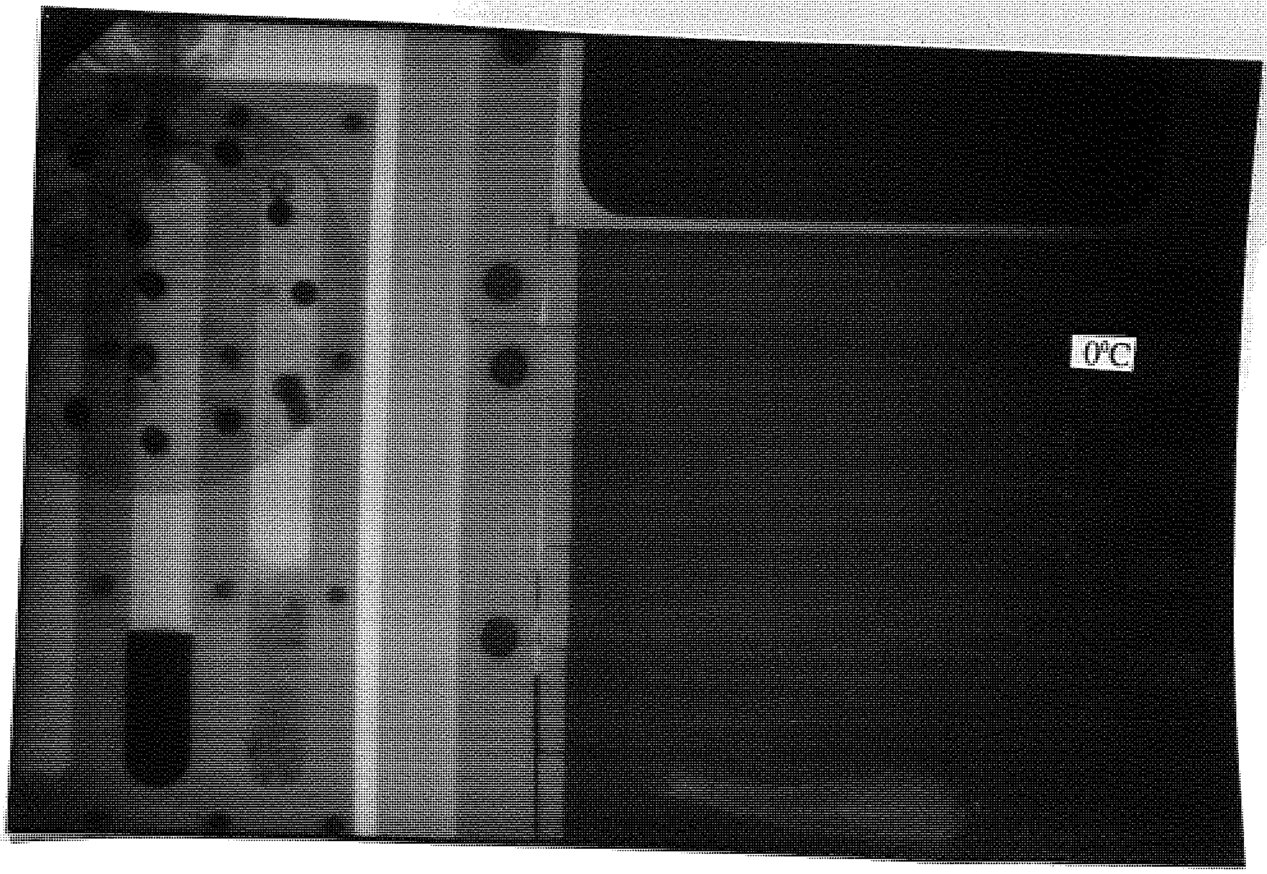

TEST 2. Time 93 minutes

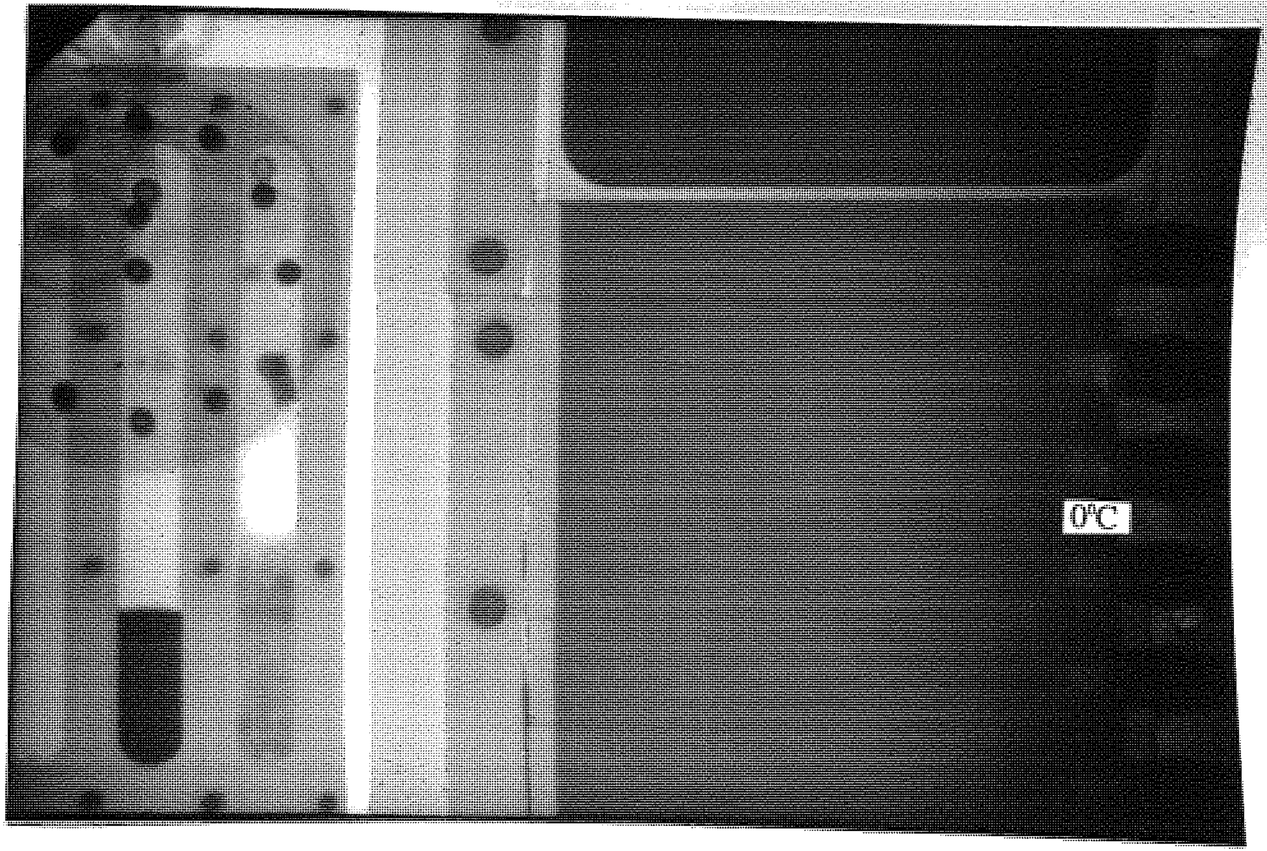

TEST 2. Time 128 minutes

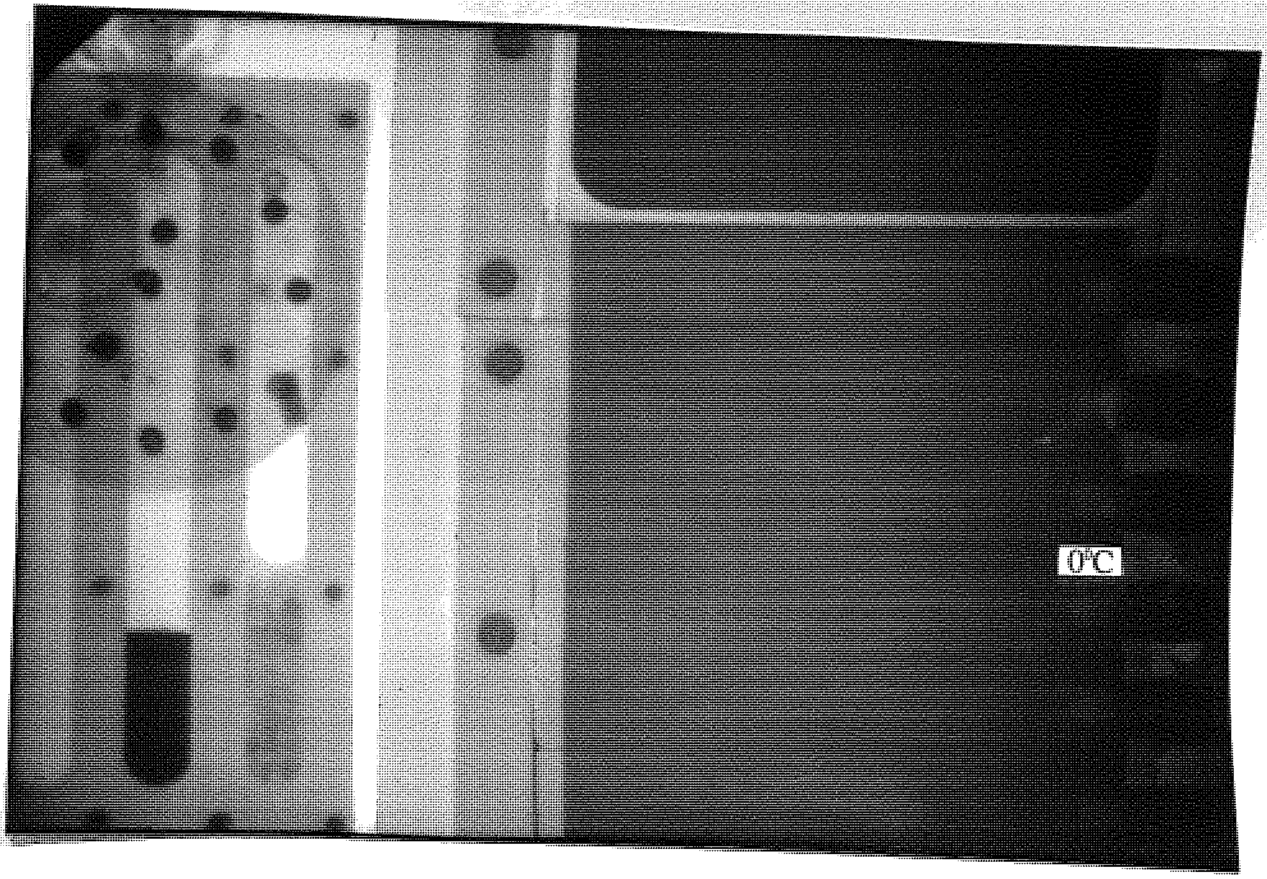

TEST 2. Time 160 minutes

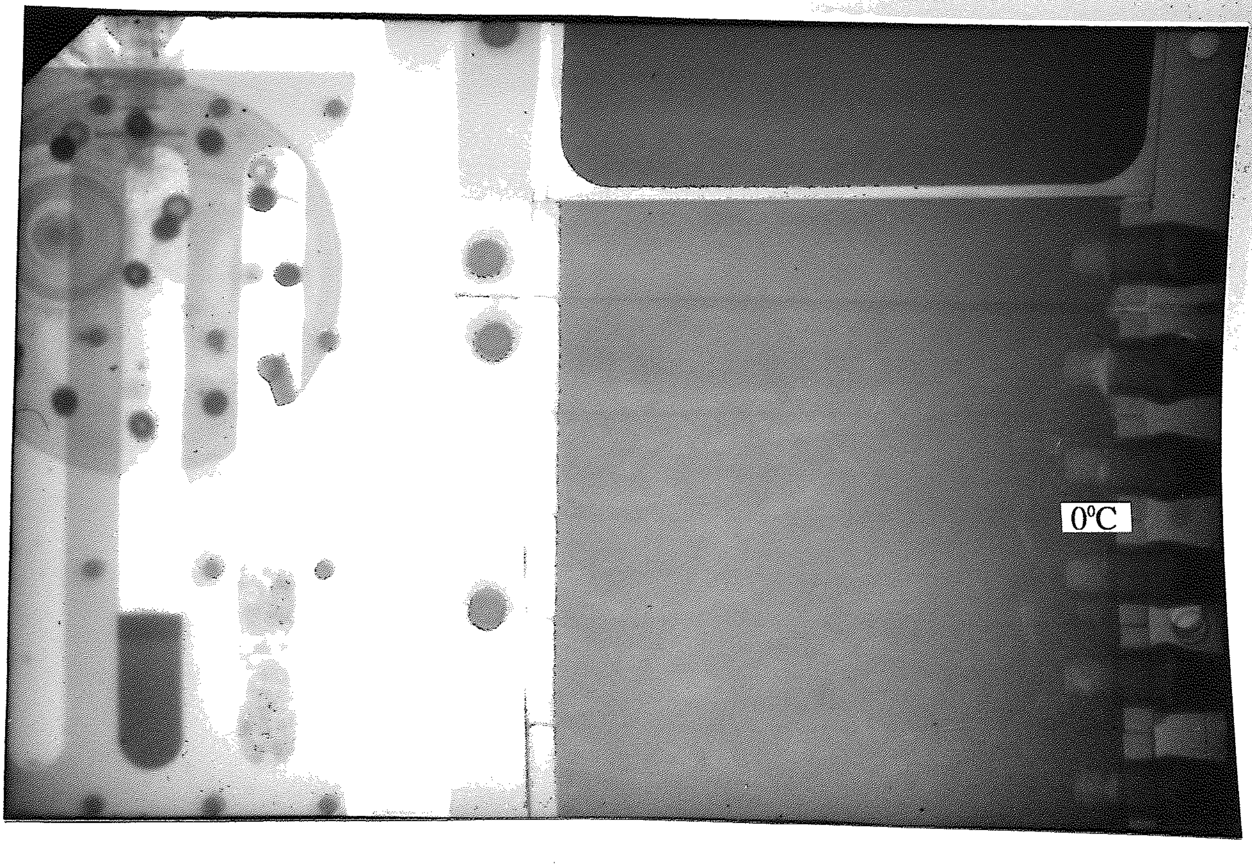

TEST 2. Time 213 minutes

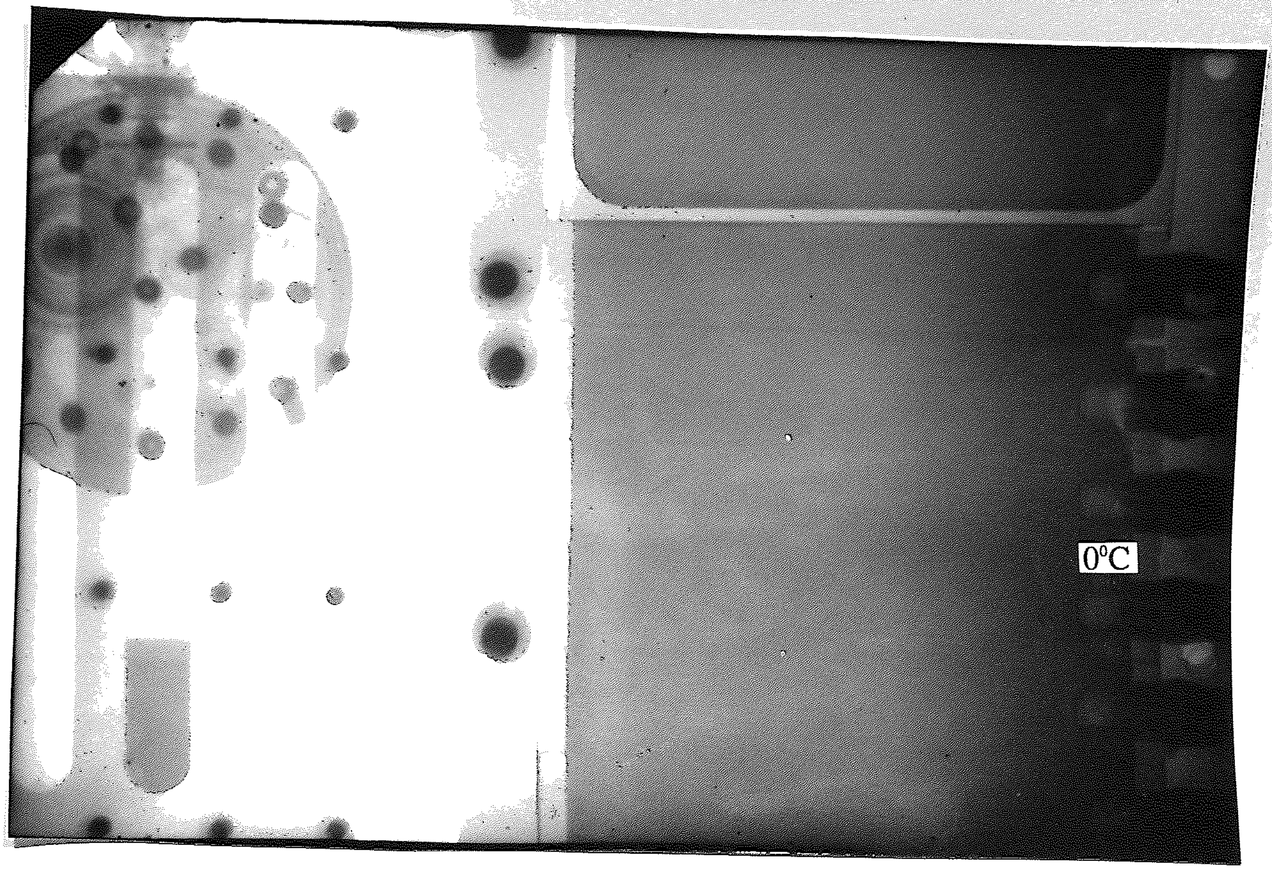

TEST 2. Time 248 minutes

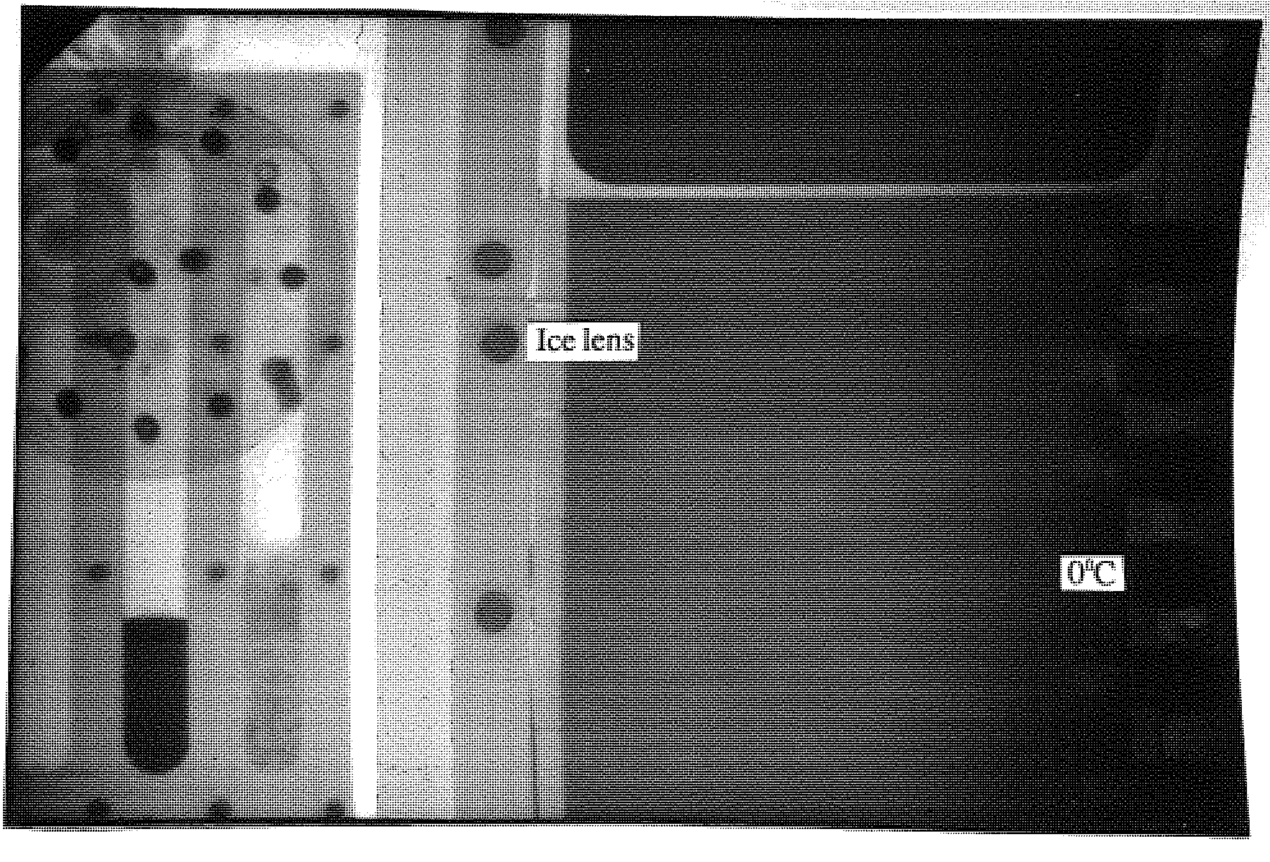

TEST 2. Time 280 minutes

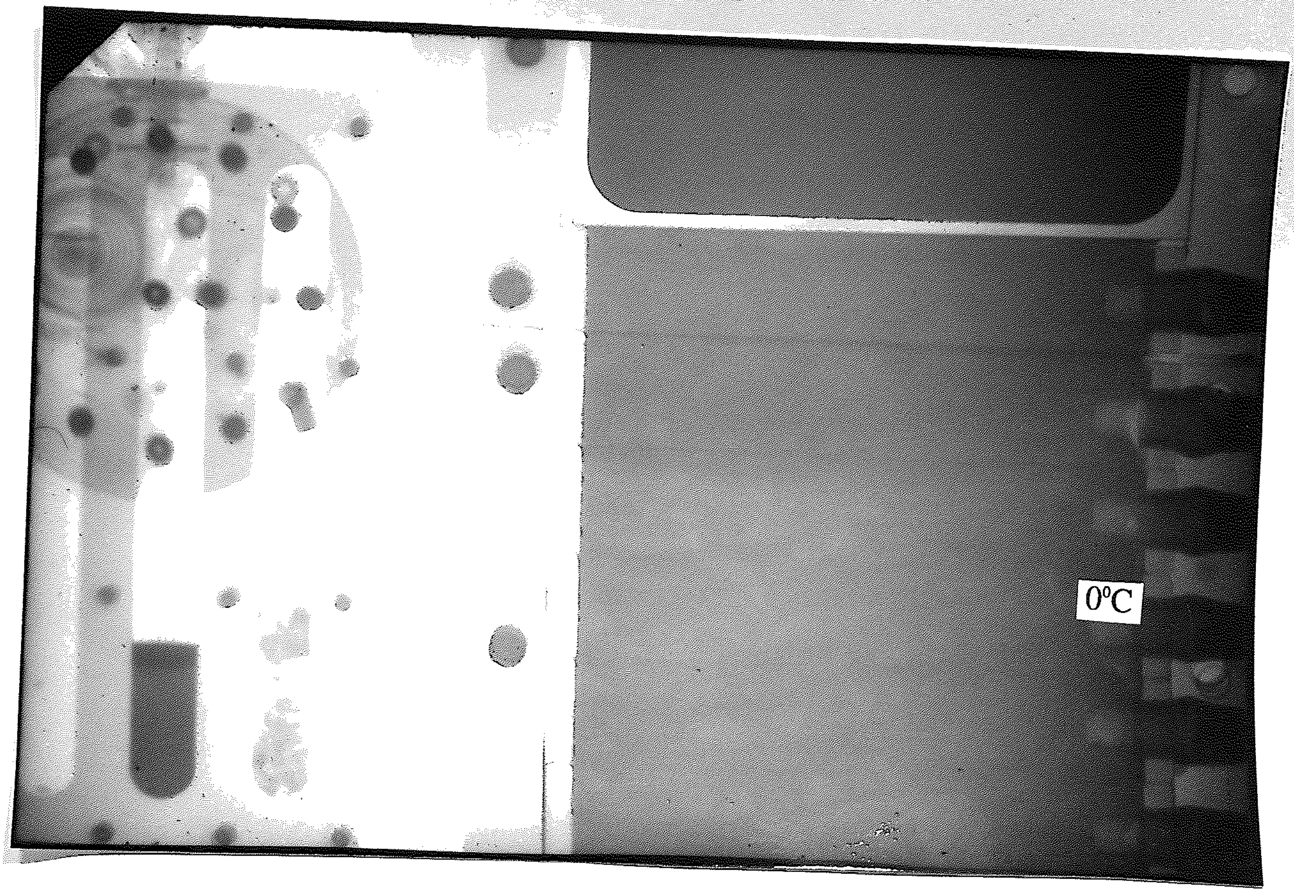

TEST 2. Time 315 minutes

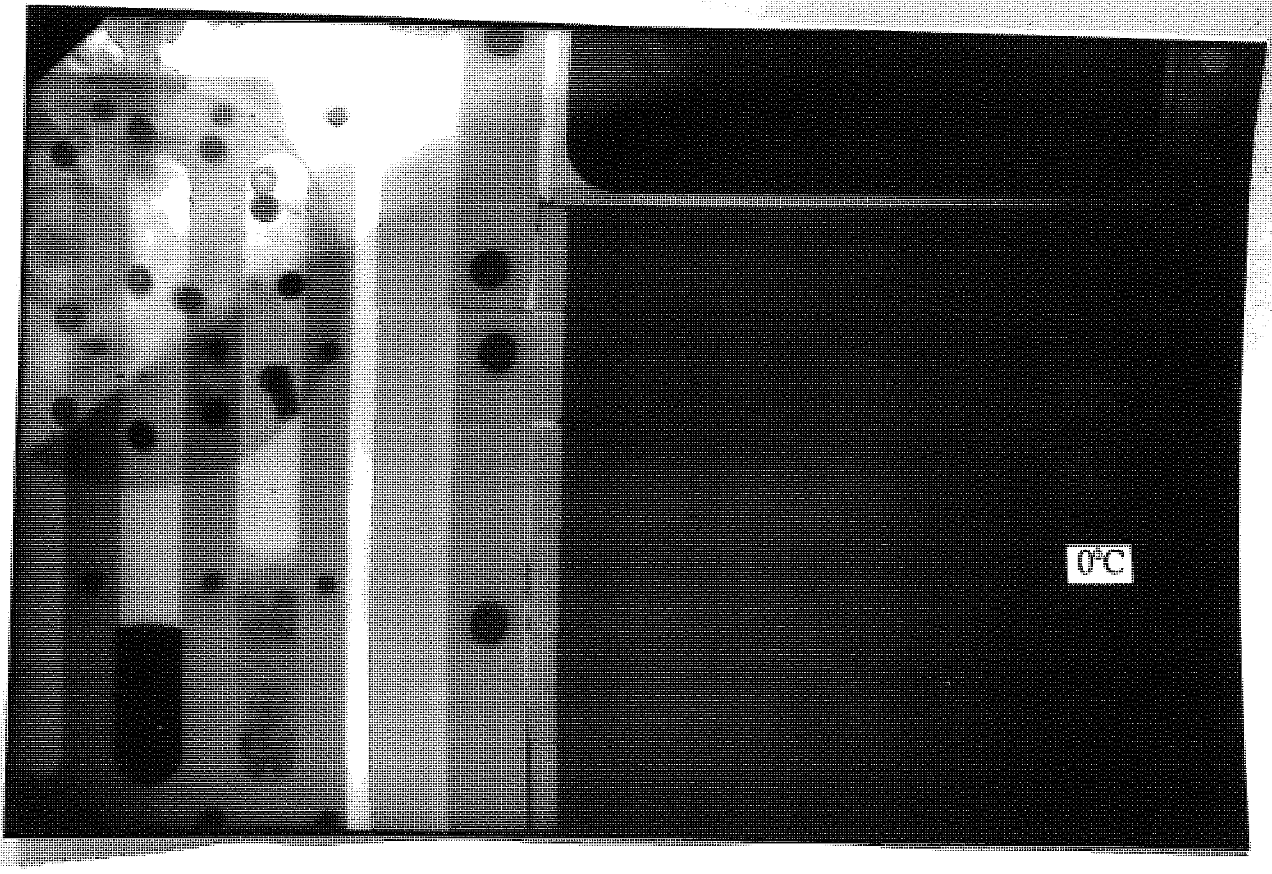

APPENDIX 5. GRAPHICAL REPRESENTATION OF RESULTS

Hydraulic potential, moisture content, electrical resistance and temperature plots against time, for each psychrometer location, are shown in the following pages for tests 1 and 2.

Potential against Time (Test 1)

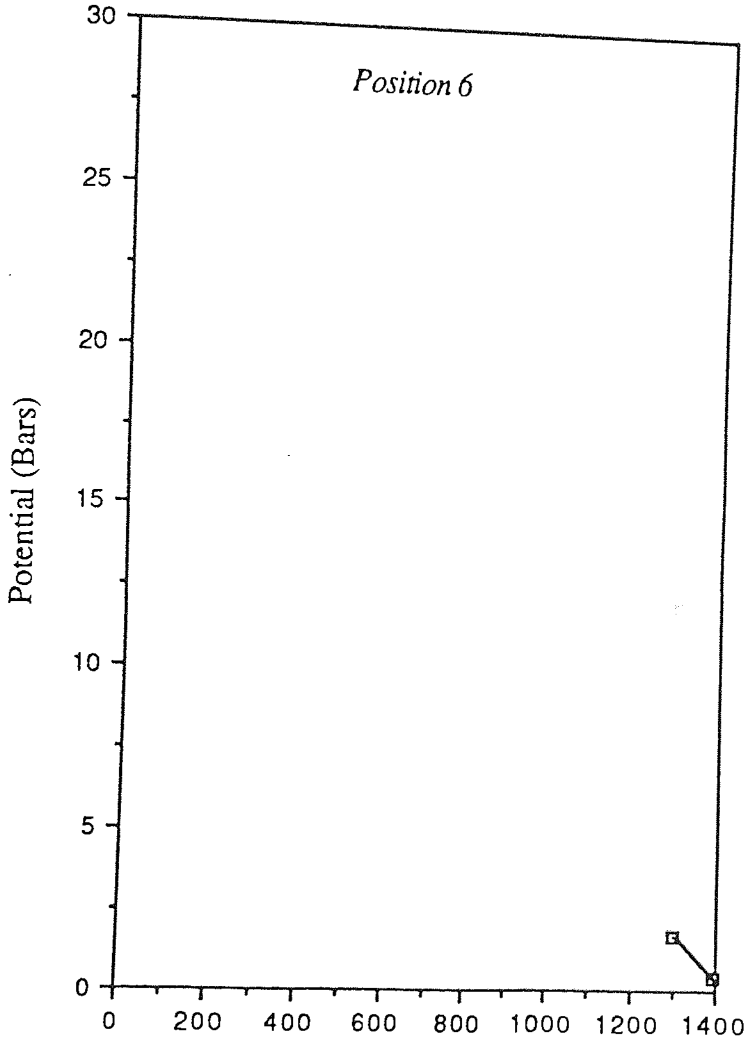

Time (minutes)

Potential against Time (Test 1)

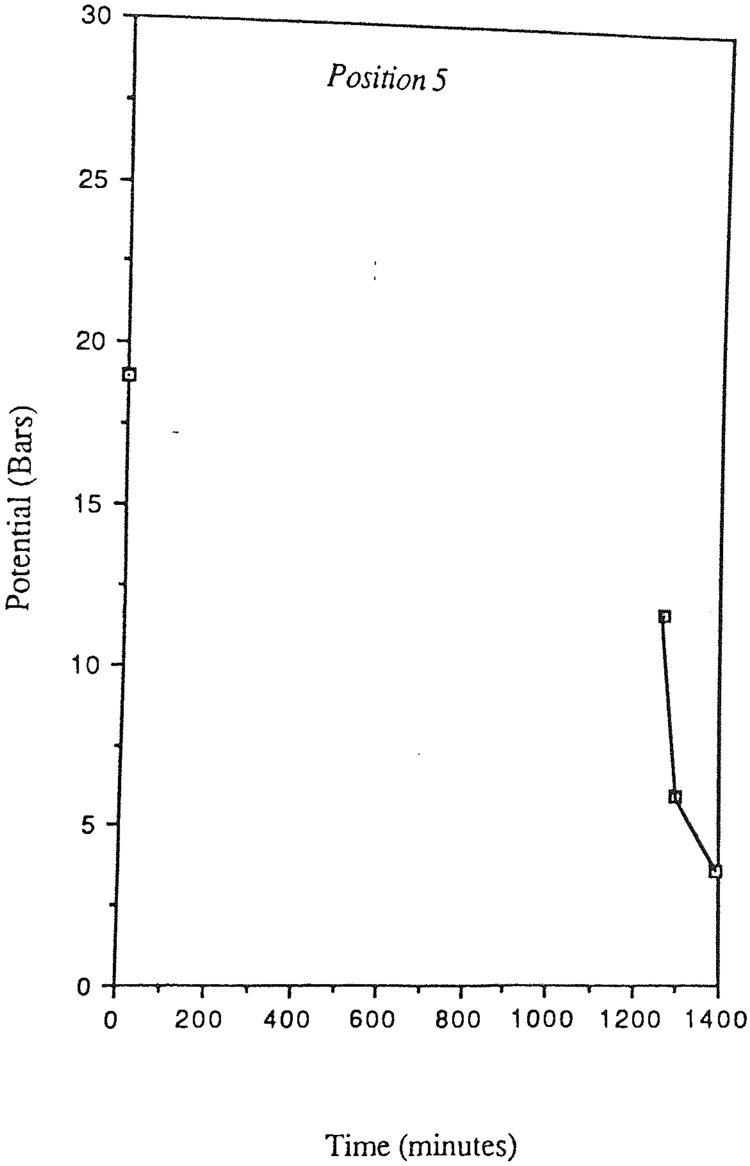

Potential against Time (Test 1)

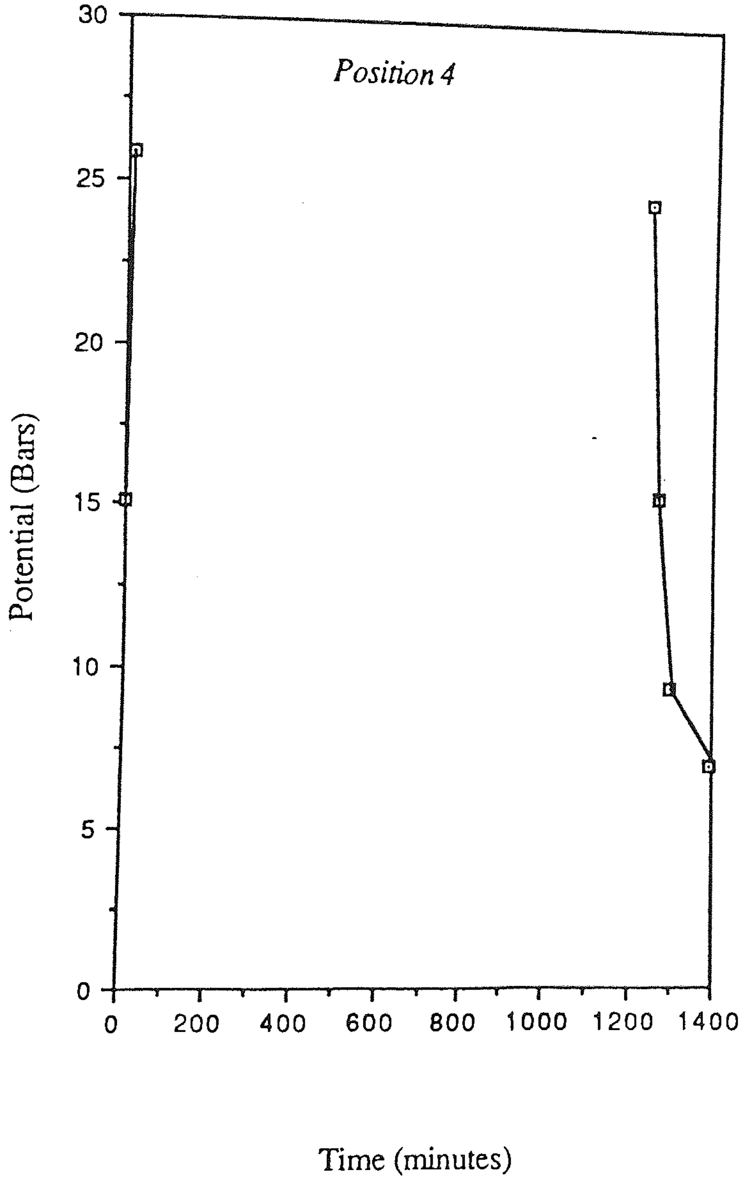

Potential against Time (Test 1)

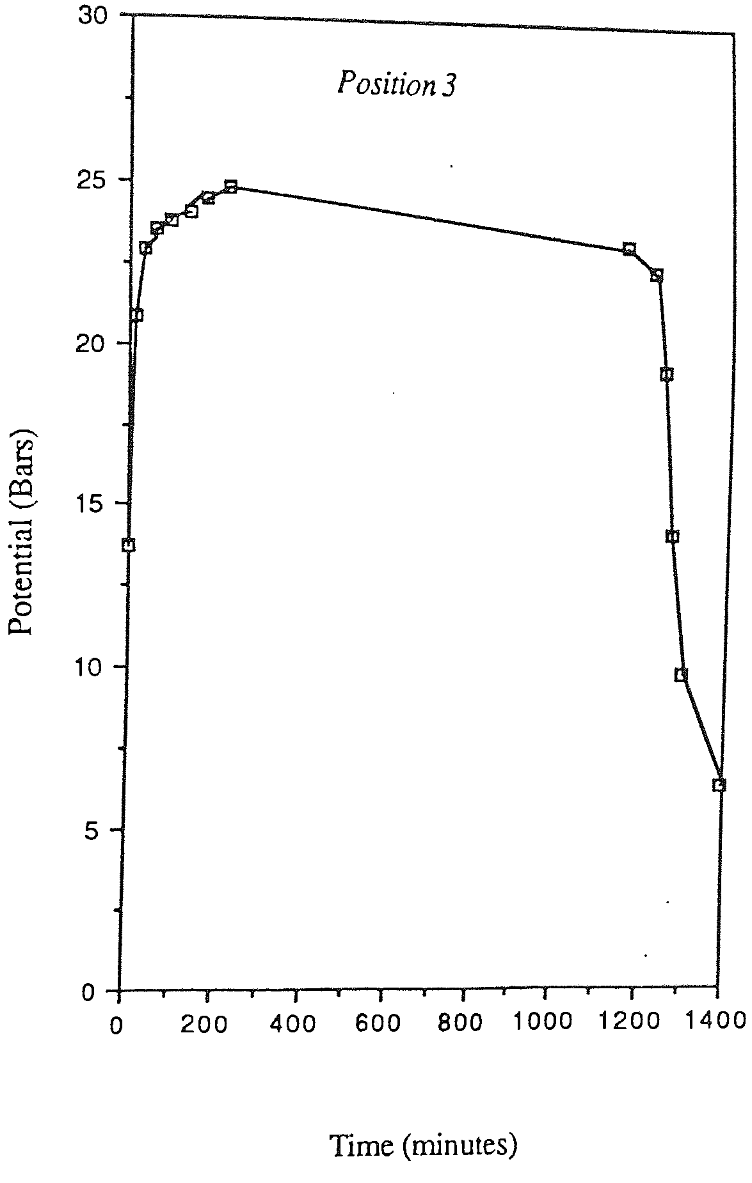

Potential against Time (Test 1)

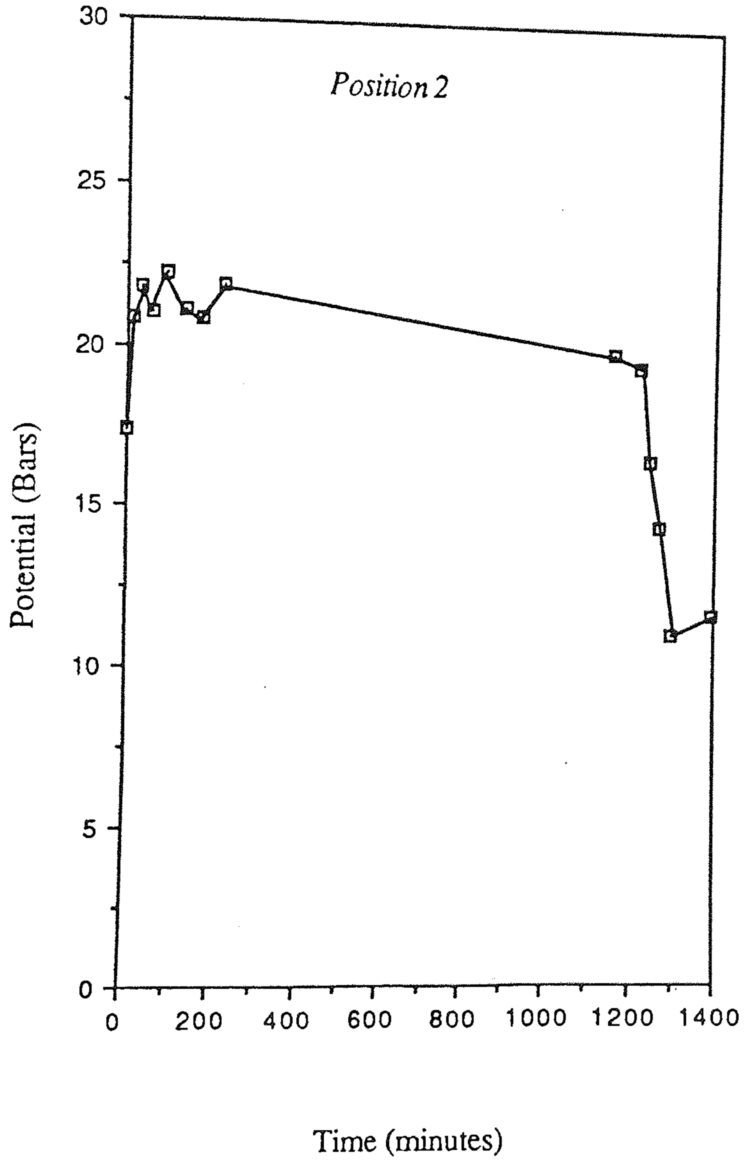

Moisture Content against Time (Test 1)

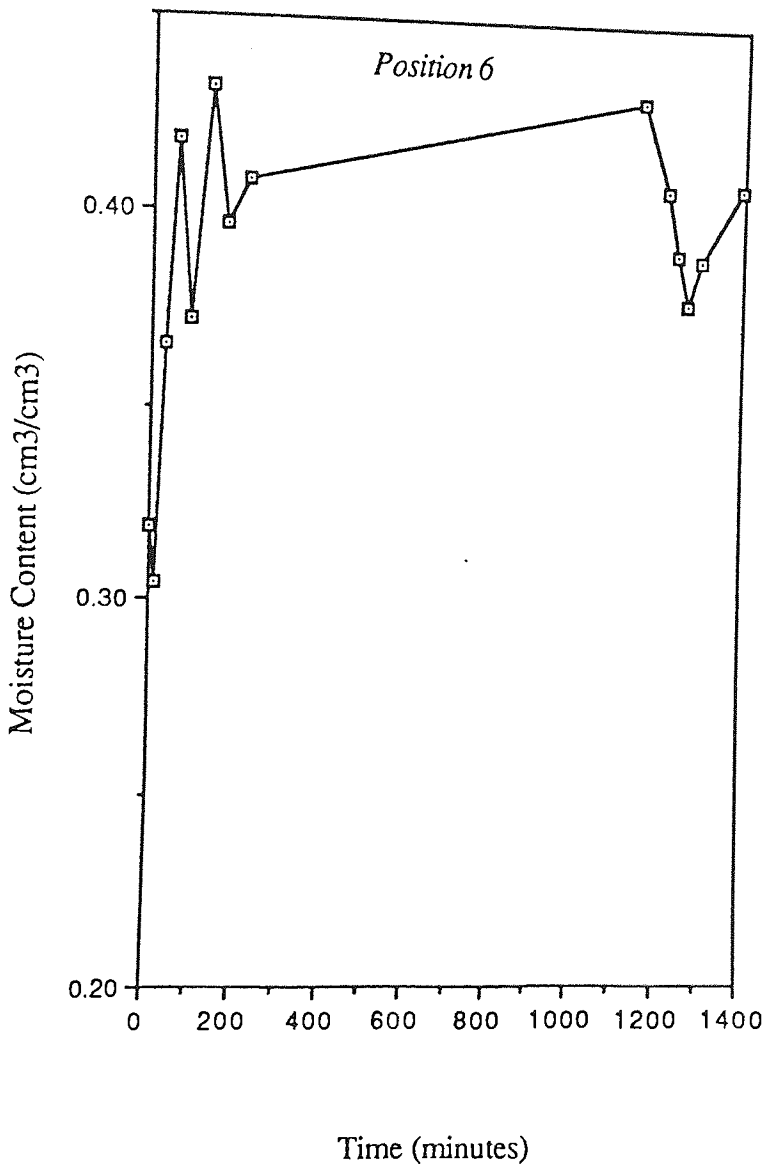

Moisture Content against Time (Test 1)

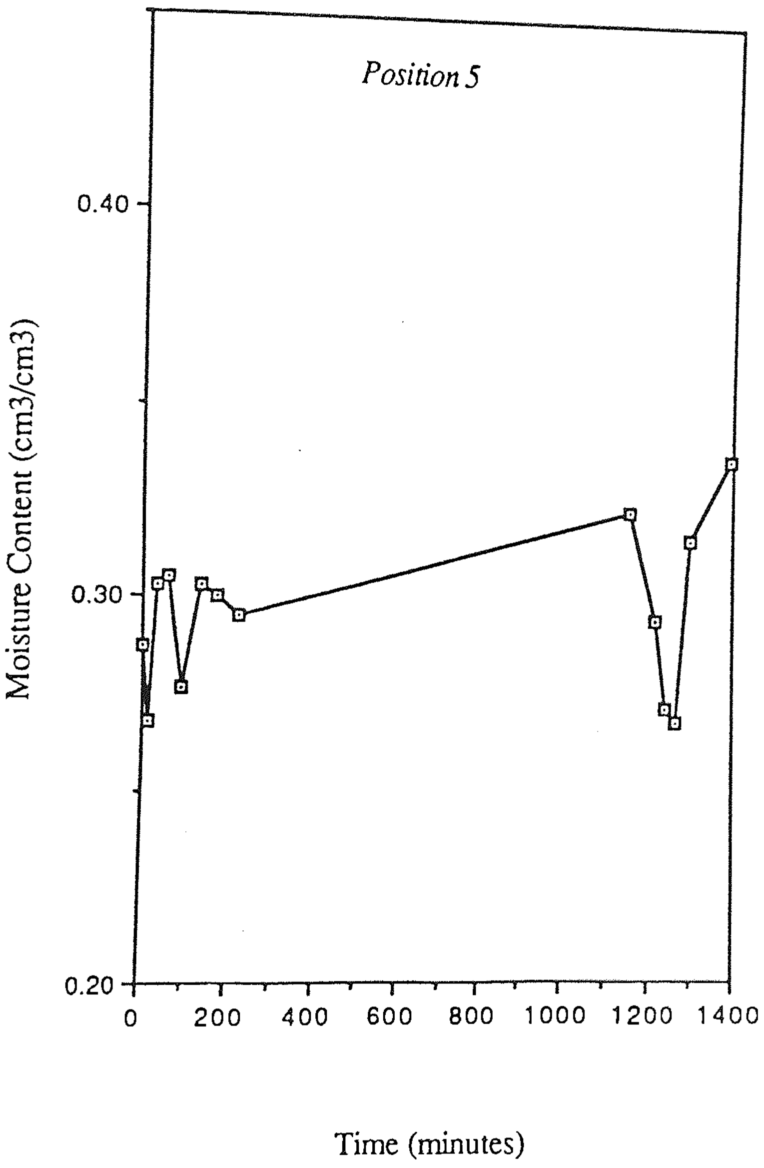

Moisture Content against Time (Test 1)

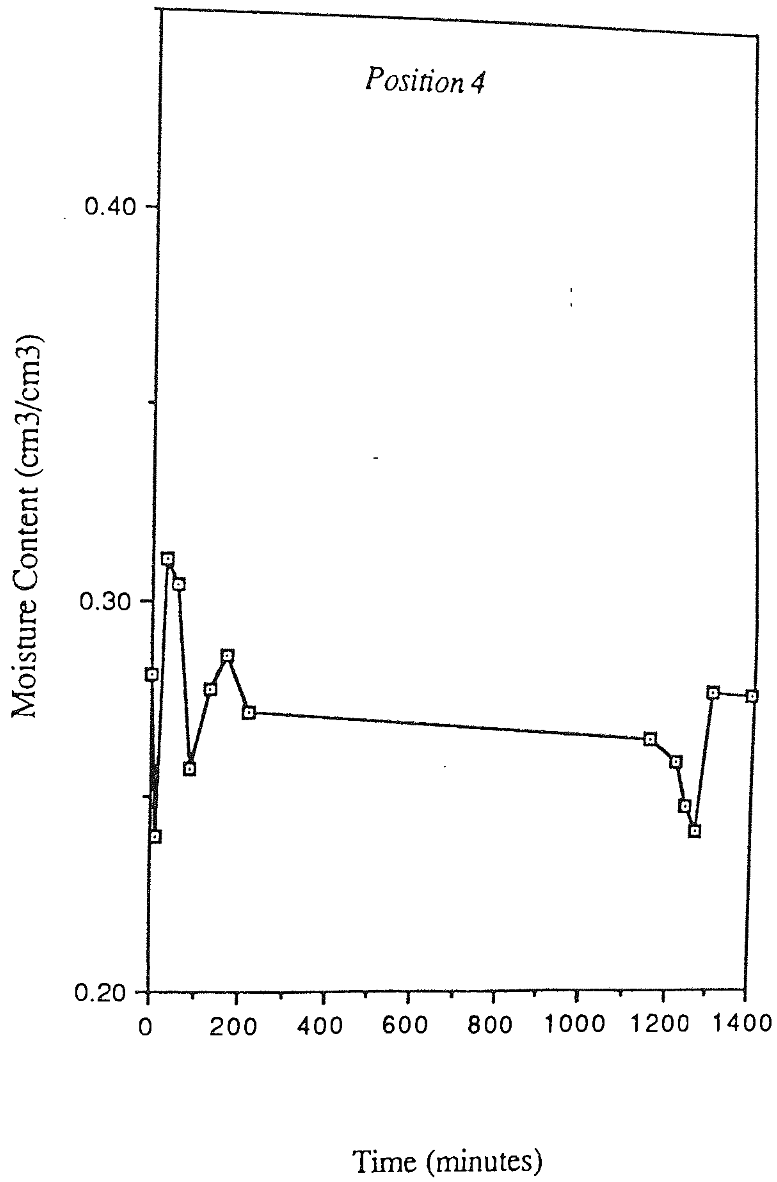

Moisture Content against Time (Test 1)

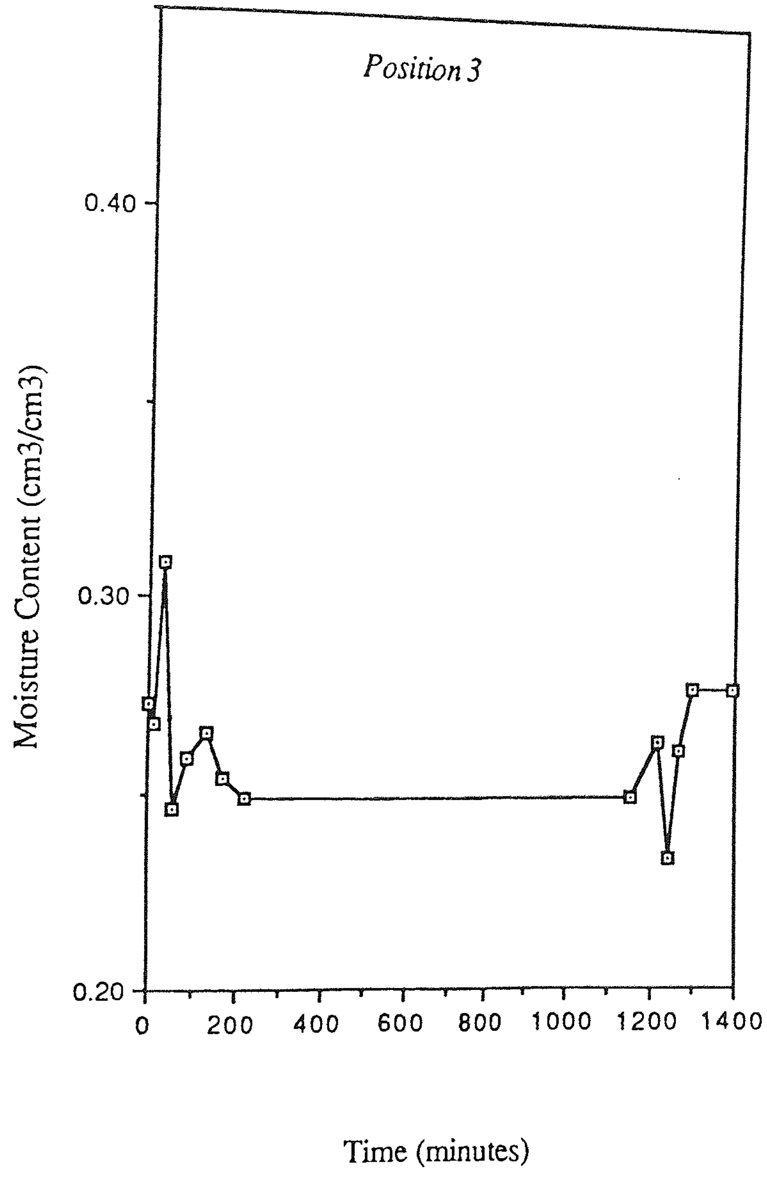

Moisture Content against Time (Test 1)

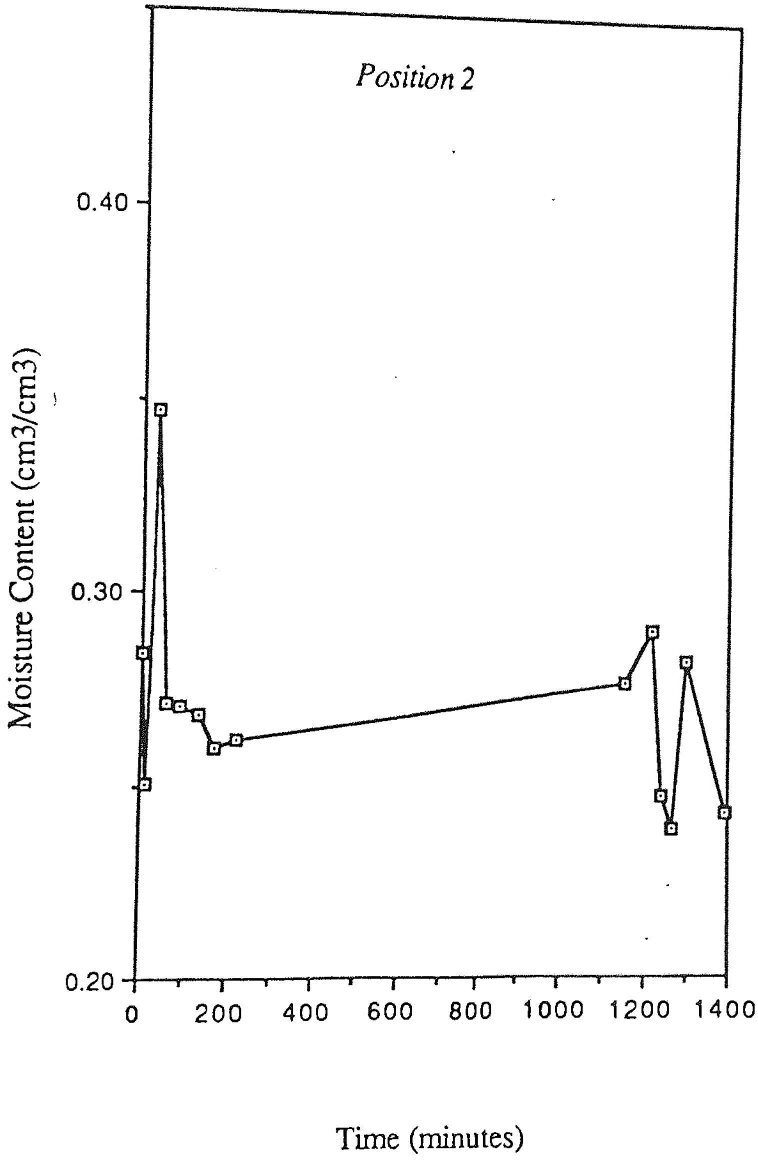

Electrical Resistance against Time (Test 1)

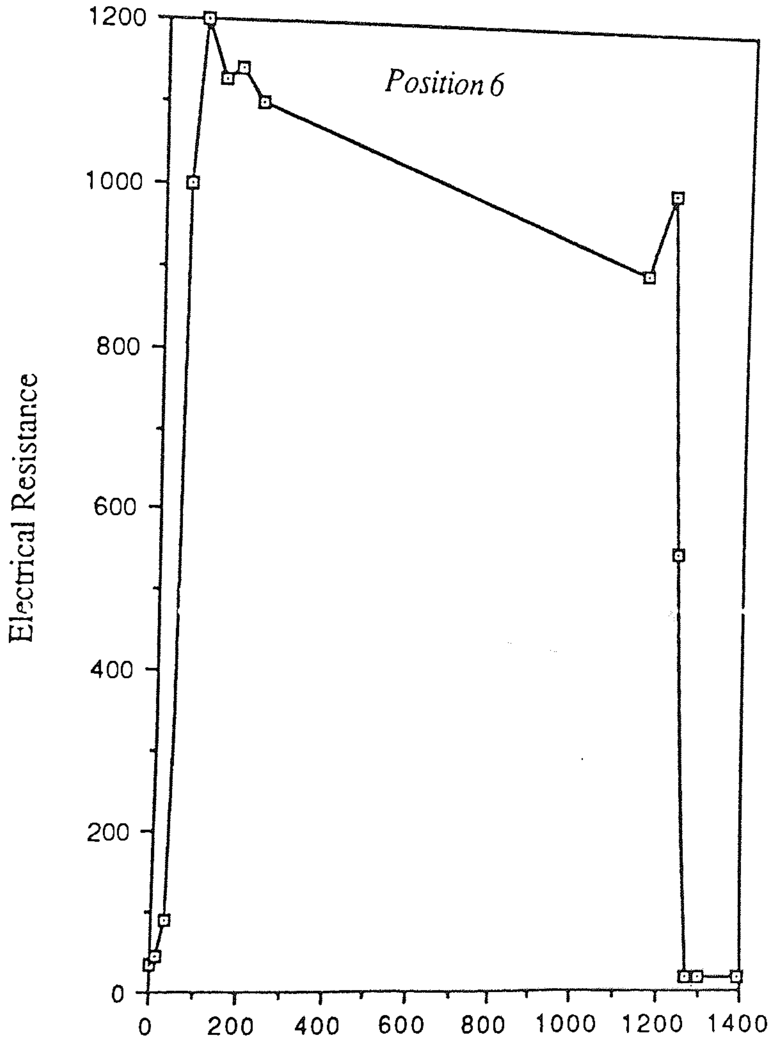

Time (minutes)

Electrical Resistance against Time (Test 1)

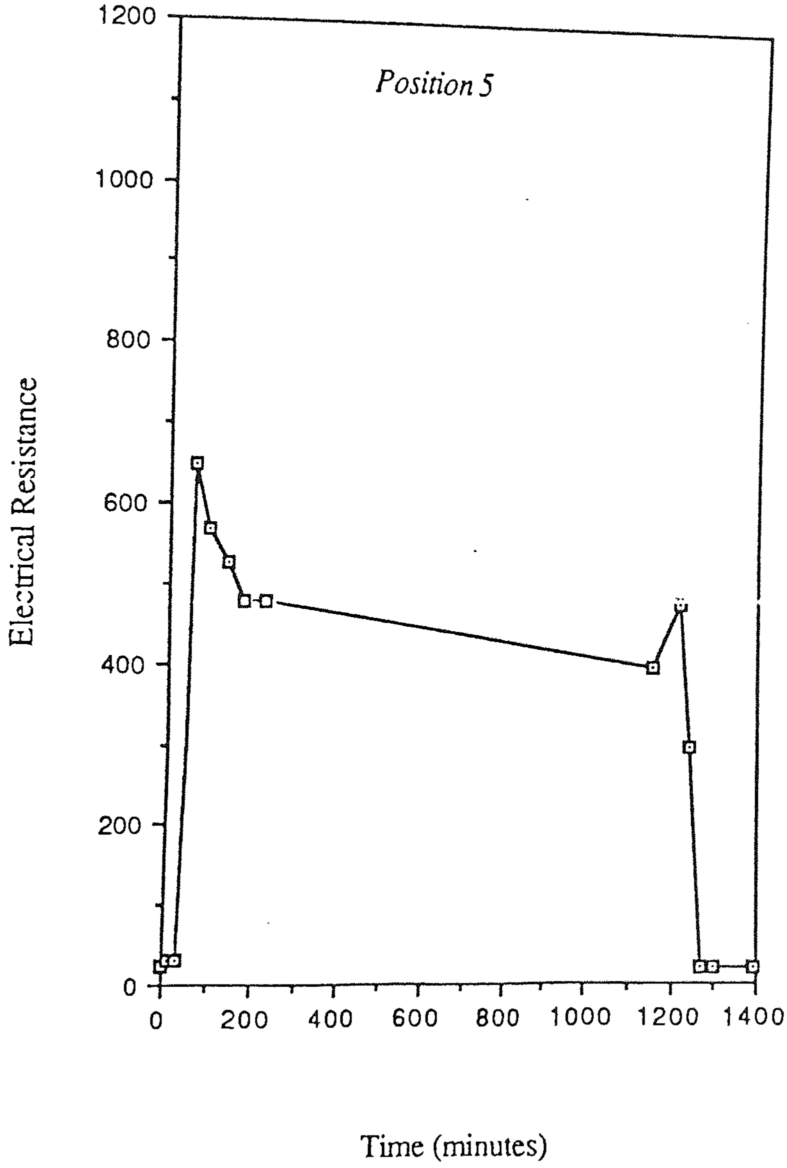

Electrical Resistance against Time (Test 1)

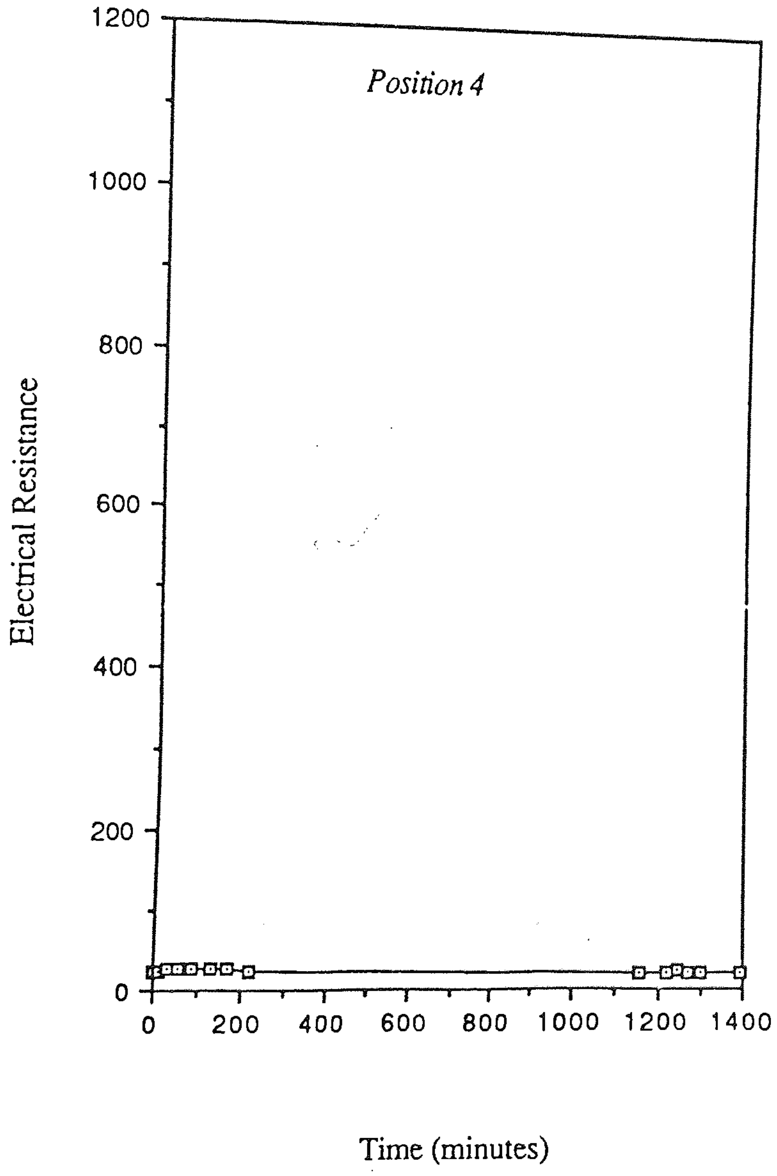

Electrical Resistance against Time (Test 1)

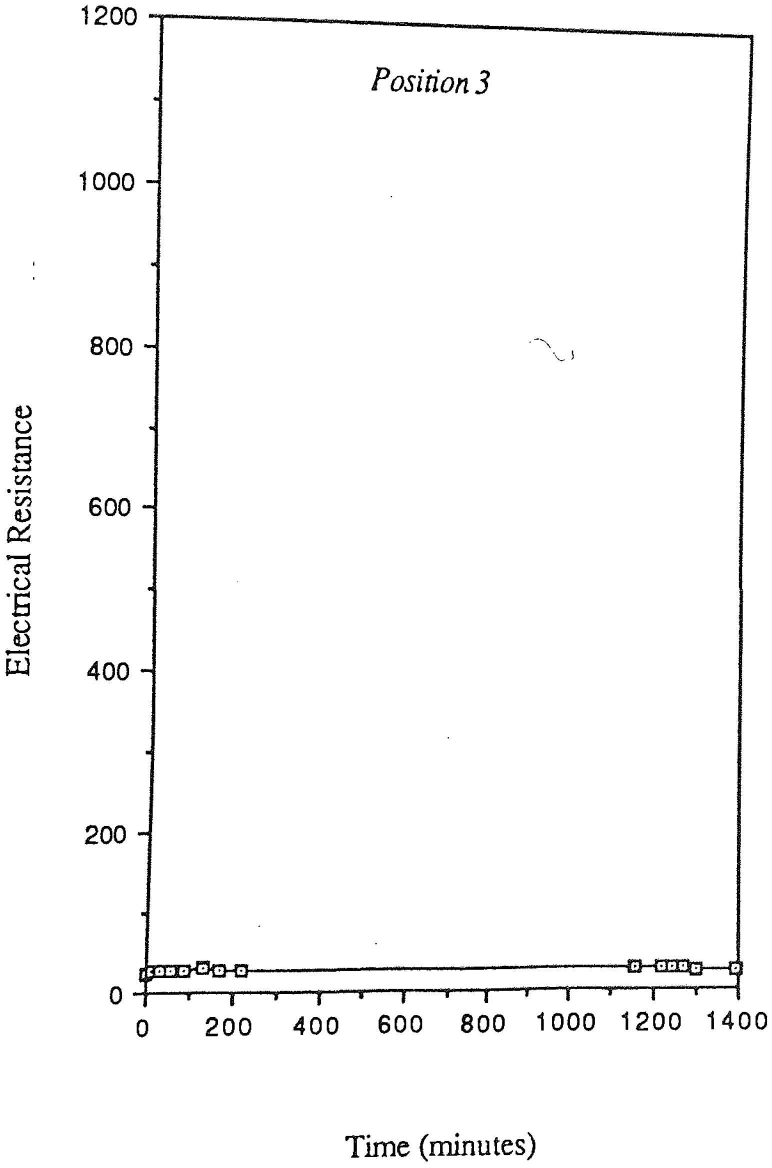

Electrical Resistance against Time (Test 1)

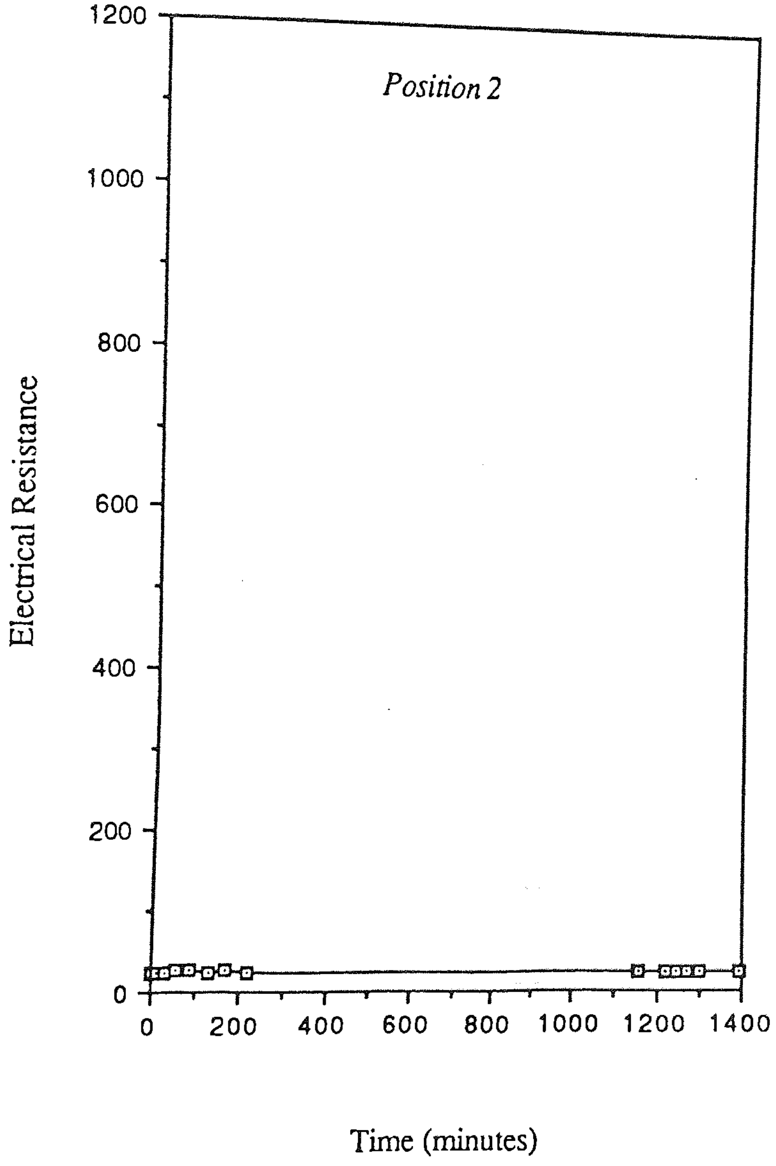

Temperature against Time (Test 1)

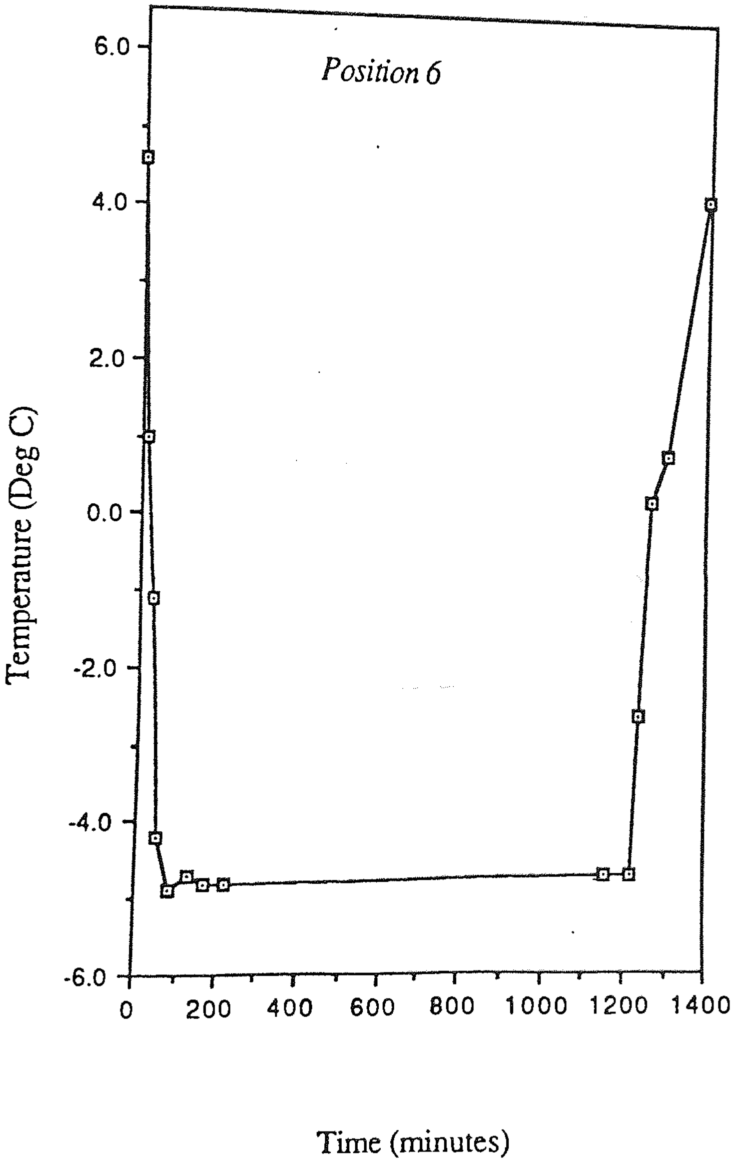

Temperature against Time (Test 1)

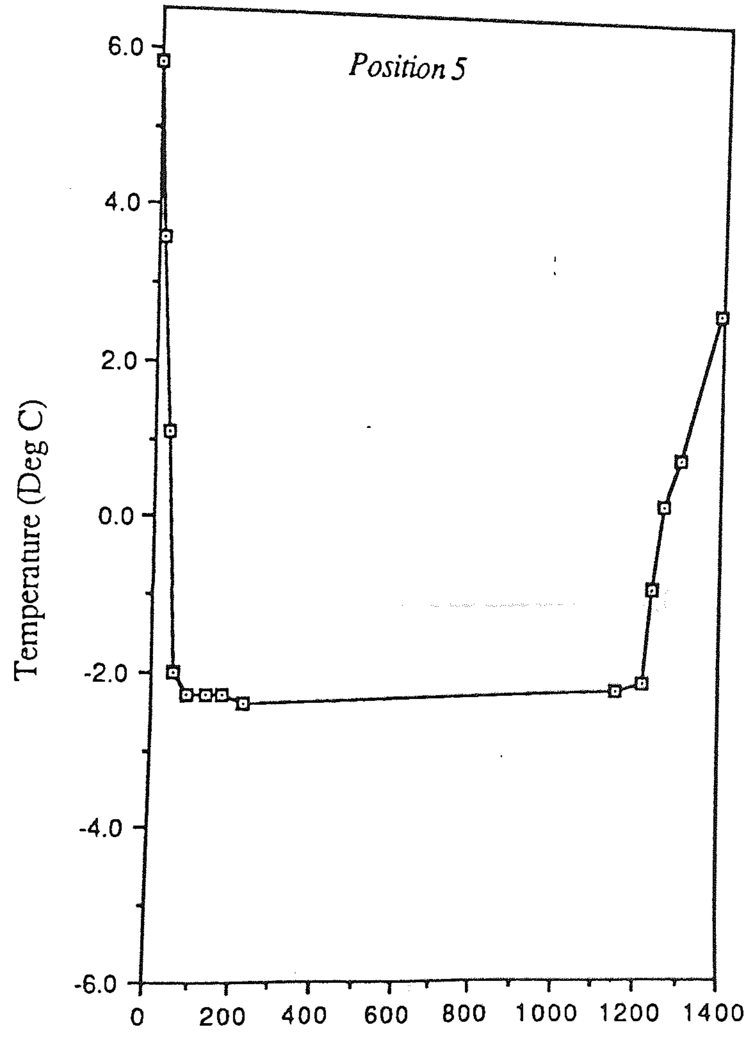

Time (minutes)

Temperature against Time (Test 1)

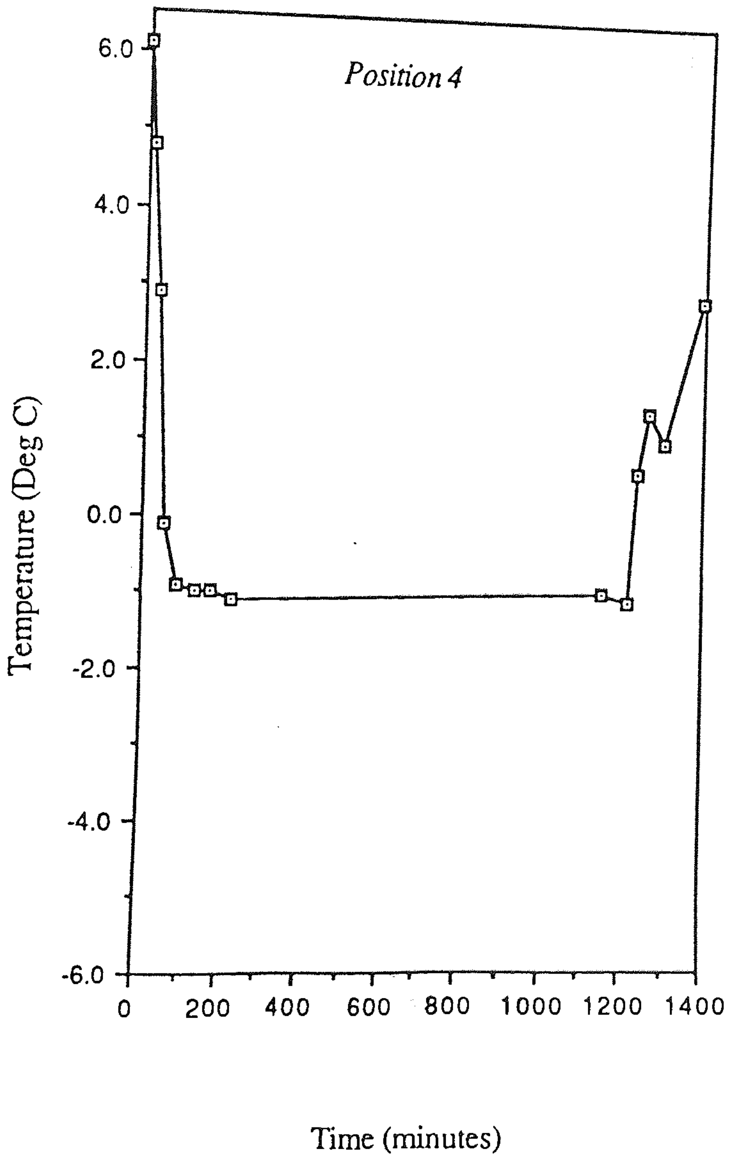

Temperature against Time (Test 1)

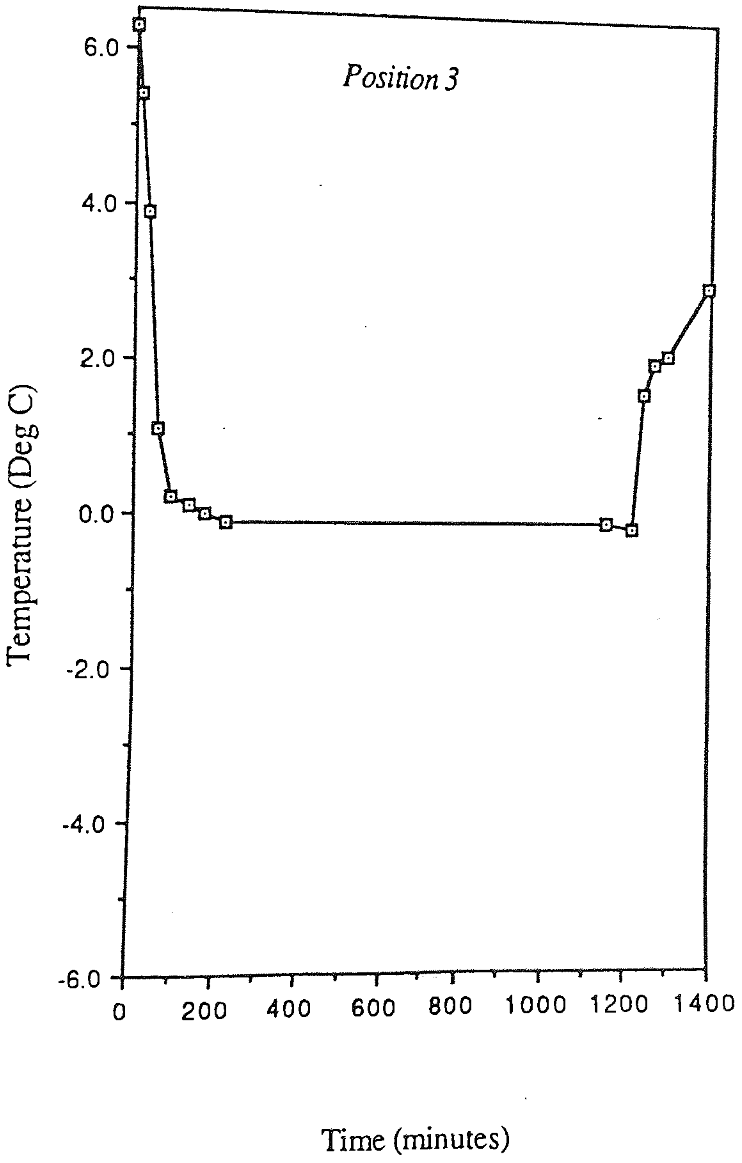

Temperature against Time (Test 1)

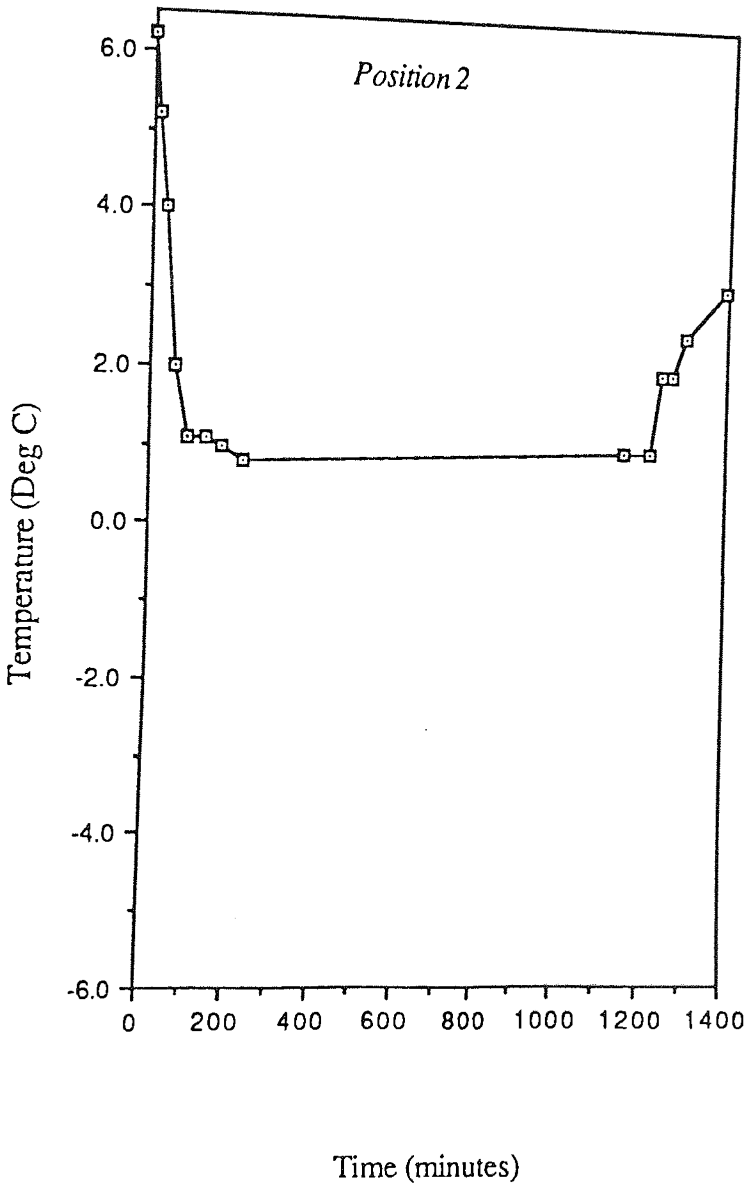

Temperature against Time (Test 1)

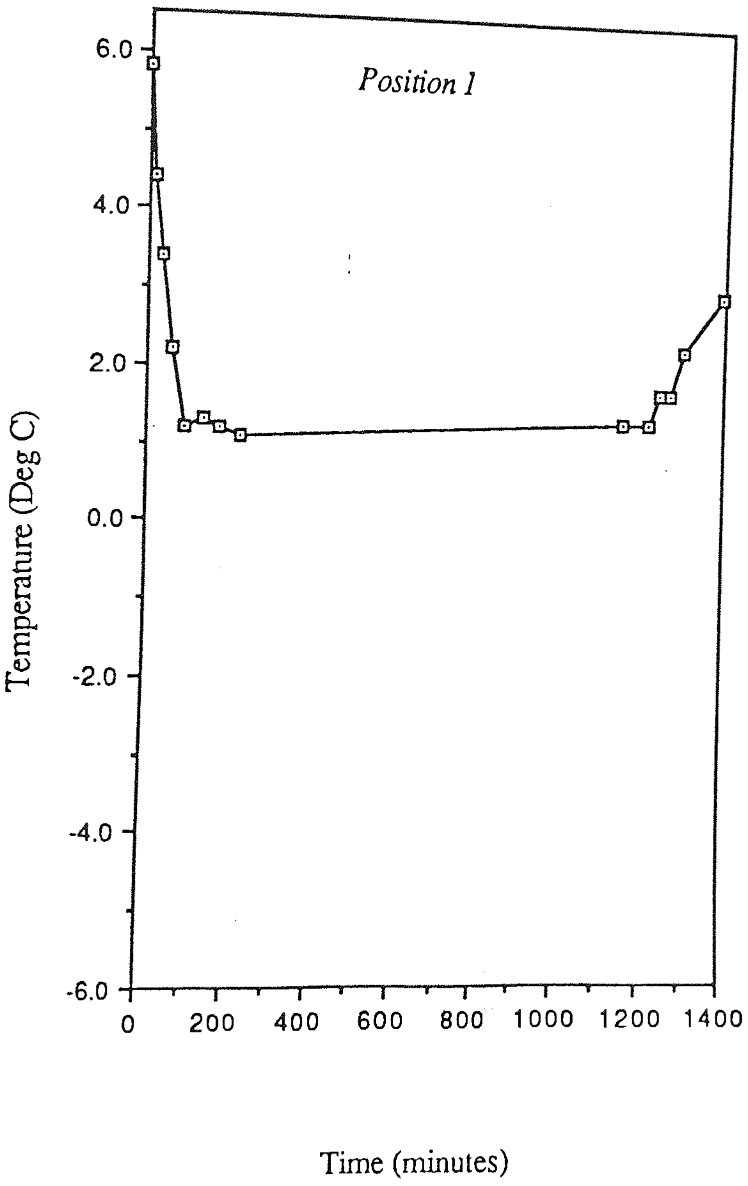

Potential against Time (Test 2)

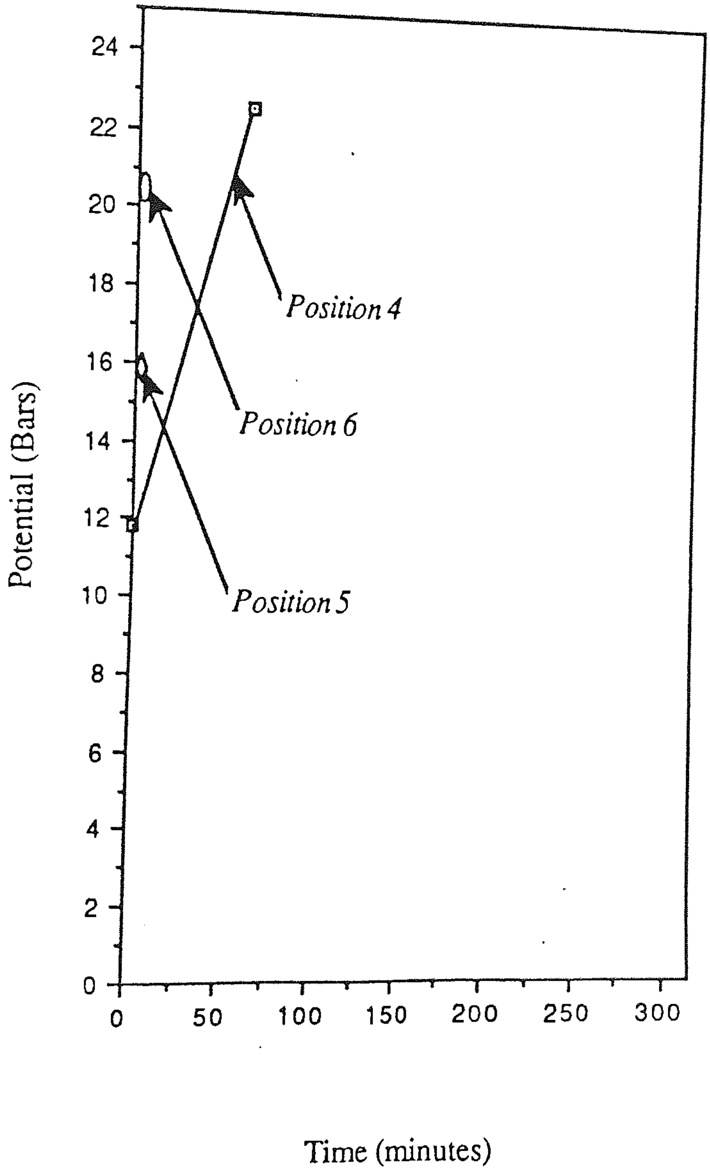

Potential against Time (Test 2)

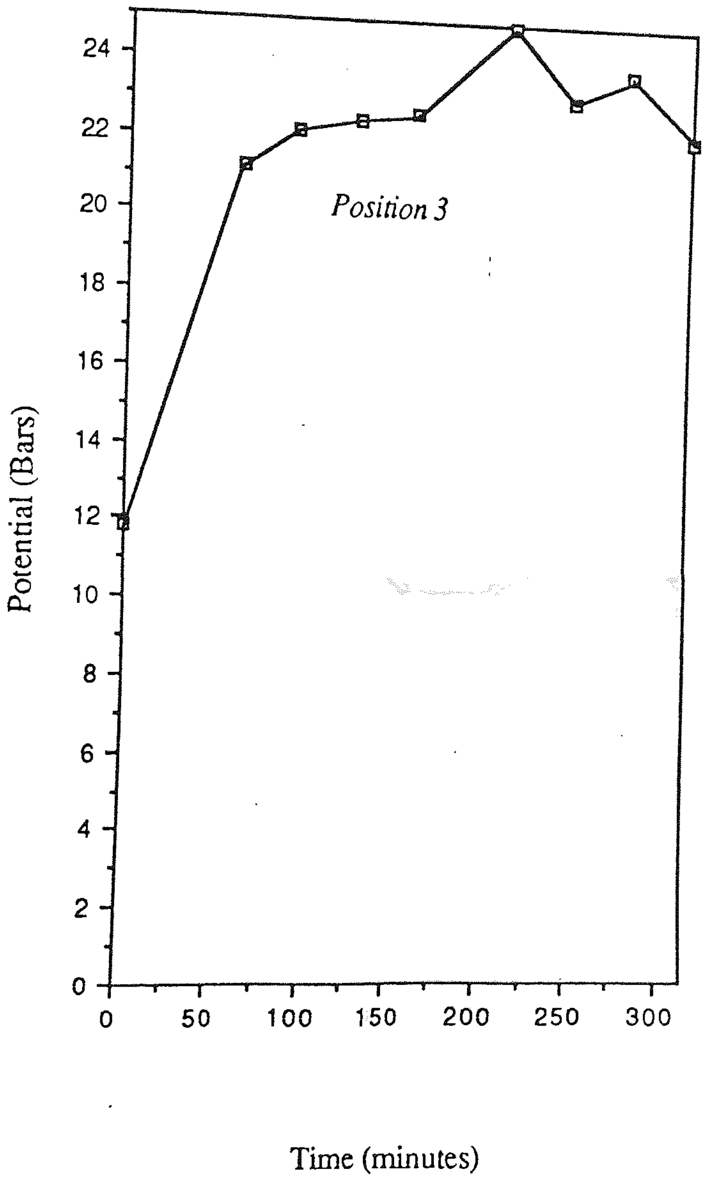

Potential against Time (Test 2)

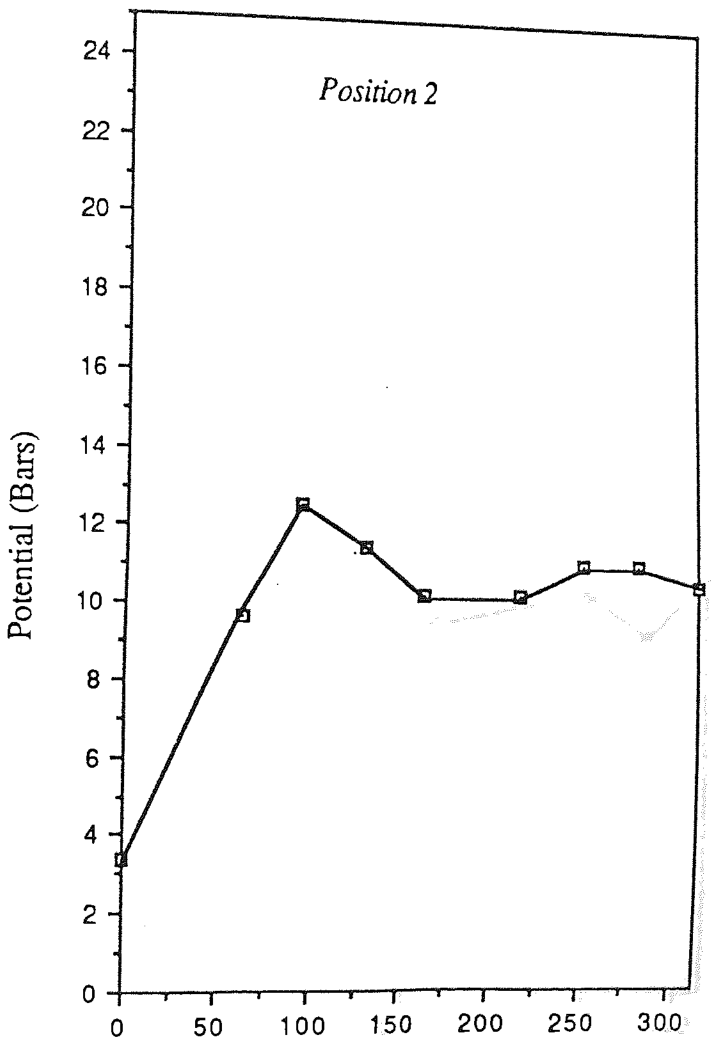

Time (minutes)

Potential against Time (Test 2)

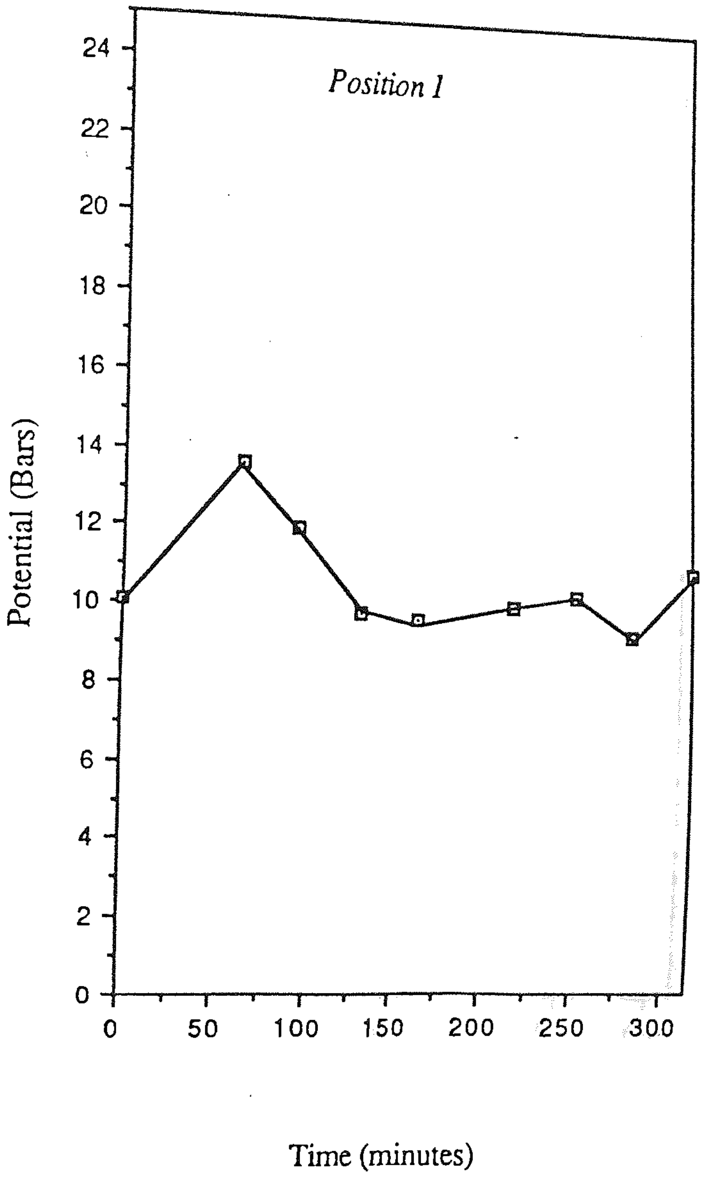

Moisture Content against Time (Test 2)

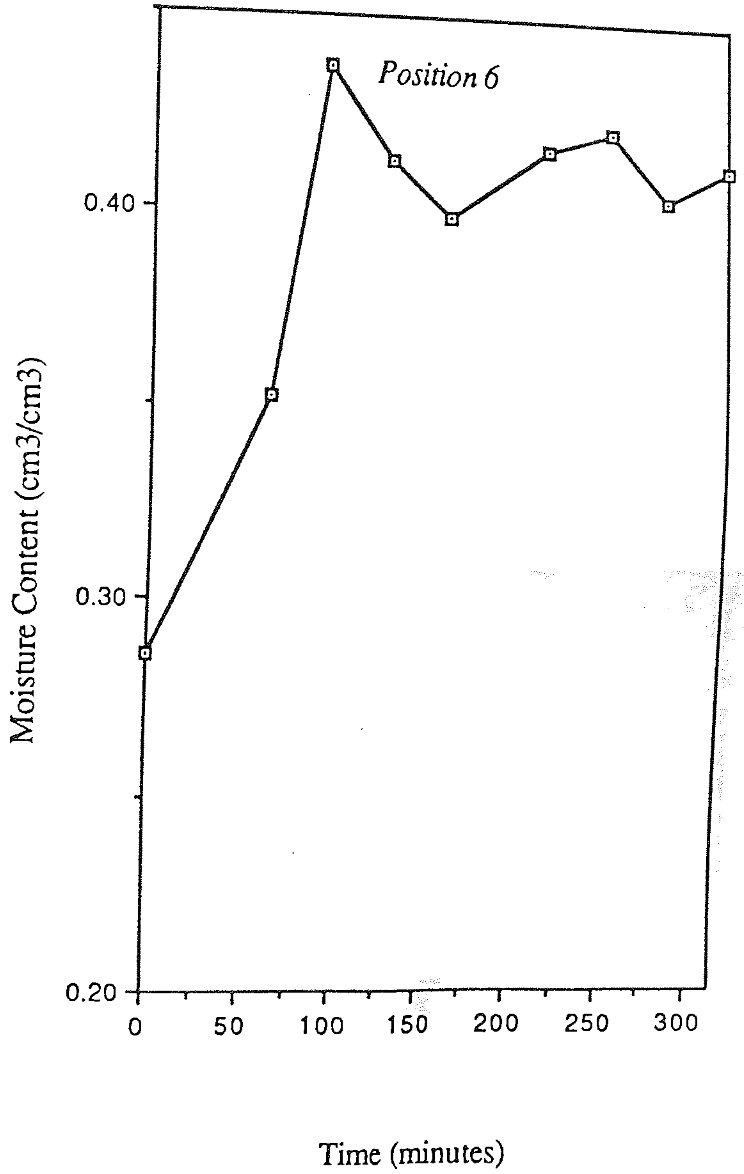

Moisture Content against Time (Test 2)

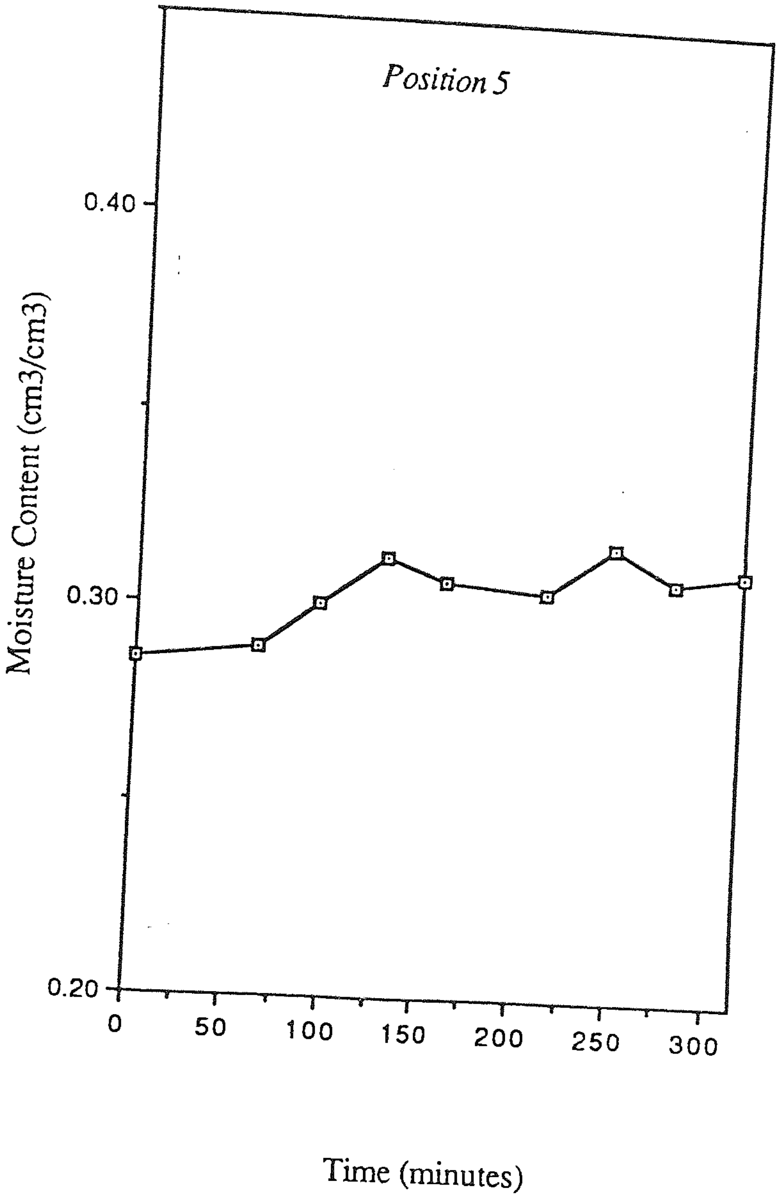

Moisture Content against Time (Test 2)

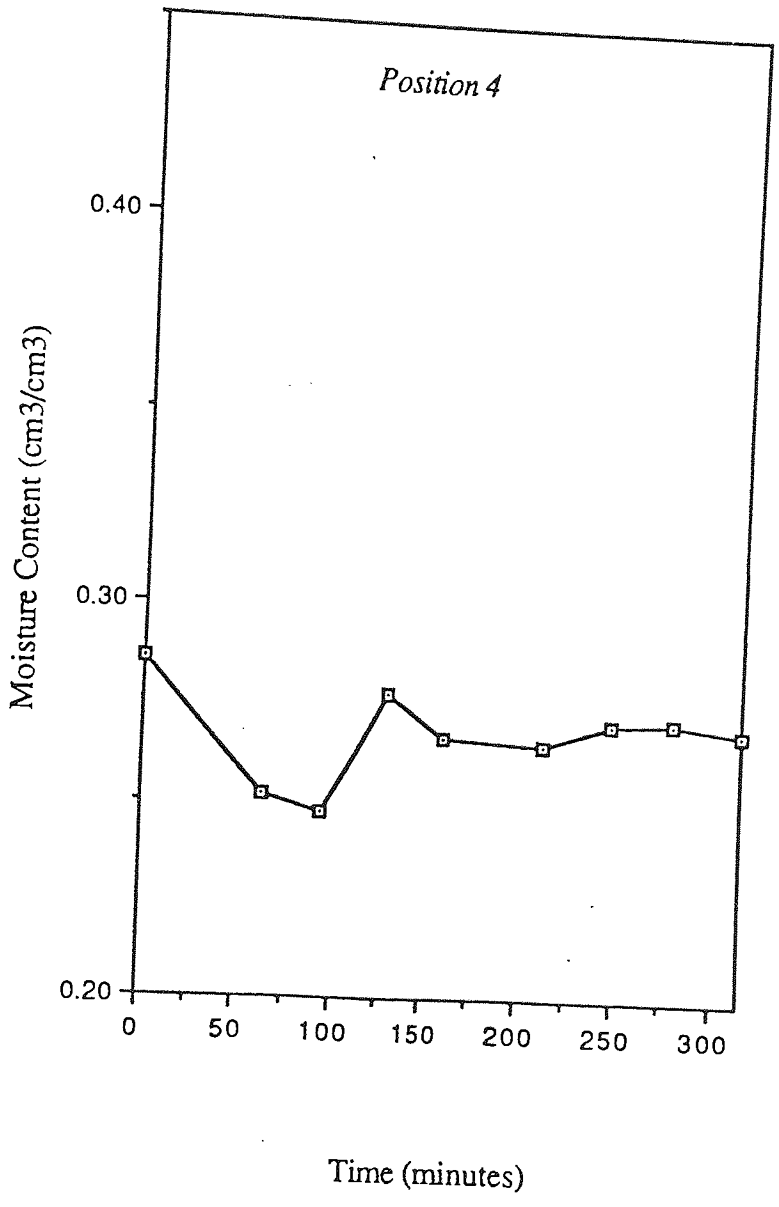

Moisture Content against Time (Test 2)

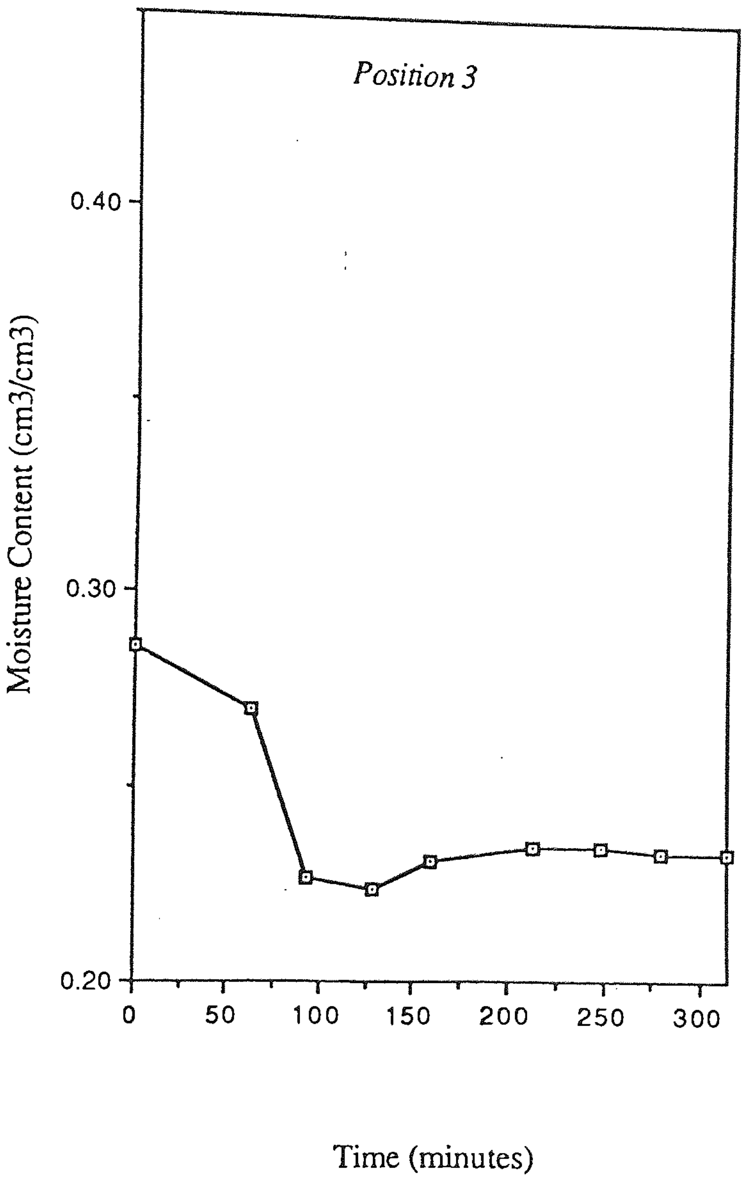

Moisture Content against Time (Test 2)

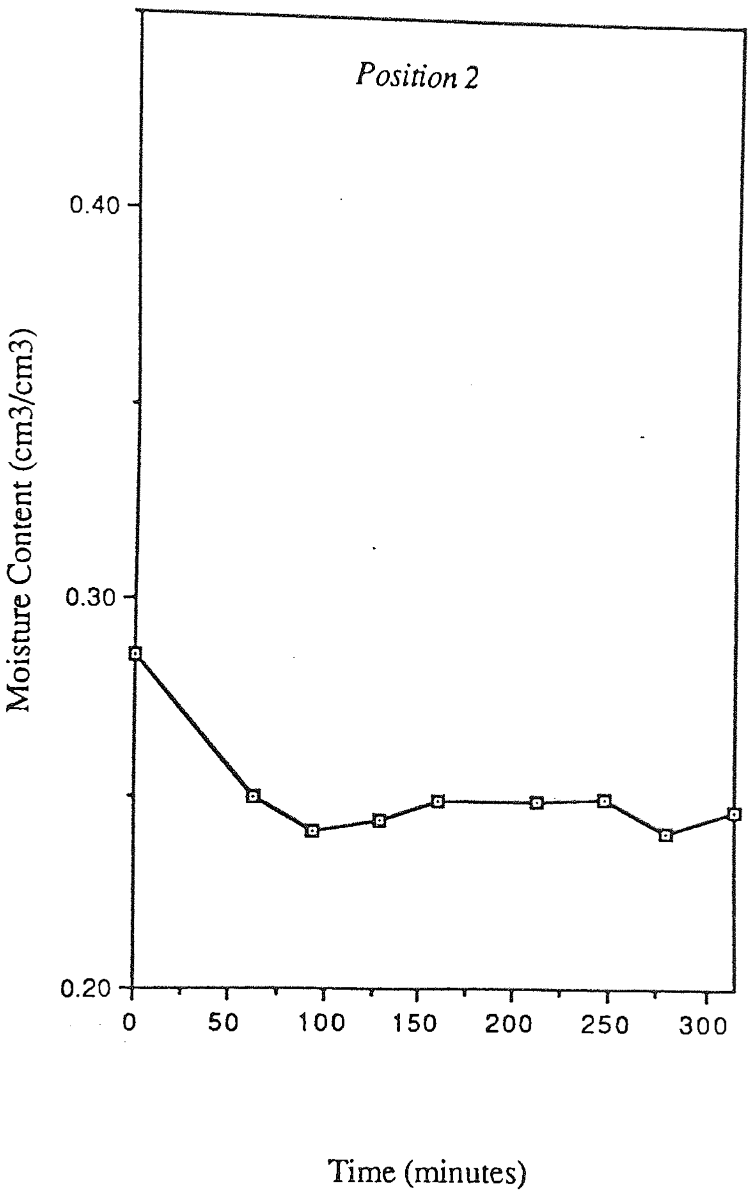

Moisture Content against Time (Test 2)

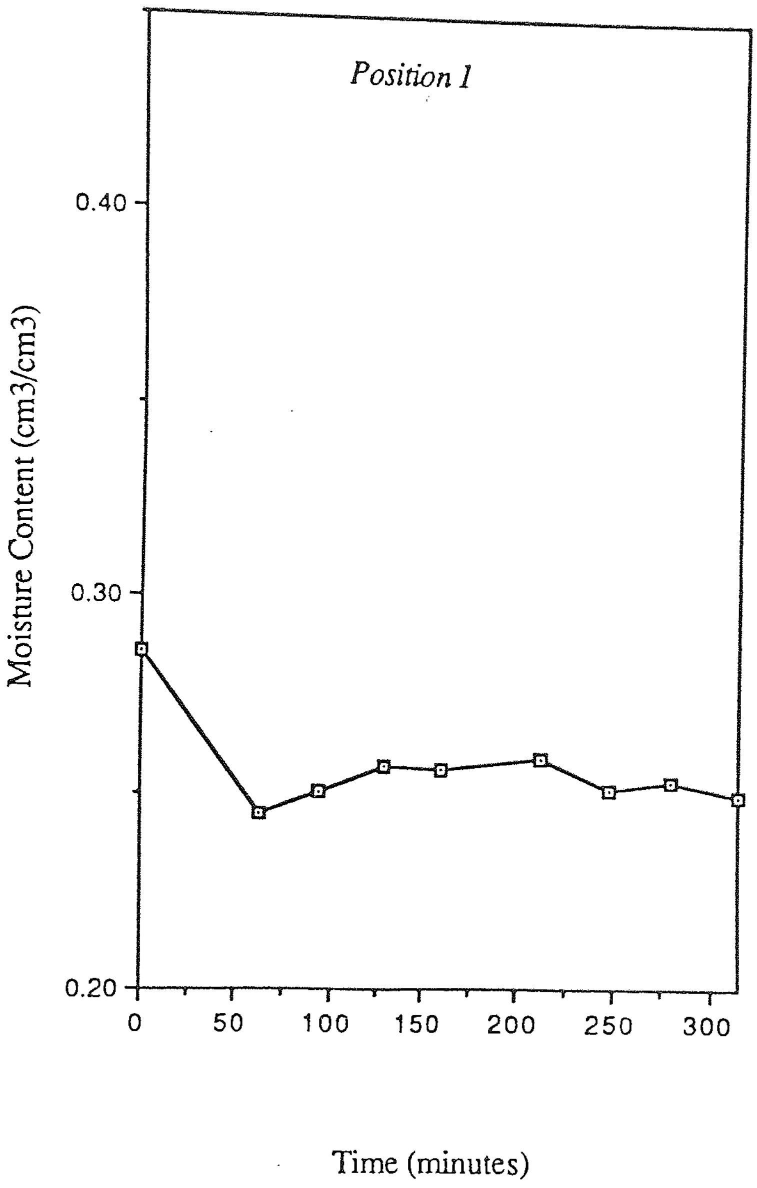

Electrical Resistance against Time (Test 2)

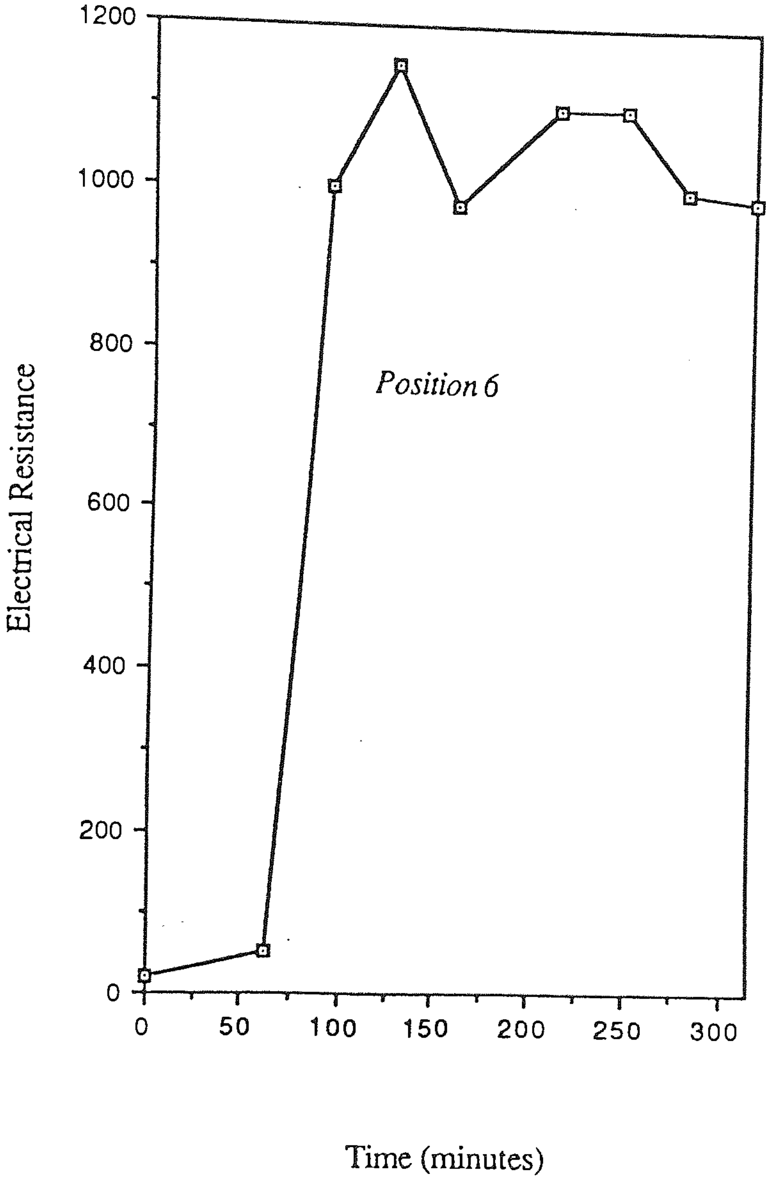

Electrical Resistance against Time (Test 2)

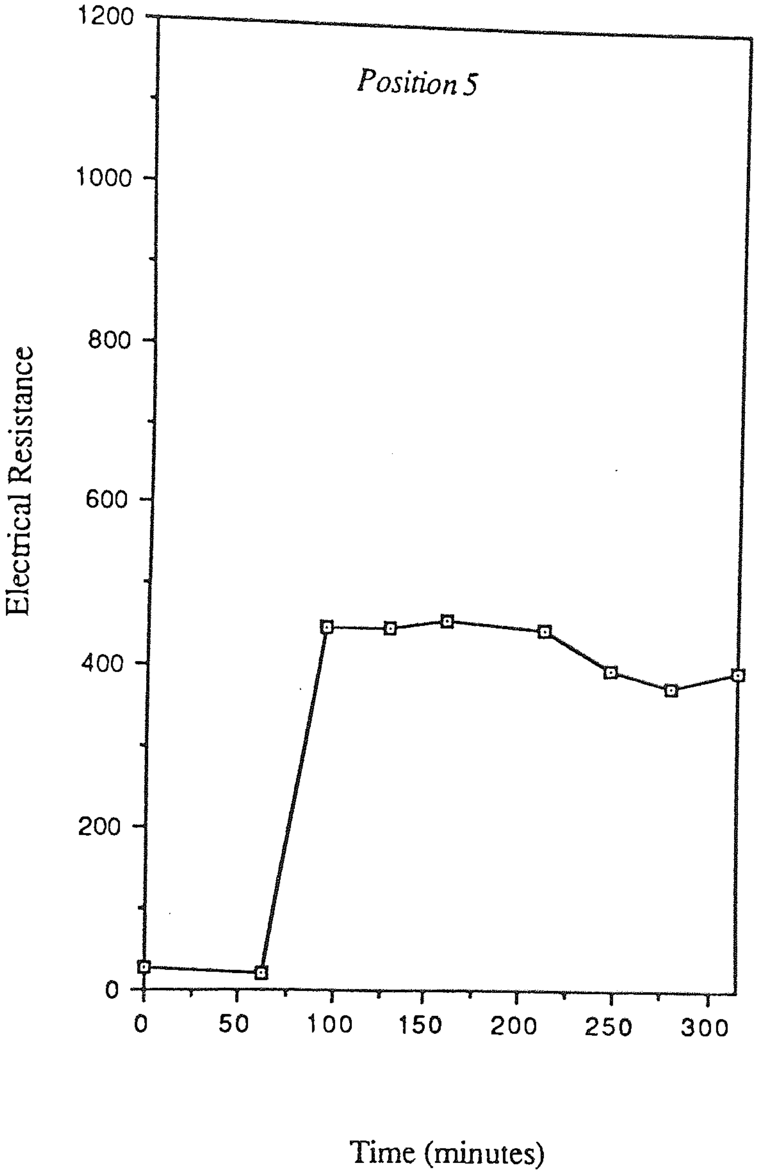

Electrical Resistance against Time (Test 2)

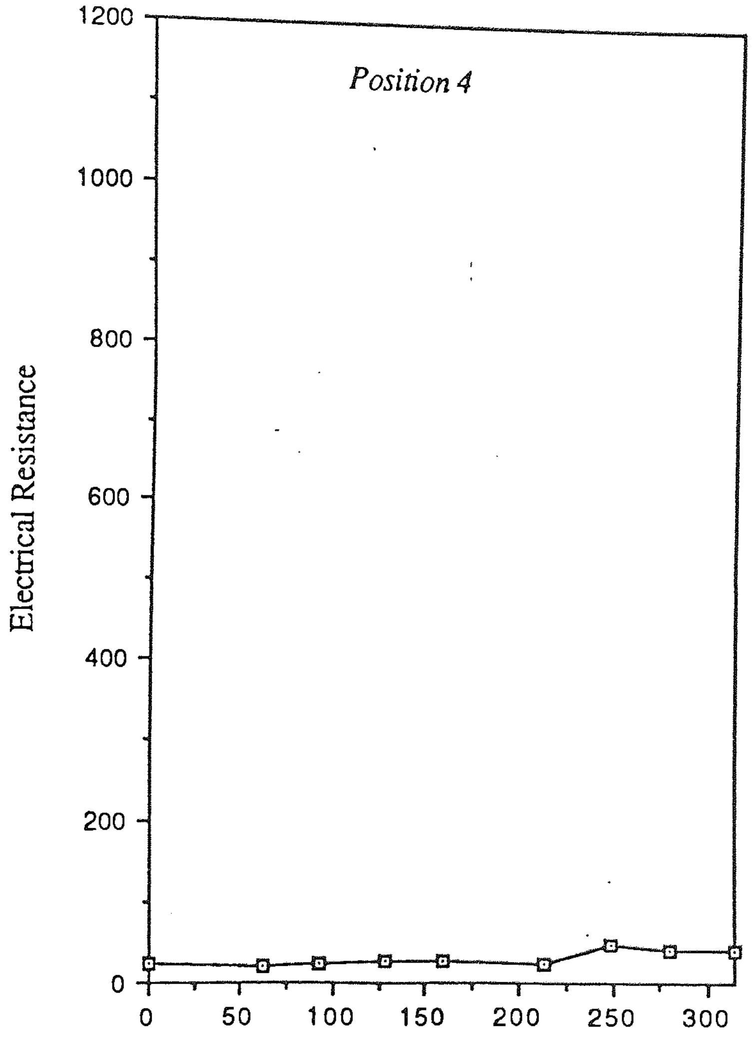

Time (minutes)

Electrical Resistance against Time (Test 2)

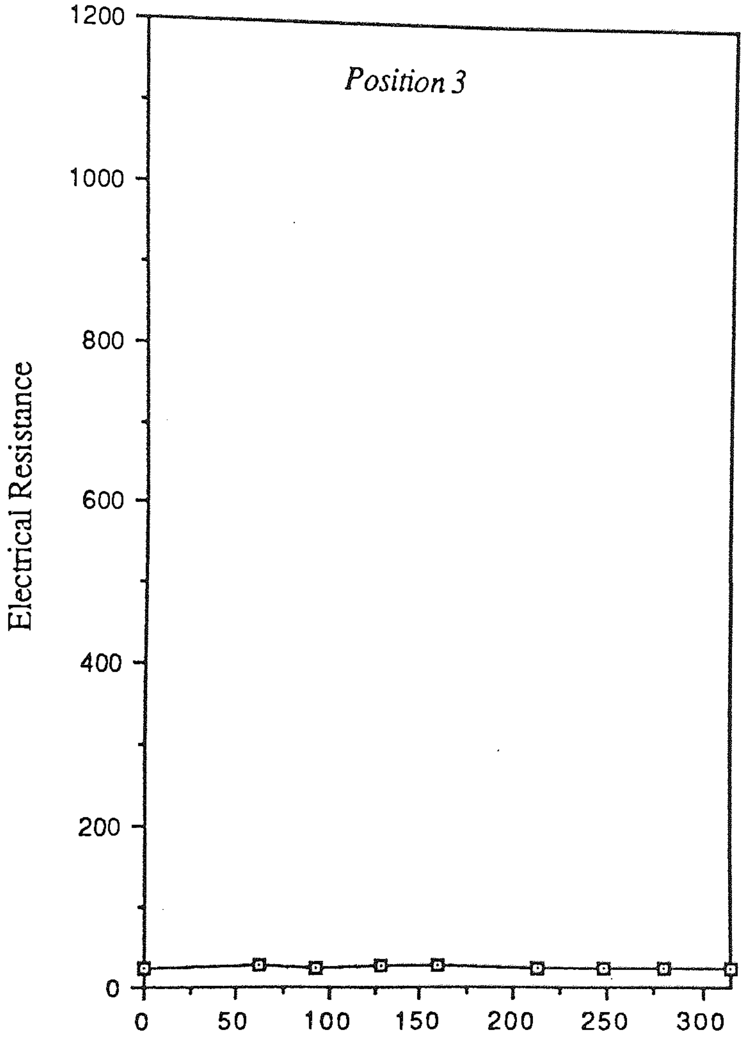

Time (minutes)

Electrical Resistance against Time (Test 2)

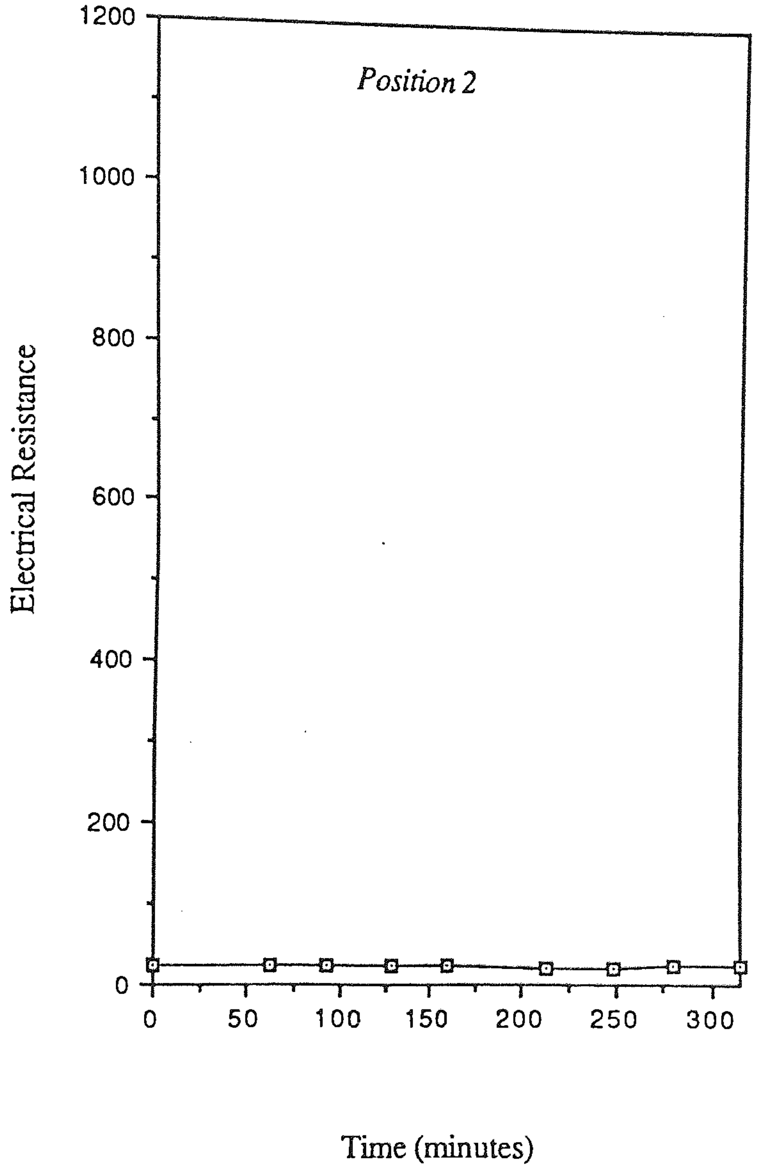

Temperature against Time (Test 2)

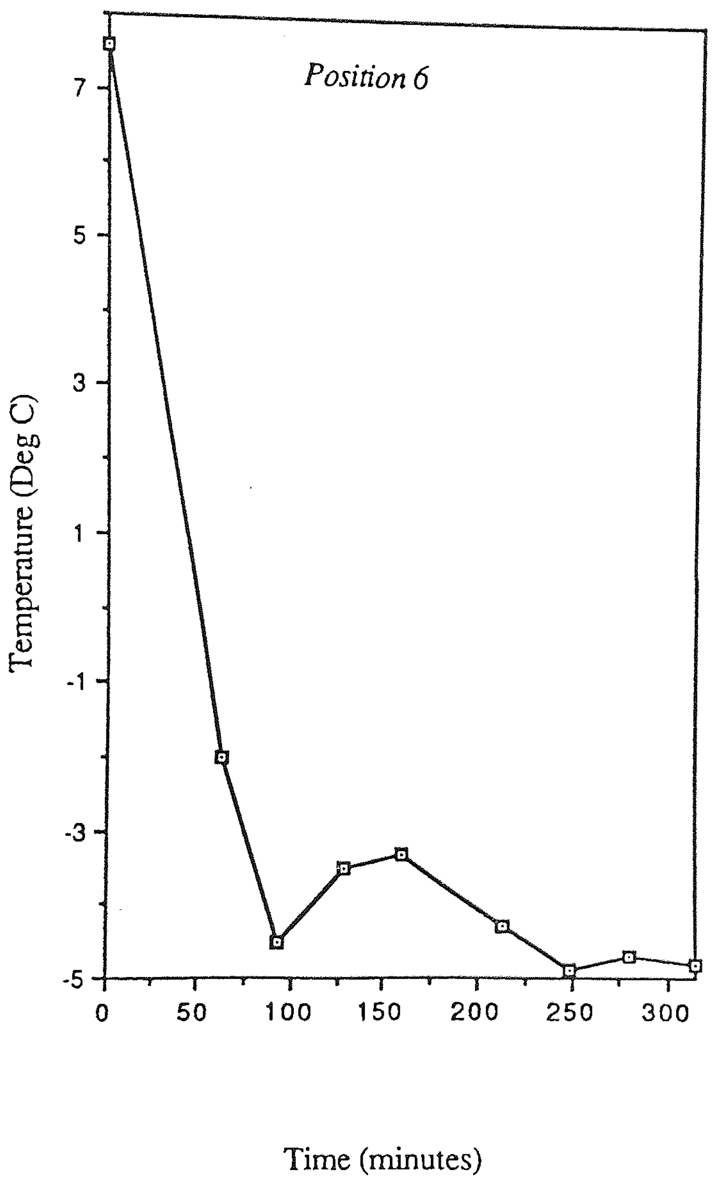

Temperature against Time (Test 2)

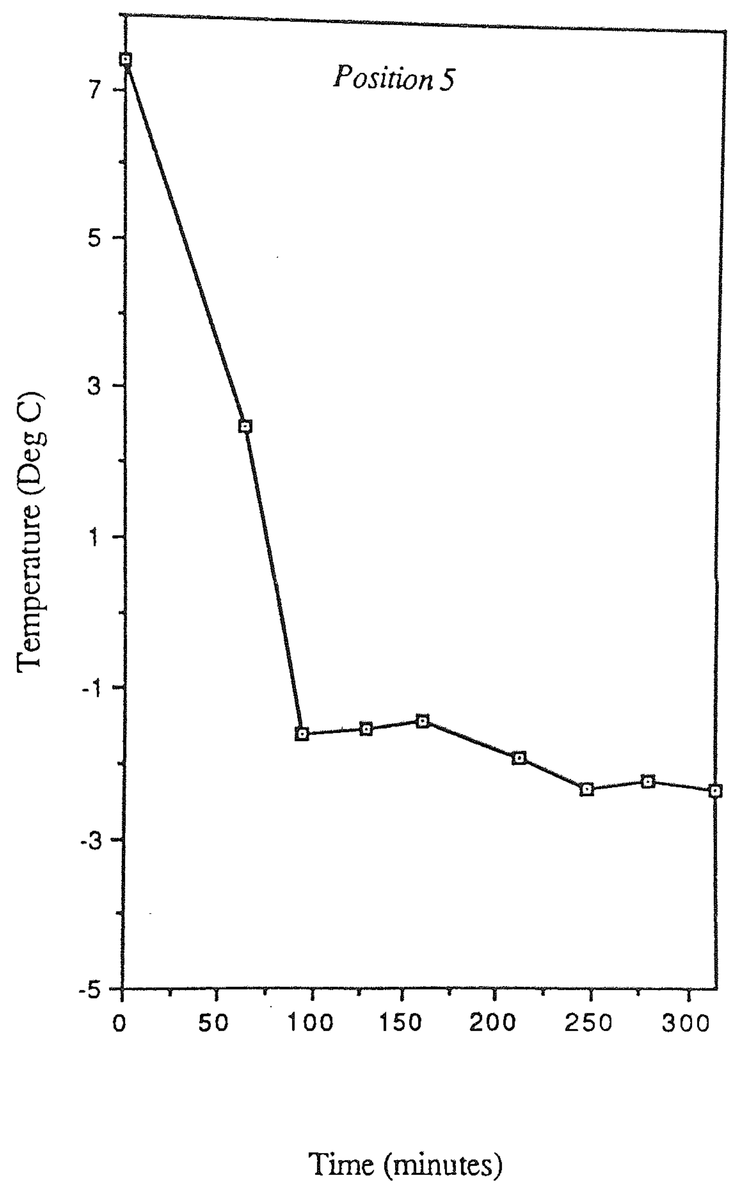

Temperature against Time (Test 2)

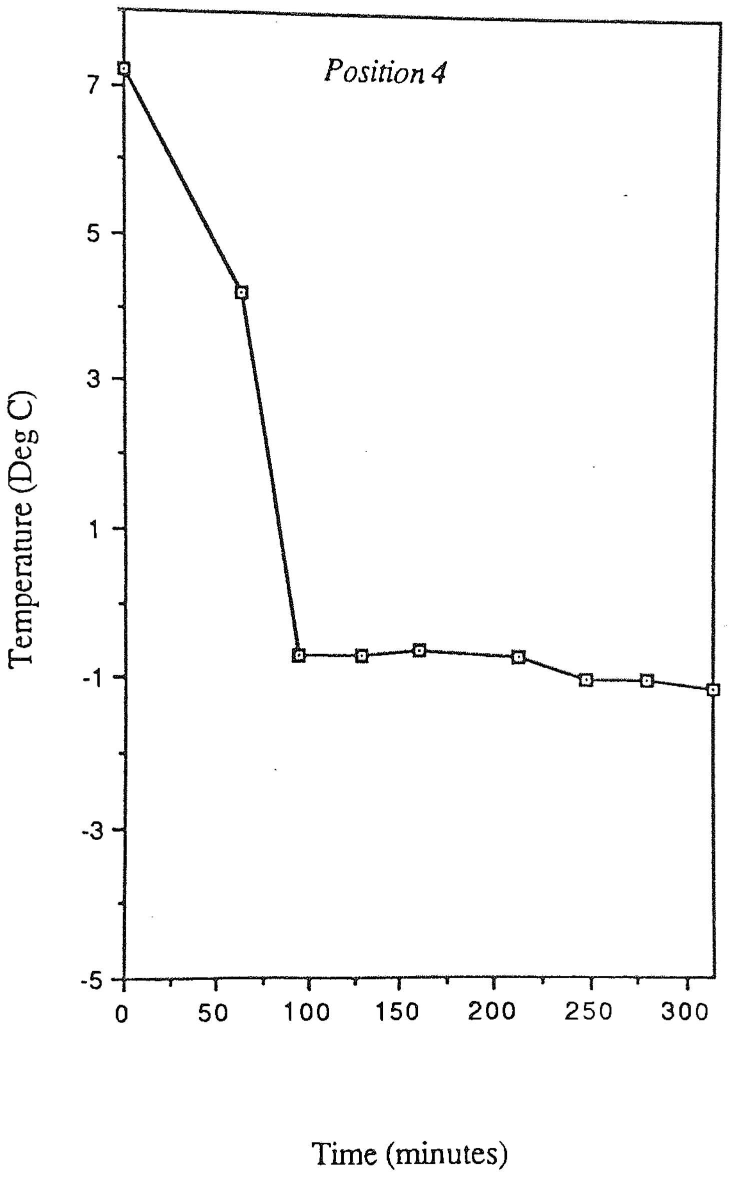

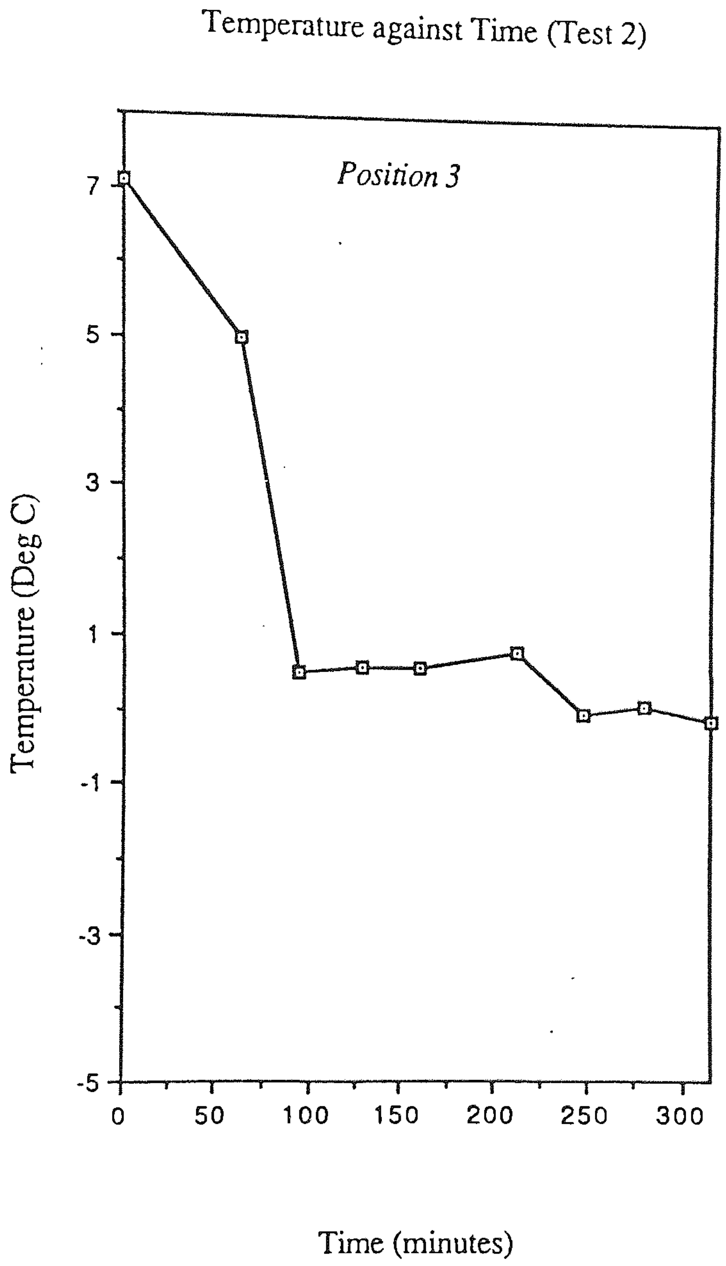
Temperature against Time (Test 2)
Position 3
Temperature (Deg C)
7
5
3
1
-1
-3
-5
0
50
100
150
200
250
300
Time (minutes)

Temperature against Time (Test 2)

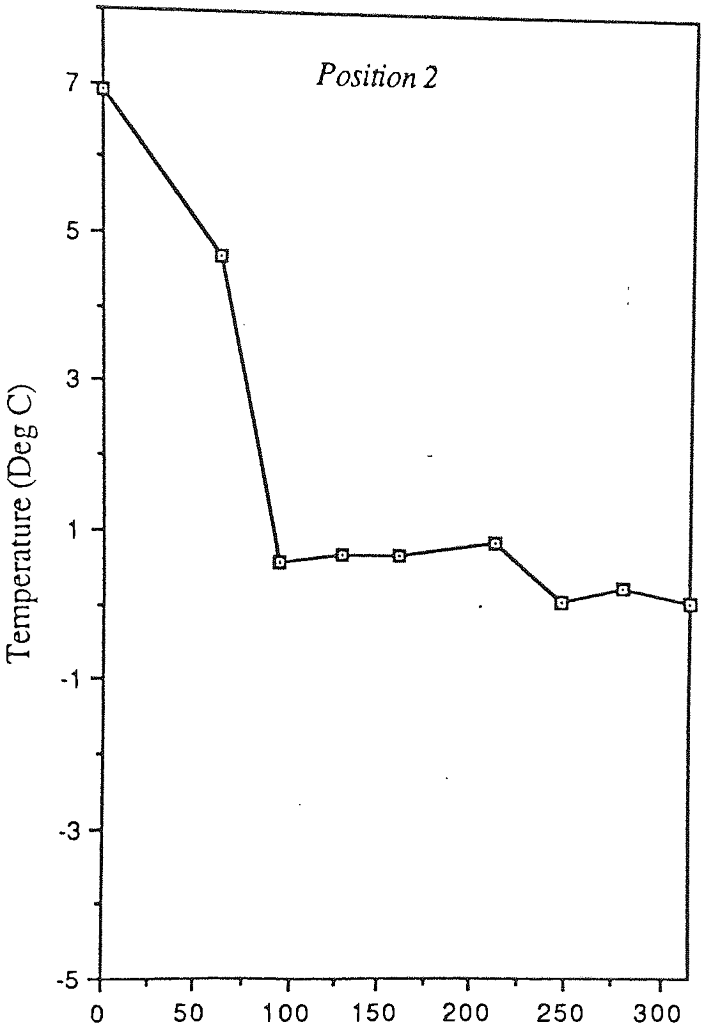

Time (minutes)

Temperature against Time (Test 2)